©2017

Xuanxuan Lu

ALL RIGHTS RESERVED

Fabrication of Edible Biocompatible Carbohydrate Particle-based Pickering Emulsions

By

XUANXUAN LU

A dissertation submitted to the

Graduate School-New Brunswick

Rutgers, The State University of New Jersey

In partial fulfillment of the requirements

For the degree of

Doctor of Philosophy

Graduate Program in Food Science

Written under the direction of

Qingrong Huang

And approved by

_____

_____

_____

_____

_____

New Brunswick, New Jersey

OCTOBER 2017

ABSTRACT OF THE DISSERTATION

Fabrication of Edible Biocompatible Carbohydrate Particle-based Pickering Emulsions

By XUANXUAN LU

Dissertation Director

DR. QINGRONG HUANG

Different from conventional emulsions, Pickering emulsions are stabilized by interfacially-adsorbed solid particles. Pickering emulsions have gained great interest in the past decades due to their high stability against coalescence, Ostwald ripening, and the possibility to avoid the deleterious effects linked to emulsifiers used in conventional emulsions. To fulfill the strong market trend of formulating products that are not only edible in theory, but also maintain the consumer perception of being natural, "clean label" and "green", this study was dedicated to developing particles from biomass-based resources to form Pickering emulsions with potential application in food, cosmetic and pharmaceutic products.

As a simple, organic solvent-free process, media-milling was applied to modify two major biomass materials, native starch and cellulose. Three maize starches (normal maize starch, high-amylose maize starch and waxy maize starch) with different amylose/amylopectin ratios were physically modified through media milling process to form milled starch particles. The physiochemical properties of these starches during milling process, including particle size, crystallinity and gelatinization properties were studied. Emulsions

stabilized by milled starch particles with different amylose/amylopectin ratios exhibited significant difference in terms of stabilization capability and rheological properties. Milled high-amylose maize starch particles have the best stabilization ability, followed by milled normal maize starch particles. Furthermore, the stabilization capacity of the milled starch particles improves with the increase of milling time.

To investigate the feasibility of Pickering emulsions stabilized by milled starch as a novel food-grade formulation for encapsulation and delivery of lipophilic bioactive compounds, curcumin was selected as model delivery target and encapsulated in the oil phase of Pickering emulsion. The digestion profile of curcumin-loaded Pickering emulsion was studied using three *in vitro* digestion models, simulated static small intestinal digestion model, pH-stat lipolysis model and TNO's gastrointestinal model (TIM-1). Simulated static small intestinal digestion model and pH-stat model indicated that the bioaccessibility of curcumin encapsulated in Pickering emulsion was enhanced compared with free curcumin suspended in bulk oil phase. A significant improvement of curcumin bioaccessbility was also observed in an emulsion system vs in bulk oil when using TIM-1 model, which simulates the entire human GI tract. Overall, the study's findings showed that curcumin encapsulated in Pickering emulsion stabilized by milled starch possesses benign stability against harsh gastric conditions as well as improved dissolution profiles in small intestinal tract. All are suggested that Pickering emulsion stabilized by milled starch exhibit high potential as encapsulate and delivery system for lipophilic bioactive compounds.

Milled cellulose particles of sizes ranging from 38 nm to 671 nm with rod-like shapes have also been successfully fabricated using media milling. Media milling process led to

a notable decrease in the particle size and crystallinity of milled cellulose particles with the increase of milling time. The milled cellulose particles were irreversibly adsorbed at the oil/water interface and formed stable emulsions with droplet size around 60~42 μm, which exhibited benign stability over a month storage. Milled cellulose stabilized emulsions also exhibited good stability against a wide range of pH (3, 5, 7, 9) and salt conditions (0.1~100 mM) with slight change in the droplet size. The rheological tests indicated the formation of gel network in the emulsions, which promoted the stability of the emulsions.

The *in vitro* digestion profile and phase behavior of Pickering emulsions stabilized by milled cellulose were evaluated to investigate their feasibility for encapsulation and delivery of lipophilic bioactive compounds. Curcumin encapsulated in Pickering emulsions exhibited benign stability with less than 50% degraded after storage of 30 days. The digestion behavior of emulsions under simulated small intestinal conditions was characterized using a pH-stat lipolysis model. The digestion profiles of emulsions were markedly dependent on the type of lipid and digestion buffer employed in lipid digestion experiments. The rate and extent of lipolysis of emulsions with medium chain triglycerides (MCT) was greater than emulsions with long chain triglycerides (soy bean and canola oil), reaching complete hydrolysis during lipolysis process independent of bile salt and phospholipids concentration. The structure changes of emulsions during digestion were analyzed using optical and fluorescent imaging. Although the initial digestion rate of curcumin encapsulated in Pickering emulsions with soy bean and canola oil was slower than the corresponding conventional emulsions stabilized by Tween/Span, their total extent of lipolysis was higher than that of conventional emulsions under both

fasted and fed intestinal digestion conditions. The bioaccessibility of curcumin encapsulated in Pickering emulsions was higher than in corresponding surfactant stabilized conventional emulsions.

High-amylose maize starch with different fatty acids (C12:0, C14:0, C16:0, C18:0, C18:1) were complexed using two heat-moisture methods. The structure properties of different starch-fatty acid complexes, including size and shapes of nanoscale supramolecular structures formed, through heat and moisture treatment, were studied. Optical microscope and SEM analysis showed that starch-fatty acid complexes retained the Maltese cross and granular morphology of native starch. X-ray diffraction revealed the crystalline morphology of starch-fatty acid complexes with B- and V-type crystallinity. And the crystallinity of the complexes varied depending on the fatty acids and methods used. USAXS/SAXS experiments demonstrated that fatty acid chain length and level of saturation affected both the lamellar structure as well as the B-type crystalline of the complexes. Moreover, the processing methods also exhibited major influence on the nanostructure of complexes.

The resistance of these starch complexes against enzymatic hydrolysis was increased based on the *in vitro* digestion measurements. And the hydrophobicity of these complexes was enhanced. This was manifested by increased contact angles. The capacity of these starch-fatty acid complexes to form Pickering emulsions was characterized. Starch-saturated fatty acid complexes were able to form stable emulsions that endured heat treatment of 60, 80 and 100℃. However, starch-unsaturated fatty acid complexes could not form stable emulsions. The barrier properties of these emulsions could be adjusted by heat treatment, which led to swelling of starches. Lipolysis profile of PMFs

loaded emulsions suggested that certain heat treatment could reduce the accessibility of lipase towards oil droplets and release of PMFs during lipolysis by enhancing the coverage of granules onto the oil-water interface.

In conclusion, particles derived from biomass resources starch and cellulose have been successfully fabricated to form Pickering emulsions using simple, environmental-friendly procedures. The resulting formulations were edible, ‘green’, have exhibited exceptional stability and a practical potential to encapsulate and control release of lipophilic ingredients, making them suitable for various applications in cosmetic, food and pharmaceutical industry.

ACKNOWLEDGEMENT

I would like to express gratitude to my advisor, Dr. Qingrong Huang for giving me an opportunity to work in his group, and his tremendous guidance and support for my study, research and life at Rutgers University. He also gave me precise suggestion and opportunities on my career plans. I am deeply grateful to have Qingrong Huang as a kind hearted and very considerate advisor.

I would like to thank Dr. Chi-Tang Ho, Dr. Shiming Li and Dr. Alan King for their willingness to be my committee members, and for their valuable suggestions and help with my research. I also would like to thank Dr. Yunqi Li and his students from Changchun Institute of Applied Chemistry, Chinese Academy of Sciences for their help with some important characterizations and analysis.

I would like to thank all my friends, previous and current labmates, a number of visiting scholars, for their support and help with my research and life here. Their encouragements and valuable suggestions have helped shape my thesis and give me insights into various areas of food research. Special thanks to Jieyu Zhu for working together with me for TIM-1 model, etc., Yijun Pan for HPLC analysis, Yin Wang for X-ray analysis, Hongwei Zhang and Lang Liu for some experimental support. I am thankful to meet and get to know all my labmates, colleagues and friends here who have made my time at Rutgers a memorable experience.

I also want to express my gratitude to China Scholarship Council for supporting my living expenses here at Rutgers University.

TABLE OF CONTENTS

LIST OF TABLES

LIST OF FIGURES

RATIONALE AND HYPOTHESIS

Conventional emulsions are generally stabilized by amphiphilic emulsifiers, either small molecular weight surfactant (molecular size ~1 nm) or polymeric emulsifiers (soluble proteins/polysaccharides, molecule size 1~10 nm), through decreasing the interfacial tensions of the emulsions. Besides, particles with dual wettability can also spontaneously accumulate at the oil-water interface to form stable emulsions, which are known as Pickering emulsions. Since the kinetic energy of collision between droplets will be insufficient to remove the particles once adsorbed at the oil-water interface, Pickering emulsions usually display long-term stability, and are even more stable against coalescence and Ostwald ripening than emulsions stabilized by small molecular weight surfactants.

Although a wide variety of particles with different shape and size have been used to stabilize Pickering emulsions, most of them are inorganic or synthetic particles, which are expensive, non-degradable and have low biocompatibility. Development of particulate emulsifiers derived from natural biopolymers has received reasonable attention in considering of their inherent superiority and wide application, especially in food, cosmetic and pharmaceutic products. With abundance supply, low cost, non-toxicity, well biocompatibility and biodegradability, starch and cellulose are attractive material sources to produce particle stabilizers for Pickering emulsions. Since the ability of native starch and cellulose to stabilized Pickering emulsions is minimal, modification methods need to be applied to improve their emulsifying capacity.

Media-milling is a simple, cost-saving and environmental friendly physical method, during which the target material would be modified by the mechanical force of grinding

balls. When a media-milling process was used to modify starch and cellulose, the original structure of starch and cellulose were damaged gradually. As a result, their physicochemical properties such as particle size, oil/water wettability were changed.

Native starch is composed of linear amylose and the branched amylopectin. The amylose can adopt the configuration of a single helix conformation when suitable guest molecules are present. Since the outside surface of the single left-handed helix is hydrophilic and the inner surface of the helical channel is hydrophobic, amylose forms complex structure by accommodating lipophilic guest molecules of appropriate dimension. Medium/long-chain fatty acids are one group of such lipophilic compounds which form V-type amylose-fatty acid complexes with starch. With collapsed helical conformation and crystalline structure from the hydrophobic interaction between amylose and fatty acids, the resulting amylose-fatty acid complex is resistant to enzyme hydrolysis. Through combination with medium/long-chain fatty acids, the lipophilic property of starch particles would increase, which can change their wettability in the oil-water interface.

Based on the above rational, **I hypothesize that (1) the emulsifying capacity of natural biopolymers, namely starch and cellulose in Pickering emulsion can be enhanced through a milling process, (2) by forming amylose-fatty acid complexes with medium- or long-chain fatty acids, native starch would become resistant starch, whose ability to stabilize Pickering emulsions would be increased.**

CHAPTER 1: INTRODUCTION

1.1. Overview of Pickering emulsion

Emulsions are generally colloids of two or more immiscible phase with one dispersed in another. Many of the food products we eat, the personal care products used, the pharmaceuticals consumed are formulations based on emulsions. Conventional emulsions are normally stabilized by small molecular weight amphiphilic molecules, which can decrease the interfacial tension between different phases, increase the steric hindrances and/or the electrostatic repulsion between the dispersed droplets (*1*). Polymeric emulsifiers, such as soluble proteins or polysaccharides with intermediate wetting properties, could also be used to stabilize conventional emulsions. Through spontaneous accumulated at the oil-water interface, solid particles with partial dual wettability can form stable emulsion, which known as Pickering emulsions. The concept of Pickering emulsion actually was firstly proposed in the early 20^{th} century, when Ramsden in 1903 (*2*) and Pickering in 1907 (*3*) independently reported the stable mixtureof two immiscible phases by solid colloidal particles.

The stabilization of emulsions using particles is highly related to their partial dual wettability. Compared to conventional emulsions stabilized by surfactants, Pickering emulsions exhibit higher stability against coalescence and Ostwald ripening during long-term storage. The diameter of particles to stabilize Pickering emulsions is often larger than 100 nm, while the relative size of small molecule surfactants is about 1 nm and soluble protein/polysaccharide molecules approximately 1-5 nm. As a result, the particles could adsorb at the oil-water interface to create a physical barrier through volume exclusion, thus preventing interfacial interaction between droplets. Moreover,

there is no fundamental difference between particle stabilization and other macro-molecular emulsifiers, such as soluble protein. The free energy needed to detach a spherical particle of radius r from the oil-water interface could be calculated by the following equation:

$$E = \pi r^2 \gamma_{ow}(1-|cos\theta|)^2 \quad (1)$$

where E is the detachment energy, r is the particle radius, γ_{ow} is the oil-water interface tension, θ is the particle contact angle at oil-water interface. For particles with contact angles between 30° and 150°, the energy of desorption per particle is normally in the order of several thousand kT, which indicates that the adsorption of particles onto interface is practically irreversibly (*1*). While the desorption energy of small molecular surfactant was less than 10kT, the surfactant molecules exist in a dynamic equilibrium, rapidly adsorbing and desorbing from the oil-water surface of emulsion droplets (*4*). This diffusion process and interfacial exchange promote Ostwald ripening and droplet coalescence, which would eventually result in measurable droplet size distribution changes. Conversely, there is no such processes in particle stabilized emulsions, which possess high stability against droplet size distribution change (*5*). According to the contact angle of particles absorbed at the oil-water interface, particles with intermediate wetting ability could stabilize either an oil-in-water (o/w) or water-in-oil (w/o) emulsion. Since the side of interface where the majority of particles exist would be the continuous phase, particles with contact angle less than 90° would lead to the formation of oil-in-water emulsions, whereas particles of contact angle more than 90° would form water-in-oil emulsions (*6*).

The development of particles to stable Pickering emulsions has generate great interest

in the past decade or so due to their distinctive features and promising applications in a wide range of products. Compared to conventional emulsions stabilized by surfactants, particle-stabilized emulsions enjoy the advantages of avoiding the adverse effects of some small molecular weight surfactants, such as tissue irritation, metabolic syndrome and environment pollution (*7-9*). Research on food grade Pickering emulsions with application in food and pharmaceutic industry has been a growing research field.

1.2. Development of particles to stabilize Pickering emulsions

A wide variety of particles with different shape and size have been developed to form Pickering emulsions. Most of the particles used to stabilize the Pickering emulsions are inorganic or synthetic particles, such as silica, latex, clay (*10-13*). In order to fulfill the strong market trend of formulating product, that is edible in theory and maintain the consumer perception of being natural, “green” or “clean label”, particulate emulsifiers derived from natural biopolymers have received reasonable attention in consideration of application in food, cosmetic and personal products (*14*, *15*). Recently, environmentally benign microparticles and nanoparticles emulsifiers originated from biomass resources have been developed to form Pickering emulsions. These biomass resources could be polysaccharide, protein, fat and oil, or other materials (*1*). Particles derived from polysaccharide materials include starch (*16*), cellulose (*17*), chitin (*18*), etc. Fat and oil based particles mainly refer as fat crystal (*19*). Protein based particles include particles from various protein resources, such as zein (*20*), kafirin (*21*), etc. Miscellaneous particles consist of particles from flavonoids (*22*), cocoa particles (*23*), etc.

The approaches to obtain biomass based particles generally could be divided into three categories. They could be synthesized from biomass molecules using aggregation, precipitation, crosslinking, crystallization, etc. Particles generated from this method

include solid lipid particles (*19*), chemical modified starch nanoparticles (*24*), soy protein particles, etc. They could be from existing structures with reduced sizes modified by milling, crushing, hydrolysis, etc. Particles from this method are cellulose nanocrystals (*25*), cryo-milled starch particles (*26*), etc. They could also from isolation of some intrinsic biological structures. These particles could be lactoferrin nanoparticles (*27*), bacteria chitosan networks (*28*), etc .

Although a wide variety of biomass-based particles has been developed, research on natural biomass based particle emulsifiers is still much less compared with the amount of study regarding inorganic or synthetic particles. Furthermore, in order to meet the large scale application in industrial products, the isolation, generation and production of particle emulsifiers from natural origin on a scale or at a suitable price is still of great importance.

1.3. Biomass materials: starch and cellulose

1.3.1. Starch and starch derivate particles

Starch is a type of carbohydrate formed by a large number of glucose units linked by glycosidic bonds, which can be isolated from a variety of green plants, mainly from tubers and cereals. The basic formula of starch is $(C_6H_{10}O_5)_n$, and the glucose monomer is called α-D-glycopyranose (or α-D-glycose). As semi-crystalline granule, native starch generally consists of amylose, long linear chain molecules with a few branches, and amylopectin, highly branched large molecules with short chains. Some native starches might also contain a third intermediate component (*29*). Based on its botanical origin, native starch has a wide variety of shape (round, oblong, sharp edged polyhedral etc.), size (0.5 to 100 nm) and composition (i.e. amylopectin/amylose ratio). The proposed multiscale structure of starch is depicted in **Figure 1**.

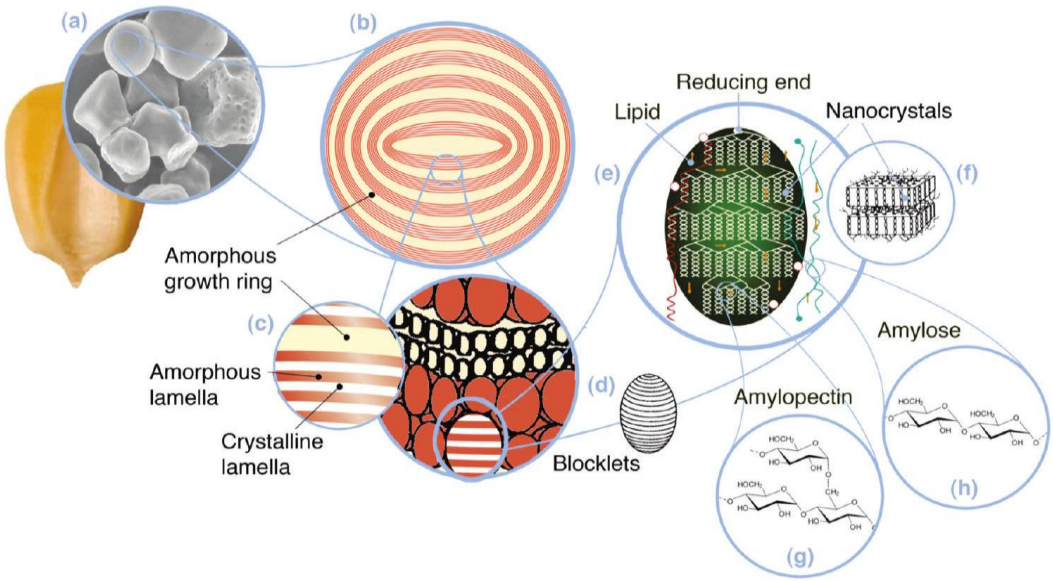

Figure 1. Starch multiscale structure: (a) starch granules from normal maize (30µm), (b) amorphous and semicrystalline growth rings (120-500 nm), (c) amorphous and crystalline lamellae (9 nm), magnified details of the semicrystalline growth ring, (d) blocklets (20-50 nm) constituting a unit of the growth rings, (e) amylopectin double helixes forming the crystalline lamellae of the blocklets, (f) nanocrystals: other representation of the crystalline lamellae called starch nanocrystals when separated by acid hydrolysis, (g) amylopectin's molecular structure, and (h) amylose's molecular structure (0.1-1 nm)(*30*).

The amylose/amylopectin ratio of starch plays a vital role in the structural as well as many significant physical, functional and technological properties of starches, such as gelatinization temperature, viscosity, water binding capacity and solubility. With the short amylopectin chains forming double helices, which associated into clusters forming crystalline lamellae, amylopectin is the main component of the crystallinity structure of starch granules (*31*). The molecular ordered structures, the amount of double helices in starch granules, was found increased with increasing amylopectin content (*32*). The majority of amylose presents in the amorphous growth ring. Only a small amount of amylose involve in the formation of crystalline lamellae by co-crystallizing with short

amylopectin chain in the crystalline lamellae (*32*, *33*). Increase the amylose content of starch results in a decrease of crystallinity in starch granules. Amylose content has also found to be correlated with the short chains to long chains ratio and average chain-length of amylopectin, which exhibits close relationship with crystal type of starch granules (*34*). Crystallinity change of A-type for normal and waxy maize starch to B-type for high amylose maize starch (i.e., amylose content >40%, w/w) is observed (*35*). And the melting thermodynamic properties of starches with different amylose contents suggest that the melting temperature of starches is directly linked with the amylose content (*36, 37*).

With large abundance, nontoxicity, low cost, inherent biodegradability and annual renewal, starch is one of the most promising natural polymers for producing particle stabilizer of Pickering emulsions (*30*). Although some native starch granules, namely rice, waxy maize, wheat and potato starch have been used to stabilize Pickering emulsion (*38*), the emulsifying ability of these starch is low and the stability of obtained emulsions is poor, especially emulsions stabilized by starch granules with relative large size. Therefore, modification processes need to be developed to improve the properties of starch as Pickering emulsion emulsifiers. These methods include using nanoprecipitation procedure to fabricate starch nanospheres, acid hydrolysis to produce starch nanocrystals, chemical cross-link to create hydrophobic starch (*24, 26, 39, 40*). The starch particles obtained from these methods exhibit good emulsifier capacity. However, these methods still have some limitations, such as involving the usage of hazardous organic solvent/chemicals, corrosive strong acids, time and labor consuming, which make it difficult to be applied in general industrial use, especially in food industry.

1.3.2. Cellulose and cellulose derivate particles

As the most abundant natural polymer, cellulose is a practically inexhaustible resource for the production of biodegradable, biocompatible and environmentally friendly products (*41*). Although having the same basic formula as starch, $(C_6H_{10}O_5)_n$, cellulose is a linear homopolymer of β(1,4)-D-glucose residues with semicrystalline structure where highly ordered regions (crystallites) are interrupted along the microfibril axis by disordered domains (amorphous phase) (*42*). The multistructure of cellulose has been presented in **Figure 2**. As a solid rod-like particles derived from biomass, cellulose has attracted great interest as Pickering emulsion stabilizer because of being environmentally friendly and possessing a potentially wide range of applications. Moreover, since cellulose cannot be digested by human, consumption of cellulose stabilized Pickering emulsions will inhibit the possible blood glucose response and calorie burden in human compared with starch stabilized Pickering emulsion.

Since cellulose is not surface active due to the lack of hydrophobicity and great tendency to aggregate, modification methods are required for it to stabilize Pickering emulsions. Various types of cellulose derivate particles, including cellulose nanocrystals (*43-45*), cellulose fibrils (*17, 46*), microcrystalline cellulose (*47*), bacterial cellulose (*48, 49*), and cellulose derivatives (*50*) have been developed to stabilize Pickering emulsions. However, the production of these cellulose rod-shape particles has some drawbacks, such as presence of contaminants, time-consuming, low productivity, which limit their general application in industry.

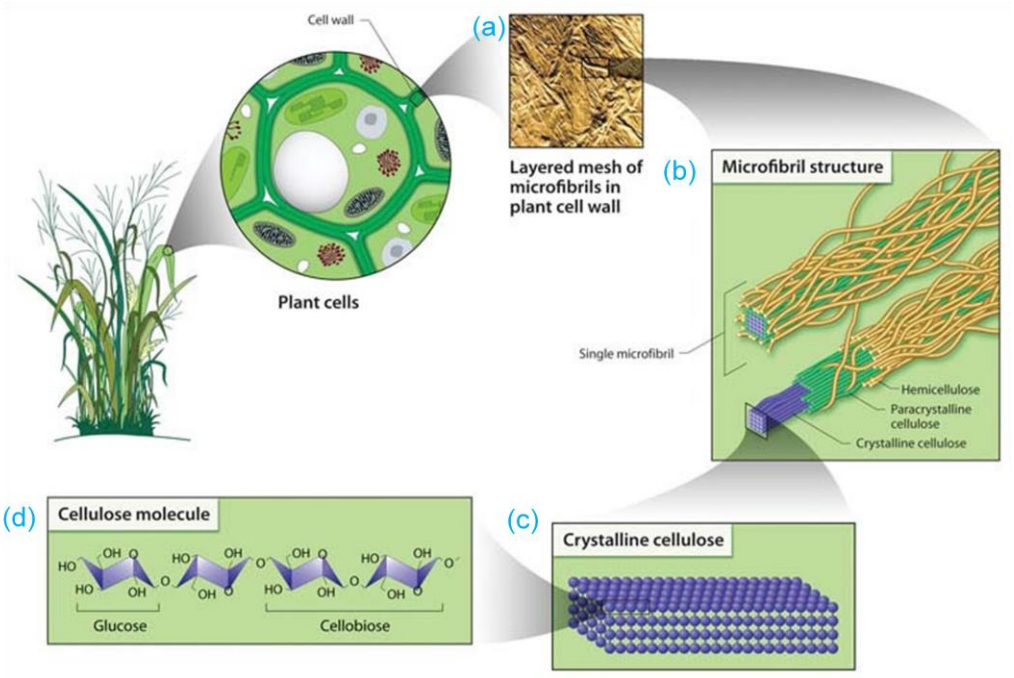

Figure 2. Cellulose multistructure: (a) linear microfibrils from plant cell wall (10-20 nm in diameter), (b) microfibril crystalline and paracrystalline (amorphous) cellulose core surrounded by hemicellulose, (c) 3D lattice-like structure of crystalline cellulose linked by high degree of hydrogen bonds, (d) cellulose's molecular structure (*51*).

1.4. Media-milling process and its application in starch and cellulose modification

As a simple, cost-lowering and environmental friendly physically method, ball milling treatment has long been used to produce particles mainly in micrometer scale (*52-54*). Derived from stirred ball milling, media milling was commercially introduced in 1948 as a sand milling (*55*). Its comminution efficiency was highly improved due to the use of more densely packed and rapidly rotated media (*56*). The thermal impact on the materials during milling process was minimized by using high efficiency temperature control system and the development in the grinding chamber (*57*). Media milling is a popular method to produce nanoparticles in pharmaceutical industry while its application in food research is limited (*58*). The structure of media-milling machine has been depicted in **Figure 3**. The target materials will be suspended in water. Under the influence

of friction, impact, compression, and shearing forces from the milling beads, grinding chamber and material itself, the materials will be damaged and their sizes will be gradually reduced (*59*). Since the nanoparticles would be in suspension, which would not float into the air, thus decreasing hazard to environment and human respiration system.

For semicrystalline materials, such as starch and cellulose, media-milling process has been proved to effectively reduce their particle sizes, producing nano/submicrometer particles (*60, 61*). When the starch granules were mechanically damaged and partially fragmented by the shearing and impact forces from the grinding media, starch granules would flake off layer by layer from the surface to interior, which would ultimately break into anomalous particles (*62*). The resulting micronized starch exhibited changes in functional properties, such as improved cold water dispersibility, reduced crystallinity, decreased viscosity, gelatinization temperature and heat for gelatinization (*61, 63-66*). Chen et al. reported the production of starch particles with number-average diameter of 260 nm using media milling, and the presence of particles smaller than 100 nm was confirmed (*67*). Liimatainen, et al. (*68*) and Yeh, Huang and Chen (*60*) have also used media-milling process to produce cellulose particles of several hundred nanometers. Media milling has been used to produce a variety of nano/submicrometer particles from other food materials, such as yam (*54*), soybean (*52*), wheat bran dietary fiber (*69*), chitosan (*70*) and *Ganoderma tsugae* (*53*). The media milling process was found to enhance the content of bioactive compounds in the materials and the resulting nanoparticles were not toxic to certain cells (*53, 54, 69*).

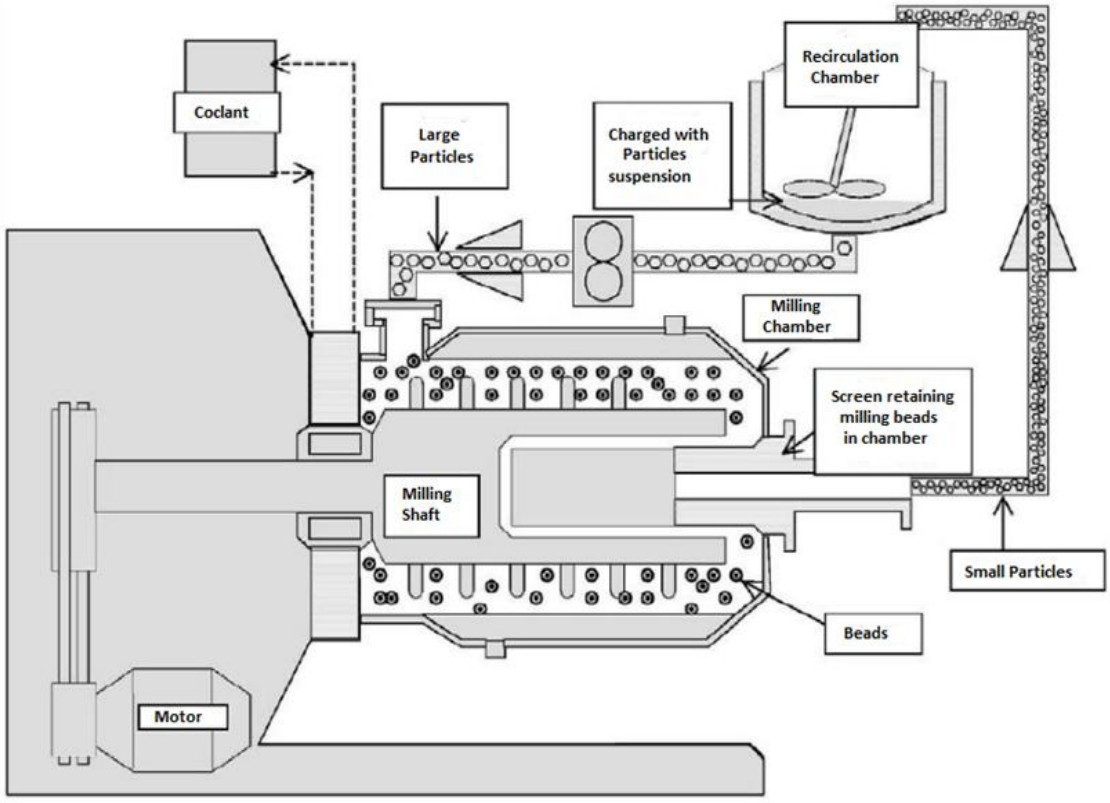

Figure 3. The structure of media-milling machine.

For particles to stabilize Pickering emulsions, the particle size and wettability, i.e. to create as small as possible particles with a contact angle close to 90 º, are the focus of much optimization (*1*). Through modifying with media-milling process, the obtained nano/submicrometer starch or cellulose particles might be benign particle emulsifiers for Pickering emulsions since their particle size would be reduced (*61*). Media-milling procedure might be a technique of great potential to produce emulsifiers for Pickering emulsions by modifying the size and solvent solubility of target material.

1.5. Resistant starch

1.5.1. Definition and category resistant starch

Starch is the major dietary source of carbohydrates. Based on their hydrolysis behavior when incubated with enzymes without prior exposure to dispersing agents,

starches can be classified into three categories by the Englyst test (*71*).

Rapidly digestible starch (RDS). RDS refers as the fraction of starch that is converted to the constituent glucose molecules at the first 20 min of enzyme digestion. It is generally made of amorphous and dispersed starch, which exists in large amount in starchy foods cooked by moisture and heat process, such as rice and bread.

Slowly digestible starch (SDS). SDS is similar to RDS, which would be completely digested in the small intestine. However, the digestion of SDS is more slowly. It refers as the fraction of starch that is converted to glucose during a further 100 min of enzyme digestion.

Resistant starch (RS). RS refers as a small fraction of starch that is resistant to *in vitro* enzymatic hydrolysis treatment by exhaustive α-amylase and pullulanase after 120 min of incubation (*72*). Since the undigested starch might be fermented by the gut microflora when reaching the large intestine, RS has now also referred as the amount of starch, which is not completely digested and absorbed in the small intestine. RS is measured as the difference between total starch (TS) and the amount of RDS and SDS after enzyme digestion.

$$RS = TS - (RDS + SDS) \quad (2)$$

RS can be subdivided into 5 fractions: RS_1, RS_2, RS_3, RS_4 and RS_5. RS_1 is referred as starch that is in physically inaccessible form. It includes partly milled grains or seeds and some processed starchy foods with high dense. RS1 is heat stable in most cooking conditions (*73*). But its resistant degree could be reduced by milling and chewing.

RS_2 is referred as starch that is resistant to enzyme digestion in a certain granular form. It is chemically determined as the difference between the released of glucose from

a boiled homogenized sample under enzyme digestion and that from an unboiled, nonhomogenized sample. Since starch molecules of raw starch granules exist in a radial pattern with tightly packing and relatively dehydration, the packing structure restricts the accessibility of digestive enzymes (*74*), which explains the resistant nature of ungelatinized starch. Food products, such as raw potato, green bananas, high amylose corn, contain certain amount of RS_1. Food processing and cooking can reduce the resistant degree of RS_2.

RS_3 is referred as retrograded starch formed after the cooling of gelatinized starch. The formation of RS_3 involves in the leaching of amylose from starch granules under complete hydration, the reassociation of this polymer chain as double helices upon cooling and the packing of double helices in hexagonal unit cell during retrogradation (*75*). It is resistant to dispersion of boiling and enzyme digestion, and can only be dispersed by dimethyl sulphoxide or KOH (*76*). Unlike RS_1 and RS_2, which are slowly digested in the small intestine with incompletion, RS_3 is entirely resistant to the digestion reaction of pancreatic amylases. Cooked starchy food, such as bread, rice, often contains RS3 after being kept at low or room temperature (*74*). RS_3 is thermal stable in most cooking conditions.

RS_4 often refers as starch that has been chemically modified with new chemical bonds formed. It includes modified starches with various types of chemical treatment, such as starches that have been esterified, etherized or cross-linked with chemicals like distarch phosphate ester. RS_4 is less susceptible to *in vitro* digestibility.

RS_5 refers as starch that contains V-amylose single helical complex. It can be formed by complexing amylose with lipids, such as monoglyceride, fatty acids. These complexes

are resistant to hydrolysis of enzymatic digestion (*77*). Since these complexes often possess higher dissociation temperature (*78*), RS_5 is less susceptible to food processing and *in vitro* digestibility. The existing of complexes could also restrict the swelling of the granules and further reduce the susceptibility of the starch to amylolysis.

1.5.2. Functional properties of resistant starch

Since the frequently consuming food containing rapidly digestible starch has been linked with the development of insulin resistance and metabolic syndrome, such as diabetes, obesity, and cardiovascular disease (*79, 80*), it is recommended to increase the consumptilon of RS, which could intervene insulin resistance and metabolic syndrome by reducing piostprandial plasma-glucose and insulin response (*81, 82*). Consumption of RS could also rnkeduce the occurrences of obesity and cardiovascular disease by reducing the rate of lipolysis, lipogenesis, and cholesterogenesis (*83, 84*). There are many potential functional properties and health benefits have been linked with RS. Consuming RS can reduce the energy value and available carbohydrate content in the foodstuffs. It can also accelerate the onset of satiation through enhancing the fiber content of food (*85*). RS would produce a number of fermentation products when reaching the large intestine, such as methane, carbon dioxide, hydrogen, organic acids (e.g. lactic acid) and short chain fatty acids (SCFA). However, compared to other non-digestible oligosaccharides, fructo-oligosaccharides and lactulose, RS only produce a modest rate of these gases (*86*). The functional properties of RS is largely relied on the production of SCFA including butyrate, acetate and propionate (*87*). As the preferred respiratory fuel of the cells lining the colon, SCFA could lower luminal pH, enhance colonic blood flow, and restrict the development of abnormal colonic cells (*88*).

The health benefits of RS have been listed as follows:

(i) The fermentation product of RS in the large intestine produces high level of short chain fatty acids, especially butyrate, which have an inhibitory effect on colonic cancer. As one of the main energy substrates for large intestinal epithelial cells, butyrate could inhibit the malignant transformation of these cells, thus decreasing the occurrence colonic cancer (*76*).

(ii) The metabolism of RS takes 5-7 h after consumption. The slow digestion of RS gives a control release of glucose, which would reduce postprandial glycemia and increase the period of satiety (*89*). The hypoglycaemic effects of RS may a significant role in decreasing the incidence and providing improved metabolic control of type II diabetes.

(iii) The production of SCFA indicated the possible interaction between RS and ingested bacteria (*87*). Research also has suggested that RS could serve as a prebiotic to enhance of growth of some beneficial microorganisms, such as *Bifidobacterium* (*90*).

(iv) RS has been observed to affect the lipid metabolism, such as lowering the levels of serum total cholesterol and VLDL + IDL + LDL cholesterol. The hypocholesterolemic effects of RS have been widely demonstrated (*73*).

(v) RS could be categorized as a type of dietary fiber due to its highly resistant to mammalian enzyme. Reducing total carbohydrate content in the meal through consuming RS could promote postprandial lipid oxidation, thus inhibiting fat accumulation in the long run (*91*).

(vi) Other health benefits of RS have also been revealed, including enhancing absorption of minerals (such as calcium and iron) in the intestinal, reducing the formation of gall stone due to lower secretion of insulin and synthesis of cholesterol (*92*).

1.5.3. Formation of starch-fatty acid complexes and its potential as particle emulsifier

Starch is composed of two polymers, the linear amylose and the branched amylopectin. The linear amylose can adopt the configuration of a single helix conformation when suitable guest molecules present. Since the outside surface of the single helix is hydrophilic and the inner surface is hydrophobic, amylose could accommodate lipophilic guest molecules. The proposed structure is presented in **Figure 4**. By interacting with fatty acids, the resulting starch will be resistant to enzyme hydrolysis due to the forming of amylose-lipid (*79, 93*). As mentioned previously, starch-fatty acid complexes are categorized as RS_5. The complex exists in two forms: amorphous amylose-lipid complex (form I) and crystalline complex (form II) (*94, 95*). Compared with amorphous complex, the crystalline complex has higher melting temperature and is more enzyme-resistant. After complexing with fatty acid, the swelling of starch granules will be restricted during cooking, which will decrease the accessibility of amylase to the starch molecules (*96*). The health benefit effects of this type of resistant starch actually have been investigated in vivo. Human-feeding study showed that substantially lower postprandial plasma-glucose concentration and insulin response was observed in human consuming bread with this resistant starch than white bread (*97*). Animal study showed that the azoxymethane-induced preneoplastic lesions (colon cancer precursors) in the colon was reduced in rat fed with cooked fatty acid complexed high-amylose starch, suggesting the ability of this resistant starch to suppress colon carcinogenesis (*98*).

Several preparation methods have been investigated in previous researches. Starch granules were firstly pretreated with debranching enzyme (isoamylase and pullulanase), then complexed with lipids (*79, 99*). Annealing of starch was performed before forming

complexes with lipid (*100*). Starch granules were dissolved in alkali solution or dimethylsulfoxide (DMSO) before interacting with lipids (*101, 102*). Complexing with lipids after gelatinization of starch and leaching out of amylose was reported (*103*). And interaction of starch granules and lipids under heating and low moisture conditions has also been reported (*103*). The last method has been applied in my research since the resulting starch complexes could mostly maintain the original granular structure, which would be an important factor for particle emulsifiers. Moreover, this method possesses advantages, including simple operation procedures and avoiding the usage of hazardous chemicals.

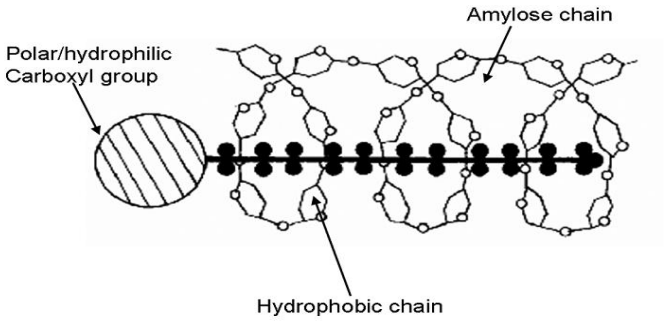

Figure 4. Single amylose helix complexed with a ligand, of which the polar head is located outside the helix, whereas its aliphatic chain is situated in the helix cavity (*104*).

Native starch is highly hydrophilic because of the hydroxyl groups. It is possible that the hydrophobicity of fatty acid-amylose complex resistant starch would be increased due to the existance of fatty acids. In my research, development of medium/long-chain fatty acid-amylose complex resistant starch will be conducted to stabilize Pickering emulsions. Compared with Pickering emulsions stabilized by conventional starch, the resulting resistant starch-stabilized Pickering emulsions might be more stable in the digestion system with lower effects on blood glucose, and more health beneficial effects.

CHAPTER 2 DEVELOPMENT OF MILLED STARCH TO STABLIZE PICKERING EMULSIONS

2.1 Introduction

In the past decades, Pickering emulsions stabilized by solid particles have attracted scientific interests due to their high stability against coalescence and Ostwald ripening than conventional emulsions stabilized by surfactants (*4, 105*). Besides, particle-stabilized emulsions avoid the side effects that linked to some hazardous surfactants (*8*). A wide variety of particles with different shapes and sizes have been used to stabilize Pickering emulsions, among which most are inorganic or synthetic particles, such as silica, latex, and clay (*10-13*). Recently, particulate emulsifiers derived from natural biopolymers have received reasonable attention in consideration of applications in food, cosmetic and personal products (*14, 15*). Some particles originated from cellulose, chitin or protein have been developed to form Pickering emulsions (*18, 106-108*). However, research relating to particle emulsifiers from natural biopolymers is still much less compared to the amount of study into organic and inorganic particles. Furthermore, in order to meet the large-scale production for industrial applications, exploration of inexpensive particulate emulsifiers from natural origin is still of great importance.

With large abundance, low cost, low toxicity, good biocompatibility and biodegradability (*30*), starch is an attractive material source to produce stabilizer for Pickering emulsions. Several native starch granules, namely rice, waxy maize, wheat and potato starch have been shown to stabilize Pickering emulsion (*38*). Starch nanospheres fabricated by nanoprecipitation procedure presented good stabilization in Pickering emulsions (*24*). Starch nanocrystals prepared by acid hydrolysis of waxy maize starch

granules, have been also utilized as Pickering emulsion stabilizer (*40*). However, the previously reported methods involved the use of corrosive strong acids for starch hydrolysis during Pickering emulsion formulation, which requires long processing time and has low yield. In addition, fabrication of chemically modified starch particles is complicated and often involves the use of several chemicals, which may not be desirable for food applications.

In this research, native starch will be physically modified through a media milling procedure, which is derived from stirred ball milling, a simple, environmentally friendly process being long employed to modify starch. During ball milling, the starch granules will be mechanically damaged by the force of grinding balls (*109*). The milling process exhibited different extent of damage on amylopectin and amylose fraction in the starch granules. Some amylopectin was observed to break into low molecular weight fragments (*110*). Amylose is less affected by this physical grinding since only a slight depolymerization of amylose was observed (*111*). Compared to balling milling, media milling has higher comminuting efficiency due to more densely packed and rapidly rotated media (*56*). Moreover, with improved temperature control system and development in the grinding chamber, the influence of thermal impact on the materials is minimized during media milling (*57*). Media milling has been widely used in pharmaceutical industry to produce nanoparticles (*58*). However, its application in food research is limited. Only a few researches were reported, where a variety of nano/submicrometer particles from food materials, such as yam, soybean, cellulose and starch were obtained using the media milling method (*52, 54, 60, 67*).

The objective of this study was to study the effects of media-milled starch with

different amylose/amylopectin ratios on the stability of starch particles-stabilized Pickering emulsions. Three maize starches of different amylose/amylopectin ratios were modified with media-milling process, and their physical properties were assessed by laser light scattering, differential scanning calometry (DSC) and X-ray diffraction. The emulsion microstructure, storage stability as well as rheological properties of the obtained Pickering emulsions were also investigated.

2.2 Materials and methods

2.2.1 Materials

Normal maize starch was purchased from Sigma-Aldrich (St. Louis, MO). High-amylose maize starch and waxy maize starch were obtained from Ingredion (Bridgewater, NJ). The soy bean oil was purchased from a local supermarket. The ethanol, hydrochloric acid and sodium hydroxide were purchased from VWR International, LLC. Milli-Q water was used throughout the experiments.

2.2.2 Media-milling treatment

The maize starch was first suspended in deionized water at a ratio of 7% (w/w). Media (yttria-stabilized tetragonal zirconia) of 0.2 mm were placed in the milling chamber (200 ml) at a filling ratio of 20% v/v. Then the starch suspension was added into a MiniSeries mill machine (Netzsch LLC, PA, USA), where the starch was ground under a pump speed of 100 rpm, mill speed of 3000 rpm and mill power of 0.13 kw. During the total grinding time of 25 h, samples were withdrawn every 5 h. To minimize the influence of milling-derived heat effect on milled starch, the milling process was paused for an hour cooling process after every 5 h milling period in addition to using the high efficiency cooling system. The temperature of milling chamber was monitored, which was below 30℃ during the entire milling process. The obtained milled-starch

suspensions were then used for emulsion preparation. In the meantime, the weight content of starch in the suspension was precisely measured through a moisture test. And rest of the milled-starch suspensions were freeze-dried to obtain milled-starch powder for further analysis.

2.2.3. Preparation of emulsions

The fresh milled-starch suspensions were throughly mixed with oil phase at a ratio of 1:1 (v/v) using an IKA Ultra-Turrax T25 homogenizer under 13,000 rpm for 3 min. Each emulsion was processed for three times. The starch concentration was expressed as weight content relative to the water phase based on the prior moisture tests.

2.2.4. Particle sizes of milled starch particles

The particle sizes of milled-starch particles at different processing times were monitored by a dynamic light scattering-based 90 Plus Particle Analyzer (Brookhaven Instruments Corporation, U.S.A) at a scattering angle of 90°. The starch suspension was diluted to around 1 mg/ml for measurement. The reflection index used was 1.33 and the laser wavelength was 660 nm.

2.2.5. X-ray diffraction (XRD)

The XRD patterns of native and milled starch were obtained using a RU200R X-ray diffractometer (Rigaku, Tokyo, Japan). The X-ray source used was Cu-Kα filtered radiation (λ=0.154 nm). The X-ray tube was set at 40 mA and 40 kV. The scattering angle (2θ) scanned was range from 5° to 40° at a scanning rate of 0.02°/min. The crystallinity of samples were determination based on a previous study (*112*) using the following equations:

$$\text{crystallinity (\%)} = A_c/(A_c+A_a) \times 100 \quad (3)$$

where A_c is the area of the crystalline peak and A_a is the area of the amorphous peak.

2.2.6. DSC analysis

The thermal properties of native and milled starch were investigated by a Perkin-Elmer DSC-8000 differential scanning calorimeter equipped with a thermal analysis data station (Norwalk, CT, USA). The sample and deionized water were added into an aluminum pan at a starch concentration of 25% (w/w). The pan was sealed and equilibrated at room temperature for 12 h before measurement. Analyses were conducted at a temperature range of 30~120℃ with a scanning speed of 10℃/min.

2.2.7. Light microscopy of starch-stabilized Pickering emulsions

The samples were stored at room temperature for 24 h before analyzed by using a Nikon Eclipse TE2000-U (Japan) microscope, which was equipped with a 1392×1040 resolution digital camera. The samples were placed on a glass microscopic plate without cover glass. The obtained images were then processed using ImageJ program. The average droplet size was the mean droplet size of at least fifty droplets.

2.2.8. Stabilization capacity

The stabilization index (EI), which was expressed as the volume of the emulsion to the total volume of the sample, was used to evaluate the stabilization capacity of the starches. The EI was calculated according to the equation (4) (*113*). And the remaining starch (RS), the amount of starch settled at the bottom of the test tube, was also calculated based on equation (5).

$$EI = \frac{\text{Volume of cream layer}}{\text{Total volume of emulsion}} \quad (4)$$

$$RS = \frac{\text{Volume of sediment starch}}{\text{Total mass of added starch}} \quad (5)$$

2.2.9. Rheological measurements

The rheological measurements were conducted by an Advanced Rhemetric Expansion System (TA Instruments, New Castle, USA) at room temperature. A plate and cone

geometry with a diameter of 25 mm was used for all tests. The rheological properties of the emulsions were analyzed after storage of 24 h at room temperature to reach an equilibrium status. The samples were placed on the bottom plate with edges covered with a thin layer of silicone oil to prevent moisture evaporation. The gap height used for emulsions was 1.2 mm. Before each measurement, twenty minutes were allowed for resting. Oscillatory tests were performed in the frequency range of 0.1-15 Hz under linear viscoelastic range, which was verified by oscillatory stress sweep tests performed in the strain range of 0.01-75 % at a frequency of 10 rad/s. The shear viscosity (η), storage (G') and loss (G") modulus were measured.

2.2.10. Statistical Analysis

All the experiments were conducted in triplicate (n=3) and data was analyzed with SPSS program version 16.0. Data were expressed as the mean ± standard deviation and analyzed using analysis of variance (ANOVA).

2.3. Results and Discussion

2.3.1. Particle size reduction

The size reduction of normal maize starch, high-amylose maize starch, waxy maize starch and physically modified starch by media-milling process at different milling time was determined by dynamic light scattering (**Figure 5**). During the milling process, the energy of friction created between starch granules and the wall of milling chamber and between starch and milling balls facilitated the breakdown of the granule structure and subsequently led to the reduction of particle size. The particle size of milled starch of 5 h milling process was several micrometers, which was beyond the measure range of the dynamic light scattering. The results were not presented here. Generally, the size of milled starch particles decreased gradually when milling time was increased. After a

milling process of 25 h, the milled waxy maize starch had the smallest particle size of around 500 nm, followed by milled normal maize starch of around 700 nm and milled high-amylose maize starch of around 900 nm. These results might imply that the increase of amylose content in the native starch enhance the endurance of starch granules against mechanical forces of media balls. Similar phenomena were observed in starch damage during cryo-milling and dry-milling process (*114, 115*). It was suggested that amylose can be a mechanical plasticizer in starch granules, which tended to act as shock absorber in the amorphous regions and provided a cushioning effect limiting breakdown of amylopectin in non-waxy starches during milling process (*114, 115*). A previous study has reported the production of nano/submicrometer milled starch particles of diameter around 700 nm when media milling was used to modify normal maize starch, which was in line with our results (*67*).

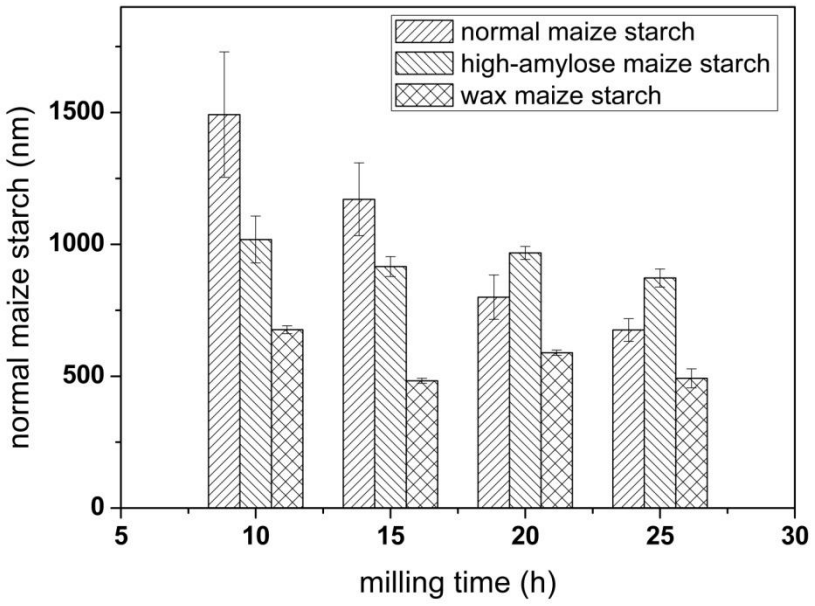

Figure 5. Particle size change of three milled starch particles with different milling times.

2.3.2. X-ray diffraction analysis

The X-ray diffraction patterns of normal maize, high-amylose maize and waxy maize starch at different milling times were displayed in **Figure 6**. Native normal maize starch and waxy maize exhibited a typical A-type diffraction pattern with four strong reflections at around 15°, 17°, 18°, 23°. Native high-amylose starch exhibited a typical B-type pattern with peaks at about 5.5°, 17°, 22°, 24°. With double helixes structure, some amylose might be able to form a crystalline structure (*116*). The crystalline structure of starch granules are mainly from the double helices of amylopectin side chain clusters, which are arranged in parallel composition by hydrogen bonds between adjoining glucose residues (*116-118*). It is explainable that with the increase of amylose content, the scattering intensity of native starch granules for almost every diffraction peak decreases, except that at 2θ = 20°. The mechanic forces from the milling beads could lead to relaxation of the crystalline clusters, emerge of disorder and defects in the crystals, as well as breakdown of starch granule structure (*119*). During the milling process, the proportion of crystalline structure decreased gradually, meanwhile the non-crystalline fraction increased. After milling for 5 h, there was a noticeable decrease in the diffraction peaks of all the starches, especially for normal maize and waxy maize starch, which suggests that the hydrogen bonds were broken and crystalline arrangements of the double helices were disintegrated. When the milling time prolonged to 15 h or more, the diffraction signals showed a halo peak and no further significant decrease in the crystallinity was observed, which means the crystallinity structure of the starch particles might be completely destroyed. The observed decrease in the crystallinity of starch granules during the media milling is in agreement with the findings in ball milling process. Morrison and Tester (*120*) reported an increase of low molecular weight

amylopectin content and reduction of cyrstallinity in the wheat starch during ball-milling process while the amylose content did not change.

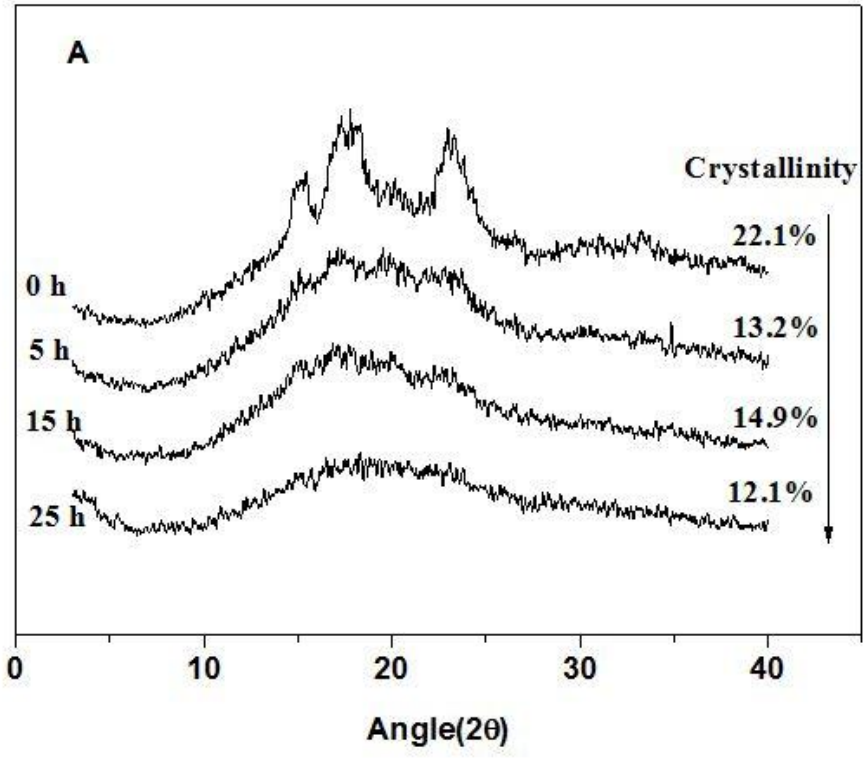

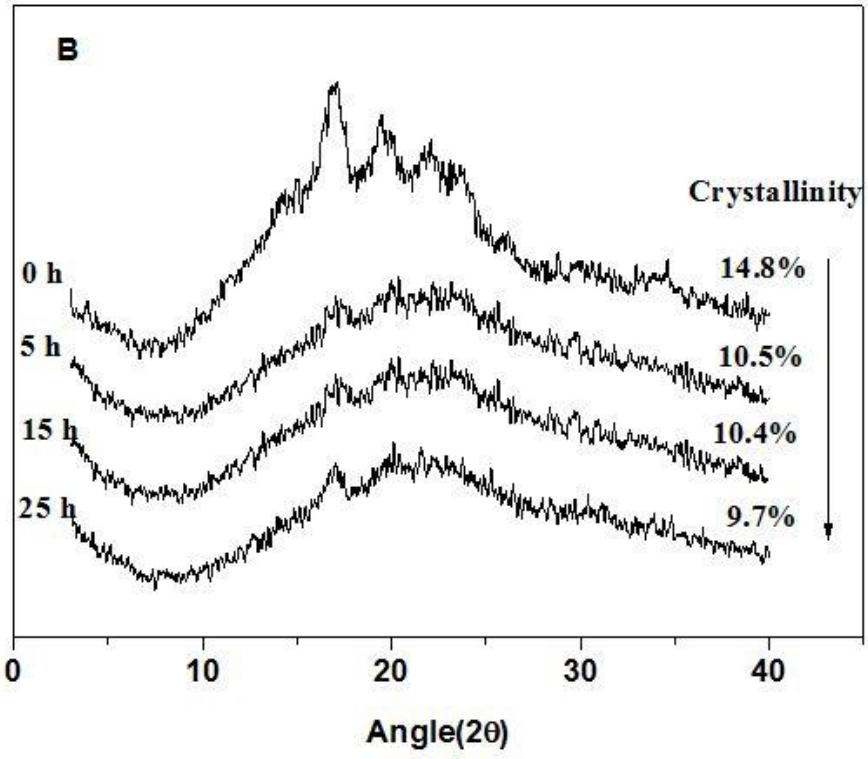

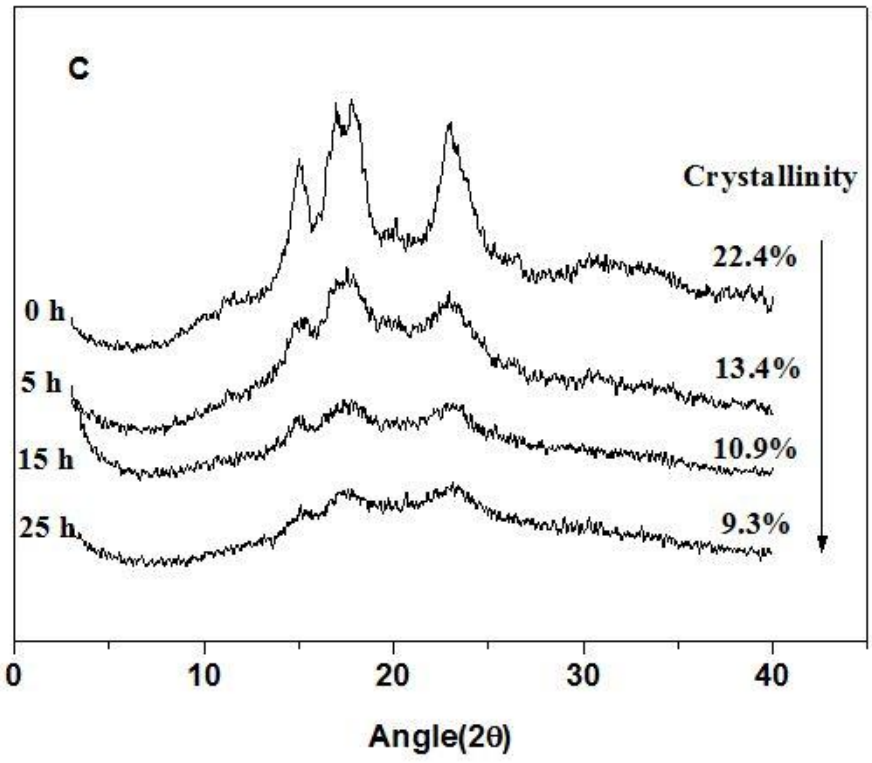

Figure 6. X-ray patterns of three native and milled starches with different milling times. (A) normal maize starch; (B) high-amylose starch and (C) waxy maize starch.

2.3.3. Thermal properties

The gelatinization parameters obtained from the DSC profile of native starch and milled starch are depicted in **Table 1**. Non-milled normal maize and waxy maize starch depicted an endothermic peak between 63~79℃ and 68~74℃, respectively. Native high-amylose maize starch exhibited an unsymmetrical melting endotherms at relatively high temperature ranging around 75~110℃. These endothermic peaks reflect the transformation of starch from polycrystalline granule states to noncrystalline gelatinized states during heating. Generally, the endothermic peak at the low-temperature is due to the melting of crystalline lamellae and the peak at the high-temperature is related to the melting of single helical crystallites, such as V-type, and the disaggregation of the amylose-lipid complexes (*121*). Since the amylose content in waxy maize starch is extremely low, almost no high-temperature transition was observed (*122*, *123*). The onset, peak, and conclusion temperatures (T_o, T_p, and T_c) of all milled starch were deceased continuously with the increase of milling time. There is a dramatic decrease in the endothermic enthalpy of gelatinization (ΔH) for three different milled maize starches after milling process. The observed reduction in ΔH with the increase of milling time is correlated to the decrease of crystallinity in the starch as supported by the X-ray results. The decrease of enthalpy in the milled starch indicated that the crystallinity and double helical order arrangements were damaged by the media milling treatment. The endothermic peak was completely disappeared when waxy maize, normal maize starches were milled for 15, 15, 25 h, and high-amylose maize starch milled for 25 h, which indicates that these milled starches have become a completely amorphous structure. It is noted that the decrease of ΔH in milled starches of 15 h milling time was the most prominent in waxy maize starch but the least in high-amylose maize starch, which

implies that the increase of amylose content in the starch particles would enhance the resistance of milled starch particles to media milling treatment. These results strongly suggest that the damage of starch particles during milling process is largely resulted from the disruption of double helices.

Table 1. Thermal properties of different milled starches at different milling times.

Milling time (h)	Thermal parameters			
	T_o (℃)	T_c (℃)	T_p (℃)	ΔH (J/g)
Normal maize				
0	63.5±0.7	79.5±0.6	70.5±0.9	9.8±0.8
5	60.8±0.9	76.2±0.4	67.6±0.6	5.1±0.5
15	-	-	-	-
25	-	-	-	-
High-amylose maize				
0	75.6±0.5	110.2±0.9	84.4±0.8	11.7±0.6
5	75.4±0.4	92.9±0.6	82.7±0.9	6.0±0.4
15	75.5±0.6	89.2±0.5	81.6±0.4	1.4±0.2
25	-	-	-	-
Waxy maize				
0	68.1±1.1	84.7±0.8	75.2±0.6	10.3±0.9
5	66.4±0.9	78.1±0.6	70.4±0.5	4.6±0.4
15	-	-	-	-

25	-	-	-	-

*T_o, T_p and T_c represent the onset, peak and conclusion temperature of starch gelatinization, respectively. ΔH refers to the enthalpy change of gelatinization.

2.3.4. Stabilization capacity of starches and storage stability of emulsions

The emulsions stabilized by three maize starch particles with different milling time (5, 10, 15, 20, 25 h) after the storage of 2 months are shown in **Figure 7**. The microscopic images of emulsions are depicted in **Figure 8** and the droplet sizes of the emulsions are presented in **Table 2**. The stabilization capacity parameters of these milled starch particles are listed in **Table 3**. Since starch granules are hydrophilic, the Pickering emulsions stabilized by starch particle are generally O/W emulsions (*26, 38, 124*). The concentration of normal maize, high-amylose maize and waxy maize starch in water phase was 7.14%, 6.97%, 7.36% (w/w), which was determined after the milling process. When the maximum surface coverage concept was applied, the required starch mass per volume of oil phase to produce starch particles stabilized Pickering emulsion at a given mean droplet size could be estimated by the following equation (*1*):

$$C_{s/o}=4\rho_s\varphi\frac{d_s}{d_{32d}} \quad (6)$$

where $C_{s/o}$ is the starch particle to oil phase ratio (mg/ml), ρ_s is the density of starch particle, φ is the packing density, d_s is the particle size of starch and d_{32d} is the surface mean diameter of the oil droplets to be stabilized. Based on this equation, the larger the starch particles, the higher the amount of starch particles required to cover an equal interfacial area. With the increase of milling time, the stabilization capacity of three milled maize starch particles enhanced gradually. The enhanced stabilization ability of the milled starch could be due to higher amount of starch particles are available to stabilize larger interfacial areas when starch particles go through the mechanical damage

effect of milling process. The amount of starch particles available in the emulsions also affects the packing pattern of particles at the interface. As shown in **Figure 8**, the droplet surface coverage increased with the increase of milling time. At short milling time of 5 h, the surface coverage of emulsion droplets was low and monolayer close-packed “clumps” of milled starch particles were observed on the interfacial surface (*125*). The droplet surface coverage increased with the increase of milling time and the milled starch particles exhibited monolayer dense packing. The dense packing of starch particles on the interface could enhance the stability of adjacent droplets against coalescence by forming a strong steric barrier (*38*). Since longer milling time resulted in higher concentration of milled starch particles to stabilize larger total interfacial area, smaller average emulsion droplets might form. Remarkable decrease in the average droplet size of the emulsions was observed when the milling time was prolonged from 5 h to 10 h. Further increase of milling time led to a gradual reduction in the average droplet size. It is notably that although the average droplet size of the Pickering emulsions stabilized by milled starch particles is ranged from several hundred micrometers to one hundred micrometer, which is much larger than that of conventional emulsions, all the emulsions exhibited benign stability against coalescence over the storage. The excellent stability of starch-stabilized Pickering emulsions with large average droplet size has also been demonstrated in previous researches (*26, 126, 127*).

Three maize starches with different amylose/amylopectin ratios exhibited different stabilization properties. The free energy of detachment of a particle adsorbed at the oil-water interface could reflect how strongly the particles are adsorbed at the oil-water interface. When the gravitational effect is neglected, the detachment energy could be

estimated from the following equation $E = \pi r^2 \gamma_{ow}(1-|cos\theta|)^2$ (*1*). Since the detachment energy is positively related to the radius of particles, emulsions stabilized by larger particles would exhibit higher long-term stability. According to **Figure 5**, milled waxy maize starch particles have the smallest particle size than normal and high-amylose maize starch particles at the same milling time. The desorption energy of milled waxy maize starch is relatively smaller than the other two milled starches, which might indicate that the emulsions stabilized by milled waxy maize starch is less stable against coalescences. Among the three starches, high-amylose starch exhibited the best stabilization capacity follow by normal maize starch. Significant creaming was observed for emulsions stabilized by waxy maize particles of different milling time. The creaming effect no longer existed in emulsions stabilized by high-amylose maize starch and normal maize starch with milling time longer than 15 and 20 h, respectively. The disappearance of creaming effect could be due to the formation of network of particle-bridged between droplets by the aggregation of particles (*26, 124*). It is noticeable that emulsions stabilized by milled high-amylose starch particles exhibit a gel-like structure, which might be due to the formation of three-dimensional network between droplets through amylose molecules. The three-dimensional network formed by amylose in the starch particles could further inhibit the creaming effect in the emulsions.

Table 2. Droplet sizes (μm) of emulsions stabilized by three different milled starch particles at different milling times.

Milling time (h)	Starch type		
	Normal maize	High-amylose maize	Waxy maize
5	468.3 ± 91.4	279.4 ± 47.7	191.4 ± 55.1
10	189.1 ± 73.7	142.9 ± 54.9	125.0 ± 31.5
15	154.2 ± 62.1	135.7 ± 50.6	115.2 ± 43.8
20	117.1± 52.4	123.9 ± 64.9	103.7 ± 26.1
25	102.9 ± 41.7	117.5 ± 52.4	91.3 ± 24.0

Table 3. Stabilization capacity of three different milled starch particles at different milling times (after 7-day storage).

Milling time (h)	Normal maize		High-amylose maize		Waxy maize	
	EI	RS (mm^3/mg)	EI	RS (mm^3/mg)	EI	RS (mm^3/mg)
5	0.87	0.54	0.91	0.32	0.54	0.58
10	0.93	0.38	0.98	0.13	0.63	0.47
15	0.97	0.21	1.00	0	0.69	0.39
20	1.00	0	1.00	0	0.76	0.34
25	1.00	0	1.00	0	0.79	0.28

EI, stabilization index.

RS, remaining starch.

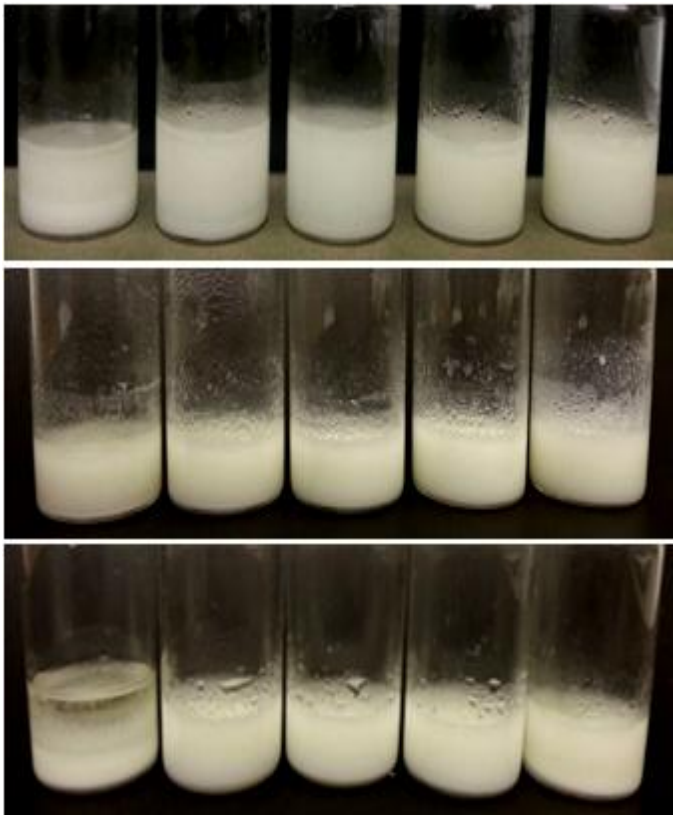

Figure 7. Vessels containing Pickering emulsions stabilized by three different milled starches after 2-month storage at different milling times. From left to right: 5 h, 10 h, 15 h, 20 h, and 25 h (milling time). From up to down: normal maize starch, high-amylose maize starch, waxy maize starch.

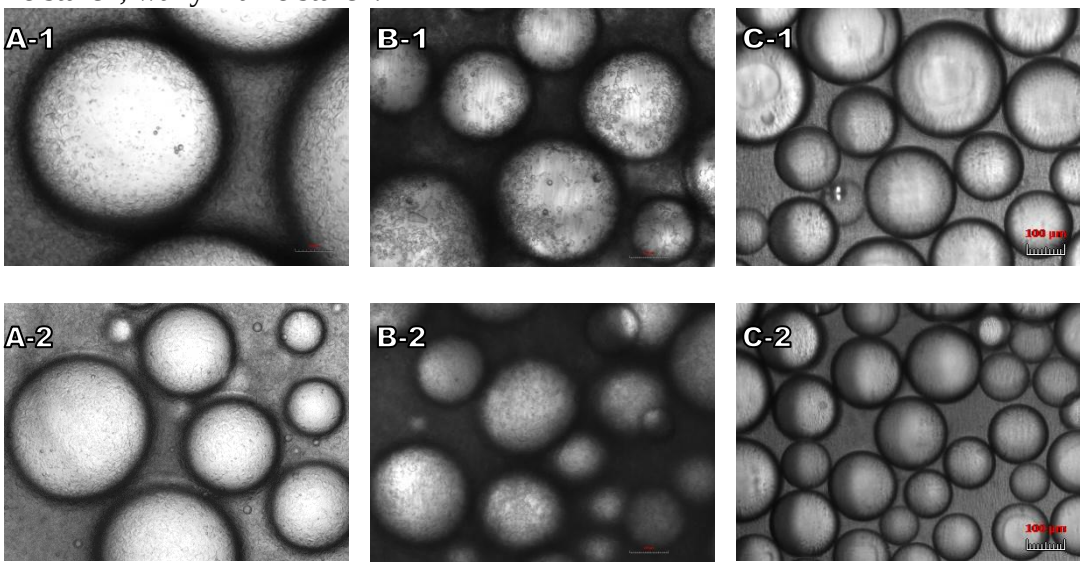

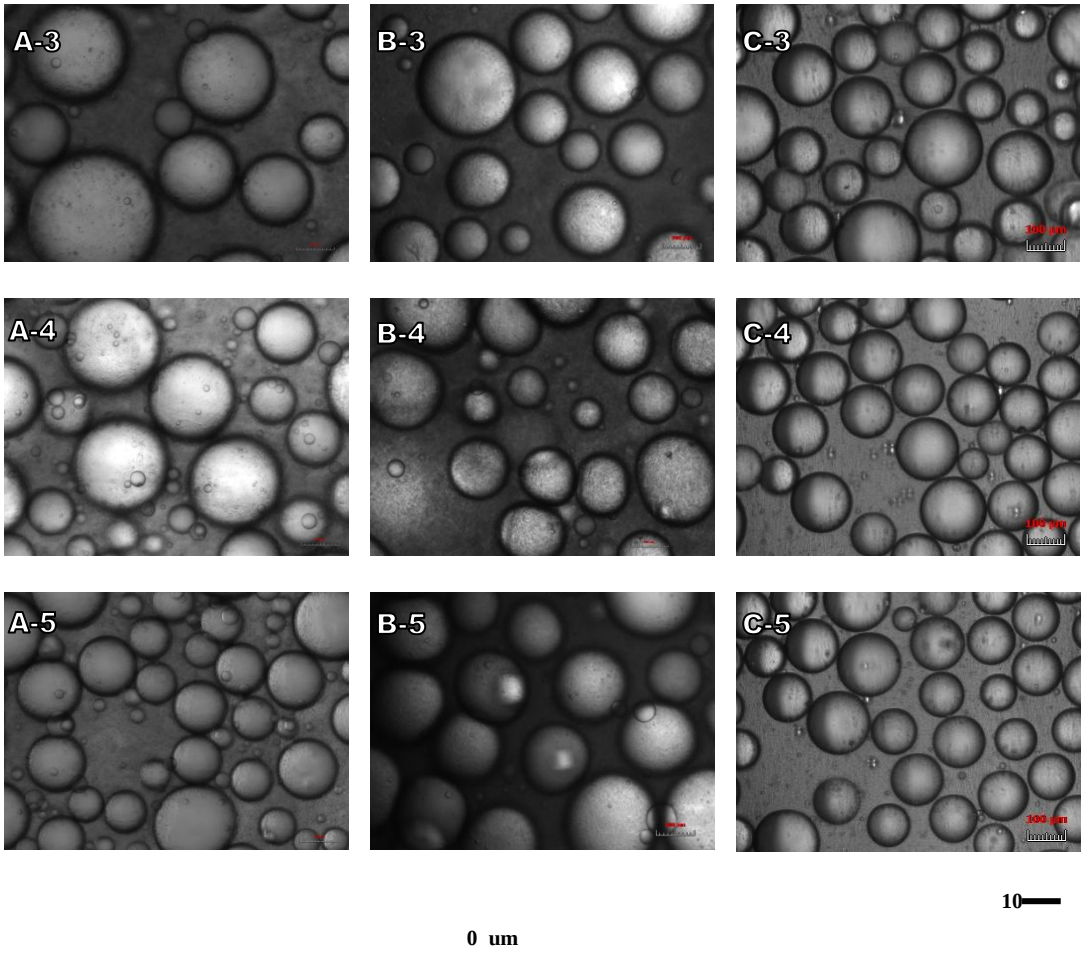

Figure 8. Microscopic images of emulsions stabilized by three different milled starches at different milling times. (A) normal maize starch 7.14% (w/w); (B) high-amylose maize starch 6.97% (w/w); and (C) waxy maize starch 7.36% (w/w). From up to down: 5 h, 10 h, 15 h, 20 h, and 25 h (milling time).

2.3.5. Rheological properties of emulsions

The rheological properties of Pickering emulsion stabilized by milled normal maize, high-amylose maize and waxy maize starch particles were further investigated. The linear viscoelastic region of the emulsions was identified through dynamic strain sweep tests and the results are presented in **Table 4**. Pickering emulsion stabilized by milled high-amylsoe starch particles has the largest linear viscoelastic region (0.1~9%), followed by emulsions stabilized milled normal maize starch (0.1~2%). The extremely short linear viscoelastic region (0.1~0.2%) was observed in milled waxy maize starch particles stabilized emulsions. The frequency dependence of the storage and loss moduli (G', G") of emulsions was analyzed by dynamic frequency tests and the data were presented in **Figure 9**. The storage modulus of Pickering emulsion stabilized by milled high-amylose maize starch was always higher than its loss modulus at all frequencies and was almost independent on frequency. The storage modulus of milled normal maize starch stabilized emulsion is also higher than its loss modulus. However, the storage modulus of milled normal maize starch stabilized emulsion shows no dependence on frequency, while its loss modulus shows slight dependence on frequency. The higher value of G' than G" implies that these emulsions possess typical characteristics of a weak gel system (*128*). The storage modulus of emulsion stabilized by milled waxy maize starch has been surpassed by its loss modulus with the increase of sweep frequency, which indicates that the weakening of the interactions between droplets in the emulsion. It should be noted that emulsions stabilized by milled maize starch with different amylose/amylopectin ratios also exhibit major difference in the range of G', G" values. Milled high-amylose maize starch stabilized emulsion has the highest G', G" values, followed by milled normal maize starch stabilized emulsion. Since the stability of an

emulsion system is positively related to its elastic modulus (G'≫G") (*129, 130*), emulsions stabilized by milled high-amylose starch possess the highest stability compared with other two emulsion system. The benign emulsion capacity of milled high-amylose maize starch particles could be attributed to its high amylose content. During the milling process, native starch granules would swell and undertake severely damage, which would lead to the leach out of amylose from the starch granules. The leached-out amylose could enhance the stability of emulsions through forming a three-dimensional network in the system (**Figure 10**) (*131*). While the entanglements and interconnection between droplets stabilized by milled waxy maize starch particles was weak as there was almost no amylose existed in the system. The three-dimensional networks formed by amylose were relative weak, which endured a progressive breakdown into smaller clusters when strong mechanical deformation was applied.

Table 4. Linear viscoelastic region of Pickering emulsions stabilized by three different milled starch particles.

Starch type	Strain range (w/w)
Normal maize	0.1-2%
High-amylose maize	0.1-9%
Waxy maize	0.1-0.2%

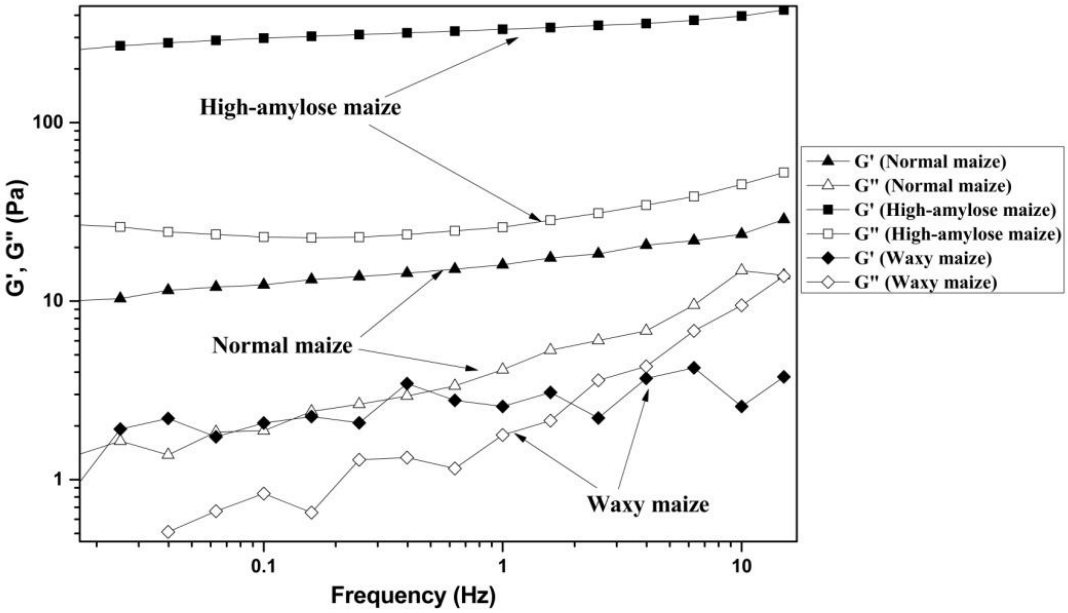

Figure 9. Frequency sweep curves for emulsions stabilized by three different milled starches at different milling times.

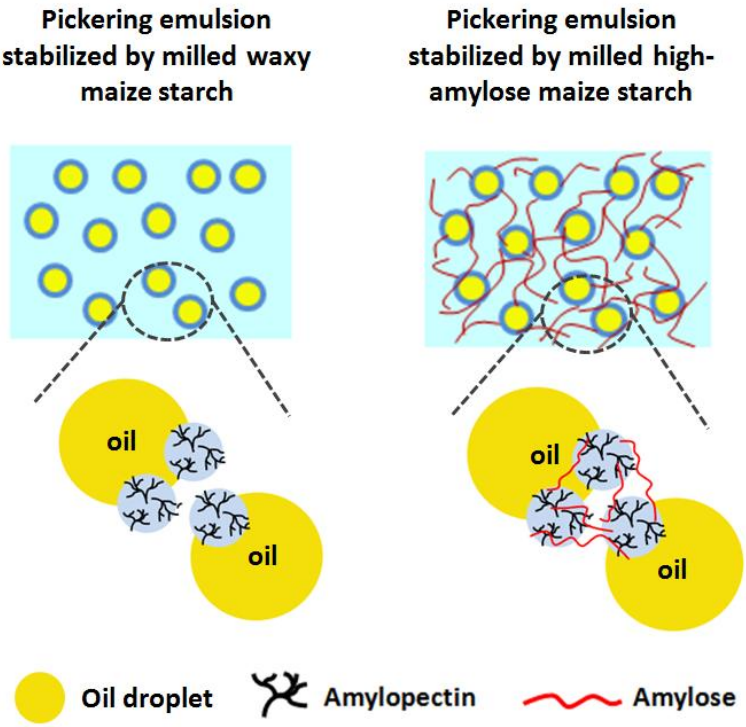

Figure 10. Schematic representation of Pickering emulsions stabilized by different milled starches under diluted (top) and concentrated (bottom) conditions. The amylose molecules are shown to promote networking systems.

2.4. Conclusions

In summary, media milling treatment could lead to the decrease of particle size, crystallinity, gelatinization temperature and enthalpy in the milled starch. Through milling process, the stabilization ability of maize starch with different amylose/amylopectin ratios to stabilize Pickering emulsions could be improved by breaking native starch granules into smaller particles. The required mass of milled starch to cover an equal interfacial area is much lower than that of native starch. As the result, the lowest critical starch particle concentration capable of stabilizing a Pickering emulsion was decreased. The high amylose content in the original starch has the most impact on the stabilization properties of the milled starch. Milled high-amylose maize starch particles exhibited the best stabilization ability, followed by milled normal maize starch particles. The stabilization ability of milled waxy maize starch particles was the lowest. The milling time also had some influence on stabilization behavior of the milled starch. With the increase of milling time, the obtained milled starch possessed the better stabilization capacity. Although, the droplet size of the milled starch stabilized Pickering emulsions are relatively large (in the ranging of hundred micrometers), the emulsions exhibited benign stability during long-term storage.

CHAPTER 3 ASSESSMENT OF BIOACCESSIBILITY OF CURCUMIN ENCAPSULATED IN MILLED STARCH STABILIZED PIKCERING EMULSIONS USING THREE IN VITRO DIGESTION MODELS

3.1. Introduction

Although the biological benefits of various natural nutritional substances have been identified, the dose efficacy of these lipophilic bioactive compounds are often insufficient after oral administration due to their poor water solubility, limited stability against degradation and low bioavailability (*132-136*). In order to improve their health benefits, emulsion-based delivery systems have been widely used in food and pharmaceutical industries as inherent vehicles for the oral delivery of lipophilic functional compounds (*134, 135*). Through dissolving lipophilic components in the oil phase, and then homogenizing the oil phase with the aqueous phase, emulsions could be formed under the function of emulsifiers. Extensive studies have been carried out to understanding the encapsulation and delivery properties of various conventional emulsions stabilized by small molecular weight surfactants or biopolymers (*137, 138*). Recently, the use of solid colloid particles to form emulsions, known as Pickering emulsions, has obtained rising attention due to their unique physical properties, including benign stability against coalescence and Ostwald (*4, 105*). With the development of solid particles from various natural biomass-based resources, including cellulose, starch, chitin, protein and lipid (*18, 19, 24, 40, 139*), Pickering emulsions stabilized by these particles exhibit high potential as edible delivery vehicle for encapsulating, protecting and releasing of various bioactive

lipophilic regents in application of food and pharmaceutical industries. Beside from superior stability, Pickering emulsion delivery systems possess the advantage of reducing tissue irritation, intestinal inflammation and metabolic syndrome that linked to some surfactants used in conventional emulsions (*9, 140*).

Since lipids digestion, encapsulated lipophilic components release and uptake in the GI tract is a complex process, some analytical tools have been developed to screen the efficacy of the various emulsion-based delivery systems. The use of *in vivo* method, which involving animal or human subjects, is usually expensive, time-consuming, relating to some ethical and practical issues. Consequently, *in vitro* digestion models have gained much attention in order to understand the basic physicochemical processes during lipid digestion and their impact on the release and uptake of encapsulated lipophilic compounds (*141*). Dialysis approach is one of the widely used methods to measure the release of hydrophobic compounds from emulsions and other encapsulation systems (*142, 143*). And this method has been used to simulate the digestion of silica-stabilized Pickering emulsions (*144*). The pH-stat lipolysis model has been extensively used for quantifying the lipid digestion process and the release of lipophilic substances under simulated small intestinal condition within pharmaceutical and food research (*137, 145, 146*). The pH-stat lipolysis model is based on the measurements of free fatty acids (FFAs) released during lipids digestion by lipase around neutral pH values. The tested sample is mixed with simulated small intestinal fluid, which contains appropriate levels of major compounds related to lipid digestion, including bile salts, lipase, colipase, phospholipids, and mineral ions. The mixture is then placed within a temperature-controlled chamber, where lipid molecules, mainly triglycerides, are hydrolyzed by lipase resulting in the

production of one monoacylglycerol and two FFAs per TAG molecule. To neutralize the FFA generated during lipid digestion and maintain the initial preset digestion pH value, alkali (NaOH) then is titrated into the digestion cell, and its concentration is recorded versus time. The amount of lipophilic bioactive component released into the mixed micelle phase after lipolysis process which is the fraction available for absorption can be taken as a marker of its bioaccessibility. As a relatively simple technique, pH-stat lipolysis model is able to comparing different lipid formulations under similar digestion conditions and rapidly screens the physicochemical factors that affect lipid digestion.

TIM-1 is a dynamic multicompartmental gastrointestinal digestive system, which simulates the *in vivo* dynamic physiological processes that occur within stomach, duodenum, jejunum, and ileum part of human (*147, 148*). The four successive compartments of TIM-1 system reproduce the following conditions: (i) secretions of enzymes and relevant cofactors such as bile salts and coenzymes, (ii) change of pH in gastric compartment and from the duodenum to ileum, (iii) peristaltic movements and proper blending during digestion, (iv) control of physiological transit time during each stage of digestion, and (v) passive absorption of released small molecules and water. Validation experiments demonstrate that TIM-1 simulates digestion conditions with reliable reproduction and possesses good consistency with *in vivo* experiments (*149, 150*). Compared to *in vivo* studies, TIM-1 system have some advantages, such as easy manipulation, relatively higher repeatability due to the elimination of biological variation, the feasibility to collect samples during any stage of digestion, and free from ethical restrictions (*147*). TIM-1 system has been used to evaluate the release of bioactive compounds from various delivery systems during digestion (*151, 152*).

This work is dedicated to investigate the potential of milled starch stabilized Pickering emulsion as oral delivery vehicles for nutraceticals. For this purpose, the responsiveness of emulsion loaded with curcumin, a model lipophilic compound, to the simulated digestion environment was investigated using the three *in vitro* digestion models, simulated static small intestinal digestion model, pH-stat lipolysis model and TIM-1 model.

3.2 Materials and methods

3.2.1 Materials

Normal maize starch and 3-(4,5-dimethylthiazol-z-yl)-2,5-diphenyl tetrazolium bromide (MTT) were purchased from Sigma-Aldrich (St. Louis, MO). The corn oil was purchased from a local supermarket. Curcumin was a gift from Sabinsa Corporation (Piscataway, NJ), which contains 85% curcumin, 11% demethoxycurcumin and 4% bisdemethoxycurcumin (*153*). Pepsin from porcine mucosa, lipase type II from porcine pancreas, bile salt, sodium chloride, calcium chloride, and potassium dihydrogen phosphate were purchased from Sigma-Aldrich (St. Louis, MO). Pancrex V powder (lipase activity = 25000 units/g, protease activity =1400 units/g, and amylase activity = 30000 units/g) was purchased from Paines & Byrne. Fresh pig bile was purchased from Farm to Pharm (NJ). Rhizopus lipase (150000 units/mg F-AP-15) was obtained from Amano Enzyme Inc. (Nagoya, Japan). Trypsin from bovine pancreas (7500 N-α-benzoyl-Larginine ethyl ester (BAEE) units/mg, T9201) was purchased from Sigma-Aldrich (St. Louis, MO). Dialysis cassettes (molecular weight cut off 3500 Da) were purchased from VWR International, LLC. Lipase type II from porcine pancreas, potassium dihydrogen phosphate, calcium chloride, sodium chloride, and bile salt were purchased from Sigma-Aldrich (St. Louis, MO). Fetal bovine serum (FBS) was

purchased from Atlanta Biologicals (Lawrenceville, GA). Dulbecco's modified Eagle's medium (DMEM), phosphate-buffered saline 1x (PBS, pH 7.2) and non-essential amino acids 100× were purchased from Gibco Life Technologies (Grand Island, NY, USA). 100× penicillin and streptomycin, 0.25% trypsin with ethylenediaminetetraacetic acid (EDTA) were purchased from Fisher Scientific (Pittsburgh, PA).

Cell culture. Caco-2 cell line was provided by Dr. Judith Storch from Department of Nutrition at Rutgers University. Caco-2 were cultured in DMEM containing 0.1% non-essential amino acids, 10% fetal bovine serum, 100 μg/ml streptomycin and 100 units/ml penicillin. Cells were cultured in incubators at 37 ℃ under 5% CO_2 and 95% relative humidity.

3.2.2. Media-milling treatment

A MiniSeries media mill machine (Netzsch LLC, PA, USA) equipped with a water cooling machine was used to modify the maize starch. The starch sample was suspended in deionized water at a ratio of 7% (w/w). Then the starch suspension was poured into the milling machine and ground at a mill power of 0.13 kw, pump speed of 100 rpm and mill speed of 3000 rpm. After a milling process of 25 h, the milled starch suspension was used to prepare Pickering emulsion. And a moisture test was conducted to calculate the accurate weight of milled starch in the final suspension.

3.2.3. Preparation of blank and curcumin-loaded emulsions

Curcumin was dissolved in corn oil at concentration of 15 mg/ml under heating for 30 min to reach a transparent solution. The oil phase containing curcumin was throughly mixed with fresh milled starch suspension at a ratio of 1:1.5 (v/v) using an IKA Ultra-Turrax T25 homogenizer under 13,000 rpm for 3 min. The emulsion was set at room temperature. Blank emulsion was prepared using the same method except that no

curcumin was added into the oil phase. Each emulsion was prepared in triple.

3.2.4. Optical characterization of curcumin-loaded Pickering emulsions

After stored at room temperature for 24 h, the microstructure of emulsion samples were characterized by an Nikon Eclipse TE2000-U (Japan) microscope equipped using a 1392×1040 resolution CCD camera (Retiga EXi, QImaging). The emulsion was added on a glass microscopic plate without cover glass for microscopic observation. Fluorescence images of emulsions were captured under fluorescence mode using blue filter.

3.2.5. Simulated gastric digestion

Digestion of curcumin encapsulated Pickering emulsions under simulated gastric conditions was conducted based on a previous method (*154*). Simulated gastric fluid (SGF) was prepared by dissolving 5 g sodium chloride and 5 ml HCl into 1 L of deionised water and adjusting its pH to 1.2 by adding 1 mol/L HCl/ NaOH. Then the pH of the emulsion was also adjusted to 1.2 using 1 mol/L HCl/NaOH. Dissolving 0.018 g of NaCl and 0.032 g of pepsin into 1 ml SGF, then mixed with 9 ml Pickering emulsion sample (pH 1.2). Add this mixture in a dialysis cassette, and put the dialysis cassette in 1 L of SGF incubated at 37℃. Emulsion sample (200 μL) was pipetted out every 30 min during the total digestion process of 2 h. The curcumin concentration of the sample was measured using the method described earlier. And the structure of Pickering emulsions during the digestion was captured using the microscope.

3.2.6. Simulated static small intestinal digestion model

0.05 mol/L potassium dihydrogen phosphate solution with pH 7.5 was used as simulated intestinal fluid (*155, 156*). Adjusting the pH of Pickering emulsion (30 ml) to 7.5 with 1 mol/L NaOH, then mixed with simulated intestinal fluid (30 ml) containing 1.5 g of bile salts, 0.2 g calcium chloride and 0.6 g lipase. The mixture was incubated at 37 ℃

and 10 ml of samples were taken out at 0.5, 1, 2 and 3 h, respectively. The structure of the Pickering emulsion after digested for 3 h was analyzed using fluorescence microscope. The samples were centrifuged at 30,000 rpm for 30 min to separate the digestion mixture. The micelle phase (from the middle) was collected using a syringe and the structure was analyzed using fluorescence microscope. The absorbance of micelle phase was measured at 425 nm after diluted with water by 100 times. Pickering emulsion that did not contain curcumin was digested following the same procedure to use as a control sample to correct the absolute absorbance value of encapsulated sample. To compare the release efficiency of Pickering emulsion and pure oil during digestion, a mixture of pure oil (12 ml, containing same amount of curcumin with the emulsion) and water (18 ml) was also digested and the released curcumin concentration was measured using the same procedure. The bioaccessibility (%) of curcumin was calculated using following equation (8).

3.2.7. pH-stat lipolysis model

The pH-stat lipolysis model used was based on a method described previously (*157*). 1 g pancreatin was added into 5ml fed-state buffer (Tris maleate 50 mM, NaCl 150 mM, $CaCl_2$ 5 mM, NaTDC 20 mM, Phosphatidylcholine 5 mM) and stirred for 15 min. The suspension was centrifuged at 2,000 rpm for 15 min and the supernatant were pipetted out and kept on ice. Pickering emulsions containing 250 mg oil phase, with 9 ml fed-state buffer were placed in a clean beaker, in an oil bath at 37℃ for 10 min under stirring. The resultant mixture was adjusted to pH 7.5 with 0.25 M NaOH solution. Finally, 1 ml ice-chilled pancreatin was added in to initiate the digestion. The pH of digestion solution is maintained at 7.5 ± 0.1 by adding 0.25 M NaOH. Digestion process was performed for 2 h. The volume of NaOH solution added during the digestion process was recorded

throughout the lipolysis experiments, which was assumed to equal to the amount of free fatty acids (FFAs) generated by lipolysis of triacylglycerols. Digestion of blank sample (250 mg water phase) was also conducted using the same procedure.

The amount of FFAs released from the system was calculated using the following equation:

$$\% \text{ FFAs released} = \frac{(V_{\mathrm{NaOH}} - V_{\mathrm{blank}}) C_{\mathrm{NaOH}} M_{\mathrm{w,lipid}}}{2\, m_{\mathrm{lipid}}} \times 100 \qquad (7)$$

where ml_{ipid} is the total mass of lipid existed in the sample (g), $M_{\mathrm{w,lipid}}$ is the average molecular weight of the lipid (g/mol), C_{NaOH} is the concentration of NaOH added during titration process (mol/L), V_{NaOH} is the volume of NaOH added into the reaction vessel to neutralize the released FFAs, and V_{blank} is the volume of NaOH added into the reaction vessel during digestion of blank sample. This equation was based on the assumption that all the triacylglycerols are converted to two free fatty acids during titration.

To determine the bioaccessibility of curcumin, the digestion media were ultracentrifuged for 40 min at 4°C, 40,000 rpm immediately after the complete of digestion, which were separated into an opaque sediment phase, an aqueous phase containing formulated curcumin micelles in the middle, and sometimes an oily phase at the top. The micelle phase was collected using a syringe and the volume was calculated. The concentration of curcumin in the micelles was analyzed using HPLC. The bioaccessibility (%) of curcumin was calculated using following equation:

$$\text{Bioaccessibility (\%)} = \frac{\text{amount of solubilized curcumin in micelle}}{\text{amount of curcumin in the formulations}} \times 100\% \qquad (8)$$

3.2.8. Gastrointestinal (TIM-1) model

The dynamic in vitro gastrointestinal model TIM-1 (TNO, Zeist, The Netherlands), whose schematic diagram was depicted in **Figure 11**, consists of four compartments

which simulate the stomach, duodenum, jejunum, and ileum. This model mimics the transit through the gastrointestinal tract, the gastric and intestinal pH profiles, and the secretion of digestive juice over time to study the preabsorption events after ingestion. The formulations "meals" were tested in a simulated fed-state digestion program of the TIM-1 model for 6 h. The half-life of gastric emptying was 70 min. Lipase and pepsin was used for the gastric phase (reducing the pH from 5.5 to 1.5 with a half time of 40 min). The pancreatin and bile extract were used in the three phases of intestinal digestion: duodenum (pH 6.4), jejunum (pH 6.9) and ileum (pH 7.2). The adjustment of pH conditions, secretion of digestive juices, the digestion temperature (37 °C) were controlled by computer program according to the published method (*158*). The "meal" (300 g) was the mixture of 20 g sample (curcumin encapsulated Pickering emulsion or oil and water dispersion with same curcumin content), 95 g gastric electrolyte solution, 0.011 g amylase, 5 g gastric enzyme solution and 180 g water. Each compartment was first filled with defined start residues that resemble the actual physiological gastrointestinal conditions. All system parameters used were summarized in **Table 5**.

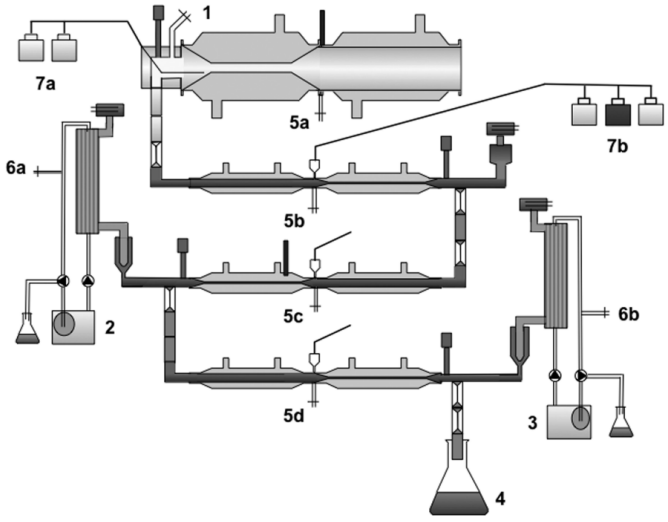

Figure 11. Schematic diagram of the in vitro gastrointestinal model, TIM-1: (1) food inlet,

(2) jejunum filtrate, (3) ileum filtrate, (4) ileal colorectal valve, (5a) gastric compartment, (5b) duodenal compartment, (5c) jejunum compartment, (5d) ileal compartment, (6a) hollow fiber membrane from jejunum, (6b) hollow fiber membrane from ileum, (7a and 7b) secretion pumps.

Table 5. Parameters of gastrointestinal digestion in the TIM when simulating digestive conditions of a healthy adult after intake of a solid meal

	Gastric compartment	Duodenal compartment	Jejunal compartment	Ileal compartment
Start residue	5 g Gastric enzyme solution	60 g Small intestinal electrolyte Solution (SIES) : 15 g Pancreatin solution: 15 g Bile: 30 g Trypsin solution (2 mg/cup): 1 cup	160 g SIES: 40 g Pancreatin solution: 40 g Bile: 80 g	160 g SIES
pH/time (min)	6/0, 5.7/15, 4.5/45, 2.9/90, 2.3/ 120, 1.8/ 240, 1.6/ 300	maintained at 6.4	maintained at 6.9	maintained at 7.2
secretion	0.25 ml/min pepsin 0.25 ml/min lipase 0.25 ml/min of HCl 1.5 M if necessary	0.5 ml/min bile salts (4% during the first 30 min of digestion then 2%) 0.25 ml/min pancreatic solution 0.25 ml/min SIES 0.25 ml/min $NaHCO_3$ 1 M if necessary	10 ml/min jejunal fluid solution 0.25 ml/min $NaHCO_3$ 1 M if necessary	10 ml/min ileal fluid solution 0.25 ml/min $NaHCO_3$ 1 M if necessary

To study the bioaccessibility of curcumin in encapsulated in the milled starch stabilized Pickering emulsion and in pure oil phase during the digestion, the samples were introduced into the stomach compartment. To monitor the typical physiological processes of GI tract, aliquots (1 ml) was taken from each digestion compartment at suitable time points. Gastric compartment liquid was collected at 15, 30, 45, and 60 min, whereas the duodenal compartment was collected at 30, 60, 90, 120 and 180 min. The jejunum and ileum compartment contents were collected at 30, 60, 90, 120, 180, 240, 300, and 360 min. During the digestion, the curcumin released in the jejunum and ileum compartment passed the semipermeable hollow capillary membranes with a pore size of

0.05 μm (Spectrum Milikros modules M80S-300-01P) through passive diffusion and entered the jejunum and ileum dialysis fluids. The amount of curcumin available for absorption was calculated based on its concentration in the dialysis fluids. Dialysis fluids of jejunum and ileum were collected at 30, 60, 90, 120, 180, 240, 300, and 360 min. The total bioaccessibility of curcumin was calculated as the accumulated amounts of curcumin in jejunal plus ileal dialysis tube. The efflux was sampled from outlet of the ileal compartment at 90, 120, 180, 240, 300, and 360 min. The total fluid volume from these three compartments was careful measured for each sample volume. All samples were ice-chilled until subsequent HPLC analysis. Duplicate experiments were conducted. The curcumin availability for absorption was measured as accumulated amounts of curcumin in jejunum or ileum compartment. Total curcumin availability for absorption was measured by combining accumulated amounts of curcumin in the jejunum compartment, ileum compartment and in fluids collected after the ileal colorectal valve.

To determine the curcumin content of samples come from the dialysis fluids and efflux, 5 ml of sample was inoculated with an internal standard (β-estradiol, 100 μg/ml) that was then extracted by mixing with 1 ml of ethyl acetate and centrifuged at 10,000 rpm for 10 min at ambient temperature. The internal standard was chose based on a previous research and its structure was presented in **Figure 12** (*159*). After being centrifuged, the supernatant was obtained and dried under nitrogen flow, then dissolved by 500 μl methanol for HPLC analysis. For samples from the gastric, duodenal, jejunum and ileum compartment, 1ml of sample was inoculated with an internal standard and extracted by mixing with 0.5 ml ethyl acetate and centrifuged at 10,000 rpm for 10 min. After being centrifuged, the supernatant was obtained and dried under nitrogen flow, then

dissolved by methanol (100 µl ~ 5 ml) for HPLC analysis.

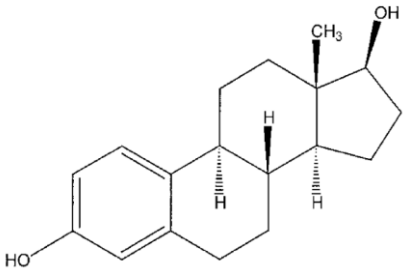

Figure 12. Chemical structure of the internal standard, β-estradiol.

3.2.9. High-performance liquid chromatography (HPLC) analysis of curcumin

The concentration of curcumin was analyzed by using an UltiMate 3000 HPLC system equipped with a 25D UV-VIS absorption detector (Dionex) and a Nova-Pak C18 3.9×150mm column (Waters). Fifty microliters of samples were injected in the system. The detection wavelength was set at 420 nm. The mobile phases used were: (A) water with 2% acetic acid, and (B) acetonitrile. The flow rate was 1 ml/min. The following elution condition was used: 0 to 2 min, held at 65% A /35% B; linear gradient from 65% A /35% B to 45% A /55% B at 17 min; followed by a flat profile for the next 5 min and then a linear change back to 65% A /35% B at 22 to 23 min. The standard curve of the absorption peak area versus curcumin concentration was plotted and fitted with a linear function. Besides using a visible wavelength of 430 nm to detect curcumin, an ultraviolet wavelength of 280 nm was used to detect the internal standard β-estradiol when necessary.

3.2.10. *In vitro* anti-cancer activity assay

Anti-cancer activity of digested curcumin-loaded Pickering emulsion was determined using the MTT assay. Caco-2 cells were cultured at a density of 10,000 cells per well in 96 well cell culture plates containing 100 µl of media. After incubated for 24 h, the cells

were treated with DMSO-dissolved curcumin, micellelar phase of digested curcumin-encapsulated emulsion sample or micellelar phase of digested emulsion sample without curcumin from D.3.1.7, respectively. Cells without any treatment were set as control. After 24 h treatment, cell culture media were aspirated and cells were incubated with 100 μl MTT solution (0.5 mg/ml in DMEM) for 2 h at 37 ℃. Then MTT solution was aspirated and the formazan crystals formed in cells were dissolved with DMSO (100 μl per well). Light absorbance at 560 nm was recorded with Absorbance Microplate Reader (Molecular Devices, Sunnyvale, CA). Relative cell viability was calculated as percentage of A560 compared with that of the untreated wells. Data were presented as mean ± standard deviation with three-well repeats. Cell viability was expressed as:

$$\textit{Viability (\%)} = N_t / N_c \times 100 \quad (9)$$

N_t is the light absorbance of cells treated with sample and N_c is the absorbance of the untreated cells.

3.2.11. Cellular uptake assay

The cellular uptake of curcumin in digested Pickering emulsions was investigated by fluorescence microscopy. Caco-2 cells were seeded at a density of 1×10^5 cells per well in 12-well Tissue Culture Plates and incubated at 37 ℃ for 12 h in a cell culture incubator (NAPCO 5400, Fisher Scientific, PA) under 5% CO_2 and 95% humidity. The cells were incubated with curcumin contained micelle phase from D.3.1.7 at a constant concentration (10 μM) and native curcumin at the same concentration (first dissolved in DMSO and then diluted 1000 times with DI water). After incubated for certain time (0, 30, 60, 90, 120 and 180 min), the tissue culture plates were taken out from the incubator. The cells were washed with 0.5 ml PBS (0.01 M, pH 7.4) to remove the micelle phase and native curcumin solution. After adding 0.5 ml fresh Dulbecco's phosphate buffered

saline into the plates, the images of cells were captured at 100× under both bright field and fluorescence with blue filter using a Nikon Eclipse TE2000-U.

3.2.12. Statistical analysis

Experiments were conducted at least in triplicate. Results were in table expressed as mean ± standard deviation. Error bars on figures represented standard deviations.

3.3. Results and Discussion

3.3.1 Characterization of Pickering emulsion

The bulk appearance of curcumin encapsulated Pickering emulsion stabilized by milled starch is depicted in **Figure 13 (A)**. And the microscopic and fluorescence images of the emulsions are presented in **Figure 13 (B)** and **(C)**. Based on the moisture test after the milling process, the obtained concentration of milled starch in the aqueous phase was 7.3% (w/w). Since starch is typically hydrophilic, the Pickering emulsion stabilized by milled starch is oil-in-water emulsion. Due to the relatively large size of the starch particles, the drop size of the emulsions was over several micrometers, which is much higher than conventional emulsion system. There were no crystals of curcumin detected in the emulsion as supported by the microscopic and fluorescence images, which suggested that the curcumin was still dissolved after encapsulated in the Pickering emulsions. The emulsion was very stable with no creaming, phase separation or precipitation of curcumin happened during the storage of emulsion for two months.

Ⓐ

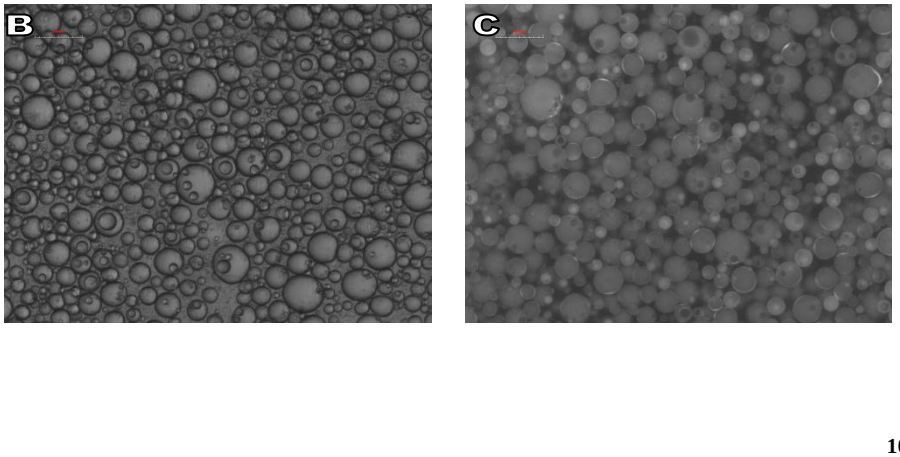

Figure 13. (A) Photograph of curcumin encapsulated emulsion stabilized by milled starches after two months' storage; (B) Microscopic and (C) Fluorescence images of curcumin encapsulated emulsions stabilized by milled starches.

3.3.2. *In vitro* gastric digestion of curcumin-encapsulated Pickering emulsions

Due to the acidic pH condition and digestion enzymes, gastric cavity is where the severe breakdown of various food materials. To protect the encapsulated bioactive lipophilic compounds against the harsh gastric environment, good stability of emulsion in gastric environment is of great importance for an encapsulation system (*160, 161*). A simulated gastric environment was used to investigate the stability of emulsion and release of encapsulated curcumin as a function of time. The release kinetic of curcumin from Pickering emulsion was presented in **Figure 14** and the structure of emulsion after simulated gastric digestion for 0.5 and 2 h are presented in **Figure 15**. During the gastric digestion of 2 h, a significant release of encapsulated curcumin of around 20% curcumin from the emulsion system was observed at the first 30 min. In the next 90 min, only a slightly 3% of curcumin was further released, which suggested that this Pickering emulsion system possessed good stability against the gastric digestion conditions. This result could be further testified by the microscopic and fluorescence images of Pickering emulsions during the gastric digestion. For emulsions treated with simulated gastric fluid

for 0.5 and 2 h, there is no obvious change in the drop size of the emulsions. The exceptional stability of the starch stabilized emulsions under gastric conditions might be attributed to strong and dense viscoelastic networks formed by starch molecules, which enhance emulsion stability by physically diminishing interaction between droplets (*162*). The barrier formed around the oil droplets by hydrogen bonds between the hydrogen groups of starch molecules and water molecule, would also minimize droplet interactions and prevent droplet coalescences (*163*).

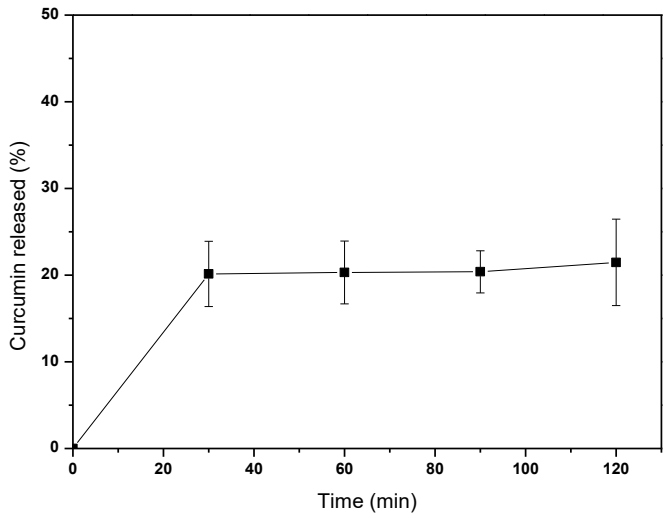

Figure 14. Release kinetics of curcumin from Pickering emulsion under simulated gastric fluid (SGF) incubation.

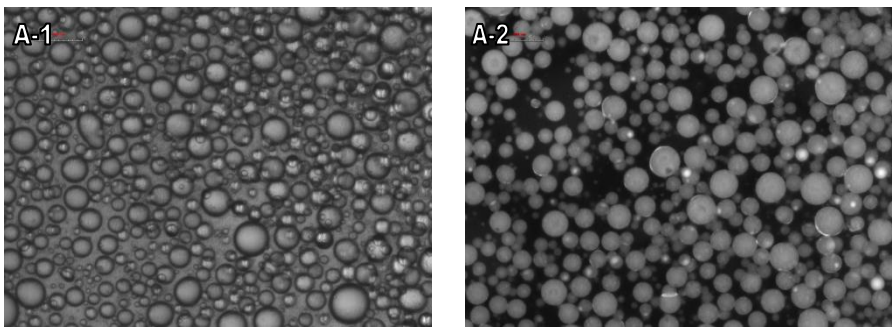

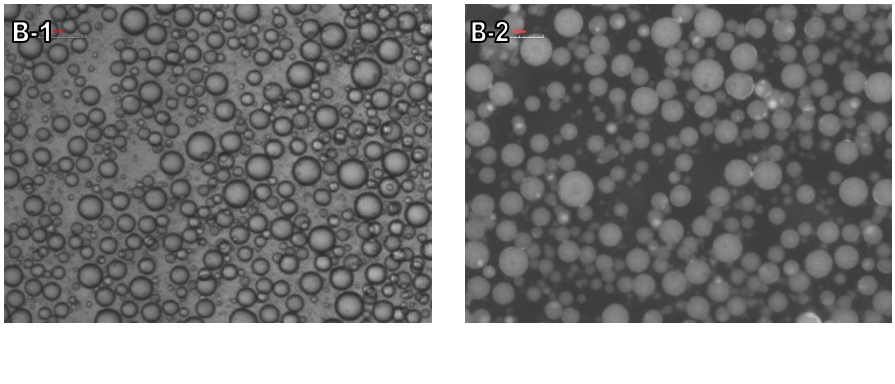

Figure 15. Microscopic and fluorescence image of (A) Pickering emulsion incubated in SGF for 0.5 h and (B) Pickering emulsion incubated in SGF for 2 h.

3.3.3. Bioaccessibility of curcumin using static *in vitro* small intestine digestion model

The low systemic bioavailability of curcumin, which might due to the rapid first-pass effect and the fast intestinal glucuronidation metabolism, is one major barrier to the clinical use of curcumin (*164*). Since the lipophilic compound released into the mixed micelle phase during lipid digestion could be regarded as a marker for its bioaccessibility, an *in vitro* small intestine digestion model was used to assess the digestion of curcumin in bulk oil and curcumin-encapsulated in Pickering emulsion in order to assess whether curcumin-encapsulated in starch stabilized Pickering emulsion can enhance bioaccessbility of curcumin. The release kinetics and bioaccessbility of curcumin in Pickering emulsion and bulk oil under simulated intestinal fluid (SIF) incubation was presented in **Figure 16**. As presented in Figure 33, a biphasic release was observed with a rapid release of about 18% and 8% curcumin in Pickering emulsion and in bulk oil at the first 30 min followed by sustained release of about 28% and 11% in the following 90 min. The bioaccessibility of curcumin loaded in Pickering emulsion was significantly enhanced by 2~3 times than curcumin in bulk oil phase during the 3 h incubation in SIF incubation. This might due to the increase in the surface area of the lipid phase in the

Pickering emulsion exposed to the aqueous phase compared with bulk oil, which enhances the interactions between lipase and oil phase (*141*). The structure of curcumin-loaded Pickering emulsion after digested for 3 h and resulting micelle phase was depicted in **Figure 17 (A)** and **(B)**. With a few oil droplets still observable, the major of the emulsion droplets in the Pickering emulsion was damaged during the 3 h digestion, which might suggest that the starch particles confer some protective effects to the oil droplets and raise the possibility to the control release of encapsulated lipophilic bioactive compounds during digestion.

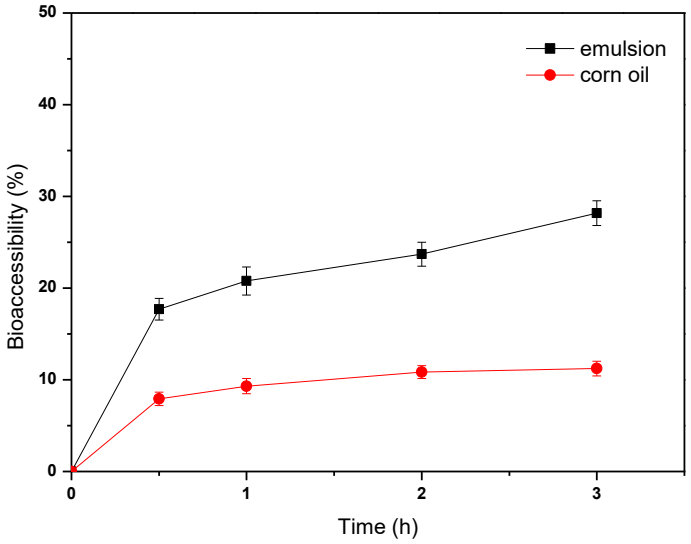

Figure 16. Release kinetics and bioaccessbility of curcumin in Pickering emulsion and bulk oil under simulated intestinal fluid (SIF) incubation.

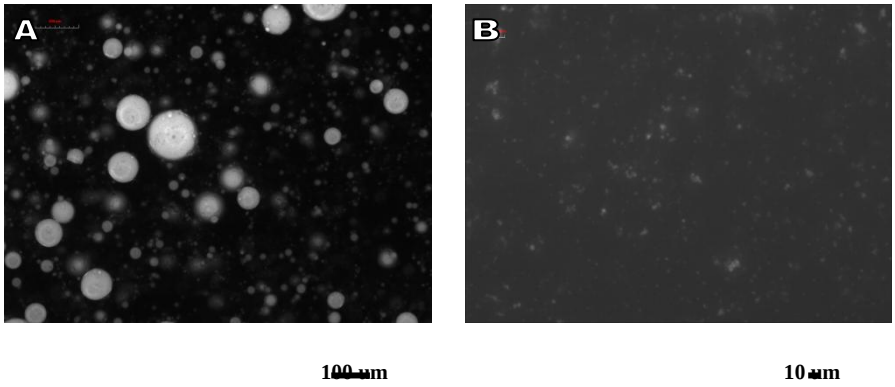

Figure 17. Fluorescence image of (A) Pickering emulsion incubated in SIF for 3 h (B) micelle phase.

3.3.4. Bioaccessibility of curcumin using pH-stat lipolysis model

The digestion of curcumin loaded Pickering emulsion and bulk oil containing same amount of curcumin were monitored using a dynamic in vitro lipid digestion model (**Figure 18**). Compared to bulk oil sample, the initial rate of FFAs released was faster for the emulsion sample. And the extent of lipolysis of the Pickering emulsion is higher than bulk oil sample, which suggested that the digestion of lipid phase would increase after been emulsified with milled starch particles. The bioaccessibility of curcumin encapsulated in the Pickering emulsion was 27%, which was higher than that of bulk oil sample (12%).

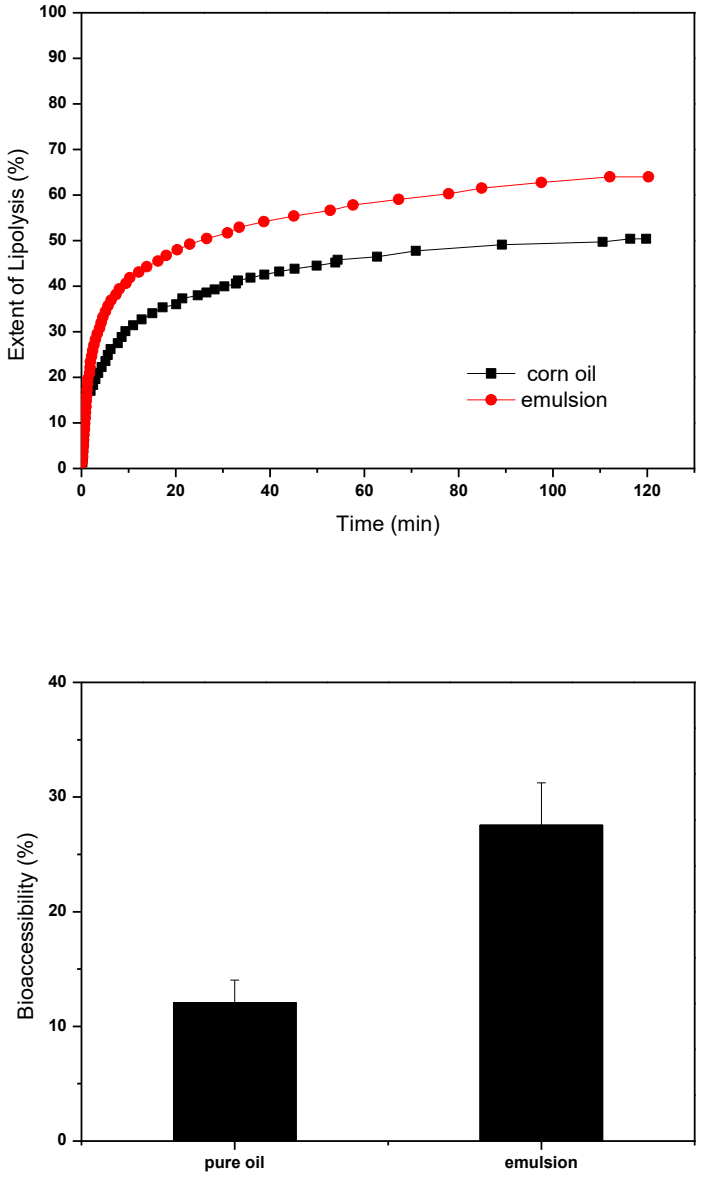

Figure 18. Release kinetics of curcumin from Pickering emulsion and bulk oil under simulated dynamic intestinal fluid (SIF) incubation.

3.3.5. Bioaccessibility of curcumin using TIM-1 model

The concentration of curcumin dissolved in corn oil and encapsulated in Pickering emulsion stabilized by milled starch passing though each compartment of TIM-1 apparatus during the digestion process has been shown in **Figure 20A**. And the

accumulated curcumin availability for absorption in jejunum, ileum and efflux fluid were presented in **Figure 20B**. For sample of curcumin dissolved in corn oil (control), the curcumin concentration in the gastric compartment reached the highest number at 30 min and then decreased significantly in the next 30 min. The concentration of curcumin in the duodenum compartment was much lower, however, exhibited similar fluctuation as in gastric compartment. The concentration of curcumin in the jejunum compartment was similar to that in duodenum and was lowest in the ileum compartment. During the digestion process of pure oil sample, curcumin availability for absorption in both jejunum, ileum compartment showed a slightly increase in the first 2 h of digestion. Then a steady growth was observed in the next 4 h, reaching 13% in jejunum and 3% in ileum, respectively.

The curcumin concentration and availability for absorption profiles of curcumin loaded Pickering emulsions was substantially different from that of the control sample in the simulated GI tract. As presented in **Figure 19**, Pickering emulsion stabilized by milled starch remained its original structure after being incubated in the gastric compartment for 30 and 60 min. Compared to digestion of free curcumin in corn oil, the curcumin concentration of Pickering emulsion in the gastric compartment exhibited similar profile, but was higher. The curcumin concentration in the duodenal compartment was 0.03 mg/ml at 15 min point, then increased steadily and reached a maximum of 0.12 mg/ml at 60 min, after which the curcumin content decreased gradually. Notably, the maximum curcumin concentration in the duodenal section was similar to that in the stomach compartment at that time point and was much higher than was the case with control sample. Curcumin concentration in the jejunum compartment in the first 120 min

was also much higher than in control sample, reaching the highest concentration of 0.1 mg/ml at 120 min, then dropping significantly in the following 60 min. Like control sample, curcumin concentration was the lowest in ileum compartment during the entire test period. Unlike curcumin in pure oil, profile of curcumin in emulsion availability for absorption exhibited a rapid increase during initial stage, then gradually reaching a plateau. The curcumin concentration distribution in each compartment and profiles of availability for absorption suggest that the Pickering emulsion stabilized by milled starch could partially endure the digestion of enzymes and severe acidic conditions of gastric compartment, and curcumin was gradually released from the emulsion in the gastric, duodenum and jejunum compartment after oral administration. The recoveries for curcumin in the corn oil suspension and curcumin-loaded Pickering emulsion were 18.0% ± 1.2% and 62.8% ± 5.7%. The majority of recovered curcumin was in the jejunum compartment, indicating that this section was the main part for absorption in small intestine despite the samples status. However, the curcumin concentration in and the availability for absorption in different sections of TIM-1 apparatus were affected by status of the sample during digestion process.

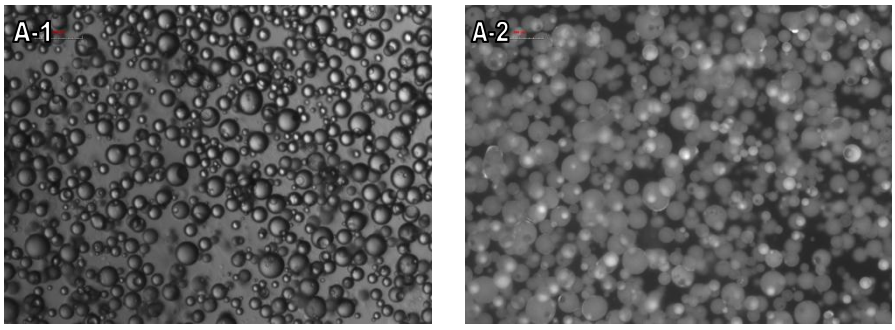

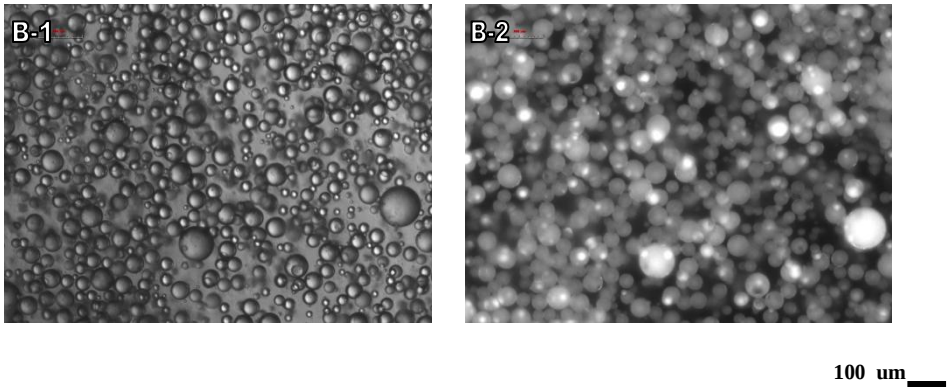

Figure 19. Microscopic and fluorescence image of Pickering emulsion incubated in TIM gastric compartment for (A) 30 min and (B) 60 min.

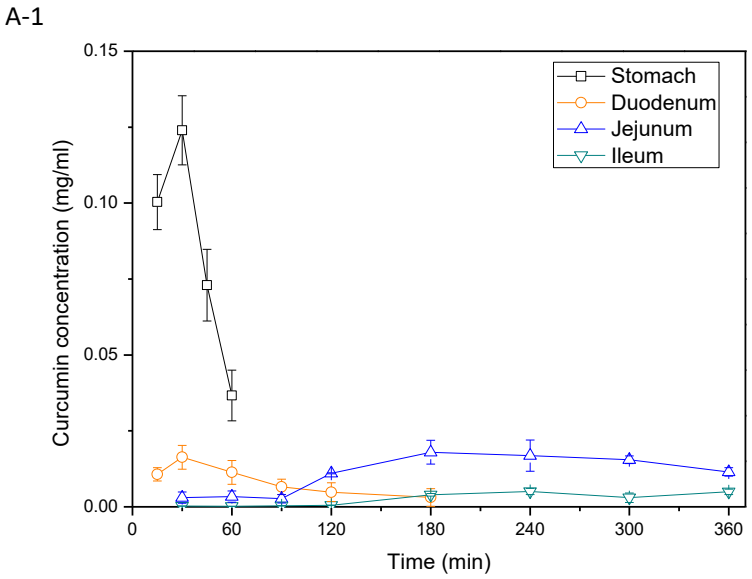

A-2

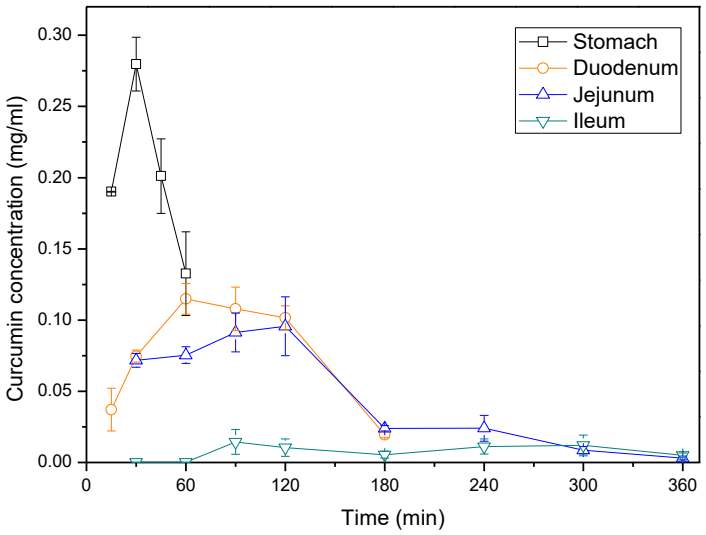
Stomach
Duodenum
Jejunum
Ileum
Curcumin concentration (mg/ml)
0.00
0.05
0.10
0.15
0.20
0.25
0.30
0
60
120
180
240
300
360
Time (min)

B-1

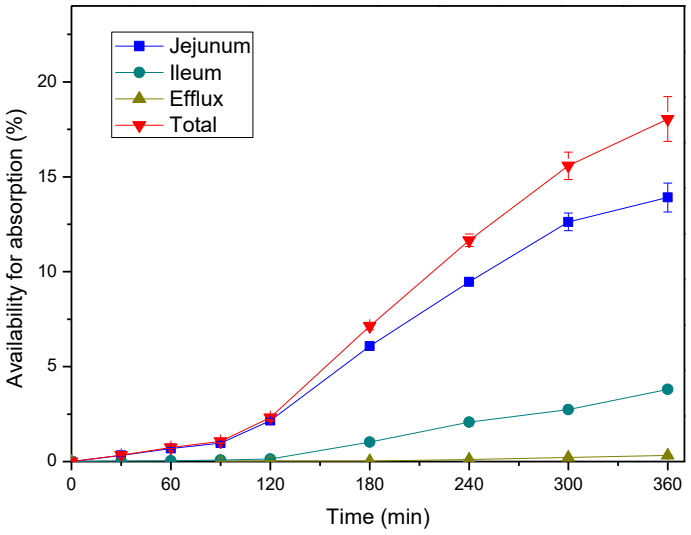
Jejunum
Ileum
Efflux
Total
Availability for absorption (%)
0
5
10
15
20
0
60
120
180
240
300
360
Time (min)

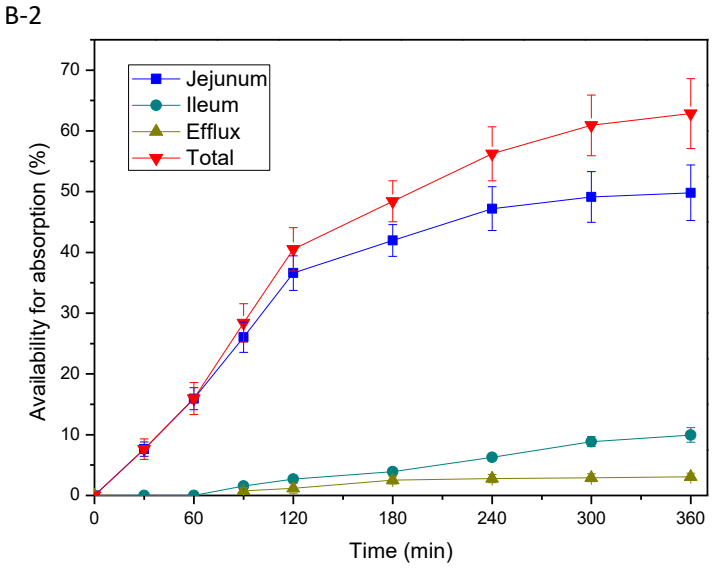

Figure 20. Curcumin concentration (A) and availability for absorption profiles (B) in the different segments of TIM-1 apparatus after feeding (1) curcumin corn oil suspension and (2) curcumin-loaded Pickering emulsion.

Since the filtration section of jejunum and ileum compartment can allow only solubilized compound to pass, the portion collected from jejunum and ileum filtrate is considered bioaccessible for absorption. While the portion collected without further filtration from the efflux outlet is considered as not bioaccessible or simply not absorbed in the GI tract. The accumulative bioaccessibility of curcumin of the samples in jejunum, ileum and the combined (jej+ile) total plotted as a function of time were presented in **Figure 21**. The amount of curcumin in the jejunum filtrate accounted for the largest portion of bioaccessible curcumin, which suggest that the major absorption of curcumin was happened in the jejunum apartment. The accumulative bioaccessibility curve of curcumin in emulsion sample exhibited an “S” shape curve, featuring a prominent delay with around 4% of the total curcumin in the jejunum dialysis fluid during the first 60 min. The bioaccessibility of curcumin then increased significantly around to 40% and reached

level off after 4 h. The release of over 30% of bioaccessible curcumin exhibited near-zero-order kinetics in the simulated conditions, suggesting that the emulsion sample would give sustained release of encapsulated curcumin over a period of 4 h. It is also notable that higher efflux recovery rate of curcumin was found in emulsion sample, which means that consumption of curcumin encapsulated in emulsion could not only enhance the curcumin bioaccessibility but also lead to faster GI clearance rate. The recovery of curcumin was defined as the amount of curcumin recovered from both the jejunum and ileum segments in relative to the original input weight. The recovery and bioaccessibility of curcuminin in the testes samples were analyzed and presented in **Table 6**. The total bioaccessibility of curcumin increased 7 times when encapsulated in Pickering emulsion stabilized by milled starch than suspended in pure corn oil. The recovery of curcumin in the emulsion was around 62%, which was also much higher than that of free oil sample. These results suggested that the delivery system of Pickering emulsion stabilized by milled starch could enhance rapid absorption during oral consumption through improving the stability, solubility and bioaccessibility of lipophilic compounds.

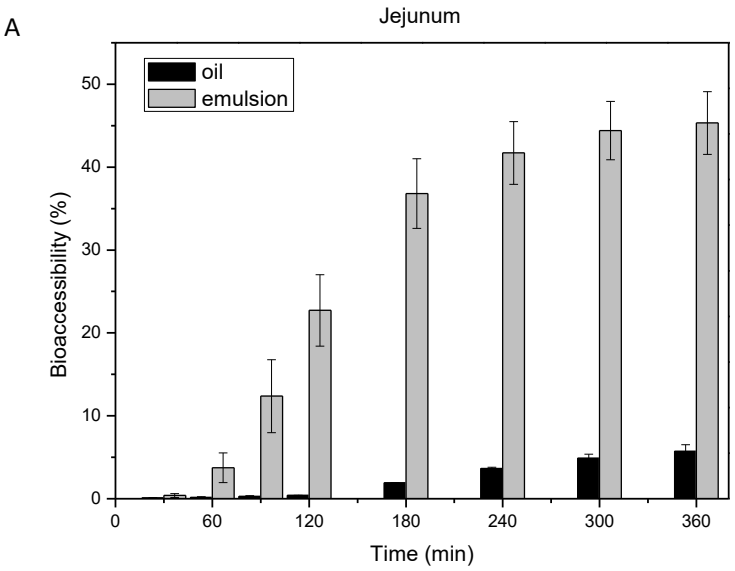
A
Jejunum
oil
emulsion
Bioaccessibility (%)
0
10
20
30
40
50
0
60
120
180
240
300
360
Time (min)

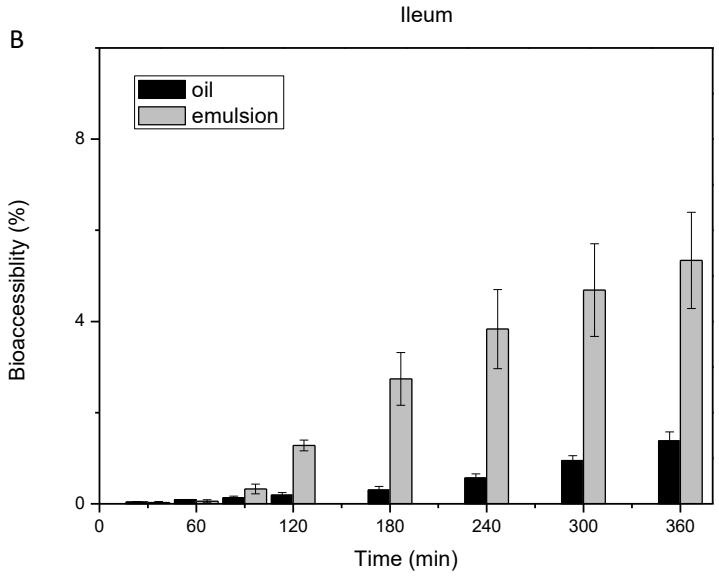
B
Ileum
oil
emulsion
Bioaccessiblity (%)
0
4
8
0
60
120
180
240
300
360
Time (min)

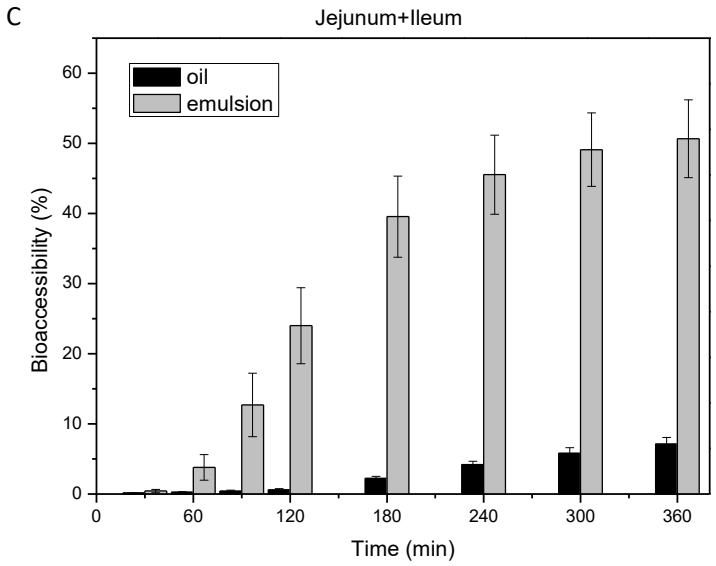

Figure 21. Cumulative bioaccessibility profiles of curcumin from (A) Jejunum section, (B) ileum section, and (C) total of the TIM-1 system expressed as percent of input concentration.

Table 6. Bioaccessibility of curcumin measured by TIM-1 system.

formulation	Curcumin input (mg)	Total recovery (mg)	Total recovery as of input (%)	Bioaccessibility as of input (%)	Efflux as of input (%)
Corn oil	120	21.6±1.4	18.0%±1.2%	7.1%±1.0%	1.4%±0.2%
Emulsion	120	75.4±6.8	62.8%±5.7%	50.6%±5.5%	5.3%±1.0%

Discussion

The Pickering emulsion sample exhibited higher curcumin bioaccessibility than in oil sample in all the three simulated in vitro systems tested. The bioaccessbility of curcumin in the emulsion and pure oil were similar when using the static *in vitro* small intestine digestion model and pH-stat lipolysis model. While 50% of the curcumin determined bioaccessible in the TIM-1 model for Pickering emulsion, this is significant

higher than the 28%, 27% in static *in vitro* small intestine digestion model and pH-stat lipolysismodel. And the content of bioaccessible curcumin in the TIM-1 model was relatively lower in oil sample than that of the other two models (TIM-1: 7%; static *in vitro* small intestine digestion model and pH-stat lipolysis model: 11%, 12%). The differences in the bioaccessibiliy results are due to differences in the complexity and accuracy of the system designs and simulations. As simplified digestion models, the static *in vitro* small intestine digestion model and pH-stat lipolysis model only controlled the temperature, initial endogenous bile salts and pancreatin concentrations for digestion. Although pH-stat lipolysis model has control the pH of the digestion process, many other important factors have been overlooked. For the emulsion sample containing milled starch and long-chain triglyceride (corn oil), a significant amount of starch and oil phase are unable to be digested in the static *in vitro* small intestine digestion model and pH-stat lipolysis model, which inhibit the release of curcumin during the digestion process. With the presence of the digestive enzymes (amylase, pepsin, trypsin, and pancreatin), degradation of starch and digestion of oil phase no doubt contributed to the release of curcumin when using the TIM-1 experiment, which might explain its significant higher bioaccessibility of curcumin in the emulsion sample.

3.3.6. *In vitro* anti-cancer activity of curcumin encapsulated in Pickering emulsion

To investigate the *in vitro* anti-cancer activity of curcumin encapsulated in starch stabilized Pickering emulsions, Caco-2 cells were treated with digested curcumin-encapsulated Pickering emulsion, digested curcumin in oil phase and DMSO-dissolved curcumin of the same concentrations, respectively. To examine the possible cytotoxicity of blank emulsion and digestion medium, digested blank Pickering emulsion without curcumin was also used to treat Caco-2 cells as control. The cell

viability was determined using MTT assay after treatment for 24 h. As showed in **Figure 22**, digested curcumin-encapsulated Pickering emulsion, digested curcumin in oil phase and curcumin dissolved in DMSO exhibited dose dependent anti-proliferative effect. And the anti-proliferation effect of encapsulated curcumin was more effective than that of DMSO-dissolved curcumin and digested curcumin in oil phase. At the concentrations of 5, 7.5, 10 and 15 μM, the encapsulated curcumin was significantly higher than DMSO-dissolved curcumin and digested curcumin in oil phase in anti-carcinogenesis ($P < 0.05$). The cell viability against increasing concentration of curcumin, and the estimated half-maximal inhibitory concentration values for curcumin in oil phase and encapsulated curcumin were found to be 11.71 and 4.28 μM, respectively. While curcumin dissolved in DMSO has relatively weak anti-carcinogenesis effect, its IC50 value was not detected in the tested concentration range. And digested blank Pickering emulsion exhibited no cytotoxicity to cells as it did not show any effect on cell viability at any the concentrations testified, which indicates no toxicity of Pickering emulsion or digestion medium in these cells. Since inadequate water solubility and subsequent precipitation largely hinder the effective exposure of cells with free curcumin, the enhanced cytotoxicity of encapsulated curcumin could be attributed to the increased water solubility of curcumin in the micelle phase. Instability and degradation of curcumin in aqueous phase with neutral pH due to rapid hydrolysis could also diminish the cytotocicity effect of free curcumin (*165*). The micelle phase is capable of exhibiting protective effect for encapsulated curcumin against hydrolysis when curcumin was entrapped in the core of micelle structure. Curcumin encapsulated in other micelle system have also been observed to improve its stability (*166*). These results clearly suggested

that the anti-cancer activity of curcumin encapsulated in Pickering emulsion was significantly increased as compared to curcumin in oil phase and dissolved in DMSO, which indicates that encapsulation is more effective to deliver curcumin to cancer cells.

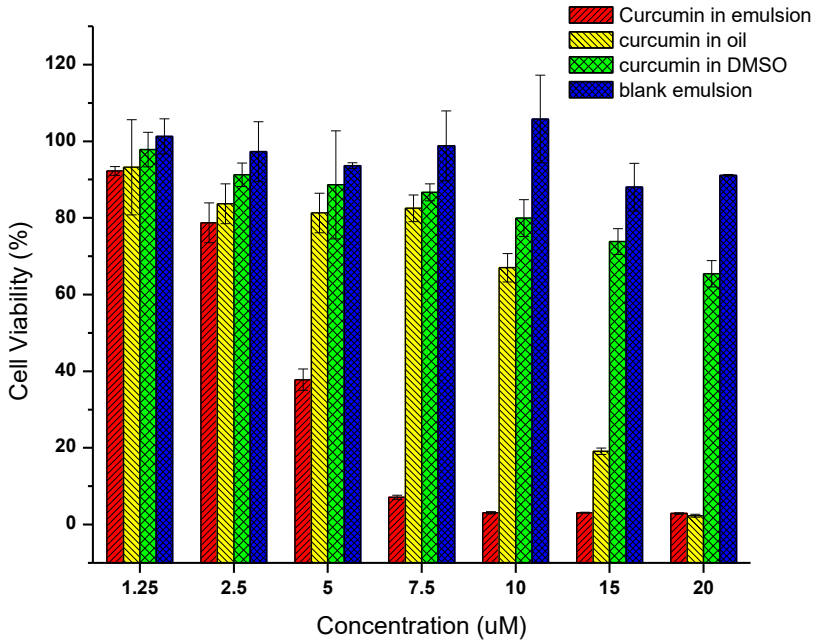

Figure 22. Cell viability of native curcumin in DMSO, digested curcumin encapsulated emulsion, digested curcumin in oil and digested blank emulsion

3.3.7. Cellular uptake of curcumin

As a useful model for studying the transport and metabolism of phytochemicals, Caco-2 human intestinal cell line has been used to assess absorption of lipophilic compounds, such as carotenoid and retinol in small intestinal (*167*, *168*). Using a Caco-2 cell culture model coupled with an in vitro digestion procedure, bioavailability of encapsulated curcumin in Pickering emulsion was assessed. With green intrinsic fluorescence, curcumin could be traced inside the cells without being tagged by any fluorescent dye. The time dependent cellular uptake studies of digested curcumin

encapsulated Pickering emulsion and free curcumin in DMSO were done by visualizing the intrinsic fluorescence of curcumin using fluorescence microscopy. **Figure 23** displays the microscopic and fluorescence images of treated cells. Control cells without any exposure to curcumin did not show any fluorescence. For cells treated with free curcumin in DMSO, faint fluorescence signal in cells was detected after 120 min of treatment, which suggests that the cellular uptake of free curcumin is rather slow and inefficient. While the internalization of encapsulated curcumin exhibited green fluorescence in cells treated with 60 min. The cellular uptake of encapsulated curcumin increased with prolonged time and the intensity was observed uniformly from the entire cell. These images indicated that Caco2 cells took up the micelles more efficiently compared to free curcumin, which further confirms that low aqueous solubility of free curcumin hinders its entry to cells. This results suggest that curcumin encapsulated in Pickering emulsion could effectively uptake by the epithelial cells after digested in the small intestinal.

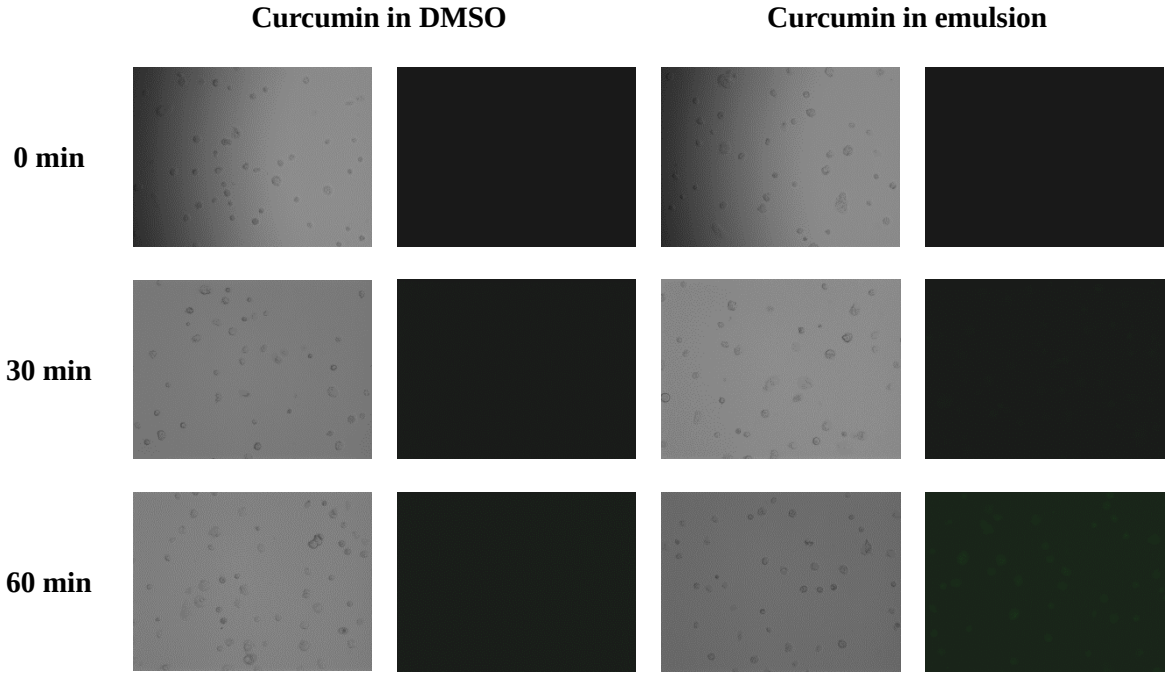

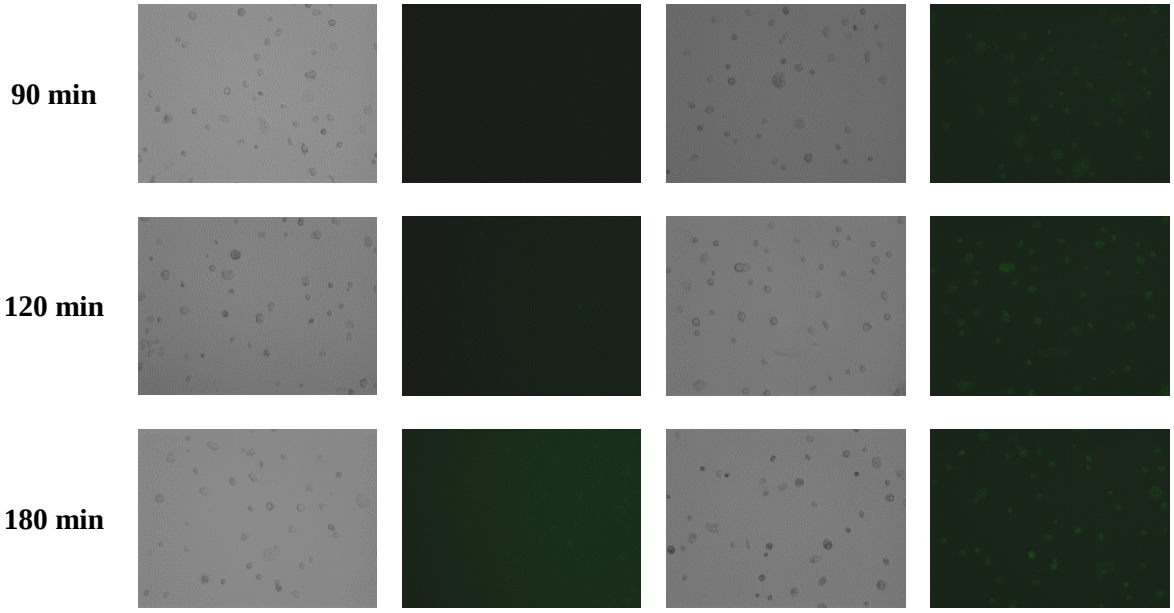

Figure 23. Cellular uptake of native curcumin and curcumin in micelle phase at different harvest time points

3.4. Conclusion

Development of suitable delivery system for poorly water-soluble bioactive compounds, such as curcumin, which suffer from low bioavailability problem, is vital for improving their therapeutic activity. Our study suggests that starch stabilized Pickering emulsion system could be a promising delivery system for administering curcumin without compromising its activity. By encapsulated in starch stabilized Pickering emulsion, the solubility and stability of curcumin were enhanced significantly. And benign stability against harsh gastric conditions as well as improved dissolution profiles in small intestinal tract was also observed in encapsulated curcumin. The curcumin-loaded micelle phase from the digested emulsion system exhibited great *in vitro* cytotoxicity and effective cellular uptake behavior. This work highlighted the potential of utilizing starch stabilized Pickering emulsion as delivery vehicle for lipophilic bioactive compounds.

CHAPTER 4 FABRICATION OF MILLED CELLULOSE PARTICLES-STABILIZED PICKERING EMULSIONS

4.1. Introduction

Emulsions are the mixture of two immiscible liquids with one dispersed in another. Besides from small molecular weight surfactants or soluble proteins/polysaccharides, solid colloid particles have been proven to be able to adsorb at the oil-water interface to form "Pickering emulsions". The stability mechanism relies on the accumulation of particles at the oil-water interface to form a densely packed layer against emulsions coalescence and Ostwald ripening (*4, 105*). The stability of the emulsion largely depends on the difficulty to remove those particles from the interface. For particles with contact angles between 30° and 150°, the energy of desorption per particle is normally in the order of several thousand kT, which indicates that the adsorption of particles onto interface is practically irreversibly (*1*). The contact angle of the particles also determines the nature of the emulsion. Since the side of interface where the majority of particles exist would be the continuous phase, particles with contact angle less than 90° tend to form oil-in-water emulsions, whereas particles of contact angle more than 90° would form water-in-oil emulsions (*6*). Compared to conventional emulsions stabilized by surfactants, particle-stabilized emulsions enjoy the advantages of avoiding the adverse effects of some small molecular weight surfactants, such as tissue irritation, metabolic syndrome and environment pollution (*7-9*).

Most of the studies related to Pickering emulsions dealt with the usage of inorganic or synthetic particles, such as silica, latex, clay, etc (*10-13*). Although, silica nanoparticles (labeled as food additive E551) are approved with application in food products,

consuming these silica particles might be potentially deleterious to health since exposure of the intestinal epithelia to these particles which could have ramifications to gut and other organs (*169, 170*). Recently, development of particles from natural resources, such as cellulose, starch, chitin, has attracted increasing attention due to their broad applications, especially in food, cosmetic and pharmaceutical industries (*1, 171*). As one of the most available biopolymers, cellulose is a good candidate due to its large abundance, low cost, biodegradability and biocompatibility. As a linear homopolymer with β(1-4)-D-glucose residues linked through glycosidic oxygen bridges, cellulose is formed by stacking of microfibrils, where highly ordered crystalline regions are interrupted by disordered domains (amorphous or less ordered regions) (*172*). Since cellulose is not surface active due to the lack of hydrophobicity and great tendency to aggregate, modification methods are required for it to stabilize Pickering emulsions. Cellulose derivatives, such as micro-fibrillated cellulose, the moderately degraded microfibrils (5-10 μm long), have been used to form Pickering emulsions (*17, 49*). However, with long length relative to the size of the droplets, these particles promote network formation rather than individual droplets. To control the emulsion characteristics, researches have been conducted to reduce their particle sizes. As a heterogeneous process involving in acid diffusion into the fibers and glycosidic bonds cleavage (*173*), acid hydrolysis is a widely used method to produce well-defined naocrystalline particles, whose properties highly depend on the cellulose origin and acid hydrolysis conditions (*174, 175*). Various cellulose nanocrystals have been reported to stabilize Pickering emulsions (*25, 43, 176*). Although cellulose naocrystals are now commercially available, the production process involves harsh acid conditions. In addition, the production rate is

low, and the products might present contaminants.

As a simple, cost-saving and environmentally friendly physical method, media-milling process has long been applied to produce nano/submicrometer particles via a top-down concept (*52*, *54*). Derived from a stirred ball mill, media mill was first commercially used in 1948 as a sand mill. With more densely packed and rapidly rotated media, the efficiency of comminuting has been highly improved (*56*). The thermal impact on the materials during milling process is minimized by using high efficiency temperature control system (*57*). Under the influence of friction, impact, compression, and shearing forces from the milling beads, grinding chamber and material itself, the materials will be damaged and their sizes will be gradually reduced (*59*). For semicrystalline materials, such as starch and cellulose, media-milling process has been proved to effectively reduce their particle sizes, producing nano/submicrometer particles (*60*, *61*). In this study, media milling treatment was used to modify cellulose and the ability of milled cellulose to stabilize Pickering emulsions was characterized. To the best of our knowledge, it was the first time media milled cellulose was studied to form Pickering emulsions.. The structure and morphological changes of cellulose during milling process were analyzed by using X-ray diffraction (XRD) and scanning electron microscopy (SEM). The emulsion microstructure and rheology properties of the milled cellulose particles-stabilized Pickering emulsions were also analyzed.

4.2. Materials and methods

4.2.1. Materials

Sigmacell cellulose Type 20 and other ACS-grade chemicals including sodium chloride, hydrogen chloride and sodium hydroxide were purchased from Sigma-Aldrich (St. Louis, MO). MCT (medium chain triacylglycerol oil, Neobee@1053) was a gift

provided by Stepan Company (Northfield, IL). Deionized water with a resistivity of 18.3 MΩ cm was obtained by treatment with a Milli-Q water purification apparatus (Millipore, MA, USA).

4.2.2 Media-milling process

A MiniSeries media mill (Netzsch LLC, PA, USA) with a mill power of 0.13 kw was used to prepare samples. The pump speed and mill speed utilized were 100 rpm and 3000 rpm, respectively. Cellulose suspended in deionized water was filled in the milling chamber. The temperature of suspension was maintained below 30℃ by a cooling system. Milling process continued for 15 h and samples were withdrawn every 5 h. The milled cellulose suspensions were immediately used for emulsion preparation or freeze-dried for further analysis. Also, a moisture test was performed to determine the exact weight content of cellulose in the suspension after the milling process.

4.2.3. Morphological studies by Scanning electron microscope (SEM) and atomic force microscopy (AFM)

Native cellulose was directly mounted on circular aluminum stubs. Milled cellulose suspension was diluted for 10 times, mounted on circular aluminum stubs and dried at 40℃ overnight. Then the samples were coated with 20 nm of gold. SEM images of samples were recorded using a model 1530VP scanning electron microscope (LEO, Oberkochen, Germany) at an accelerating voltage of 3 kV. Twenty microliters of milled cellulose dispersions were diluted 50 times and dripped onto freshly cleaved mica surface. The samples were then dried by nitrogen gas. NanoScope IIIA Multimode AFM (Veeco Instruments Inc., Santa Barbara, CA) equipped with a silicon-etched RTESP7 cantilever (Veeco Nanoprobe, Camarillo, CA) was used to collect tapping mode AFM images. A silicon tip with nominal spring constant of 40 N/m was used.

4.2.4. Contact angle measurement

A sessile drop method was used to measure the water contact angle of cellulose film using a VCA Optima system (AST Products, U.S.A). Cellulose film was prepared by pouring milled cellulose suspension onto glass dishes and dried at room temperature for 12 h. The contact angles were measured at five different places on the film through placing a drop of water (2 µl) on the film using a precision micro-syringe. The reported result was the average value of all measurements.

4.2.5. X-ray diffraction analyses

The XRD patterns of native and milled cellulose were conducted using the method described in section 2.2.5.

4.2.6. Emulsions preparation

The oil-in-water emulsions were prepared by mixing the water phase containing milled cellulose and oil phase (medium chain triacylglycerol, MCT) through an IKA Ultra-Turrax T25 homogenizer at 10,000 rpm for 2 min. The oil/water phase ratios were ranged from 6:4 to 3:7. Different milled cellulose concentrations used were through diluting the original milled cellulose suspension with certain amount of water. Cellulose concentrations were expressed as weight content relative to the water phase based on the results from the moisture tests. Each emulsion was prepared at least twice.

4.2.7. Responsiveness to ionic strength

The emulsion stability aganist different ionic strength conditions were evaluated by diluting fresh prepared emulsions with same volume of defined salt concentrations of 0.1, 1, 10 and 100 mM NaCl solution. Samples were equilibrated overnight before being analyzed for appearance, structure and stability.

4.2.8. Responsiveness to different pH conditions

The stability of emulsions under different pH was evaluated by diluting fresh

prepared emulsions with the same volume of 0.2 M phosphate buffer solutions of defined pH values ranging from pH = 3, 5, 7 and 9. All samples were equilibrated overnight before further analysis.

4.2.9. Zeta potential of milled cellulose

The zeta potentials of milled cellulose at different ionic strength and pH conditions were measured using a Zeta sizer nano ZS, Malvern (UK) at 25℃. The concentrations of all measured samples remain the same at 0.05 wt%.

4.2.10. Light microscopic observation of cellulose-stabilized Pickering emulsions

The emulsions were all visualized using a Nikon Eclipse TE2000-U (Japan) microscope by the method described in section 2.2.7.

4.2.11. Rheological analyses

The rheological properties of emulsions were observed after storage for 24 h at room temperature to ensure a complete equilibration status. The measurements were performed using Advanced Rheometric Expansion System (Rheometric Inc., Germany) at room temperature using parallel plate geometry with a diameter of 25 mm and gap height of 1 mm. Five minutes were allowed for resting prior to measurement. Strain sweep tests were performed in the strain range of 0.01-60 % at a frequency of 10 rad/s to verify the linear viscoelastic region. The linear viscoelastic regions established by the strain sweep experiments were in the range of strain values between 0.01% and 1%. Oscillatory tests were conducted in linear viscoelastic range at the constant strain of 0.2% with the angular frequency range of 0.1-100 rad/s.

4.3. Results and Discussion

4.3.1. Characterization of native cellulose and milled cellulose particles

The morphology of native cellulose and milled cellulose particles revealed by SEM and AFM were presented in **Figures 24** and **25**. Native cellulose particles are rod-like

shape with particle size ranging from around 10 to 90 μm. During the milling process, the large particles of cellulose were broken into smaller ones by the mechanical forces. Although milled cellulose particles agglomerated during the sample preparation process, the SEM images revealed that most particles were in nano/submicrometer scale. The AFM height image of milled cellulose particles was presented in **Figure 25**. Based on the statistically calculation of measuring at least 100 milled cellulose particles in AFM image using ImageJ software, the mean particle size of milled cellulose particles was ~463 nm when the milling time was increased to 15 h. With high cohesive energy induced by van der Waals forces and by massive hydrogen bond networks among hydroxyl groups within and between chains (*177*), cellulose exists as highly packed resistant fibers with ordered crystalline regions, which might explain the long processing time needed for obtaining nano/submicrometer milled cellulose. Native cellulose is highly polar due to the existing of hydroxyl groups, it is nearly non-soluble in cold water, and quickly precipitates from water after mixing. Compared to native cellulose, the cold water dispersibility of milled cellulose was largely enhanced. As presented in **Figure** 24, the milled cellulose suspension was stable without any settlement after over one-month storage while complete settlement of native cellulose at the bottom was observed in storage of 2 h. The enhancement interactions between milled cellulose and water phase were attributed to the disruption of hydrogen bond network through decrystallisation of cellulose (*178*). The crystallinity change of cellulose during milling process was further verified using X-ray diffraction. The water-contact angle of milled cellulose film with milling time of 15 h was 45°, which suggested that milled cellulose was hydrophilic.

(i)

(ii)

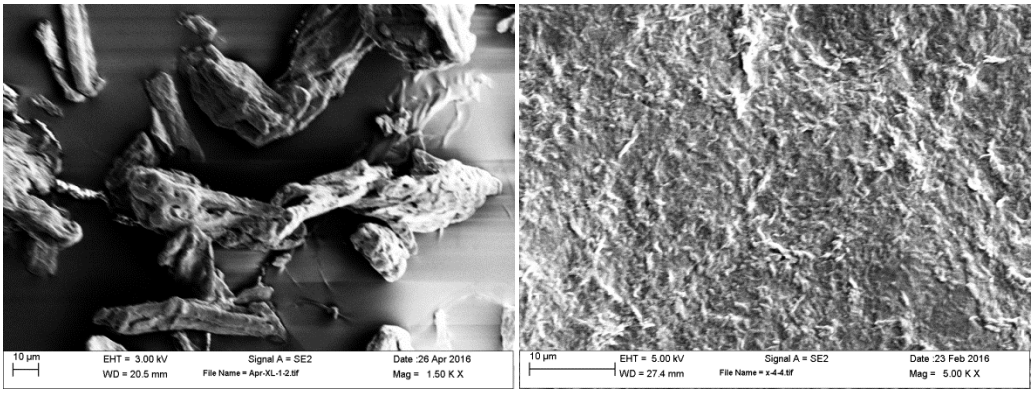

Figure 24. (i) Digital images of 3.7% (w/w) native cellulose in water (left) and milled starch after milling time of 15 h (right) after storage for different times. (ii) Scanning electron micrographs of native cellulose particles (left) and milled cellulose particles after 15 h milling process (right).

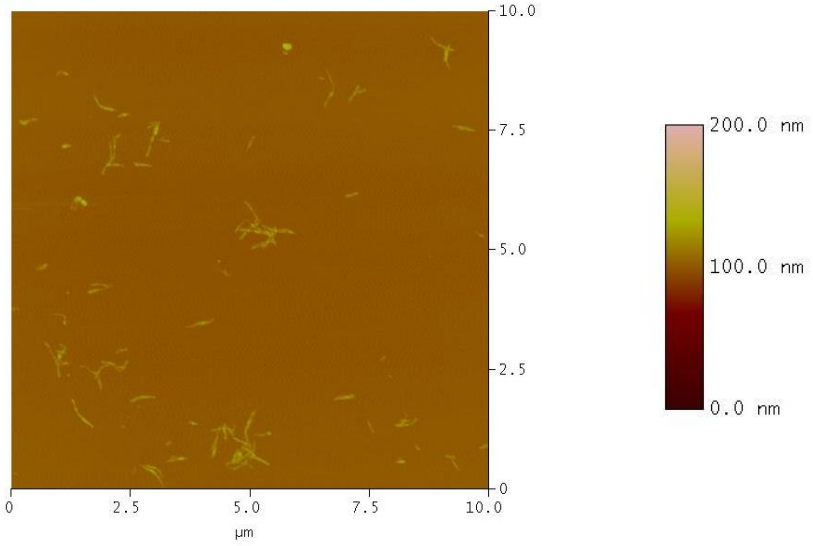

Figure 25. Atomic force micrographic height image of milled cellulose particles after 15

h milling process.

The crystallinity change of cellulose induced by the media-milling treatment was analyzed by X-ray diffraction (XRD). X-ray diffractograms of native cellulose illustrated the typical crystal lattice for cellulose I (**Figure 26**) (*179*). Diffraction peak at 22-23º exhibited the maximum intensity, which indicates the distance between hydrogen-bonded sheet in cellulose I. The broad peak at 15º corresponds to be a composite of two peaks from I_{β}, I_{α}, or both. The small peak at 34.5º represents the 1/4 of the length of one cellobiose unit and arises from ordering along the fiber direction (*180*). The intensity of these three diffraction peaks decreased as the milling was proceeded. After milling process of 15 h, these two peaks were still existed despite significant reduction was observed. These results suggest that part of crystalline structure of native cellulose could be damaged by the mechanical force from the milling process. Further analysis of XRD profiles indicated that cellulose crystallinity decreased from 38.6% for native cellulose to 31.2% for the cellulose particles after 15h milling treatment. The decrease in the particle size as well as the crystallinity in the cellulose increased the accessibility between cellulose and aqueous phase.

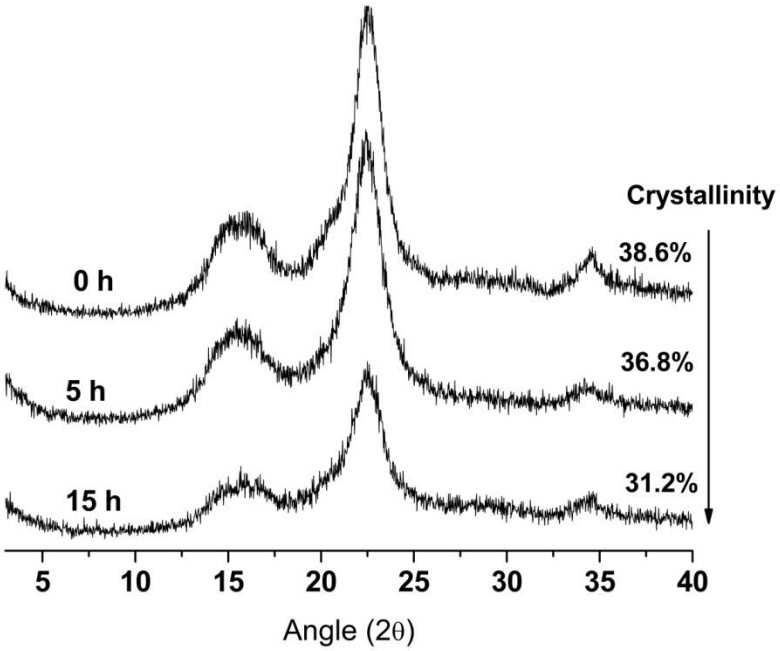

Figure 26. X-ray diffraction profiles of native (0 h) and milled cellulose particles with different milling times (5 h and 15 h).

4.3.2. Influence of milling time, cellulose concentration and oil/water ratio on emulsion formation

Milled cellulose suspensions with different milling times were used to form Pickering emulsions. The emulsifying power of particles to stabilize Pickering emulsions is related to their ability to cover the oil-water interface. Since larger particles require higher mass to cover an equal interfacial area, some particles with larger size were found to exhibit lower emulsifying power than smaller particles (*38*). Native cellulose was unable to stabilize emulsions, possibly due to its large particle size. The emulsifying capacity of cellulose particles increased steadily after milling treatment. Pickering emulsions stabilized by milled cellulose exhibited benign stability without creaming and phase separation for over one-month storage. The microscopic images of emulsions

stabilized by milled cellulose with different milling times (5 h, 10 h and 15 h) were presented in **Figure 27**. As presented in **Table 7**, the droplet sizes of the emulsions ranged from 57± 21 to 42 ± 5 μm. With increase in the milling time, the percentage of large droplets decreased possibly due to more small cellulose particles were available for adsorption at the oil-water interface. The influence of milled cellulose concentration in the water phase on emulsion formation was assessed using 0.1, 0.2, 0.4, 0.9, 1.9, 2.8, and 3.7 wt% cellulose suspension with a milling time of 15 h. Oil/water ratio of 5:5 was used in every formulation. The digital pictures of vials containing emulsions, optical microscopic images and the droplet sizes of emulsions were depicted in **Figure 28**. The droplet size of emulsions with different storage time was depicted in **Table 7**. All the emulsions formed exhibited benign stability against coalescence during long-term storage. The droplet diameters were measured twice after 24 h and after one month, and no variation in the size of the droplets was observed, which confirmed that no further coalescence occurred once the emulsion formed. With the increase of milled cellulose concentration, two distinct regimes were observed: the droplet size of emulsions decreased, which was due to the higher amount of cellulose were allowed to stabilize larger surface area, until reaching a “plateau”. By adding more milled cellulose into the system, the emulsions stability against coalescence and aggregation could be enhanced as the rate of surface coverage of droplets increased and particles adsorbed at the interface could form a thick interfacial layer around droplets. The plateau observed in the milled cellulose concentration range where the emulsion droplet size was almost constant was attributed to lacking of efficiency of the emulsification process, which was reported in other cellulose nanocrystals stabilized emulsions (*43*).

Table 7 Mean droplet size of Pickering emulsions stabilized by milled cellulose with different storage time at oil/water ratio of 1:1.

Sample	Droplet size (μm)		
	0 day	24 h	1 month
3.7% cellulose, milling time 5 h	57 ± 21	59 ± 20	67 ± 22
3.7% cellulose, milling time 10 h	49 ± 12	47 ± 11	50 ± 14
3.7% cellulose, milling time 15 h	42 ± 5	41 ± 5	45 ± 7
2.8% cellulose, milling time 15 h	42 ± 6	44 ± 7	48 ± 9
1.9% cellulose, milling time 15 h	43 ± 6	43 ± 8	47 ± 9
0.9% cellulose, milling time 15 h	46 ± 9	48 ± 11	51 ± 11
0.4% cellulose, milling time 15 h	48 ± 8	50 ± 10	42 ± 13
0.2% cellulose, milling time 15 h	52 ± 11	54 ± 12	57 ± 17
0.1% cellulose, milling time 15 h	60 ± 13	63 ± 15	68 ± 19

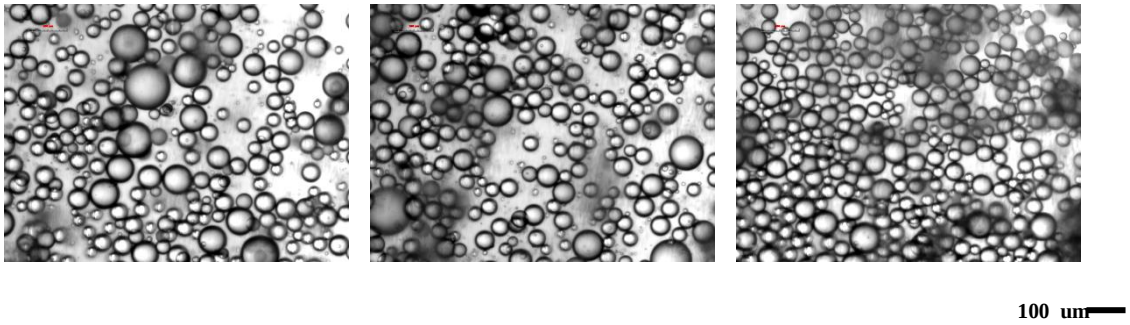

Figure 27. Optical microscopic images of Pickering emulsions stabilized by milled cellulose particles prepared at different milling times (from left to right: 5 h, 10 h, and 15 h) with cellulose concentration fixed at 3.7%.

(i)

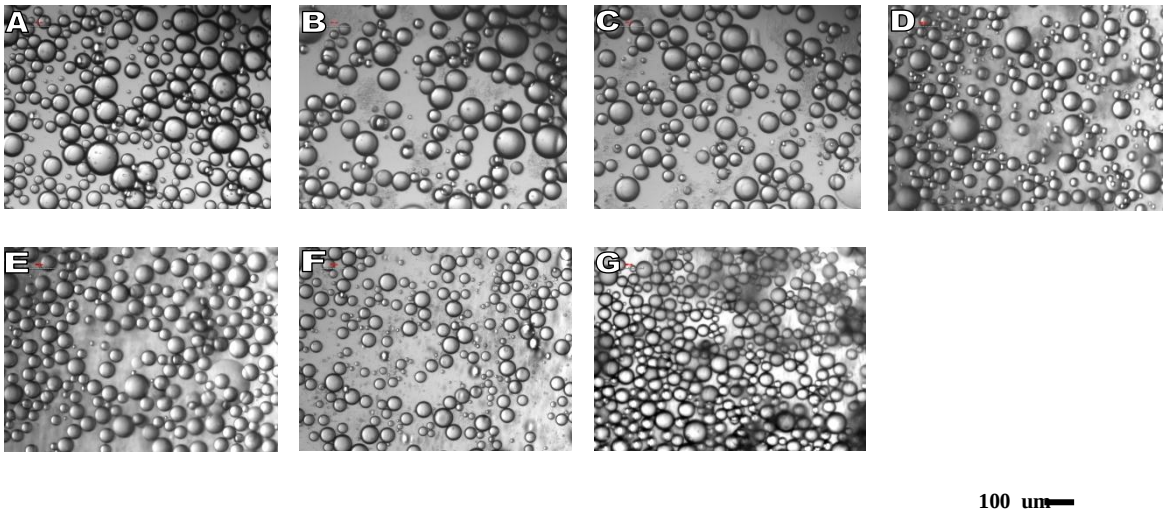

(ii)

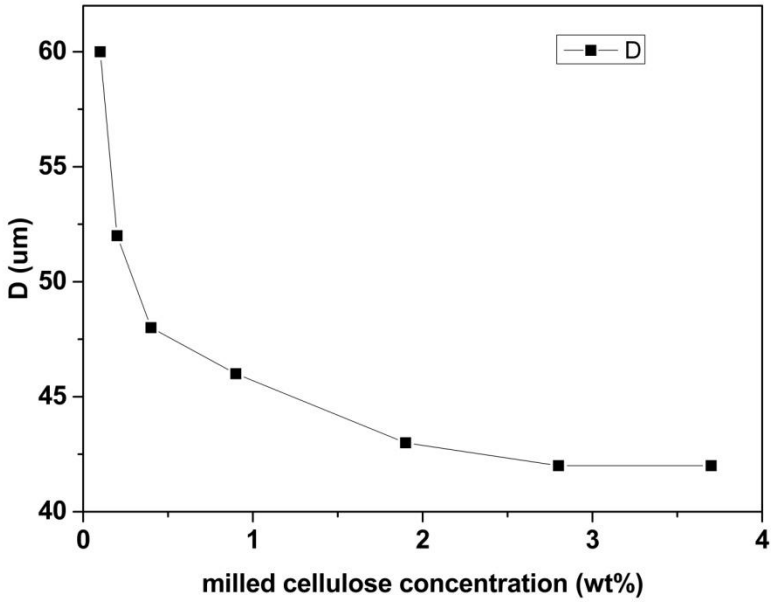

(iii)

Figure 28. Digital pictures of vials containing emulsions (i), microscopic images (ii) and droplet size of milled cellulose stabilized emulsions at different cellulose concentration (iii). The cellulose concentrations from left to right (i) and A to G (ii) are 0.1, 0.2, 0.4, 0.9, 1.9, 2.8, and 3.7%, respectively.

It is notably that Pickering emulsions stabilized by milled cellulose exhibited good stability against creaming compared with emulsions stabilized by cellulose nanocrystals. For emulsions formed by milled cellulose with different concentrations, the creaming effect was only observed in emulsions stabilized by 0.1% milled cellulose. However, creaming only disappeared when emulsions (oil/water ratio: 1:1, v/v) containing particles concentration higher than 0.25% for cellulose nanocrystals (*181*). The benign stability against creaming might be attributed to the formation of entanglements and interconnecting droplets induced by the long linear milled cellulose. Long bacterial cellulose-derived nanocrystals with length ranging from 855 ± 215 nm to 4 μm were

found to inducing an interconnected mesh-like structure when stabilizing Pickering emulsions. And this network formation was length-dependent since none was observed with short cellulose nanocrystals of length around 189 nm (*25*). The increase in the cellulose concentration could also enhance the emulsion stability against creaming and coalescence, which could be due to the increased surface coverage of oil droplets and the ability of particles to form a thick interfacial layer around droplets (*182*). Furthermore, the smaller droplets formed at relatively high particle concentrations could be responsible for slower creaming (*183*). When the milled cellulose concentration increased from 2.8% to 3.7%, the droplet size of the emulsions was almost constant. Hence, the viscosity of the continuous phase increased as more non-adsorbed cellulose presented in the aqueous phase, which could be due to the presence of excess cellulose in the continuous phase assuming the surface coverage of the emulsion droplets was not changed. Meanwhile, the resulting emulsion exhibited a gel-like structure, which was further analyzed by rheological studies.

In addition to the concentration and size of milled cellulose dispersed in the aqueous phase, the amount of oil phase used is also crucial to the emulsion droplet size. Emulsions with different oil/water ratios were prepared at milled cellulose concentration of 3.7 wt%. The microscopic images and droplet size of the emulsions were depicted in **Figure 29**. Stable emulsions were formed in all the oil/water ratios tested. And a minor change in the droplet size of the emulsions when the oil/water ratio varied from 6:4 to 3:7. The droplet size of Pickering emulsion was thought to be affected by the oil/water ratio as the amount of particles relative to the dispersed phase available to stabilize the oil-water interface was changed (*184, 185*). The slight differences in the droplet size of milled

cellulose stabilized emulsions with various oil contents might be due to the availability of enough cellulose particles in the aqueous phase for the formation of oil-water interface.

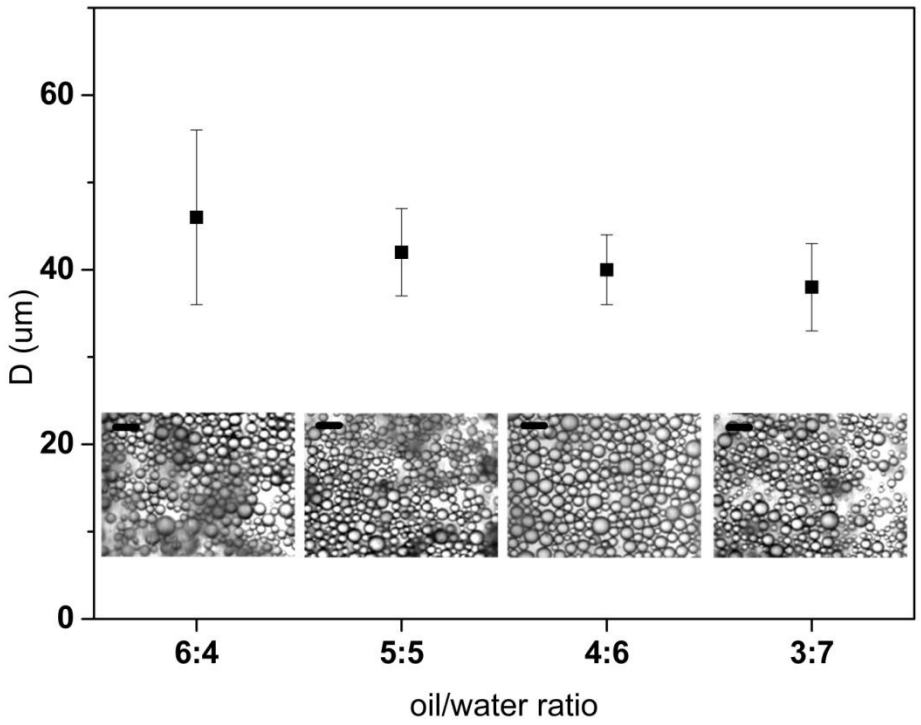

Figure 29. Microscopic images and droplet size of milled cellulose particles-stabilized Pickering emulsions with different oil/water ratios at cellulose concentration of 3.7%. Scale bar represents 100 µm.

4.3.3. Influence of ionic strength and pH condition on emulsion stability

The ionic strength and pH conditions were found to influence the packing of charged particles at the interface as the electrostatic repulsion between particles being screened (*18, 186*). The bulk appearance, microscopic images and droplet size of 1.9% milled cellulose stabilized emulsions under different ionic strengths of NaCl (100, 10, 1, 0.1 mM) were depicted in **Figure 30**. The zeta potentials of milled cellulose at different ionic strength conditions were also presented in **Figure 30**. The absolute zeta potential value of

milled cellulose decreased from 12.8 mV to 2.2 mV as the NaCl concentration was increased from 0.1 mM to 100 mM. During the media milling process, the massive intermolecular network of hydrogen bonds formed between the hydroxyl groups of cellulose monomer units in crystalline structure was disrupted. The ordered crystalline cellulose was converted to milled cellulose with smaller particle size, increased effective surface area and more amorphous structures. Compared to crystalline cellulose, amorphous cellulose was found to possess fewer hydrogen bonds per repeating monomer unit (*42*). And the β-1, 4 glycoside bonds of amorphous cellulose are more readily accessible to water and other reactants (*187, 188*). Hence, the change of structure as well as chemical bonding associations in milled cellulose facilitated the interaction of milled cellulose and aqueous phase. The negatively charged milled cellulose in an aqueous medium is thought to be due to their characteristic carbonyl and hydroxyl groups (*189-191*). Under the influence of gravity, a concentrated layer of emulsion droplets (cream) rose to the top. The emulsion prepared at 0.1 mM sodium chloride released both a significant of water and milled cellulose particles as the droplets creamed. The relatively high electrostatic repulsion between milled cellulose at 0.1 mM sodium chloride was response for the release of excess cellulose from the emulsion phase. When emulsions were diluted at sodium chloride concentrations of 100, 10 and 1 mM, only water was released and no milled cellulose was observed at the bottom, indicating the screening effect by salt led to enhancing particle interaction and entrapping of cellulose particles in the emulsion phase. The increase in salt concentration screened the negative surface charges on the cellulose particles and lowered the particle zeta potential, which would enhance the attachment of particles on the emulsion droplets. The reduction in

released of excess particles as the ionic strength increased was also observed in other Pickering emulsion systems (*186, 192*). . Small variations in the emulsion creaming behavior were observed when sodium chloride of different concentrations was added. As the emulsion droplets were not close packed in the cream, an open three-dimensional network of droplets and the particles might form in the cream. Increasing the ionic strength resulted in less electrostatic repulsion between dispersed oil droplets, which were more likely to coalesce (*13*). However, the size and polydispersity of droplets did not vary with sodium chloride concentration as depicted in the **Figure 30**. These creaming behaviors of emulsions revealed the stability of the Pickering emulsions against aggregation. When emulsions were dispersed in 0.1 mM sodium chloride solution, the release of milled cellulose seemed not to significantly destabilize the droplets to coalescence. It was possible that the emulsion droplets were re-dispersed in the sodium chloride solutions. The benign stability of emulsions might be due to the weak electrostatic repulsion between milled cellulose.

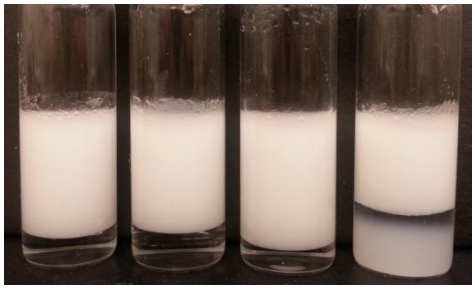

(i)

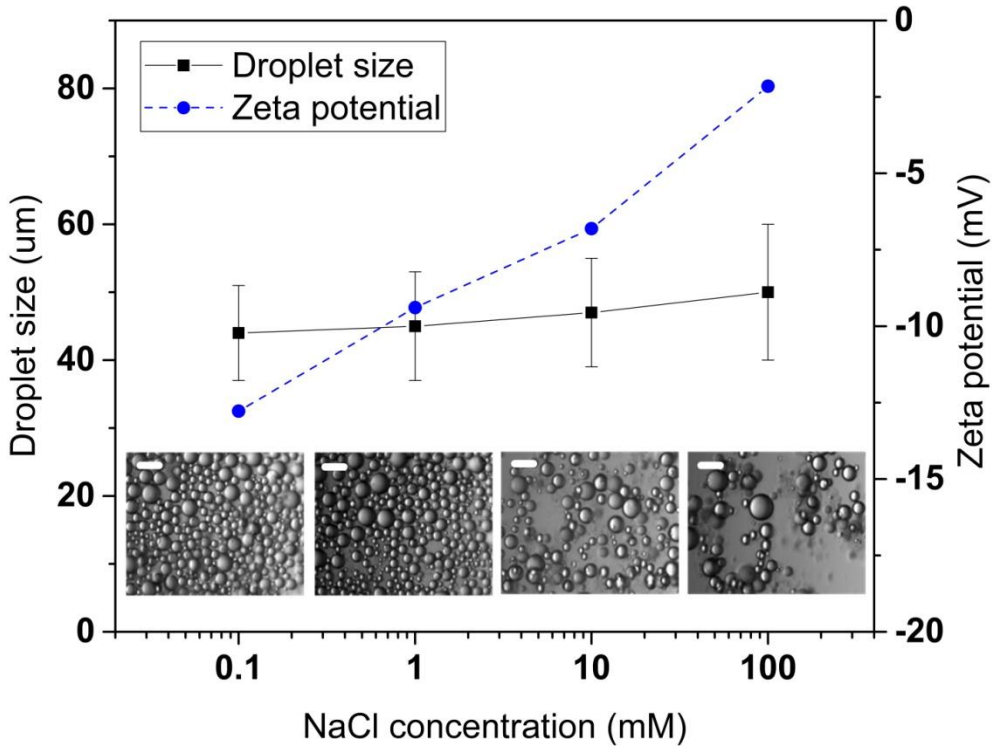

(ii)

Figure 30. (i) Digital pictures of vials containing emulsions at cellulose concentration of 1.9% (NaCl concentrations from left to right are 100, 10, 1, and 0.1 mM respectively); (ii) optical microscopic images, droplet sizes of milled cellulose particles-stabilized emulsions and zeta potential of milled cellulose at different ionic strengths.

The Pickering emulsions stabilized by 1.9% of milled cellulose were dispersed in solutions with pH = 3~9. The digital pictures of vials containing emulsions, microscopic images, droplet size of emulsions and zeta potential of milled cellulose at different pH conditions were presented in **Figure 31**. The zeta potentials of milled cellulose remained negative in the whole studied pH range, with values ranging from -6.7 mV (at pH 3) to -9.4 mV (at pH 7). The physical stability of milled cellulose particles stabilized emulsions did not appear to be responsive to changes in pH conditions. Only a slight increase in the

droplet size of emulsions was observed under pH of 3 and 9. All the samples prepared were very stable for over a month. The remarkable stability of these emulsions against acid and alkaline conditions could be due to the formation of cellulose networks in the continuous phase, which increased the viscosity of system, thereby physically limiting droplet interactions. This notion concurs with results from previous study of cellulose nanocrystals stabilized Pickering emulsions. The long cellulose nanocrystals were found to promote formation of networking system, which acted as a mechanical barrier to enhance emulsions stability against coalescence (*25*). It is notably that the exceptional stability of milled cellulose stabilized emulsions under tested pH conditions was higher than many emulsion formulations, thus offering a new formulation which might be stable under harsh conditions of gastric environment (*193*).

(i)

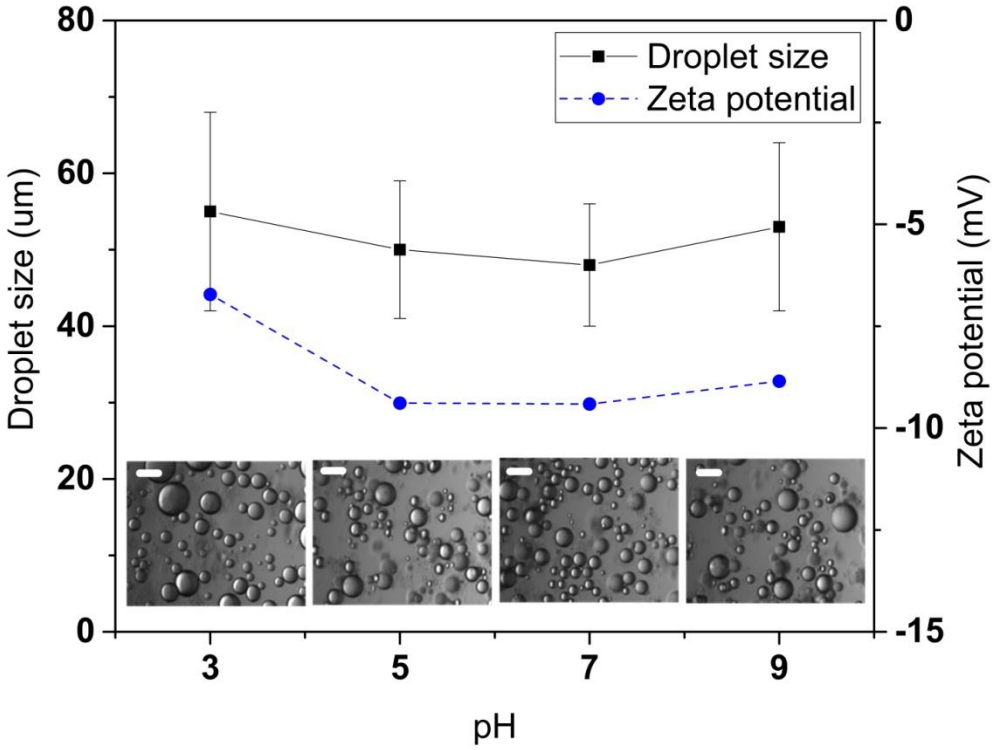

(ii)

Figure 31. (i) Digital pictures of vials containing emulsions at cellulose concentrations of 1.9% (pH values from left to right are 3, 5, 7, and 9 respectively); (ii) optical microscopic images, droplet size of milled cellulose stabilized emulsions and zeta potential of milled cellulose at different pH conditions.

4.3.4. Rheological properties of emulsions

The dynamic rheological measurements were conducted to test the viscoelastic response of milled cellulose stabilized Pickering emulsion with oil/water ratios of 3:7, 4:6, 5:5 and 6:4, respectively. Under the limit of linear viscoelastic region, the dynamic frequency measurements were carried out to investigate the frequency dependence of the storage modulus (G') and loss modulus (G"). **Figure 32** presented the effects of oil/water ratios on the storage modulus and loss modulus of Pickering emulsions. Both G' and G" showed only a slight dependence on the angular frequency. G' was much larger than G"

over the entire frequency range, suggesting that the behavior of the emulsions were predominantly elastic and there was a three-dimensional weak gel network in the emulsions (*128*). The network was mainly attributed to the bridges formed from packing of emulsion droplets stabilized by the milled cellulose particles. Similar phenomena were observed in cellulose nanocrystals stabilized Pickering emulsions, where longer cellulose nanocrystals were involved in the network formation between oil droplets (*25*). When the oil/water increased from 3:7 to 4:6, a significant decrease in the G' was observed, indicating a reduction in the gel strength. And further increase the oil/water ratio to 5:5, a moderate decrease of G' was found. However, increasing oil/water ratio from 5:5 to 6:4 led to a slight increase in the G' value. With adjusting the oil/water ratio, the rheological properties of milled cellulose stabilized Pickering emulsions were affected by the oil volume fraction and available particles. Cellulose nanorods with relatively long length tended to entanglements and bridges between droplets (*25*), which was the main cause for the formation of gel system in milled cellulose stabilized Pickering emulsions, thus explaining the high gel strength at low oil/water ratio of 3:7. Increasing the oil/water ratio could also improve the Pickering emulsion gel strength due to the close proximity between emulsion droplets and a tighter packing density with high oil volume (*192*). As the result, the rheological property of the emulsion was dominated by the oil fraction at relatively higher oil/water ratio of 6:4.

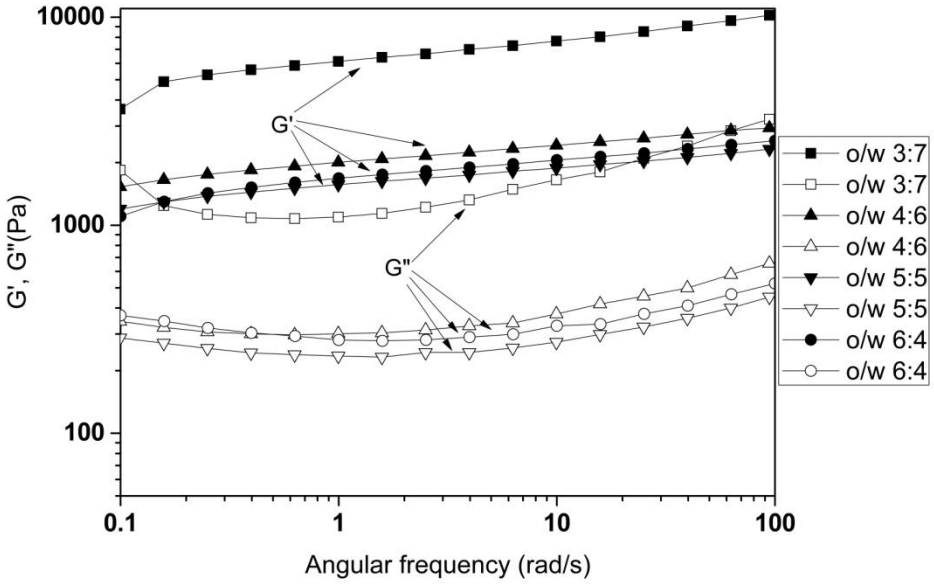

Figure 32. Dynamic frequency flow curves for emulsions stabilized by milled cellulose particles with different oil/water ratios.

4.4. Conclusions

Oil-in-water Pickering emulsions with long-term stability against coalescence could be stabilized solely by milled cellulose particles. This is the first report of preparation of stable Pickering emulsions using milled cellulose alone. These milled cellulose particles consisted of rod-like particles and exhibited efficient emulsifying ability. The emulsion droplet size was influenced by the cellulose concentration in the aqueous phase since the interfacial area was related to the amount of available cellulose particles. No creaming effects were observed when the cellulose concentration in the water phase was higher than 0.1% wt. And the resulting emulsions were stable at salt concentration as high as 100 mM and a wide range of pH conditions ranging from 3 to 9. The benign stability of milled cellulose stabilized Pickering emulsions could be due to their rod-like shape, which facilitated the formation of entangled networking systems among the emulsion

droplets. This milling process provides great potential to effectively utilize these sustainable biomolecules to build stable emulsions with applications in food, cosmetic and pharmaceutical industries.

CHAPTER 5 STABILITY AND CHARACTERIZATION OF CURCUMIN-ENCAPSULATED MILLED CELLULOSE STABILIZED PICKERING EMULSIONS

5.1. Introduction

Although the biological benefits of a variety of lipophilic compounds have been identified, their dose efficacies of oral administration are often limited since they have low stability against degradation and low bioavailability (*132-136*). By affecting gastric transit, intestinal permeability or drug metabolism, lipid-based oral delivery systems are perhaps most widely used strategy to improve the bioavailability of poorly water-soluble, lipophilic compounds through enhancing drug solubilization and dissolution in the gastrointestinal tract (*194, 195*). Encapsulation of these lipophilic functional compounds using emulsion system is a commonly used formulation approach in food, cosmetic and pharmaceutical industries (*134, 135*). Extensive studies have been conducted to evaluate the encapsulation, oxidative stability and release of bioactive compounds in conventional emulsions stabilized by small molecular weight surfactants or biopolymers. Nowadays solid particle stabilized emulsions which called Pickering emulsions, have exhibited benign stability against coalescence and Ostwald ripening (*4, 105*). Although the unique physicochemical and mechanical properties of Pickering emulsions have been extensively investigated, characterization of stability and release of functional lipophilic compounds encapsulated in these emulsions is still limited. Only some studies have studied the role of silica stabilized Pickering emulsions in digestion behavior under simulated digestion conditions, delivery and release of bioactive compounds (*144, 145, 196*). However, oral consumption of formulations containing silica nanoparticles has

gained some attention regarding its potential deleterious effects to human health. Silica with particles sizes of 5-50 and 50-500 nm have been reported to be likely to result in enhanced exposure of the intestinal epithelia to these particles which could have ramifications to health (*169*).

Recently, various particles derived from cellulose have been fabricated to stabilize Pickering emulsions with superior physical and chemical stability (*25, 50*). These particles include microfibrillated cellulose, moderately degraded microfibrils (*49*), cellulose nanocrystals, well-define naocrystalline particles from acid hydrolysis process of cellulose (*173*) and hydrophobically modified cellulosic material, such as acetylated nanofibers (*48*), carboxymethylated cellulose (*197*), or sililated microfibrils (*17*). Media milling process is a simple physical method, which has been used to produce various nano/submicrometer particles (*52, 54*). And the particle size of cellulose has been proved to be effectively reduced by media mill (*60*). Coming from natural biomass-based materials under physical modification treatment, milled cellulose particles could avoid the presents of hazardous contamination when using chemical methods. Hence, milled cellulose stabilized Pickering emulsions have the high potential as edible delivery systems to encapsulate, protect and release bioactive lipophilic compounds with application in food and pharmaceutical industries. To the best of author's knowledge there is no reported study that reveals the emulsifying capacity of milled cellulose, the encapsulation ability, stability and in vitro digestion aspects of milled cellulose stabilized Pickering emulsions.

In this work, milled cellulose particles were prepared via ball milling process, which then were used to stabilize a Pickering emulsion delivery system. As bioactive lipophilic

regent, curcumin has exhibited significant anti-cancer and anti-inflammatory properties (*198*), However, with low water solubility and stability, the systemic bioavailability and pharmacokinetics of curcumin were extremely low (*199-202*). Hence, emulsion-based delivery systems have been developed to improve the effectiveness of oral delivery of curcumin (*153, 203, 204*). To evaluate the encapsulation, protection and release capacity of milled cellulose stabilized Pickering emulsion delivery system, curcumin was encapsulated in the emulsion as a model lipophilic compound. And the structure of emulsions, the stability of encapsulated curcumin as well as the emulsions responsiveness to the simulated small intestinal digestion environments were characterized. For enhanced understanding of the stability of the emulsions under simulated digestion conditions, the structure of emulsions were analyzed using microscopic and fluorescence imaging, and the distribution of curcumin between pellet and supernatants was analyzed.

5.2. Materials and methods

5.2.1. Materials

Sigmacell cellulose (size of ~20 μm) was purchased from Sigma-Aldrich (St. Louis, MO). The soy bean and canola oil was purchased from a local supermarket. A Neobee Medium chain triglyceride (MCT) sample was requested from Stepan Company (Northfield, IL). Curcumin was a gift from Sabinsa Corporation (Piscataway, NJ), which contains 85% curcumin, 11% demethoxycurcumin and 4% bisdemethoxycurcumin (*153*). Sodium taurodeoxycholate (NaTDC) was purchased from CalBiochem (La Jolla, CA). Phosphatidylcholine (PC75 rapeseed lecithin) was a gift from the American Lecithin Co. (Oxford, CT). Lipase type II from porcine pancreas, potassium dihydrogen phosphate, calcium chloride, sodium chloride, and bile salt were purchased from Sigma-Aldrich (St. Louis, MO).

5.2.2. Media-milling treatment

The milling process was conducted using the same procedure as in section 4.2.2. Milled cellulose suspension with milling time of 15 h was used to prepare Pickering emulsion. And the accurate weight of milled cellulose in the final suspension was determined using a moisture test.

5.2.3. Preparation of curcumin-loaded Pickering emulsions

Curcumin was first dissolved in MCT, soy bean, canola oil at 8 mg/ml at 120℃ to reach a transparent solution. Then the oil phase containing dissolved curcumin was mixed with fresh prepared milled cellulose suspension at a water/oil ratio of 1:1 (v/v) and the curcumin-loaded Pickering emulsion was formed using an IKA Ultra-Turrax T25 homogenizer operating at 10,000 rpm for 2 min. The cellulose concentration was expressed as weight content relative to the water phase based on the prior moisture test. Controls emulsion sample was prepared by mixing aqueous phase containing 1% Tween 80 and Span 80 with oil phase containing dissolved curcumin at oil/water ratio of 1:4 using an IKA Ultra-Turrax T25 homogenizer operating at 14,000 rpm for 3 min.

5.2.4. Microscopy characterization of curcumin-loaded Pickering emulsions

Samples microstructures were assessed using the method described in section 3.2.4.

5.2.5. Curcumin concentration and its storage stability in emulsions

The concentration of curcumin encapsulated in the Pickering emulsion was determined using the following method. 200 μL of emulsion was thoroughly mixed with 9 ml of methanol. The mixture was then centrifuged at 14,000 rpm for 10 min. The concentration of curcumin in the supernatant was further diluted to an appropriate concentration using methanol and analyzed by HPLC. The storage stability of curcumin in the emulsion was determined as a function of storage time. Emulsion samples were stored at room temperature in dark for 30 days. And curcumin concentration in the

samples at different storage periods were measured using the same method described above.

5.2.6. *In vitro* lipolysis digestion of emulsions

The *in vitro* lipolysis digestion of emulsions was evaluated using a pH-stat lipolysis model, which is a widely used method to simulate the digestion of emulsions and predict the *in vivo* solubilization of lipophilic compounds in small intestinal (*138, 157*). With the digestion of lipids, the lipolysis products and the bile salts, endogenous phospholipids in the digestion media will form micelles and mixed micelles, which will solubilize the lipophilic compounds and make them possible to be absorbed (*138*). Since the concentration of bile salts and phospholipids in the small intestine in the fed state will be higher than in the fasted state due to the response to the consumption of food, two lipolysis buffers were prepared to simulate the different digestion environments in the fasted and fed states (**Table 8**).

Table 8 Formulation of lipolysis buffers in the fasted and fed states

	Fasted state	Fed state
Tris maleate (mM)	50	50
NaCl (mM)	150	150
$CaCl_2 \cdot 2H_2O$ (mM)	5	5
NaTDC (mM)	5	20
Phosphatidylcholine (mM)	1.25	5

The pH-stat lipolysis model was conducted according to the following procedure.

Pancreatin extract was prepared by adding 1 g of pancreatin into 5ml lipolysis buffer and stirred for 15 min. The mixture was centrifuged at 2,000 rpm for 15 min and the supernatant were collected, stored on ice. The pancreatin extracts used were fresh prepared every day. Emulsion samples containing 250 mg oil phase was mixed with 9 ml of lipolyis buffer and kept at 37℃ for 10 min under continuously stirring. Then the pH of resultant mixture was adjusted to 7.5 using 0.25 M NaOH solution. Finally, 1 ml of ice-chilled pancreatin extract was added in to initiate the lipolysis. During the digestion process of 2 h, the pH of digestion media was maintained at 7.5 ± 0.1 by adding 0.25 M NaOH and the volume of added NaOH solution was recorded as function of time. During the digestion process, 50 µl digestion media were pipetted out and viewed under optical and fluorescent microscope at digestion time of 0, 30, 120 min. And the digestion of emulsion stabilized by 1% Tween 80 and Span 80 was also conducted as control sample.

The amount of NaOH added through the lipolysis experiment was assumed to equal to the amount of free fatty acids (FFAs) generated by lipolysis of triacylglycerols. The %FFA released could be calculated based on the previously developed method (*152*).

Upon completion of the lipolysis digestion, the lipolysis media were subjected to ultracentrifugation for 40 min at 4°C and 40,000 rpm, which would be separated into a precipitated pellet on the bottom, an aqueous phase in the middle and sometimes an oily phase on the top. The amount of curcumin precipitated in the pellet was analyzed by suspending the pellet in 10 ml methanol, centrifuging at 4500 rpm for 15 min. The supernatants were diluted into suitable concentrations and injected into HPLC. The middle aqueous phase containing formulated curcumin micelles was collected and the volume was recorded. The concentration of curcumin in the micelle phase was analyzed

using HPLC. The bioaccessibility (%) of curcumin was calculated based on the equation (8).

5.2.7. High-performance liquid chromatography (HPLC) analysis

The curcumin concentration in the samples was analyzed using the same method as in section 3.2.9.

5.2.8. Statistical Analysis

Experiments were conducted at least in duplicate, and results were expressed as the mean ± standard deviation (SD).

5.3. Results and discussion

5.3.1. Characterization of curcumin-loaded Pickering emulsion

Pickering emulsions with different lipid phases were stabilized by milled cellulose from a milling process. Based on the moisture test conducted after the milling process, the cellulose concentration in the aqueous dispersion was 3.7% (w/w). The oil/water ratio of the emulsions used was 1:1. The microscopy and fluorescence images of Pickering emulsions containing MCT, soy bean and canola oil were presented in **Figure 33**. The droplets of Pickering emulsion with MCT, canola and soy bean oil had mean diameter of 46, 27 and 41 μm, respectively. Emulsion of MCT oil had similar droplet size as emulsion with soy bean oil, which was slightly higher than that of emulsion form by canola oil. These results indicated that the formation of emulsions stabilized by milled cellulose could be impacted by the type of oil phase used. The brighter regions in the fluorescence images of emulsions represented the oil droplets with dissolved curcumin owing to the emission of fluorescence from curucmin under excitation. It was notably that no apparent needle-like crystals was detected in all the emulsions, which suggested that curcumin did not precipitate after encapsulated in the these emulsions. The emulsions stabilized by milled cellulose possessed benign stability with no curcumin precipitation

and change of droplet sizes observed in the emulsions after the long-term storage of one month.

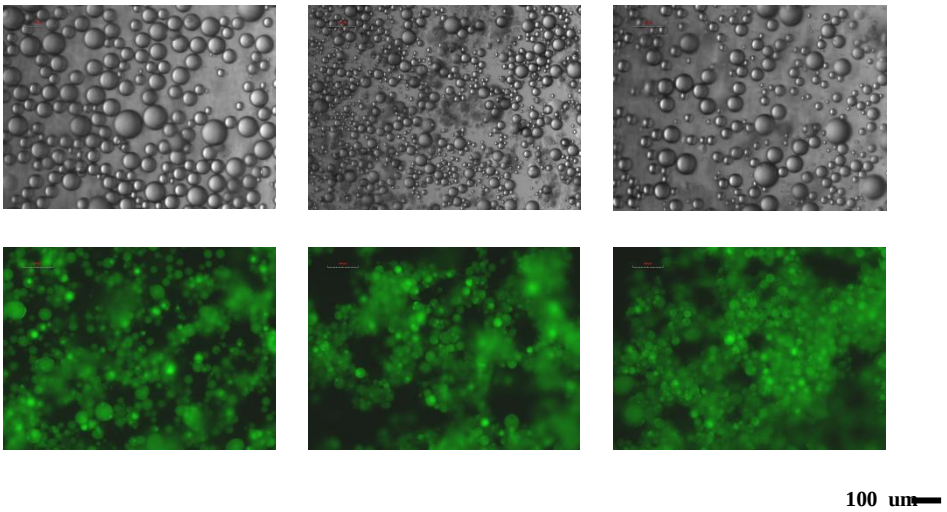

Figure 33. Microscopic images of curcumin encapsulated emulsions stabilized by milled cellulose. From left to right: MCT, canola, soy bean.

5.3.2. Stability of curcumin in milled cellulose stabilized Pickering emulsion

Curcumin has a high sensitivity to environmental conditions, which is unstable in various solvent conditions. In PBS of pH 7.2, more than 85% of free curcumin were found to degrade within 30 min of incubation (*165*). And around 80% of curcumin degraded when dissolved in water with 3% v/v of methanol (pH 5.7) for 90 min (*144*). The retention of curcumin in the milled cellulose stabilized Pickering emulsions as a function of time was depicted in **Figure 34**. Curcumin in Pickering emulsions with different oil phases exhibited similar degradation pattern. And the degradation rate was not significant different for emulsions containing different oil phases. Curcumin encapsulated in these Pickering emulsions exhibited improved stability and higher retentions. Encapsulated in emulsions with MCT, canola and soy bean oil, 64.3%, 50.8%, and 56.0% of curcumin were retained in the emulsions at the end of 30 days' storage,

respectively. It is notably that the stability of curcumin is much higher in these Pickering emulsions than in other encapsulation systems. Studies showed that approximately 40% of encapsulated curcumin was degraded within 20 h and less than 200 min of storage in sodium dodecyl sulfate micelles and liposomes (*205*, *206*). The predominant enhancement in the curcumin stability within this Pickering emulsion system indicates its high potential as functional ingredient encapsulation system with applications in food, cosmetic, and pharmaceutical industries.

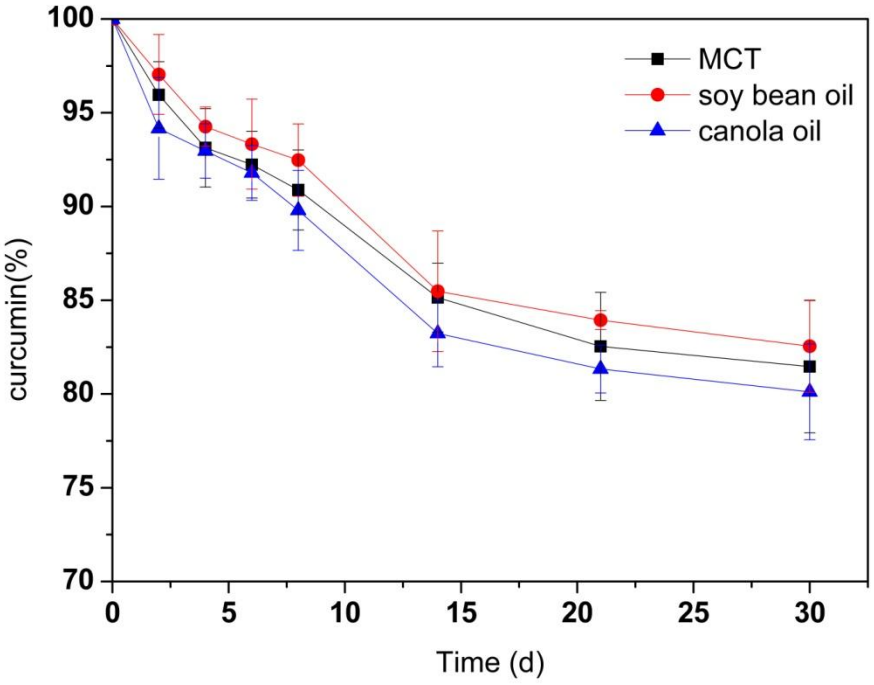

Figure 34. Stability of curcumin in Pickering emulsion with different oil phases.

5.3.3. Influence of oil type on *in vitro* lipid digestion

Curcumin encapsulated in milled cellulose stabilized Pickering emulsions were produced with different types of lipids. The influence of carrier oil type on rate and extent of lipid digestion was quantified using a pH-stat lipolysis model by monitoring the amount of free fatty acids (FFAs) released over time (**Figure 35**). The changes in the structure of emulsions during digestion process were presented in **Figure 36**. The nature of carrier oil exhibited a major impact on the kinetics of lipid digestion. MCT is mainly made of saturated medium chain fatty acids, caprylic (C8:0) and capric (C10:0) triglycerides. Soy bean and canola oils consist of unsaturated long chain fatty acids, including oleic acid (C18:1) and linoleic acid (C18:2). Compared to emulsions with soy bean and canola oil, the released of FFAs for emulsions with MCT oil was much faster and higher, with almost complete conversion to monoglyceride and fatty acids after 40 min of digestion. This is consistent with results obtained in previous study (*137*). While the digestion of emulsions with soy bean and canola oil was far from complete at the end of 2 h digestion process. The susceptible of MCT to digestion could be attributed to several factors including solubility, hydrophilicity and phase behavior. At physiological pH, medium chain fatty acids (apparent pKa 6.8 (*207*)) could be ionised to a larger extent than long chain fatty acids (apparent pKa 8 ~ 8.5 (*207*)), thus enhancing solubility and amphiphilicity. As the result, the aqueous solubility of medium chain lipolytic digestion products is significantly higher than that of long chain lipolytic digestion products, which could dissociate from the digesting interface rapidly and protrude into digestion buffer easily to either be incorporated into micellar structure or may precipitate as calcium or sodium soaps. This is in contrast to digestion of lipid with long chain fatty acids, where concentration of bile salt and solubilisation capacity of digestion media are crucial to

remove long chain FFAs. The lower extent of lipolysis for emulsions with soy bean and canola oil might be due to not enough calcium or bile salts available to remove the long chain FFAs produced during digestion, which would accumulate at lipid droplet surface to inhibit the function of lipase (*208*). During the lipolysis process of emulsions with MCT, a significant amount of needle-like fatty acid crystals were observed to precipitate out (**Figure 36**), which could be the precipitation of calcium or sodium soaps. While this kind of crystals was not existed in digestion media of emulsions with soy bean and canola oil.

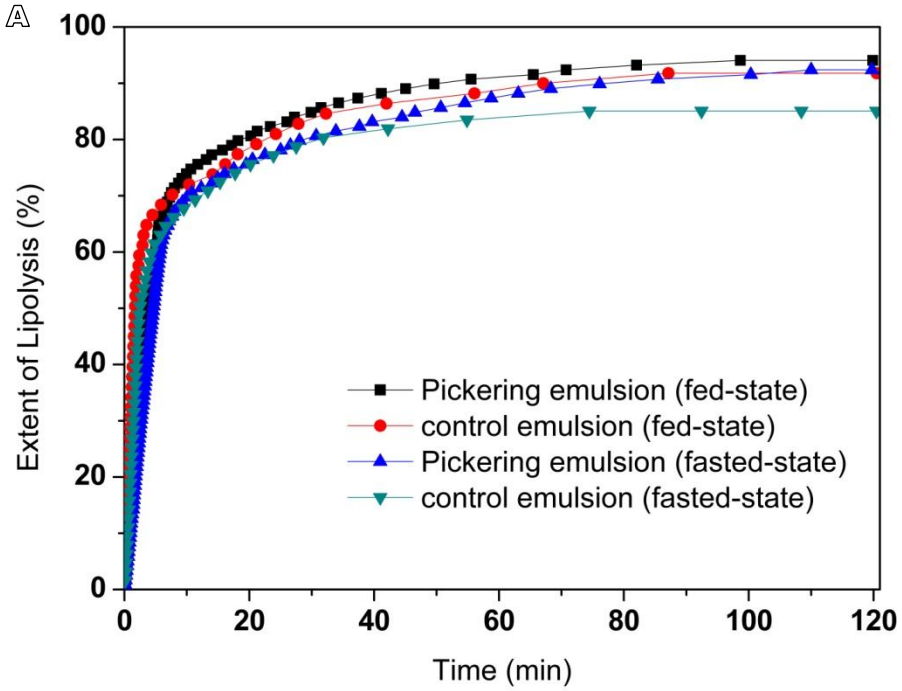

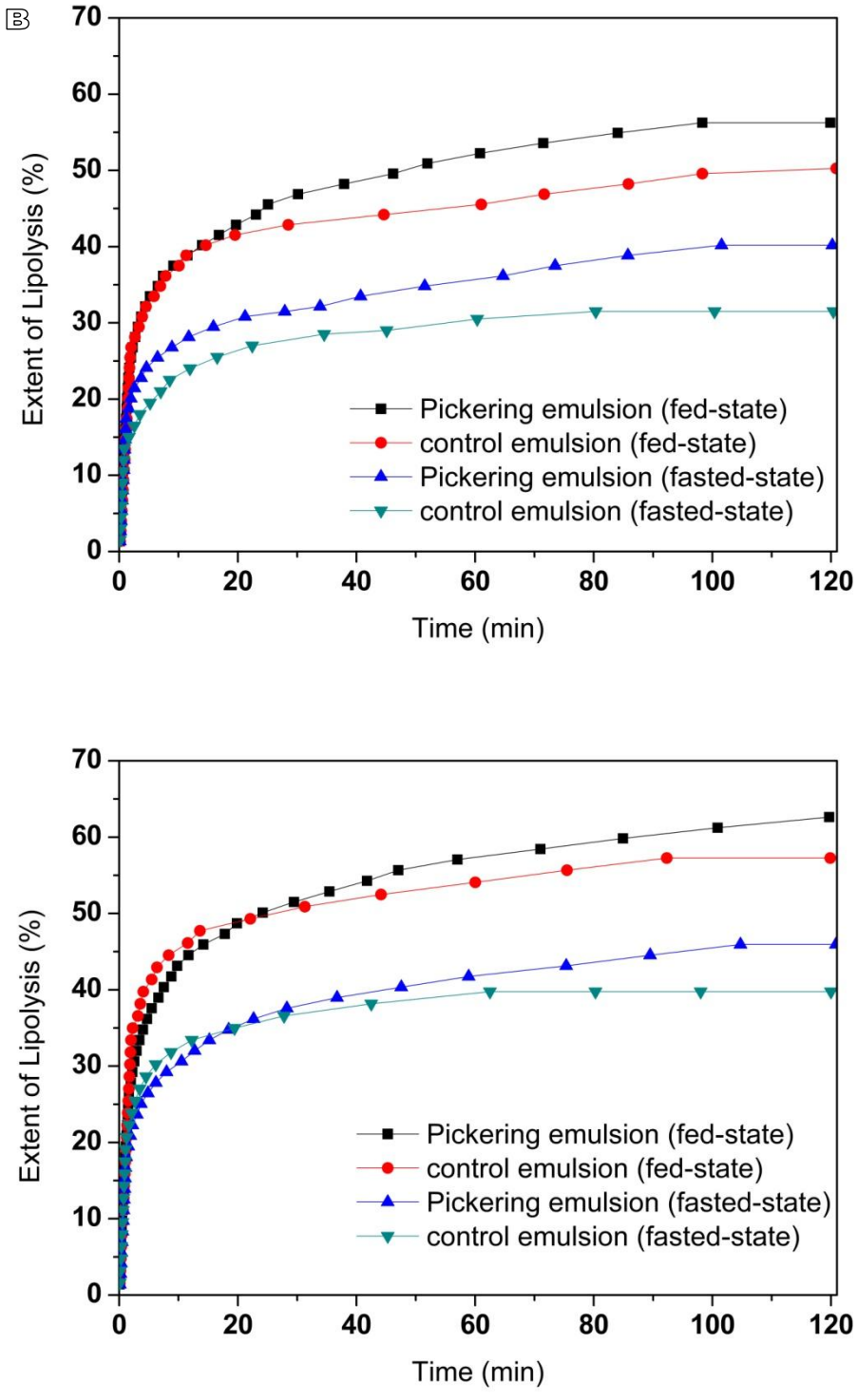

Figure 35. Release kinetics of curcumin from Pickering emulsion containing different oil phases during *in vitro* lipolysis. (A) MCT, (B) canola, (C) soy bean.

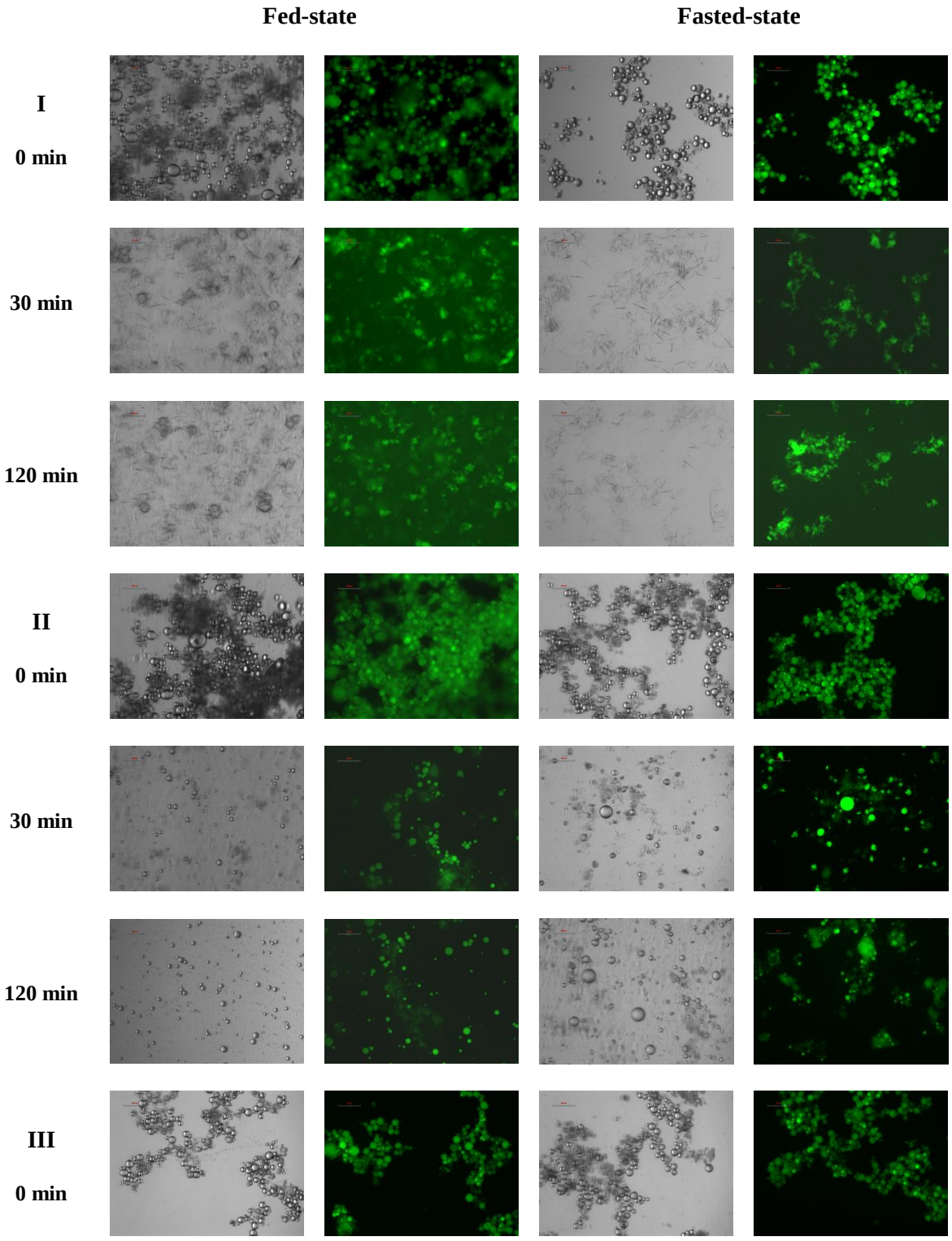
Fed-state
Fasted-state
I
0 min
30 min
120 min
II
0 min
30 min
120 min
III
0 min

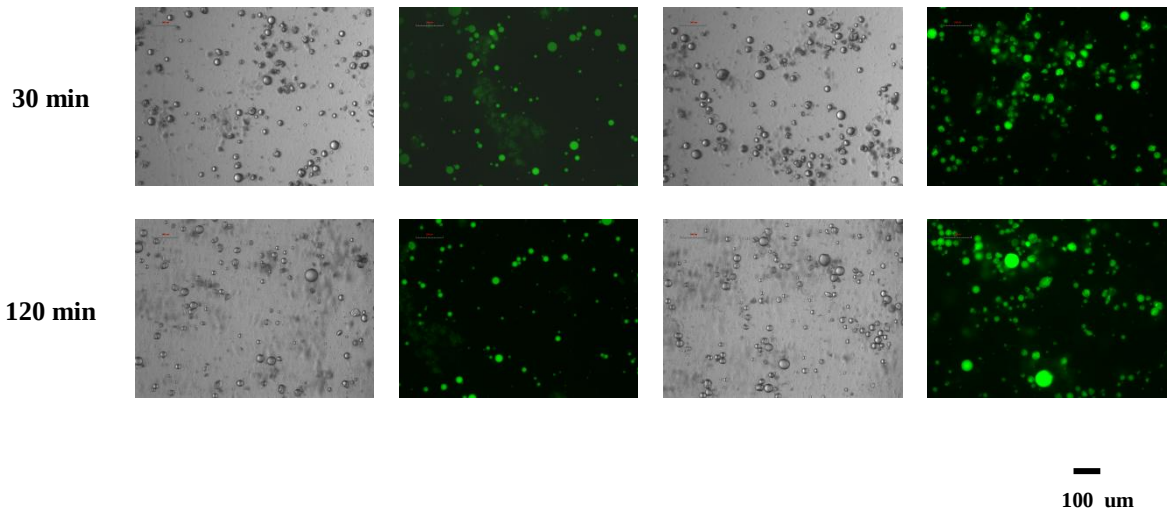

Figure 36. Microscopic and fluorescence image of Pickering emulsion containing different oil phase incubated in *in vitro* lipolysis at different time. (I) MCT, (II) soy bean, (III) canola.

5.3.4. Influence of digestion buffer on *in vitro* lipid digestion

The influence of digestion buffer on digestion of Pickering emulsions was characterized by monitoring the release of FFAs over time under simulated fasted and fed conditions. At the beginning of digestion of Pickering emulsions containing canola and soy bean oil, a continuous increase in release of fatty acid was observed as lipolysis proceeded. After 10 min's digestion, the rate of lipolysis decreased, which might result from the saturation of phospholipid/bile salt micelles with lipolytic products. At the end of 2 h digestion process, the extent of FFAs released under fed-state conditions was approximately 1.5-fold higher than that observed under fasted-state conditions. In both cases, long chain lipid was partially digested over 2 h of digestion under fasted- and fed-state conditions. The increased rate and extent digestion of long chain lipid under higher bile salt concentration is in consistent with results obtained in previous studies (*208, 209*). In the presents of colipase, bile salts could improve the digestion of long chain lipids by enhancing the removal of poorly water-soluble lipolytic compounds from

the oil/water interface through solubilisation (*209*). The effect of phospholipids on the activity of pancreatic lipase/colipase is affected by a number of factors, such as concentration of substrates, each amphiphile, the ratio of colipase and inhibitors present (*210*). In the present study, the net effect of bile salt/phospholipid addition at a fixed ratio was found to stimulate long chain lipids digestion. **Figure 35** presented the fatty acid titration profiles of Pickering emulsions with MCT oil under simulated fasted- and fed-state conditions. In contrast to digestion of emulsions with long chain lipid, the digestion profiles of emulsions with medium chain lipids under fasted-state were similar to fed-state conditions.

After ultracentrifugation, the digests of emulsions containing long chain lipid were separated into an upper oily phase, an aqueous phase and a precipitated pellet phase. And aqueous phase was separated into two layers: an opaque paste-like layer and a clear layer in digests of emulsions containing canola and soy bean oil under fed conditions (**Figure 37**). As digestion of emulsions with MCT was effectively complete and independent of bile salt concentration, the lipolytic products were separated into an aqueous phase and a pellet fraction, without an oily phase, post ultracentrifugation (**Figure 37**). The pellets principally contained insoluble crystalline calcium soaps and bile salts. The oil phase mainly contained undigested triglyceride and diglyceride. With the interaction with surface active bile salts, the lipolytic materials (mainly monoglycerides and fatty acids) would produce multilamellar liquid crystalline phases, which could gradually detach from the surface of the oil droplets to form multilamellar vesicles. These multilamellar vesicles then underwent a transformation initially to first unilamellar vesicles and later to mixed micelles upon the bile salt interaction (*211*). The aqueous phase obtained after *in*

vitro digestion contained both mixed micelles and unilamellar liquid-crystalline vesicles, which composed of bile salts, fatty acids, monoglycerides and phospholipids (*212*). However, the solubilization capacity of micellar and vesicular species were significantly affected by the lipid species and buffer conditions. The overall solubility of curcumin in the aqueous phase under different conditions were quantified and characterized later in this study.

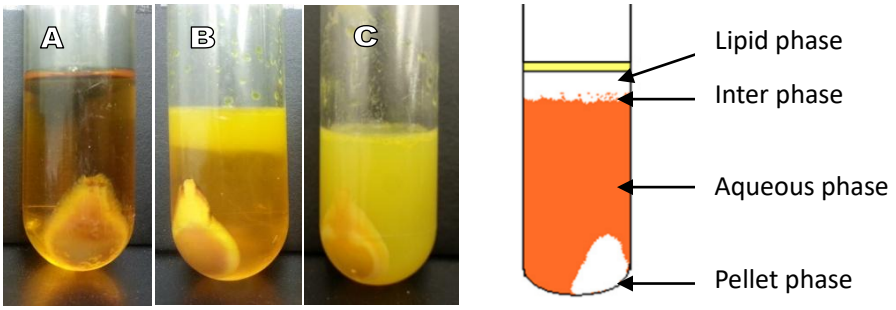

Figure 37. Different phases present after ultracentrifugation of lipolysis samples. (A) Pickering emulsion containing MCT oil under fed-state lipolysis, (B) Pickering emulsion containing soy bean oil under fed-state lipolysis, (C) Pickering emulsion containing soy bean oil under fasted-state lipolysis.

5.3.5. Influence of emulsion type on *in vitro* digestion

The *in vitro* digestion of curcumin encapsulated in milled cellulose stabilized Pickering emulsions and control emulsions containing same amount of curcumin were studied to using a pH-stat lipolysis model. The droplet size of conventional emulsions stabilized by stabilized by Tween 80 and Span 80 were around 2~30 um (**Figure 38**), which were smaller compared to Pickering emulsions. The digestion of conventional emulsions showed a more rapid increase in the hydrolysis of triglyceride in the first 10 min followed by a slower increase than the corresponding Pickering emulsions (**Figure 35**). The faster initial digestion rate of emulsions stabilized by surfactants than the

corresponding Pickering emulsion samples could be attributed to the increase in the surface area of the lipid exposed to the lipase (*213*). The extent of lipolysis of Pickering emulsions stabilized milled cellulose was higher compared to conventional emulsions stabilized by small molecular surfactant with the same lipid phase, except for emulsions containing MCT oil, which reached complete hydrolysis. The deviations in the digestion profile of Pickering and conventional emulsions might be due to the differences in the interfacial properties of emulsifiers. Non-ionic surfactants have been reported to be more surface-active than lipase, which could inhibit the binding of lipase to oil droplet surface (*214*). Addition of bile salts to the digestion system was found to restore lipase activity (*215*). When Span/Tween-stabilized emulsions were incubation with lipolysis buffer, there appeared to be some coalesced droplets present (**Figure 38**), which could due to the displacement of some Span/Tween molecules from the droplet surfaces by bile salts in the buffer, thus enhancing the binding between lipase and partially bile salts coated droplets. This could explain the rapid digestion of Span/Tween-stabilized emulsion during the first few minutes of lipolysis. Then the digestion rate reached a fairly constant value after certain time, even though not all lipids had not been digested, which might be attributed to the inhibition effect of Span/Tween molecules as some bile salts interact with lipolytic products to form micellar structure. Also, the released fatty acids during lipolysis would reduce the lipase activity (*216*). As surface active molecules, fatty acids would compete for the oil-water interface with lipases, which limited the contact between lipase and emulsified lipids. The rate of lipolysis would rely on access of lipase to the oil droplets interface as well as the remove of surface active molecules from the interface, which original existed in the system or formed during lipolysis. These results suggested

that even though the digestion of lipid phase in Span/Tween stabilized emulsions were faster than in the corresponding Pickering emulsions stabilized by cellulose due to larger surface area, the total extent of lipolysis of Pickering emulsions was higher than conventional emulsions due to the inhibition effect from the non-ionic surfactants and rapidly accumulated fatty acids.

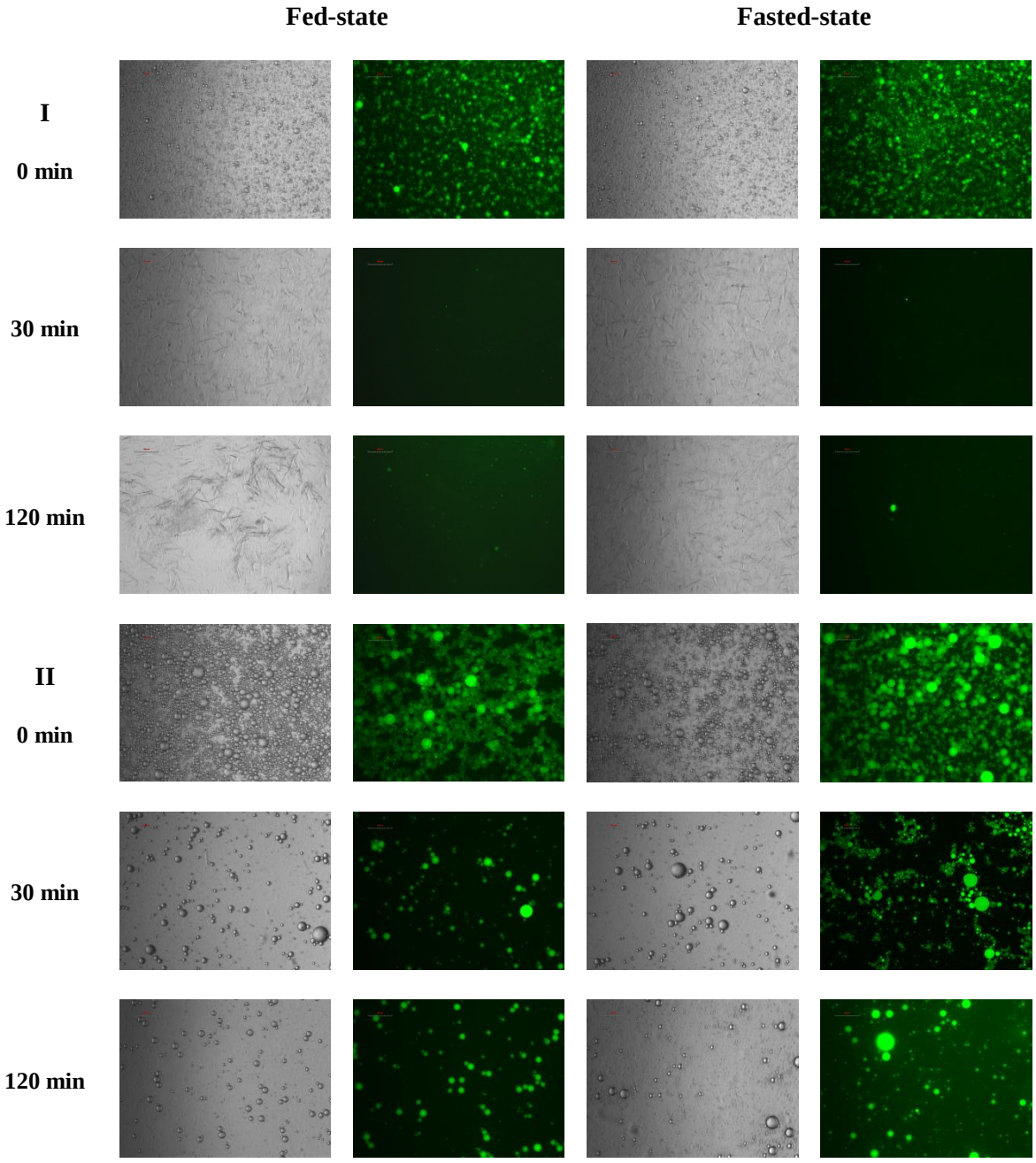

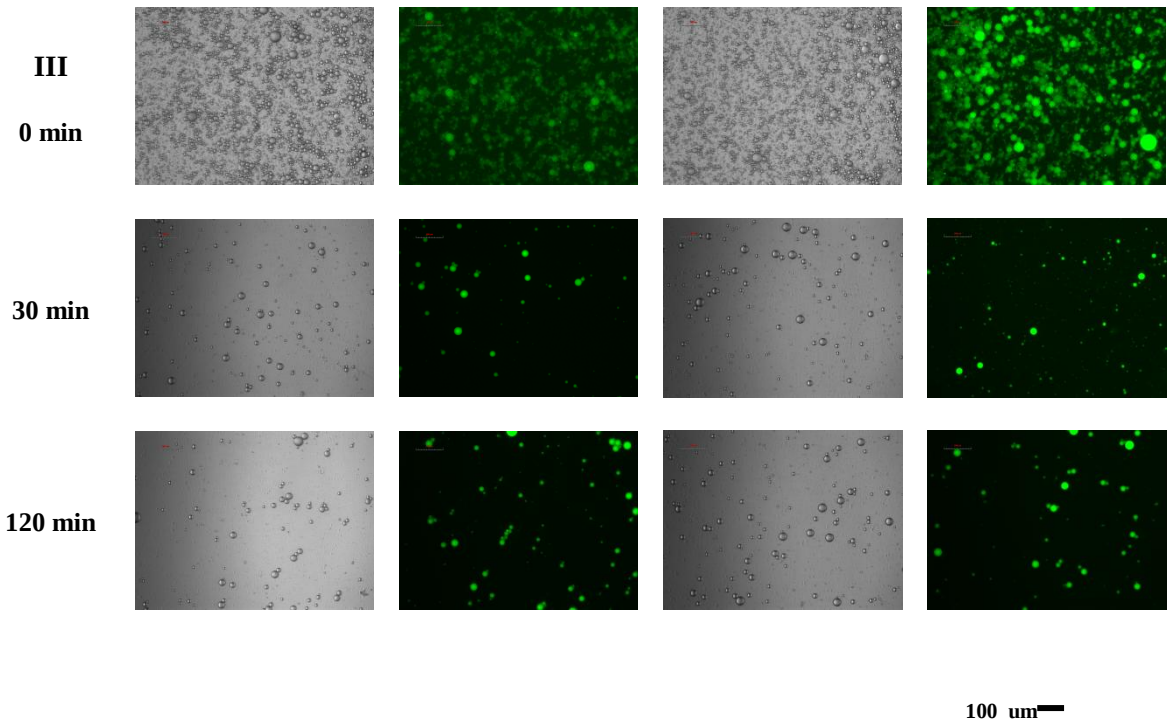

Figure 38. Microscopic and fluorescence image of control emulsion containing different oil phase incubated in *in vitro* lipolysis at different time. (I) MCT, (II) soy bean, (III) canola.

5.3.6. Influence of oil type & oil droplet size on *in vitro* bioaccessibility

The solubility and dissolution rate of lipophilic compounds could be significantly improved after administrated in a lipid formulation compared to a simple suspension formulation. During lipid digestion, lipophilic compounds are trafficked from digesting triglyceride droplets, via lipolytic products, monoglycerides and diglycerides exist on droplet surface, through to the dispersed vesicular and micellar phases from where absorption is thought to occur (*217*). The summary of extent of lipolysis and bioaccessbility of curcumin in Pickering emulsion and control emulsion were presented in **Figure 39**. The distribution of curcumin in different phases of centrifuged lipolytic buffer (oil phase, aqueous phase and precipitated pellets) was displayed in **Table 9**. The curcumin in the aqueous phase reflected the amount of curcumin incorporated into the

vesicular and micellar system, which represented the bioaccessibility of curcumin encapsulated in different emulsions. The digestion of Pickering emulsion with MCT was complete. However, the digests of MCT provided poor solubilizing conditions for curcumin. With the absence of residual oil phase to maintain curcumin in lipid phase, precipitation of curcumin from the digestion solutions was observed, leading to a significant proportion of curcumin being recovered in the pellet phase. The digestion of emulsions with long chain triglycerides (canola and soy bean oil) was incomplete and an undigested oil phase existed, resulting in retention of curcumin in the oil phase and reduced curcumin diffusion into the aqueous phase. The bioaccessibility of curucmin in Pickering emulsions with long chain triglycerides was much lower than that of in Pickering emulsions with MCT. The concentration of bile salts/phospholipids had a major influence on curcumin solubilization in the Pickering emulsion digests. The ratio of curcumin attained in the aqueous phase postdigestion was higher in digests conducted under fed state when compared to under fasted state. And the precipitation of curcumin during lipolysis in fasted state was more significant than in fed state, which might because the high concentration of bile salts/phospholipids in the lipolysis buffer of fed state enhanced the incorporation of curcumin into the micellar phase.

The trafficking of curcumin from the Pickering emulsions was related to the extent of lipolysis as the percentage of curcumin existing in the aqueous phase was well correlated with the extent of lipolysis. However, compared with Pickering emulsions, the ratio of curcumin contained in the pellet was low, and a large portion of curcumin was concentrated in the remaining undigested oil phase during the digestion of conventional emulsions with corresponding oil type. The low bioaccessibility of curcumin in

conventional emulsions might be attributed to two factors, the lower extent of lipolysis and the existing of polar compounds. With less amount of oil droplets were hydrolysis during lipolysis, less curcumin was released into the aqueous phase. Moreover, since the addition of more polar compounds (Span 20, Span 40, Span 60, Span 80 and monoolein), was found to enhance the solubility of curcumin in the oil phase (*218*), the present of Span 80 in the conventional emulsions might promote the solubilization of released curcumin into the undigested oil phase. The influence of Span 80 on curcumin solubility might also explain the low concentration of curucmin in the pellets of digested conventional emulsions.

These data suggested that the relative solubilization capacity of digested emulsions was highly dependent on the type of lipid, concentration of bile salts/phospholipids used, and that the emulsifiers utilized in the formulations was critical to effective delivery of the bioactive compounds. And milled cellulose stabilized Pickering emulsions might be a more effective approach for oral delivery of lipophilic bioactive compounds than conventional emulsions stabilized by non-ionic surfactant. However, the influence of the different emulsifiers used on the formation of colloidal species and the solubilization behavior of encapsulated lipophilic compounds during the digestion process still need to be revealed by further studies.

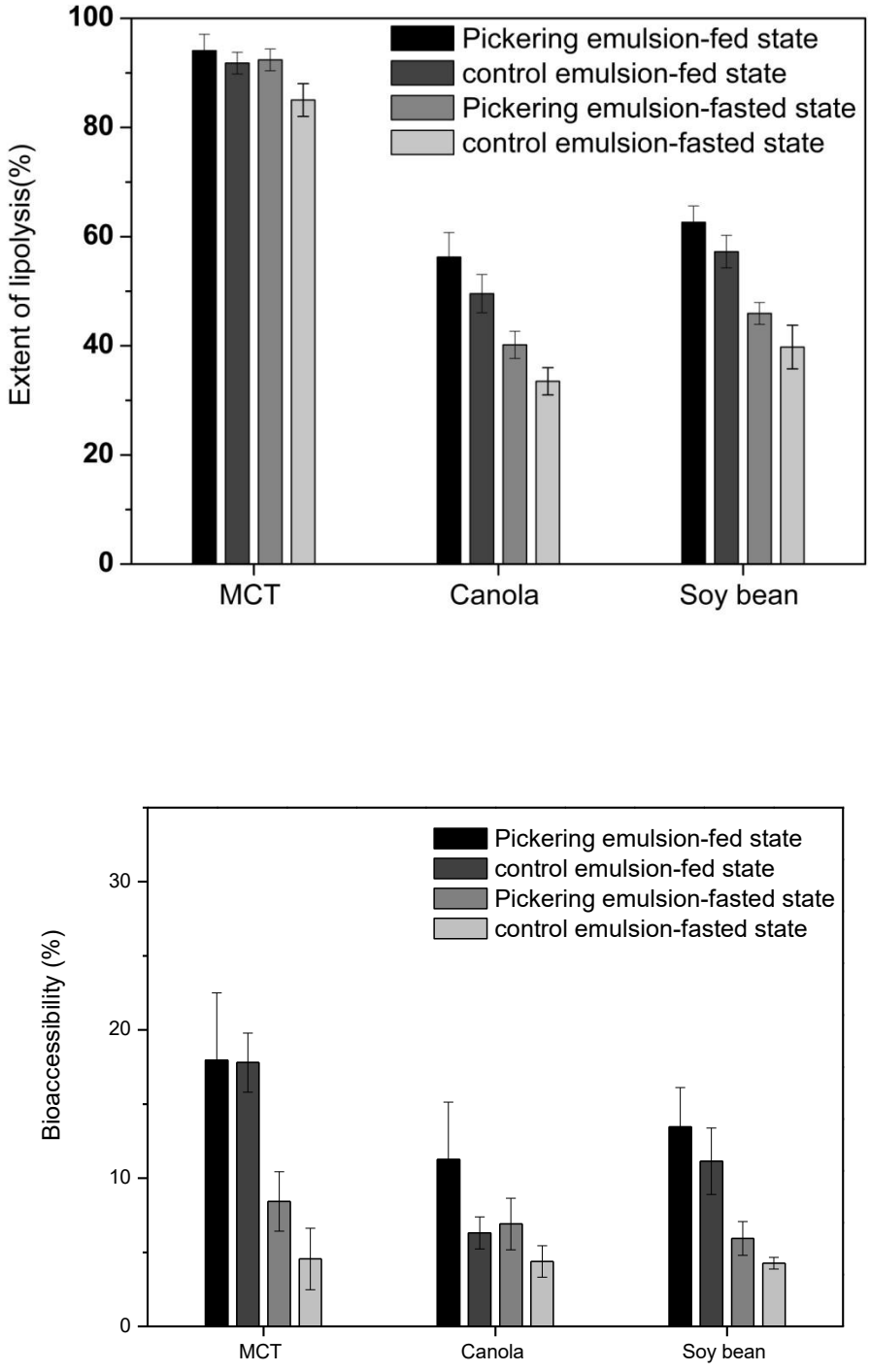

Figure 39. Extent of lipolysis and bioaccessbility of curcumin in Pickering emulsion and control emulsion.

Table 9 The distribution of curcumin in different phases of lipolysis samples after ultracentrifugation

Lipid	Fed state			Fasted state		
	% in oil	% in AP [a]	% in pellet	% in oil	% in AP	% in pellet
Pickering emulsion						
MCT	none	78.0 ± 4.5	17.5 ± 3.5	none	61.4 ± 2.0	34.8 ± 2.0
Soy bean oil	62.4 ± 5.8	13.5 ± 2.7	24.1 ± 3.1	44.0 ± 3.9	5.9 ± 1.1	50.1 ± 2.8
Canola oil	53.5 ± 6.3	11.3 ± 3.9	35.2 ± 2.4	46.5 ± 4.3	6.9 ± 1.7	46.6 ± 2.6
Convention emulsion						
MCT	none	67.8 ± 2.0	27.8 ± 2.7	none	56.6 ± 2.1	38.3 ± 2.5
Soy bean oil	72.2 ± 5.3	11.1 ± 2.2	16.7 ± 3.1	80.4 ± 4.2	4.3 ± 0.5	14.3 ± 3.7
Canola oil	81.3 ± 4.0	6.3 ± 1.1	12.4 ± 2.9	86.0 ± 2.7	4.4 ± 1.1	9.6 ± 1.6

[a]AP: Aqueous phase.

5.4. Conclusion

The current study demonstrates the potential of utilizing milled cellulose stabilized Pickering emulsions as a novel food-grade formulation for the encapsulation and delivery of lipophilic bioactive compounds. Benign stability of curcumin in the Pickering emulsions with different lipid phases was observed in a storage period of about a month. The *in vitro* digestion of Pickering emulsions was highly dependent on the type of lipids and buffer conditions used. Pickering emulsions with MCT reached complete digestion under both low and high bile salts and phospholipids conditions. However, a significant amount of curcumin precipitated during the digestion process. Digestion of Pickering emulsions with long chain triglycerides (soy bean and canola oil) was incomplete and more dependent on bile salt/phospholipid concentration. Although the ratio of precipitated curcumin decreased, their bioaccessibility was lower than that of emulsions

with MCT. Due to the inhibition effect from surface active non-ionic surfactants, the extent of lipolysis of Pickering emulsions was higher than the corresponding conventional emulsions stabilized by Span/Tween despite their higher initial digestion speed. And the bioaccessibility of curcumin encapsulated in Pickering emulsions was higher compared to in conventional emulsions. These results suggest that Pickering emulsion stabilized by milled cellulose might be a great encapsulation formulation for oral delivery of lipophilic bioactive compounds. Further studies on investigating the correlation between *in vitro* bioaccessibility and *in vivo* bioavailability of the encapsulated active ingredient in this system would be vital to reveal the delivery capacity of the Pickering emulsions *in vivo*.

CHAPTER 6 STRUCTURAL CHARACTERIZATION OF STARCH-FATTY ACID COMPLEX VIA HEAT-MOISTURE TREATMENT

6.1. Introduction

Starch consists of two glucose polymers, amylopectin which is a branched polymer, and amylose which is a linear polymer. With the presence of suitable ligands, amylose would undergo a conformation transformation from double helices to a single helix that can complex the ligands (*77*). The resulting amylose-inclusion complex, which is the so called V-amylose, has an internal hydrophobic cavity where the hydrocarbon chain (apolar part) of the ligand can reside (*77*). A variety of compounds including alcohols (*219*), fatty acids (*220*), flavor compounds (*221*) and hydrophobic organic polymers (*222*), have been shown to form V-amylose. The V-amylose complexes have exhibited potential applications, such as encapsulating sensitive flavor or bioactive ingredients (*221*, *223*), modifying rheological functionality of starch-containing products (*224*, *225*), and forming amylose nanotubes (*226*).

The formation of complex between amylose in the starch and lipid has attracted much attention in recent years. The existing of amylose-lipids complex in starch has been proved to restrict the starch swelling during cooking, decrease the accessibility and susceptibility of the starch enzyme hydrolysis (*96*, *227*, *228*). Complexation with fatty acids has been used to prepare resistant starch (*229, 230*). Studies suggested that consuming bread containing this resistant starch led to substantially lower postprandial plasma-glucose concentration and insulin response in human than eating white bread (*97*). Their potential to suppress colon carcinogenesis was verified as reduction of

azoxymethane-induced preneoplastic lesions (colon cancer precursors) in the colon of rat fed with cooked fatty acid-starch complex (*98*). Moreover, the amylose-lipid complexes could host bioactive long-chain unsaturated fatty acids as a new delivery system to encapsulate and protect the volatile and sensitive unsaturated fatty acids, such as conjugated linoleic acid (CLA), docosahexadecanoic acid (DHA), etc (*223, 231, 232*).

The amylose-fatty acid complex consists of two main crystalline polymorphic forms, namely types I and II. Type I is amorphous, while type II is made up of distinct crystalline and amorphous regions (*221, 232*). The molecular organization and physicochemical properties of the amylose-fatty acid complex have been proved to be affected by parameters including the amylose chain length, fatty acid chain length and the degree of saturation, fatty acid concentration and solubility (*77*). The thermal stability of amylose-fatty acid complex was found to be enhanced with increasing fatty acid chain length and decreasing unsaturation (*95, 233, 234*). The V-amylose complex forms an imperfect helix with a hydrophobic helical cavity, where the fatty acid partly inside, partly out (*235*). Transmission electron microscopy (TEM) study suggested that amylose-fatty acid complexes exhibited uniaxial layout of amylose molecules locally interrupted by amorphous segments. The crystal thickness increased with increasing fatty acid chain length (C8, C12, C16), and was no more than 4.6 nm (*220*). The crystalline regions of V-type amylose-fatty acid complexes are intersected by amorphous regions, and may form various supramolecular structures, such as lamellae and spherulites (*93, 223*). Atomic force microscopy (AFM) revealed aggregates of amylose-fatty acid complex with spherical or lamellar morphologies and some other ill-defined structures (*223, 236*).

Most of amylose-lipid complexes reported was prepared in excess aqueous solutions to increase the accessibility between amylose and lipids (*101, 102, 236*). Lalush et al. obtained amylose-long chain fatty acid complexes of nano-scale spherical shape with a typical diameter of 150 nm and elongated structure with a typical width of 43-160 nm via two different complexation methods involving using water/dimethylsulfoxide (DMSO) and potassium hydroxide (KOH)/ hydrochloric acid (HCl), respectively (*223*). And Zabar et al. also obtained some amylose-fatty acid complexes of average crystalline lamellar thickness of 0.16-0.46 and 0.11-0.26 using the two similar methods, respectively (*101, 102*). However, most lipids, especially long-chain fatty acids, are not dispersed in the aqueous phase and cannot penetrate into starch granules to complex with amylose. Hence, in this study, heat-moisture treatments were used to prepare starch-fatty acid complexes. The objective of the study was to increase the understanding of the interactions between starch and fatty acids in fatty acid-starch complex formed when heating high-amylose maize starch with different fatty acids before and after the hydrothermal treatment. The physiochemical properties and molecular organization of the starch-fatty acid complexes under different conditions were assessed using XRD, USAXS, SAXS and SEM.

6.2. Materials and methods

6.2.1. Materials

High-amylose maize starch (~ 70% amylose) was obtained from Ingredion (Bridgewater, NJ). Lauric acid (C12:0), myristic acid (C14:0), palmitic acid (C16:0), stearic acid (C18:0) and oleic acid (C18:1) with at least 99% purity were purchased from Sigma-Aldrich (St. Louis, MO). All other chemicals used in the study were analytical grade.

6.2.2. Formation of starch-fatty acid complexes

Starch-fatty acid complexes production was performed according to the previous method with modification (*229*). Two production methods were implemented to prepare the starch-fatty acid complexes, one is heating starch prior to the addition of fatty acid (Method I) and the other is adding fatty acid prior to heating to the starch (Method II). In Method I (MI), 1.00 g of native high-amylose starch, which was dried at 105℃ for 3 h, was mixed with 400 mg of distilled water vigorously. The starch with moisture content of 40% was sealed in stainless-steel reaction vessels and heated at 80℃ for 12 h. Then 150 mg of fatty acid dissolved in 350 mg of ethanol was added into the heated starch dispersion. After vigorously stirring, the mixture was heated at 80℃ for 5 min without cover to evaporate the ethanol. The final mixtures was sealed and heated at 80℃ for an additional 2 h.

In Method II (MII), 1.00 g dried high-amylose starch was mixed with 150 mg of fatty acid dissolved in 350 mg of ethanol. The mixture was heated uncovered at 80℃ for 5 min to evaporate the ethanol, then sealed in stainless-steel reaction vessels and heated at 80℃ for 2 h. Then 400 mg of distilled water was added into the mixture with vigorously mixing. The final mixture was heated at 80℃ for another 12 h.

All the samples obtained by both protocols were cooled to room temperature, washed with 50% distilled water-ethanol solution (v/v) and recovered by centrifugation (1500g, 10 min). This step was repeated twice before the resulting pellets were dried at 40℃ overnight and ground to fine powder.

6.2.3. Microscopic level investigation using light microscopy and scanning electron microscope (SEM)

Light micrographs were recorded using a Nikon Eclipse TE2000-U (Japan)

microscope. Samples were dispersed in water phase. Then the starch suspensions were placed on a glass microscopic slide with cover glass**.** SEM micrographs were obtained using a HITACHI S-3000N Scanning Electron Microscope (Japan). Samples were prepared through mounted on circular aluminium stubs, then coated with gold. All the other parameters were shown on images.

6.2.4. Structural characterization using X-ray diffraction (XRD)

The XRD measurements were carried out using a method descried in section 2.2.5.

6.2.5. Ultrasmall-angle X-ray scattering (USAXS) and small-angle X-ray scattering (SAXS) based nanometric level investigations

To investigate the nano-structural properties of the starch-fatty acid complexes, USAXS and SAXS experiments were performed, which covered structural information ranging from several angstroms to micrometers. These analyses probed the nanostructure of starch-fatty acid complexes at wet state. All the samples tested were prepared by adding deionized water directly to the starch and allowed to equilibrate at a total moisture level of 50% for over 6 h.

USAXS experiments were performed using the USAXS instrument at the Advanced Photon Source, Argonne National Laboratory (United States). The X-ray radiation wavelength of USAXS instrument was set at 1.13 Å. The scattering vector q is defined as

$$q = \frac{4\pi}{\lambda} sin\theta \qquad (10)$$

where λ is the wavelength of X-ray and θ is the scattering angle. The q range for USAXS was ranged from 0.00015 to 0.05 $Å^{-1}$.

SAXS measurements were conducted using a Bruker Nanostar SAXS camera. The radiation wavelength of X-ray source was 1.54 Å. The X-ray diffraction was collected using SAXS camera with a Hi-star 2D detector. Samples were loaded to sealed glass

capillaries with 2 mm diameter. The q-range for SAXS was from 0.02 to 2 $Å^{-1}$. The background scattering, which used the data obtained from the diffraction of water as a standard, was measured separately. The USAXS/SAXS profiles were obtained by subtracting the background and normalizing to sample transmission.

6.3. Results and discussion

6.3.1. Morphology of stacrh-fatty acid complexes

The morphology of starch-fatty acid complexes was analyzed using polarized light microscopy and scanning electron microscopy. The granule microstructure of different starch-fatty acid complexes was observed using microscope under polarized light (**Figure 40**). Starch-fatty acid complexes appeared as spherical and filamentous granules and exhibited a characteristic birefringence pattern of a Maltese cross centered at the hilum under polarized light, which was the same as native starch granules. The results suggested that the molecular orientation of starch-fatty acid complexes maintained intact morphology during the heat-moisture treatment.

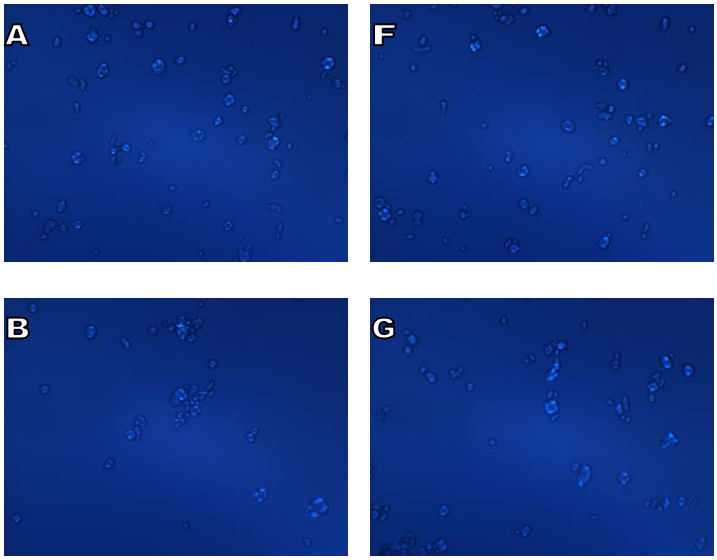

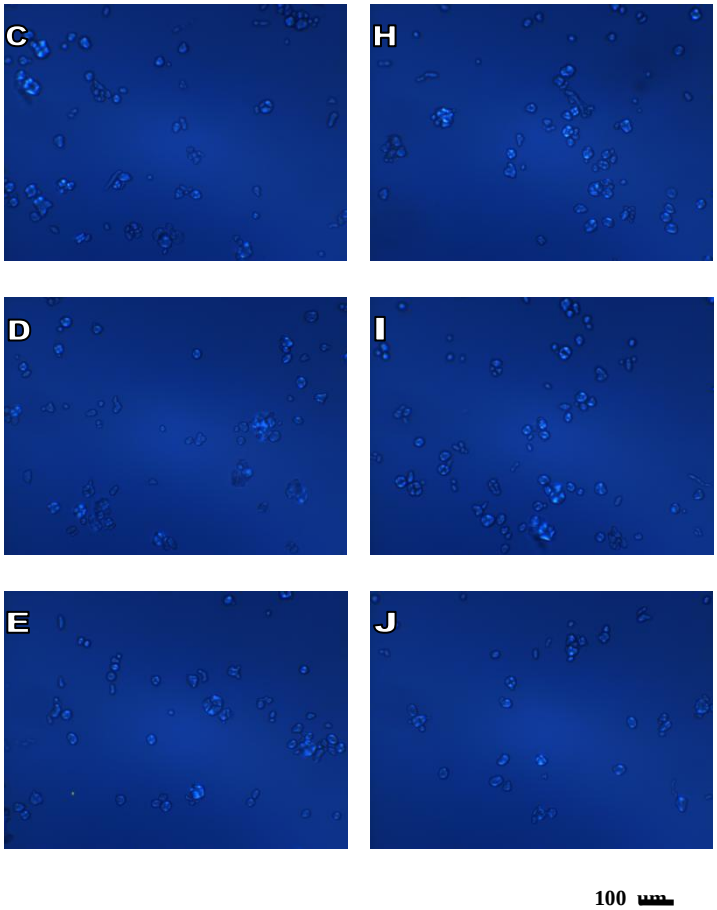

Figure 40. Polarized light microscopic images of starch-fatty acid complexes. A. starch-lauric acid complex from Method I; B. starch-myristic acid complex from Method I; C. starch-palmitic acid complex from Method I; D. starch-stearic acid complex from Method I; E. starch-oleic acid complex from Method I; F. starch-lauric acid complex from Method II; G. starch-myristic acid complex from Method II; H. starch-palmitic acid complex from Method II; I. starch-stearic acid complex from Method II; J. starch-oleic acid complex from Method II.

SEM micrographs of starch-fatty acid complexes are presented in **Figure 41**. Most of the starch-fatty acid complexes remained intact granule of round and irregular polygonal shape with smooth edges, which exhibited similar morphology as native high-amylose starch (*230*). However, starch-palmitic acid complex and starch-stearic acid complex from both the two methods exhibited a slightly roughness on the granular surface, which could indicate the partial gelatinization in these complexes. Native high-amylose maize

starch has relative high gelatinization temperature of around 70~100℃ (*237*). The reason of starch-fatty acid complexes maintaining the granule structure of native starch could due to the benign thermal stability of high-amylose maize starch. Furthermore, the added fatty acid could coat on granule surface, complex with amylose, reduce water movement into the granules, thus retarding starch gelatinization (*229*). The minor surface roughness increase of starch-palmitic acid and starch-stearic acid complex could be attributed to the relatively low solubility in ethanol and high melting temperature of these fatty acids, which hindered the interaction between fatty acids and starch granules.

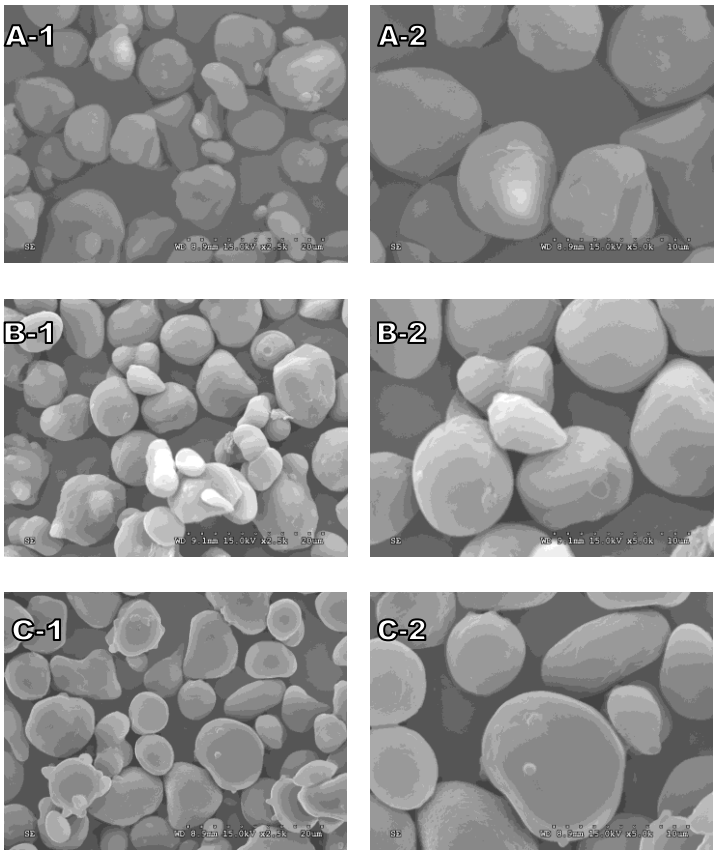

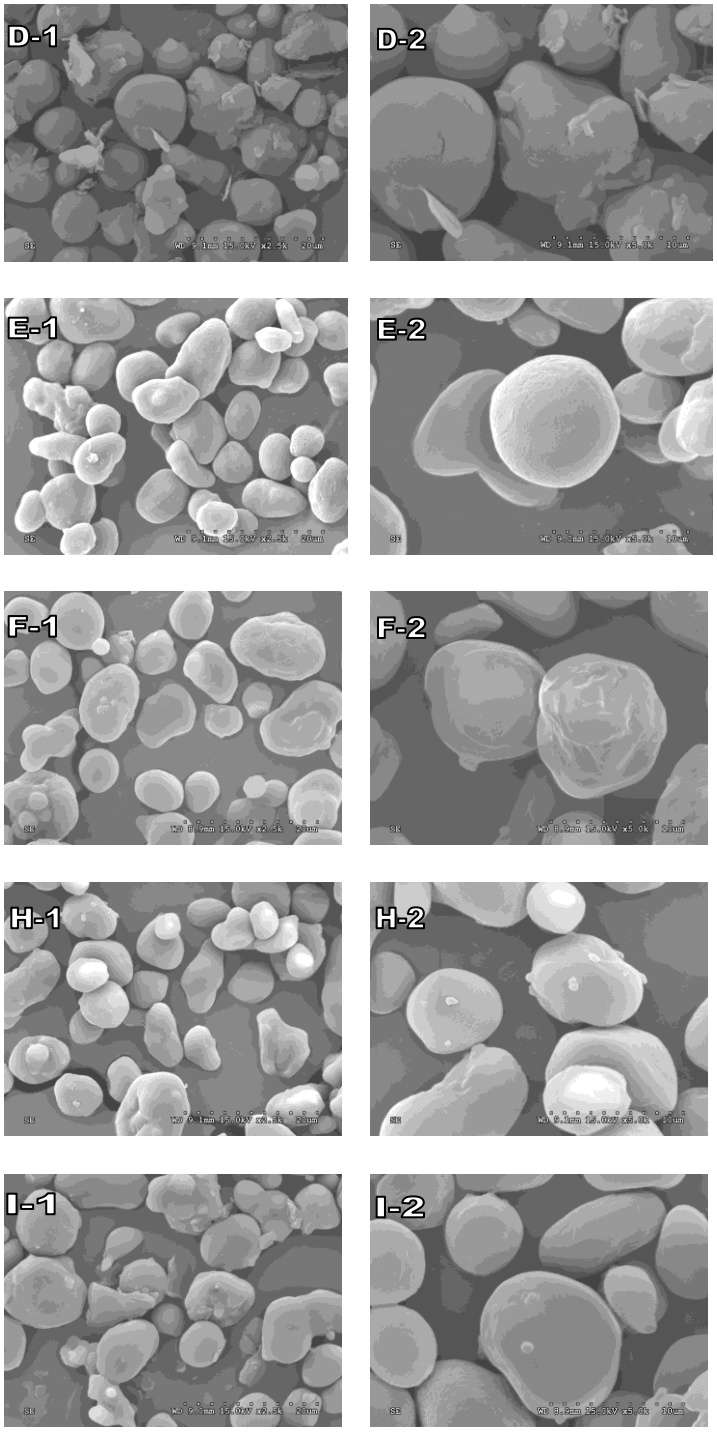
D-1
D-2
E-1
E-2
F-1
F-2
H-1
H-2
I-1
I-2

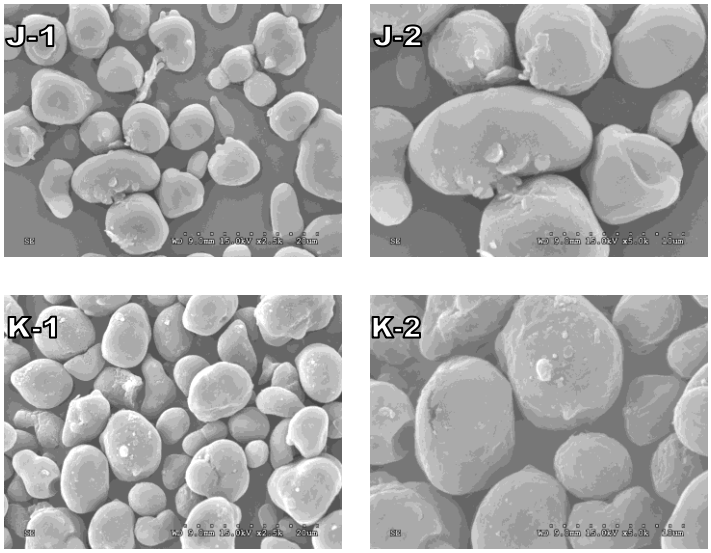

Figure 41. SEM morphology of starch-fatty acid complexes. A. starch-lauric acid complex from Method I; B. starch-myristic acid complex from Method I; C. starch-palmitic acid complex from Method I; D. starch-stearic acid complex from Method I; E. starch-oleic acid complex from Method I; F. starch-lauric acid complex from Method II; G. starch-myristic acid complex from Method II; H. starch-palmitic acid complex from Method II; I. starch-stearic acid complex from Method II; J. starch-oleic acid complex from Method II.

6.3.2. Structural characterization by X-ray diffraction

The X-ray diffraction patterns of starch-fatty acid complexes were presented in **Figure 42**. Native high-amylose starch was found to exhibit B-type pattern (*35*). The starch-fatty acid complexes showed intensity peaks at Bragg angles (2*θ)* of around 5º, 7º, 13º, 17º and 20º, which was a mixture of B-type and V-type patterns (*223*). The peaks shown at 21º and 24º, which were observed in starch-myristic acid, -palmitic acid, -stearic acid complex, were the crystallites of these fatty acids (*102, 236*). And the intensity of the fatty acid peaks enhanced correspondingly with the increase of the fatty acid chain length except for starch-palmitic acid complex from Method I, which showed the highest peak intensity. Several studies have suggested the possibility of small ligands being either included within the helices or trapped between helices or even in the

amorphous regions of V-amylose complex (*232*, *238*). Although study indicated that sequential washing with ethanol 50% (v/v) was enough to remove free decanoic acid or hexanoic acid intercalated in V-amylose complex, the trapped fatty acid in this study might not all be removed by similar treatment due to the differences in the association of the trapped fatty acid (*232*). These crystalline fatty acids might come from the physically trapped fatty acid crystals in the other regions of the complexes other than within the helices. Similar fatty acid crystalline peaks have also been observed in previous study (*236*). Although oleic acid has the same carbon-chain length as stearic acid, the peaks of 21º and 24º were not observed in the X-ray pattern of starch-oleic acid complexes from the two methods, which suggested that no oleic acid crystals existing in the complexes. These results could be due to the fact that, the crystalline temperature of saturated fatty acids with longer aliphatic chain is higher than that of unsaturated fatty acids with same chain length. Hence, these fatty acids are more susceptible to aggregation and crystallization. These findings implied that the chain length and degree of unsaturation of fatty acids affect the interaction between fatty acids and starch polymer chains and the remove of physically trapped fatty acid molecules in the complexes.

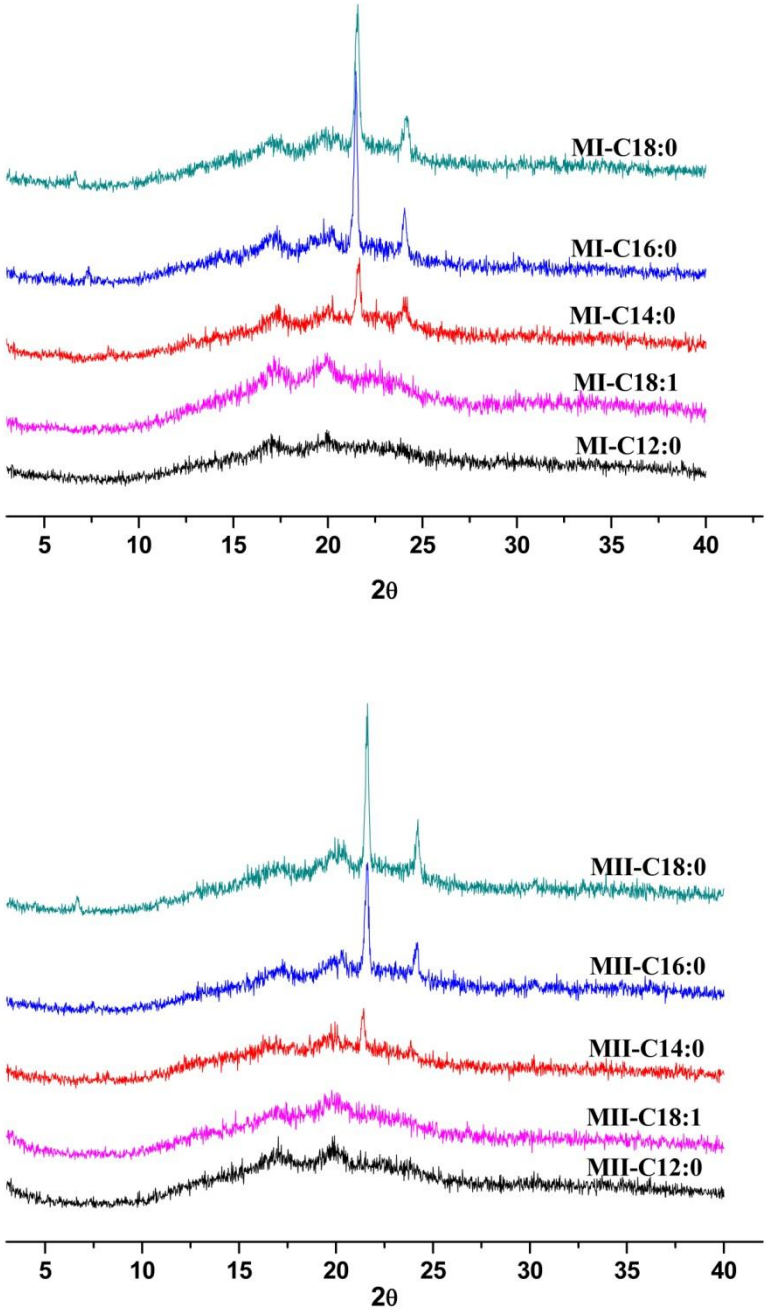

Figure 42. X-ray pattern of starch-fatty acid complexes. MI: Method I; MII: Method II.

The crystallinity of different starch-fatty acid complexes was presented in **Table 10**. When the chain length of fatty acid increased from 12 carbon atoms to 16 carbon atoms, the crystallinity of starch-fatty acids complexes from Method I and II improved from 29.7%

and 29.4% to 40.4% and 35.3%, respectively. The crystalline structure of starch-fatty acid complexes was contributed by the formation of double-helix amylopectin, single helix amylose-fatty acid complex and free fatty acids. The observed enhancement in the crystallinity of starch-fatty acids complexes could partially be attributed to the formation of fatty acid crystals. However, further prolonged the carbon atoms to 18 led to the decrease of crystallinity in starch-stearic acid complexes (38.1% and 35.2%, respectively). Since significant peaks of fatty acids was still observed in the X-ray pattern, it would suggest the ratio of double-helix amylopectin and single helix amylose-fatty acid complex in starch-stearic acid complex was much lower than in starch-palmitic acid complex. Many studies have found that the formation of V-amylose complex would be affected by the chain length of fatty acids in the lipids. However, there is no agreement on the identity of the best complexing lipids. Some researches indicated that a lipid with chain length of 14 carbon atoms is best for complex formation (*239-241*), while other studies suggested that lipid chain length of 16 or 18 carbon atoms was preferred (*241*). The results in this study indicated that fatty acid with 18 carbon atoms might not be suitable for preparing starch-fatty acid complex using heat-moisture treatment. The crystallinity of starch-fatty acid complexes prepared using Method I was higher than their counterparts from Method II, which suggested that the order of adding fatty acids (before or after the hydrothermal treatment) could also impact the formation of starch-fatty acid complex.

Table 10. Degree of crystallinity (X_c) of the different samples calculated from the X-ray diffraction data

sample	X_c (%)
MI-C12:0	29.7

MI-C14:0	34.9
MI-C16:0	40.4
MI-C18:0	38.1
MI-C18:1	32.4
MII-C12:0	29.4
MII-C14:0	33.2
MII-C16:0	35.3
MII-C18:0	35.2
MII-C18:1	28.1

6.3.3. Ultrasmall-angle X-ray scattering (USAXS) and small-angle X-ray scattering (SAXS) based nanometric level investigations

The nanostructure of various starch-fatty acid complexes was characterized using USAXS and SAXS. Addition of water has been found to affect the structural order of starch (*242*). Addition of water will lead to a transition of starch lamellar structure from nematic phase to smectic phase, where branch points of amylopectin undergo plasticization and become flexible spacers, allowing the double helices side chains to be decoupled from the polymer backbone and aligned into lamellar register (*243*). As a result, the lamellar architecture of the semicrystalline growth rings can only be detected in hydrated starch instead of dry starch granules by small-angle scattering. The USAXS and SAXS experiments were conducted at humidity conditions (50% water content) in this study. The data of different starch-fatty acid complexes after subtraction of solvent scattering are shown in **Figure 43**. All the curves exhibited a rather broad peak ("shoulder") at low $q \sim 0.07$ A^{-1}, suggesting a certain level of long-range order existing in the samples. This shoulder was attributed to the 9 nm d-spacing characteristic of native starch, defined as lamellar structure of side-chain liquid-crystalline (*101*). This peak would appear in sample suspended in water instead of dry sample, suggesting that addition of water leads to changes in the contrast: the electron density difference between the samples and the medium (air or water). The changes in the contrast affected both the

scattered intensity and s-dependence, indicating the existing of heterogeneous internal structure containing at least two electron densities in the samples (*244*). The peak at $q \sim 0.4$ A^{-1} was associated with the 100 interhelix reflection from B-type crystallinity, which could also be observed in native starch (*245*). The presence of this peak suggested the gelatinization of starch during the heat-moisture treatment was extremely low. This could due to the moisture content was only 40% and the processing temperature was 80℃, which was below the full gelatinization temperature of high-amylose maize starch (gelatinization temperature: 70~125℃) (*79*). Therefore, the water in the amorphous phase was not sufficient enough to initiate the cooperative melting of crystallites. The influence of fatty acids on the intensity of this peak in starch-fatty acid complexes from Method I was more pronounced than that from Method II. Compared with other complexes, starch-palmtic acid and -oleic acid complexes from Method I have higher 100 interhelix peak intensity, indicating a lower degree of crystallite disruption. A new peak at $q \sim 0.55$ A^{-1} observed, which didn't exist in native starch, was linked with Bragg distances of ~1.2 nm ($2\theta \sim 7°$) in X-ray patterns of V-type crystallinity (*246*). The V-crystals of starch were attributed to the formation of ordered amylose single helices with a diameter around 1.3 nm. Although the nanostructural of amylose-lipid complex produced via acidification method and using organic solvent (dimethylsulfoxide, DMSO) was characterized by SAXS (*101, 102*), this is so far the first USAXS/SAXS scattering study of starch-fatty acid complex from heat-moisture treatment. Similarly shaped USAXS/SAXS curves has been reported in the scattering studies of resistant starches formed through extrusion process (*246*).

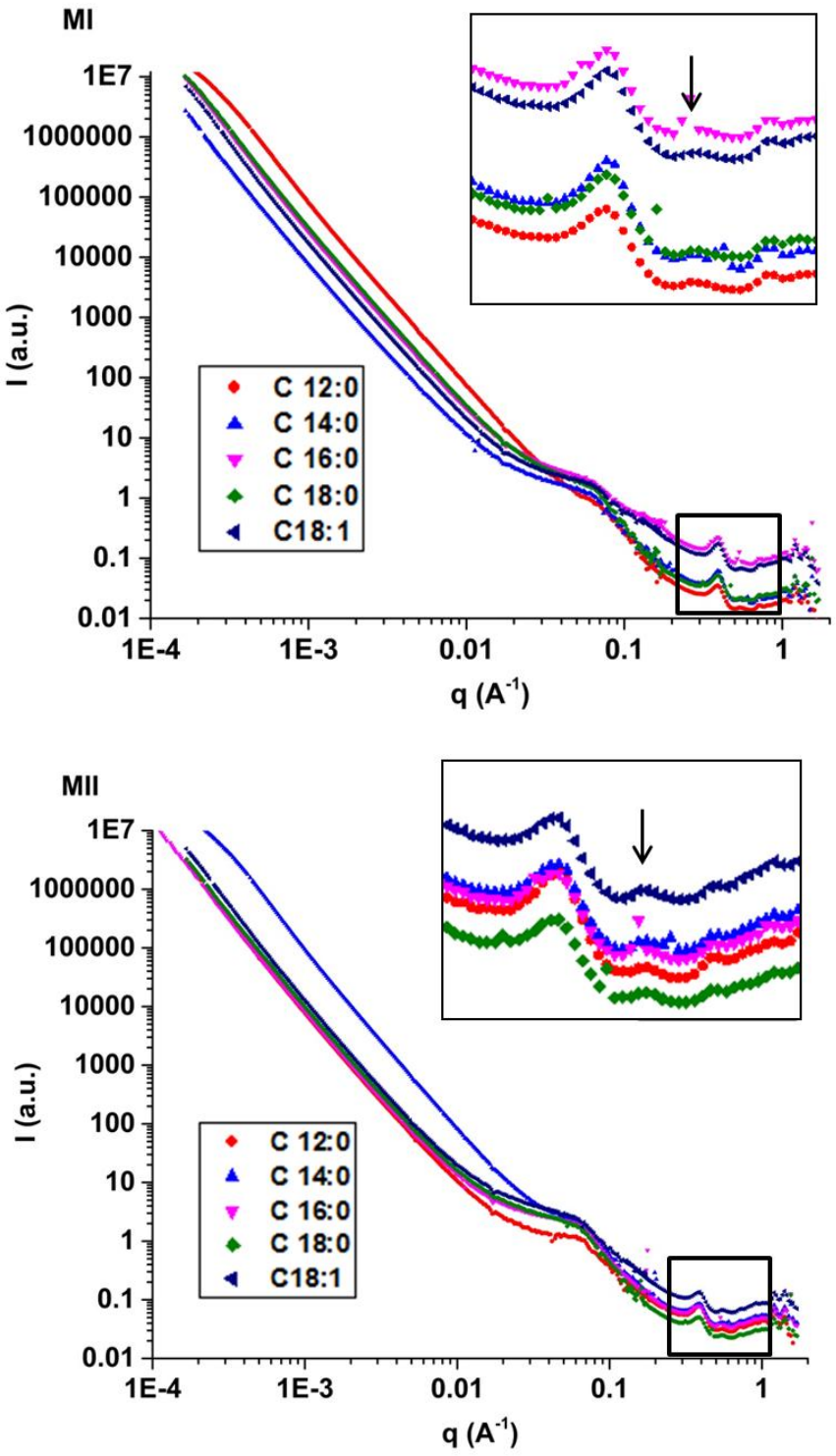

Figure 43. USAXS/SAXS curves of starch-fatty acid complexes. MI: Method I; MII: Method II.

Amylose-lipid complexes are polycrystalline powders with lamellar-like

morphology of crystallites interspersed among amorphous areas (*220*). Transmission electron microscopy (TEM) revealed that the crystal thickness increased with increasing of amylose chain length and ranged from 1.6 nm to 4.5 nm (*220*). Fitting based on SAXS data enabled the characterization of parameters, such as the average thickness of crystalline lamellar and characteristic length (*101*, *102*). The physical structure of starch-lipid complex has been only partly characterized. Nanostructure of starch-lipid complex proposed the presence of both amorphous amylose-lipid complex and crystalline complex (*95*). To characterize the nano-structural arrangements of starch-lipid complex, we considered the following model to fit USAXS/SAXS data: a model describing a "two-phase non-particulate system" combined with a Gaussian function.

$$I(q) = Aq^{-\delta} + \frac{CX_c(1-X_c)\xi^3}{(1+q^2\xi^2)^2} + I_0 \exp\left[-\frac{1}{2}\left(\frac{q-q_0}{B}\right)^2\right] + Bkgd \qquad (11)$$

The first term of the equation corresponds to a "power law" function, which describes the diffuse scattering of the USAXS/SAXS curves at low q. The *A* represents the prefactor and δ represents the power law exponent. The broad lamellar peak at around 0.07 A^{-1} is fitted using a "two-phase nonparticulate system" model by the second term of the equation, where X_c represents the degree of crystallinity (%), ξ represents the characteristic length of the system, and C referents a factor that is related to the electron density differences between the crystalline and amorphous regions. And the third term is a Gaussian function describing the second order reflection peak at around 0.4 A^{-1}, where I_0 represents the peak height, q_0 represents mean position of the peak, and *B* is the standard deviation, representing the width of the peak. The scattering data of the samples have been well fitted by the model (fitting curve of the model for starch-lauric acid complex from Method I was presented in **Figure 44)**.

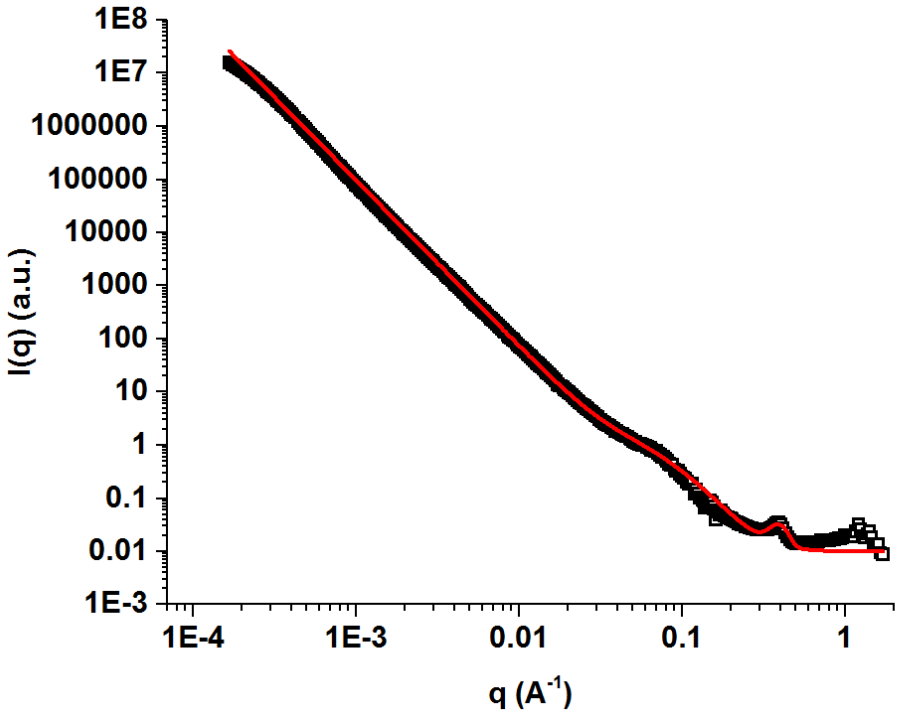

Figure 44. USAXS/SAXS curve for starch-lauric acid complex from Method I. Scattering data (square markers) fit to the model function (solid curve).

The values of fitted parameters for all samples are displayed in **Table 11**. The proposed model indicated that the exponent of power law function was with between -3.029 and -3.182. For fatty acids with 18 carbon atoms (C18:0, C18:1), the addition order during the processing didn't affect the value of exponent. While this value varies based either on the fatty acid used (C12:0, C14:0, C16:0) and its addition order. The major causes of deviations could be electron density differences among the interface or within a phase, interfacial roughness and curvature (*247*). The "two-phase nonparticulate" model, often known as the Debye-Beuche model, illustrates systems with one phase consisting of domains with sharp interfaces randomly distributed in another phase (*248*). For starch samples, this model describes the semicrystalline filaments consisting of crystallites with various sizes embedded in an amorphous matrix and has been used to

describe the scattering pattern of resistant starch before (*246*). The value for degree of crystallinity, X_c, was measured from the XRD patterns, which was not refined during the fitting. The characteristic length, ξ, corresponds to the average spacing between the crystallites and amorphous phase and is described as follows:

$$\frac{1}{\xi} = \frac{1}{\xi_c} + \frac{1}{\xi_a} \quad (12)$$

where ξ_c and ξ_a represents the average crystalline lamellar thickness and the average amorphous phase length, respectively. And these values could be measured based on the following equations (*246*).

$$\xi = (1- X_c)\xi_c = X_c\xi_a \quad (13)$$

Table 11. Value of the parameters obtained by fitting the scattering data of starch-fatty acid complexes to the model.

Sample	power law exponent (δ)	Two-phase non-particulate model			Gaussian Function		
		characteristic length (ξ)	ξ/(1-X_c)	ξ/X_c	height (I_0)	peak position (q_0)	width (B)
MI-C12:0	3.075	18.71	26.62	63.00	0.0178	0.388	0.0437
MI-C14:0	3.169	15.49	23.80	44.39	0.0369	0.389	0.0389
MI-C16:0	3.173	12.61	21.15	31.20	0.119	0.390	0.0380
MI-C18:0	3.159	15.14	24.46	39.75	0.0262	0.391	0.0367
MI-C18:1	3.182	13.39	19.81	41.32	0.0943	0.392	0.0352
MII-C12:0	3.175	11.76	16.65	39.99	0.0425	0.387	0.0422
MII-C14:0	3.029	15.30	22.90	46.07	0.0428	0.383	0.0368
MII-C16:0	3.149	12.14	18.76	34.37	0.0417	0.380	0.0366
MII-C18:0	3.159	15.38	23.74	43.70	0.0241	0.377	0.0450
MII-C18:1	3.182	15.86	22.06	56.45	0.0650	0.386	0.0446

The average characteristic length of the crystallites is calculated as ξ/(1-X_c). The values of fitted parameters from **Table 11** indicated that increasing of fatty acid chain seemed to decrease the order within the lamella. The characteristic length of starch-fatty acid complexes from Method I decreased from 18.71 to 12.61 nm when the carbon atoms of fatty acid increased from 12 to 16. The corresponding characteristic length of the

crystallites also decreased from 26.62 to 21.15 nm. However, further prolonged the carbon atoms to 18 resulted in an enhancement in the characteristic length of starch-fatty acid complexes. The effect of fatty acid chain length on starch-fatty acid complex formation seemed to exhibit a different trend using Method II. These complexes showed an increase in the characteristic length from 11.76 to 15.86 nm when the carbon atoms was prolonged from 12 to 18 except for starch-myristic acid complex. Similarly, beside from starch-myristic acid complex, an increase in crystal thickness from 16.65 to 23.74 nm was observed for complexes with fatty acid chain of 12 to 18 atoms. The critical size of amylose for complex formation was related to the lipid chain length. 20-30 glucose residues was found to be sufficient for complexation of lauric acid (C12:0), while 30-40 were required for palmitic acid (C16:0) (*220*, *249*). As the result, structure of the hosting V-amylose complexes including differences in crystallites and amorphous phase was affected when fatty acids with different chain length were used. Moreover, the addition order of fatty acids during processing also impacted the formation of V-amylose. Comparing starch-fatty acid complexes from the two methods revealed that Method I produced complexes with longer lamella crystallite, the only exception being starch-oleic acid complex. We noted that the characteristic crystallite length for MI-C16:0 was the highest among all the formed complexes, which might be related to the explicit inclusion of crystallinity for this sample. For long chain fatty acid (C18:0, C18:1), increasing fatty acid unsaturation led to decrease in crystalline lamellar thickness in both the methods used. This trend is in agreement with the findings in amylose-fatty acid complex produced using other approaches (*102*).

The Gaussian function describes the characteristic 100 reflection of B-type

crystalline in the system. With the fatty acid chain increased from 12 to 16 carbon atoms, the partial gelatinization that took place during heat-moisture treatment of the two methods decreased reflected in either increased peak height or decreased peak width, or both. This could be attributed to the stronger hydrophobic interactions between aliphatic chain of lipids and the interior of the amylose helix, resulting in the enhanced dissociation temperatures of amylose-fatty acid complexes with the increased aliphatic chain length of the lipids (*95, 231, 250, 251*). Also for fatty acids with 12 to 16 carbon atoms, starch-fatty acid complexes from Method I had lower peak height or larger peak width, compared to the counterparts from Method II, reflecting a higher degree of crystalline disruption. In Method I, starch was first heated under moisture conditions. The granules would swell and partially gelatinize before adding fatty acids. While the starch was first incorporated with fatty acid before water was added during Method II. The fatty acid coated on the granule surface would delay the penetration of water into the granules, thus hindering gelatinization. When the fatty acid further prolonged to 18 carbon atoms, the resulting complexes showed higher degree of gelatinization with decreased peak height and enhanced peak width, which might be attributed to the decrease in V-amylose yield due to higher activation energy required for complex formation with increasing acyl chain length (*252*). It is notably that starch-oleic acid complexes (C18:1) showed larger peak height and smaller peak width than starch-stearic acid complexes (C18:0), suggesting that increasing the fatty acid unsaturation resulted in less disruption in the B-type crystalline of the complexes. Since ligands to form V-type complex could be possible located within the helices, between the helices or dispersed in the amorphous regions (*232*), the low melting point of oleic acid might promote the dispersion of fatty

acid between the helices and in the amorphous regions of starch, thus delaying starch gelatinization.

Based on the data presented above, a lamellar-like structural organization of starch-fatty acid complex was proposed (**Figure 45**). Previous studies have suggested that amylose located in starch granules as individual chains, which are randomly interspersed amongst the clusters of amylopectin chains in both amorphous and semi-crystalline regions (*253, 254*). After interaction with starch, some fatty acids might be within the helices through forming complexes with amylose chains or a small amount of amylopectin helices, while uncomplexed fatty acid might be dispersed between the helices of the crystalline regions, or in the amorphous regions (*232*). In the lamellar structural organization, the amylose-fatty acid complex and amylopectin make up the crystalline phase, whereas the branching points of amylopectin, some uncomplexed amylose and free fatty acids form the amorphous phase, with the two alternating. The presence of fatty acid induces the formation of amylose helices to entrap the fatty acids. The appearance of these molecular segments in the crystalline phase leads to the disruption in the original B-type crystalline structure of native starch and transform to V-type crystalline structure.

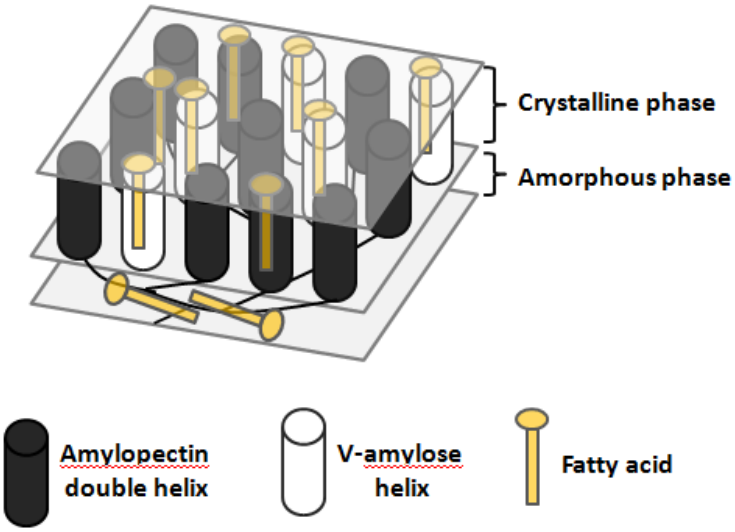

Figure 45. Schematic representation of the lamellae-like structure of starch-fatty acid complexes and possible fatty acid molecules trapped.

6.4. Conclusion

The formation of starch-fatty acid complexes is proposed to be related to the chain length of fatty acids and the order of adding fatty acids during the hydrothermal treatment. The characteristic B- and V-type XRD patterns were observed in the starch-fatty acid complexes, indicating the tendency of fatty acids to complex with amylose and amylose-fatty acid complex to form organized structure. The optical microscope and SEM images suggested that the structure change was minor at microscopic level. Fitting of the USAXS/SAXS data to a model consisting of a “two-phase non-particulate system” combined with a Gaussian function enabled the nano level characteristics of the complexes. All fatty acids induced the formation of V-amylose. However, their nanostructure, including lamellar structure, B-type crystalline, varied depending on the fatty acid chain length and level of saturation. The interactions between amylose and fatty acid were also significantly affected by the presence of water (starch mixing with fatty acids before and after the hydrothermal treatment). Generally, Method I was found to

promote the formation of longer lamella crystallite while lead to a larger disruption of B-type crystalline in the resulting starch-fatty acid complexes compared to Method II. This study provided understanding to the suprastructural arrangements of starch-fatty acid complexes from different preparation conditions at nano or micron scale, which would facilitate the production and application of tailor made V-amylose inclusion complexes.

CHAPTER 7 CHARACTERIZATION OF PICKERING EMULSIONS STABILIZED BY HIGH-AMYLOSE MAIZE STARCH COMPLEXED WITH DIFFERENT FATTY ACIDS

7.1. Introduction

A large variety of compounds with health-promoting biofunctionalities have been recognized in natural plants. However, many of these compounds are lipophilic with poor aqueous solubility, which have low bioavailability over oral ingestion. Encapsulation bioactive lipophilic compounds using emulsion system has long been applied to increase their solubility and augment their oral dose efficiency. Conventional emulsions formed by traditional emulsifiers might cause adverse effects, such as foaming, irritancy, biological interactions, even promoting colitis and metabolic syndrome (*8, 9*). An alternative way to avoid these surfactants use is to apply colloid solid particle-stabilized emulsions, so-called Pickering emulsions (*3*). Compared to conventional emulsions, Pickering emulsions also possessed higher stability against coalescence and Ostwald ripening (*162*). Most of the colloid particle used is from inorganic or synthetic resources (*10-13*). Recently, production of particulate emulsifiers from natural biopolymers has gained great attraction, especially with application in food, cosmetic and pharmaceutical industry (*14, 15*). Starch is one of the promising materials that has been studied for developing particle stabilizers owing to its overwhelming abundance and inherent biodegradability (*30*). With intrinsic hydrophilicity, the emulsifying efficiency of most native starch was unsatisfying. Hydrophobic modification of starch is a common approach used to enhance its affinity for oil phase, thus improving its emulsifying properties (*24, 26*). Currently, this approach involved the formation of chemical bonding between the hydroxyl groups of starch and

the reacting reagents.

The amylose in the starch tends to form single helix structure through complexing with suitable lipophilic molecules (*104*). Complexation between fatty acids and starch has been proved to reduce enzyme hydrolysis rate of starch, which could form a type of resistant starch (*229, 230*). In chapter 7, starch-fatty acid complexes with fatty acid chain length of 12-18 carbons have been prepared. These complexes still maintain the original intact granule shape of native starch. Since medium- and long-chain fatty acids are lipophilic, the hydrophobicity of starch-fatty acid complexes would be enhanced. Hence, the emulsifying efficiency of these complexes would be improved compared to native starch. In this study, complexes formed by starch and different fatty acids will be used to form Pickering emulsions. The resulting Pickering emulsions will possess the health benefits that linked with resistant starch, which include lower the postprandial plasma-glucose, intervene insulin resistance, serve as a potential probiotic and promote colonic health (*81, 82, 255, 256*). Although starch granules stabilized Pickering emulsions are stable against coalescence, there could be some relatively large space between starch granules at the oil-water interface even if a fully coverage interface was formed due to relatively large size of starch granules. The gelatinization of starch granules at the oil-water interface under heat treatment could adjust the barrier properties of starch granule stabilized Pickering emulsions (*257*). Since the formation of amylose-lipid complex in starch granules restricts the swelling of starch granules during heating process and enhance the resistant of starch molecules to enzymatic hydrolysis (*96, 228*), the delayed or controlled lipid digestion and controlled release of encapsulated bioactive compounds within the gastro-intestinal tract could be achieved by applying

different extent of heating treatment on the starch-fatty acid complex stabilized Pickering emulsions.

Polymethoxyflavones (PMFs) are a unique class of flavonoids that exist almost exclusively in the peels of citrus fruits. The health-promoting properties of PMFs are well-documented, which include neuroprotective, anti-inflammatory, antiatherogenic, antiangiogenic and anticancer activities (*258-261*). Monodemethylated PMFs are a unique subclass of PMFs, that have been isolated from aged citrus peels and proved to exhibit stronger bioactivities in different systems than their permethoxylated PMF counterparts (*262-265*). As lipophilic bioactive reagents, monodemethylated PMFs have low bioavailability over oral consumption due to poor aqueous solubility. Emulsion system stabilized by biocompatible lecithin has been developed to enhance the oral dose efficiency of monodemethylated PMF (*266*). However, the choline headgroup of lecithin used in this formulation acting as a labile methyl group donor led to the transformation of 5-demethyltangeretin to tangeretin during lipolysis, thus reducing its efficiency (*266*).

The aim of this research was to investigate the emulsifying efficiency of resistant starch formed by complexing high-amylose maize starch with different fatty acids to stabilize Pickering emulsions and barrier properties of resistant starch stabilized Pickering emulsions after heat treatment. To evaluate their encapsulation and delivery properties of lipophilic bioactive compounds, two key polymethoxyflavones (PMFs), 5-demethyltangeretin and 5-demethylnobiletin were incorporated in the emulsion systems. And the release profiles of the PMFs under *in vitro* small intestinal digestion conditions in Pickering emulsions after different extent of heat treatments were investigated.

7.2. Materials and methods

7.2.1. Materials

High-amylose maize starch (H-VII, ~ 70% amylose) was obtained from Ingredion (Bridgewater, NJ). The soy bean oil was purchased from a local supermarket. Lauric acid (C12:0), myristic acid (C14:0), palmitic acid (C16:0), stearic acid (C18:0) and oleic acid (C18:1) with at least 99% purity were purchased from Sigma-Aldrich (St. Louis, MO). Sodium taurodeoxycholate (NaTDC) was purchased from CalBiochem (La Jolla, CA). Phosphatidylcholine (PC75 rapeseed lecithin) was a gift from the American Lecithin Co. (Oxford, CT). Pancreatin from porcine pancreas (Cat. No. P7545) and amyloglucosidase (Cat. No. A7095, activity 300 unit/ml) were purchased from Sigma-Aldrich (St. Louis, MO). 5-Demethyltangeretin and 5-demethylnobiletin at a ratio of 3:1 (w/w) with a purity of >98% was synthesized in our laboratory using a previously published method (*267*). All other chemicals used in the study were analytical grade.

7.2.2. Preparation of starch-fatty acid complex resistant starch

The starch-fatty acid resistant starch was prepared according to a previous method with modification (*229*). The starch-fatty acid complexes were prepared using the methods in section 6.2.2.

7.2.3. Lipid content

The lipid contents of the samples were determined according to a previous study (*268*).The free lipid in the complexes was measured by extracting using Soxhlet with petroleum ether at 50℃ for 10 h. The total lipid content of the complexes was measured after acid hydrolysis process of starch. Around 1.00 g of complex was accurately weighed and well mixed with 10 ml of distilled water. Then 15 ml of 8.0 M HCl was added before heating in a boiling water bath for 25 min. After the heating process, 50.0 ml of distilled water was added. The mixture was then filtered through filter paper and washed with distilled water until the filtrate reached neutral. The residue with filter paper was dried

overnight at 40℃. The total lipid content of the dried residues was Soxhlet extracted with petroleum ether at 50℃ for 8 h. The recipients with the extracted fat were dried at 105℃ to constant weight. The lipids in the samples were composed by both free lipids and complexed lipids (complexed lipids = total lipids - free lipids). All samples were analyzed in duplicates.

7.2.4. Contact angle measurement

Starch films were formed using solution casting method. The samples were heated in distilled water at 150℃. The suspensions were poured onto glass dishes and dried at room temperature overnight. The water contact angle of the films was measured using sessile drop method on a VCA Optima-goniometer system (AST Products, U.S.A). A drop of water (2 µl) was placed on the starch film. Then the contact angle was measured at least at five different places of the film. The reported result was the average value of these measurements.

7.2.5. *In vitro* starch digestibility

In vitro digestibility of the samples was analyzed using Englyst method with slight modifications (*82*). Starch samples (600 mg, dry base), distilled water (10 ml) and five glass beads were added into 50 ml centrifuge tubes. The tubes were capped and mixed using vortex for 5 min before heated for 30 min in a boiling water bath. The tubes were vortexed in each 5 min intervals to prevent agglomeration during heating treatment. The tubes was then equilibrated in a shaking thermostat at 37℃ for 30 min before 5 ml of sodium acetate buffer containing porcine pancreatin (3×10^3 USP) and amyloglucosidase (40 units) was added. 1.00 ml of aliquots were taken at 20 and 120 min of reaction time and mixed with 10 ml of ethanol-water solution (80%, v/v) to stop enzyme reaction. The reducing sugar content in the mixture was measured using the 3, 5-dinitrosalicylic acid

method. Each sample was analyzed in duplicate.

7.2.6. Preparation of blank emulsions and PMFs loaded-emulsions

Blank emulsions without PMFs was prepared by dispersing starch-fatty acid complexes in distilled water (12 mg/ml water phase) and throughly mixing with same volume of soy bean oil using an IKA Ultra-Turrax T25 homogenizer at 12,000 rpm for 3 min. PMFs loaded-emulsions were prepared using the same method as blank emulsions except the oil phase contained dissolved PMFs (2 mg/ml). The oil/water ratio of PMFs loaded emulsions was set at 1:0.8 (v/v). To investigate the effect of heat treatment on the emulsions, the emulsions were heated at 60, 80 and 100℃ for 1 h, respectively. Then samples were equilibrated overnight before further analysis. All samples were prepared in duplicate.

7.2.7. Microstructure observation of emulsions by light microscopy

The microstructure of starch-fatty acid complexes stabilized Pickering emulsions were analyzed using a Nikon Eclipse TE2000-U (Japan) microscope by the method described in section 2.2.7.

7.2.8. *In vitro* lipolysis of PMFs in emulsions

The *in vitro* lipolysis study simulated the digestion conditions of human small intestine was performed based on a method described in section 3.2.7. The extent of lipolysis at 30 min was recorded as a measure of barrier properties of starch-fatty acid stabilized emulsions with different heat treatments on the initial rate of lipolysis.

7.2.9. Bioaccessibility determination

Upon completion of the lipolysis, the digestion buffers were ultracentrifuged at 4℃ and 40,000 rpm for 40 min, which were separated into several phases, an oily phase at the top, an aqueous phase containing incorporated PMFs micelles in the middle, and an opaque sediment phase. The volume of middle phase micelle phase which represented the

major forms of compounds for potential intestinal absorption was calculated and its PMFs concentration was analyzed using HPLC. The bioaccessibility (%) of PMFs was calculated using following equation:

$$\text{Bioaccessibility (\%)} = \frac{\text{amount of solubilized PMFs in micelle}}{\text{amount of PMFs in the formulations}} \times 100\% \qquad (14)$$

7.2.10. High-performance liquid chromatography (HPLC) analysis of PMFs

The UltiMate 3000 HPLC system equipped with a 25D UV-VIS absorption detector (Dionex) and Supelco's RP-Amide column, 15 cm × 64.6 mm i.d., 3 μm (Bellefonte, PA) was used to analysis PMFs based on a previous study (*266*). The detection wavelength was set at 320 nm. And the injection volume was thirty microliters. The gradient elution with a mobile phase of water (A) and acetonitrile (B) was used. The following elution program was used: 0 to 10 min, linear gradient from 60% A/40% B to 45% A /55% B, then linear gradient to 30% A /70% B at 15 min, followed by linear gradient to 20% A/80% B at 20 min, finally a linear change back to 60% A /40% B at 21 min and lasting for 1 min. The flow rate was set at 1 ml/min.

7.3. Results and discussion

7.3.1. Lipid content and contact angle of starch-fatty acid complexes

When fatty acids and starch were processed under heat and moisture conditions, the fatty acids in the resulting starch-fatty acid complex would exist as free fatty acid and complexed fatty acids. And the complexed fatty acids were mainly from the helical complexation between amylose and fatty acid (*103*). The amount of total lipids, complexed lipids and free lipids in starch-fatty acid complexes were analyzed and presented in **Table 12**. The modeling of fatty acid and chain length of added fatty acid were both found to affect the lipid content in the resulting starch-fatty acid complexes. Generally, the content of free lipids in the starch-fatty acid complexes from both Method

I and II increased when the chain length of fatty acids increased from 12 to 18 carbons. Meanwhile, the complexed lipid content of the starch-fatty acid complexes decreased with the increase in the fatty acids chain. Complexed lipids might be mainly from the fatty acids that formed single helix complex with linear amylose (*221*). The formation of V-amylose complex between amylose and lipids is found to be affected by the fatty acid chain length. Previous studies indicated that the V-amylose formation decreased with increased in the chain length since higher activation energy needed for complex formation with longer acyl chain (*269*). The free lipids could come from the fatty acid crystals that coated on the surface of starch granules or were physically trapped in some regions of starch granules other than within the helixes (*221*). Saturated fatty acids with longer aliphatic chain possess higher crystalline temperature and lower solubility in ethanol solutions, which are more susceptible to aggregation and crystallization during treatment. Consequently, increasing the chain length of the fatty acids led to higher content of free fatty acid residues in the complexes. The content of free fatty acids and complexed lipids in starch-unsaturated fatty acid complex was much lower than other starch-saturated fatty acid complexes. The decrease of free unsaturated fatty acid content in the complexes could be attributed to the relatively low crystalline temperature and high solubility in ethanol solutions of unsaturated fatty acid. The less efficient complexing between amylose and unsaturated fatty acids might be due to the nonlinear or kinked *cis*-double bound of unsaturated fatty acid requiring a larger helix cavity to accommodate the unsaturated portion of the acyl chain (*101, 270*).

Table 12. Lipid content of starch-fatty acid complexes.

Sample	Lipid content (g/100 g of dry starch sample)		
	acid hydrolyzed (total lipids, T)	petroleum ether extracted	T – F (complexed lipids)

		(free lipids, F)	
Method I-C12:0	2.84 ± 0.18	1.13 ± 0.47	1.71
Method I-C14:0	3.35 ± 0.32	1.68 ± 0.13	1.67
Method I-C16:0	3.47 ± 0.29	1.88 ± 0.36	1.59
Method I-C18:0	3.35 ± 0.47	1.84 ± 0.22	1.51
Method I-C18:1	2.41 ± 0.25	0.92 ± 0.19	1.49
Method II-C12:0	3.74 ± 0.31	1.33 ± 0.38	2.41
Method II-C14:0	3.58 ± 0.42	1.57 ± 0.16	2.01
Method II-C16:0	3.56 ± 0.15	1.71 ± 0.24	1.85
Method II-C18:0	3.50 ± 0.19	1.72 ± 0.28	1.78
Method II-C18:1	2.56 ± 0.23	0.99 ± 0.11	1.57

The addition modes of fatty acids (before or after heat treatment of starch) also impacted the interactions between starch and fatty acids. Starch-fatty acid complexes from Method II contained higher amount of total lipids and complexed lipids than their counterparts from Method I, while the free lipids content in complexes from Method II was lower than that from Method I except for starch-lauric acid complex. During Method I, addition of fatty acids was after the swelling and partial gelatinization of starch granules, leading to more porous and accessible structure in the amorphous and crystalline lamellae (*271*). Therefore, fatty acids were supposed to more easily penetrate into the granules, complex or entangle with the external and internal amylose. Since V-amylose formation was difficult between amylose and fatty acid with longer chain length, a large amount of the penetrated fatty acids might be physically trapped in the amorphous lamellae or between helixes of the crystalline lamellae. These physically trapped free fatty acids were hard to be removed during the washing procedure and retained in the resulting complexes. In the case of Method II, fatty acids were added before hydrothermal treatment, which provided longer reaction time between fatty acids and amylose to form V-amylose complex. And the fatty acids might coat on the surface of the starch granules, inhibiting the penetration of other fatty acids into the granules (*272*).

As a result, most of the free fatty acids were located on the surface of the granules, which could be easily removed by washing solutions. The obtained starch-fatty acid complexes would contain less free fatty acids.

The contact angles of these starch-fatty acid complexes were presented in **Table 13**. The contact angles of starch-saturated fatty acid complexes were ranged from 78.6º to 82.6º, which were much higher than that of native starch (46.1º). And the enhancement in the contact angle of the complexes was positively related to their total lipid contents. When the lipid contents of starch-fatty acid complexes prepared by Method I increased from 2.84 to 3.47 (g/100 g starch), contact angle of the complexes improved from 78.6º to 81.2º. Then the contact angle declined to 78.5º when the lipid content decreased to 3.35 (g/100 g starch). Similarly, the contact angle of complexes from Method II decreased from 82.6º to 80.9º with the lipid content decreasing from 3.74 to 3.50 (g/100 g starch). Containing higher lipid contents, starch-fatty acid complexes from Method II exhibited slightly higher contact angle than their counterparts from Method II. Compared to starch-saturated fatty acid complexes, contact angles of starch-unsaturated fatty acid complexes were much lower, which could be attributed to the low lipid content of the complexes. Increasing in the contact angle of starch-fatty acid complexes indicated the improvement of their hydrophobicity, which would adjust their affinity to the oil and water phase and might enhance their emulsifying efficiency when forming Pickering emulsions.

Table 13. Contact angle of starch-fatty acid complexes.

sample	Contact angle (º)
Native starch	46.1 ± 1.6
Method I-C12:0	78.6 ± 2.1
Method I-C14:0	79.4 ± 1.6
Method I-C16:0	81.2 ± 1.7

Method I-C18:0	78.5 ± 2.2
Method I-C18:1	62.3 ± 2.4
Method II-C12:0	82.6 ± 1.7
Method II-C14:0	82.1 ± 2.1
Method II-C16:0	81.7 ± 1.9
Method II-C18:0	80.9 ± 2.4
Method II-C18:1	64.2 ± 1.8

7.3.2. *In vitro* starch digestibility

According to previous classification method (*71*), the starch fractions hydrolyzed within 20 min and between 20 and 120 min were referred as “rapidly digested starch” and “slowly digested starch”, respectively. And the rest of the starch was categorized as “resistant starch”. The contents of RDS, SDS, and RS in different starch-fatty acid complexes were presented in **Table 14**. The RDS, SDS, and RS content of native starch were 75.2%, 6.5% and 18.8%, respectively. The addition modes of fatty acids and chain length of fatty acids were found to affect the enzymatic hydrolysis of starch. After complexing with fatty acids, the SDS and RS content of the complexes were markedly increased. The V-amylose complex formed between amylose and fatty acids is known to be resistant to enzymatic hydrolysis (*227*). These V-amylose complexes would restrict the swelling of starch during heating, and the free fatty acids coated on the surface of the starch granules, which could further reduce the accessibility of starch molecules to enzyme digestion (*96, 228*). In the case of starch-saturated fatty acids complexes, the content of RDS in the complexes from both Method I and II was decreased markedly, and the RS content increased with prolonged fatty acid chain length. The RS level in the starch-fatty acids complexes from Method II was slightly higher than that of their counterparts from Method I. The higher content of RS in complexes from Method II might be result from the more efficient formation of amylose-fatty acid complexes, which could be manifested by the higher complexed lipids content observed earlier. Compared

to native starch, the RS content of complexes was increased when complexing with unsaturated fatty acid. However, the RS level was lower than that of starch-saturated fatty acid complexes with same chain length, which might be attributed to lower thermal stability of amylose-unsaturated fatty acid complexes (*101*).

Table 14. RDS, SDS, and RS contents in the cooked starch-fatty acid complexes[a].

sample	RDS (%)	SDS (%)	RS (%)
Native starch	75.2 ± 1.4	6.5 ± 1.5	18.8 ± 0.8
Method I-C12:0	61.0 ± 0.6	13.4 ± 0.9	25.7 ± 0.5
Method I-C14:0	60.2 ± 1.4	13.5 ± 0.8	26.4 ± 1.1
Method I-C16:0	59.3 ± 1.2	13.8 ± 0.7	26.9 ± 1.3
Method I-C18:0	59.5 ± 1.5	13.3 ± 1.1	27.2 ± 1.6
Method I-C18:1	58.2 ± 1.3	14.7 ± 0.6	27.1 ± 0.9
Method II-C12:0	58.8 ± 1.7	14.0 ± 0.7	27.2 ± 0.9
Method II-C14:0	57.4 ± 1.3	13.7 ± 0.8	28.9 ± 1.6
Method II-C16:0	56.8 ± 1.6	14.2 ± 1.1	29.0 ± 1.5
Method II-C18:0	56.3 ± 1.2	14.4 ± 0.9	29.3 ± 1.7
Method II-C18:1	55.8 ± 1.4	15.6 ± 0.8	28.6 ± 0.8

[a]RDS, SDS, RS refer to rapidly digestible starch, slowly digestible starch, and resistant starch.

7.3.3. Emulsifying capacity of starch-fatty acid complexes

After complexing with fatty acids, the hydrophobicity of the resulting complexes was largely enhanced due to the long aliphatic chain of these fatty acids, which would adjust their affinity to the water and oil phase. The bulk images of Pickering emulsions stabilized by different starch-fatty acid complexes (o/w 1:1, 12 wt%) were presented in **Figure 46**. All the starch-saturated fatty acid complexes were able to stabilize Pickering emulsions, which were creaming quickly after the homogenization due to the large emulsion droplets. The emulsifying volume of emulsion stabilized by starch-lauric acid complex from Method I was the smallest and a noticeable amount of complex was settled

down at the bottom, indicating that its emulsifying ability might be less efficient than other complexes. In the case of starch-unsaturated fatty acid complexes, emulsifying phase seemed to be formed. However, a certain amount of oil phase was leaked out on the top of emulsion phase.

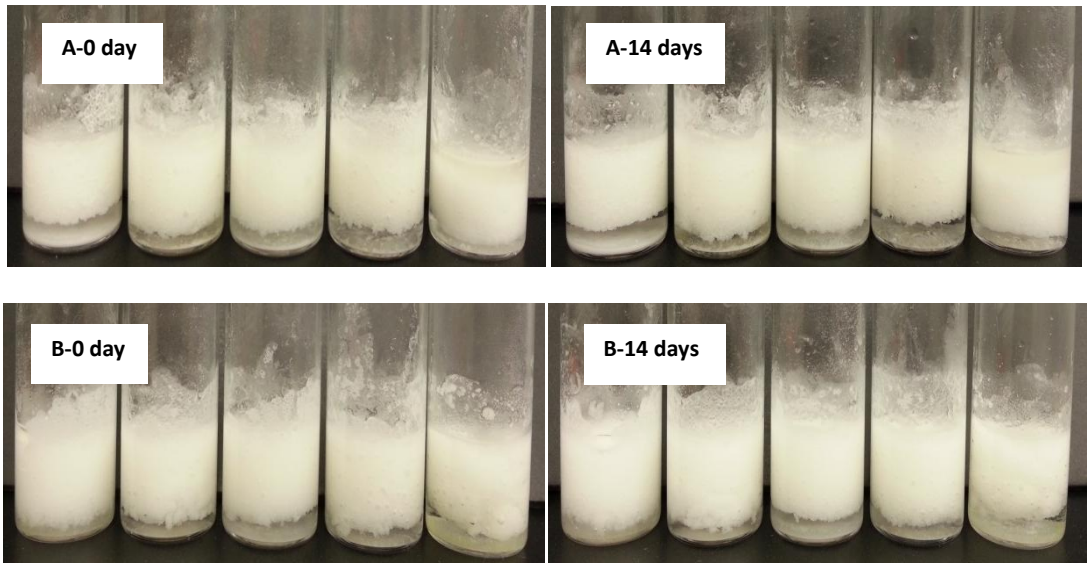

Figure 46. Vessels containing emulsions stabilized by starch-fatty acid complexes (o/w ratio 1:1). A. 12 wt% starch-fatty acid complexes prepared using Method I (From left to right: C12:0, C14:0, C16:0, C18:0, C18:1). B. 12 wt% starch-fatty acid complexes prepared using Method II (From left to right: C12:0, C14:0, C16:0, C18:0, C18:1).

The typical microscopic images, combined with average droplet size of these emulsions are presented in **Figure 47**. As evidenced from the images, the modes of adding fatty acids and chain length of fatty acids during complexes processing had a distinct influence on the size of the emulsion droplets. The difference in the emulsifying ability of these complexes was related to wettability of the complex particles at the oil-water interface, which was affected by the total lipids content of the complexes, the distribution of fatty acids in the complexes and the affinity of complexes at oil and water

phase. Emulsions stabilized by starch-fatty acid complexes from Method I seemed to have larger droplet size compared to those stabilized by complexes with same fatty acids from Method II. The energy needed to detach a particle (E) from the oil-water interface could be estimated from the equation: $E = \pi r^2 \gamma_{ow}(1-|cos\theta|)^2$, where r represents particle radius, γ_{ow} represents the oil-water interface tension, θ represents contact angle of particle at oil-water interface. Complexes from Method II contained a higher amount of total lipids, larger contact angles than their counterparts from Method I, indicating higher level of hydrophobicity. The detachment energy of complexes from Method II would be higher, and the resulting emulsions were more stable against coalescences. The distributions of fatty acids in the complexes would also adjust the position of complex particles at the oil-water interface by influencing the partial hydrophobicity of the complexes. The affinity of complexes towards oil and water phase could be affected by the solubility of fatty acids in the oil and water phase. The chain length of fatty acids exhibited small influence on the droplet size of the emulsions stabilized by complexes from Method I, while its effects on the emulsion droplets formed by complexes from Method II were more profound. The emulsions stabilized by starch-palmitic acid and -stearic acid complexes from Method II presented larger droplet size than emulsions stabilized by other starch-fatty acid complexes using the same method. The different emulsifying ability of complexes with similar amount of total lipids might be attributed to the last two factors. For emulsions stabilized by starch-saturated fatty acid complexes, densely packed starch particles could be clearly observed on the oil-water interface of discrete emulsion droplets. These packed particles would form strong steric barriers to further enhance the stability of adjacent droplets against coalescence (*38*). In the case of

starch-unsaturated fatty acid complexes, no discrete emulsion droplets were observed under microscopic images, indicating no stable emulsions were formed. These results suggested that complexing with unsaturated fatty acids might not be effective to enhance the emulsifying ability of native starch to form Pickering emulsions.

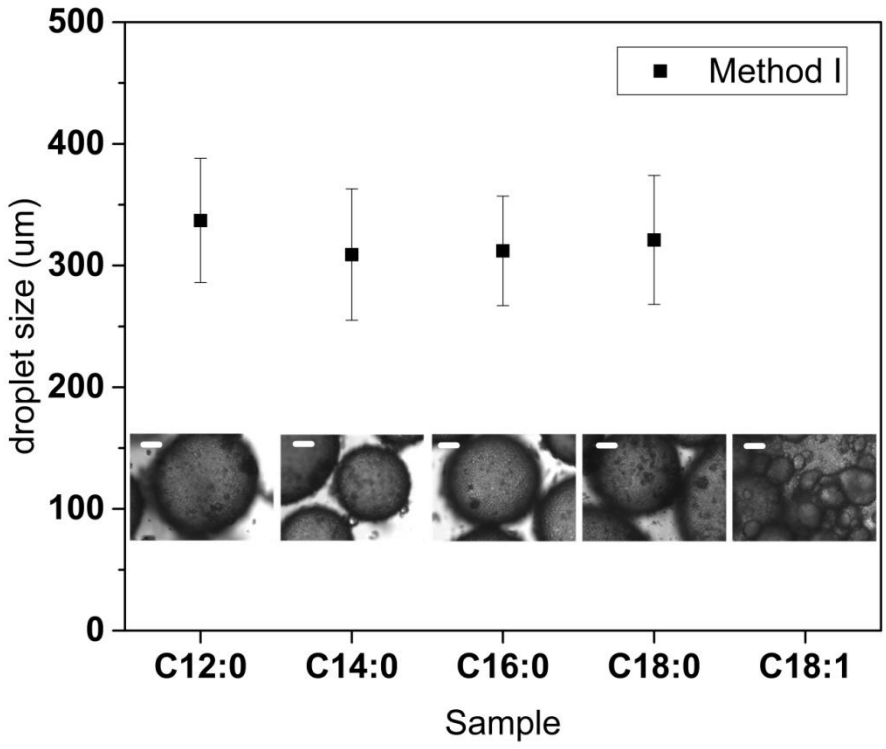

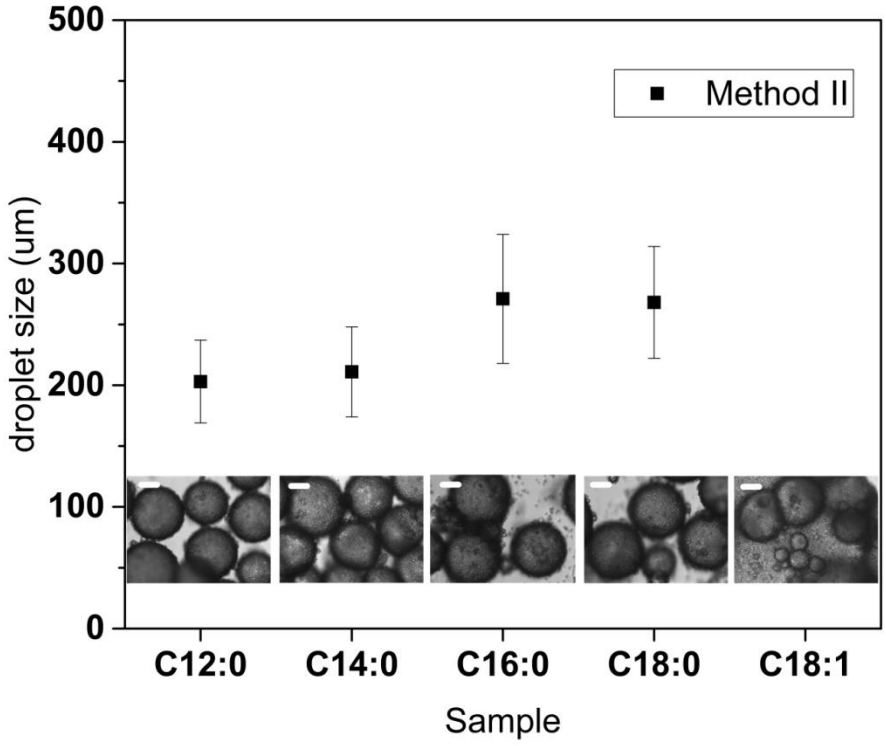

Figure 47. Microscopic images and droplet sizes of emulsions stabilized by different starch-fatty acid complexes (12 wt% starch complex, o/w 1:1). The solid bars in microscopic images correspond to the length of 100 μm.

7.3.4. Influence of heating on emulsion stability

The microscopic images and average droplet size of Pickering emulsions stabilized by different complexes under different heating conditions (60, 80, 100℃) were depicted in **Figure 48**. Studies have suggested that Pickering emulsion stabilized by starch granules remained stable under heat treatment, which led to partial gelatinized starch granules at the interface to protect the integrity of the emulsions droplets (*257, 273*). The droplet size measurements indicated that the heated emulsion droplets were slightly higher after heat treatment. And the emulsion droplets size increased with increased temperature treatment. The microscopic images showed that swelling of intact starch

granules were located at the oil-water interface. At heat temperature of 100℃, the starch-fatty acids complex granules still remained particle status besides from a noticeable swelling of these particles. The resulting emulsions were still stable with increase in the droplet size due to swelling of starch from heating. The benign stability of emulsion against heat treatment could be attributed to the relatively high gelatinization temperature of high-amylose starch (70~108℃) (*230*). Furthermore, the gelatinization temperature of starch-fatty acid complexes would be further increased due to the formation of amylose-fatty acid crystalline complex, which had high melting temperature of larger than 100℃ (*78*). The swelling of starch particles under heat treatment in starch stabilized Pickering emulsions was found to provide better barrier properties and protect the integrity of droplets under freezing and freeze-drying (*257, 273*). It suggested that these heated Pickering emulsions might have potential applications as delivery and encapsulation systems of lipophilic compounds in food and pharmaceutical products.

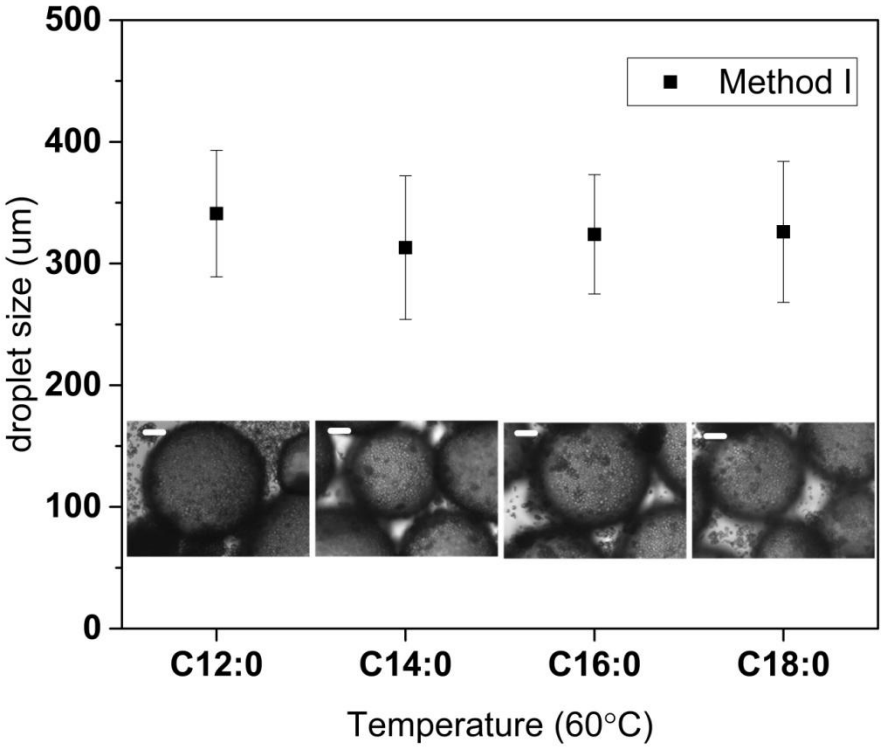
Method I
droplet size (um)
500
400
300
200
100
0
C12:0
C14:0
C16:0
C18:0
Temperature (60°C)

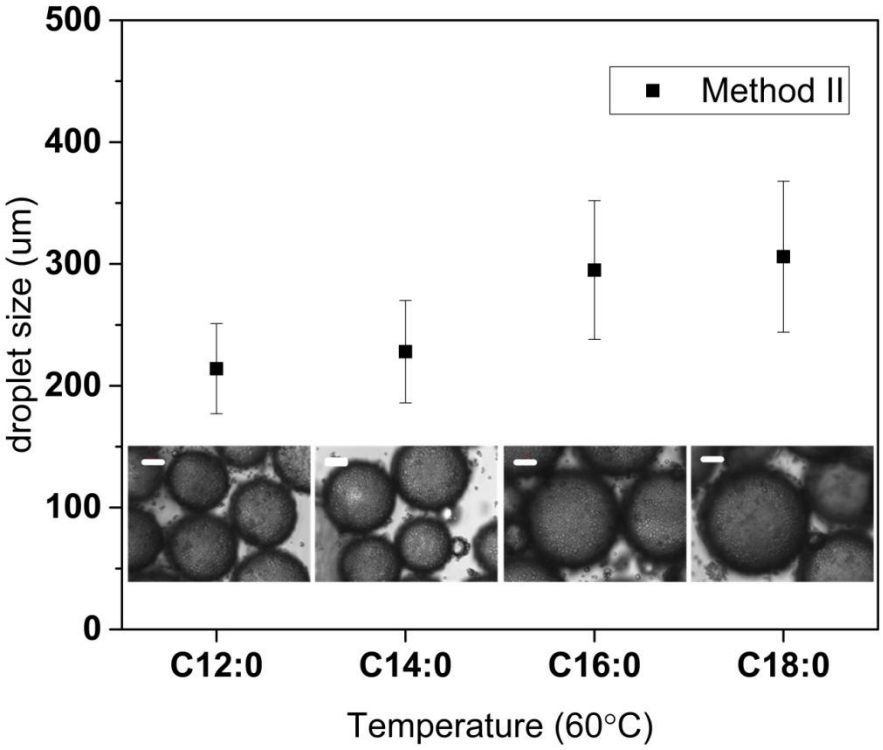
Method II
droplet size (um)
500
400
300
200
100
0
C12:0
C14:0
C16:0
C18:0
Temperature (60°C)

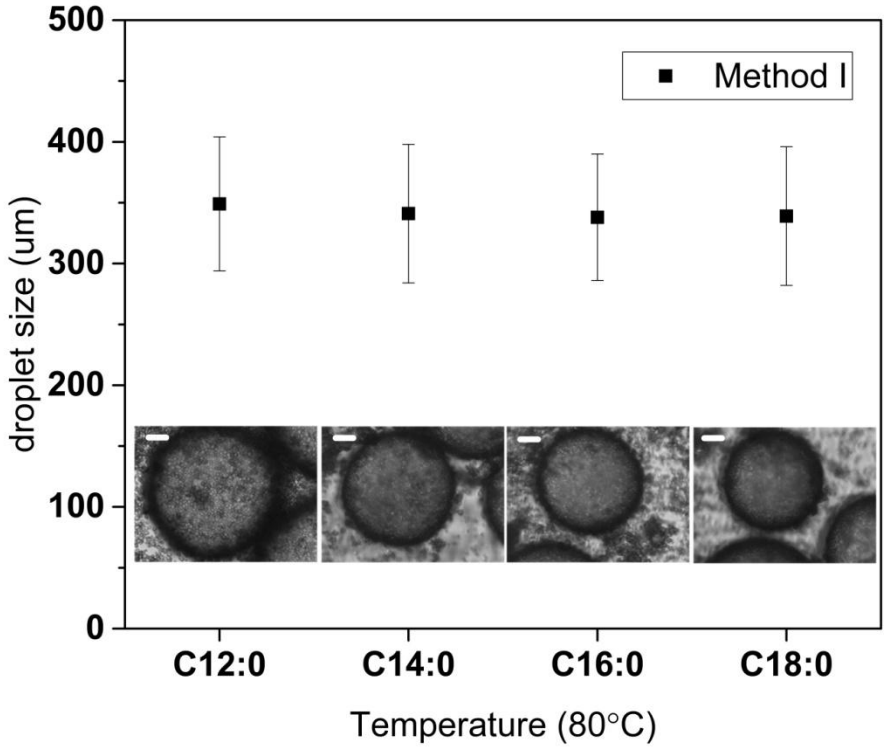
Method I
droplet size (um)
500
400
300
200
100
0
C12:0
C14:0
C16:0
C18:0
Temperature (80°C)

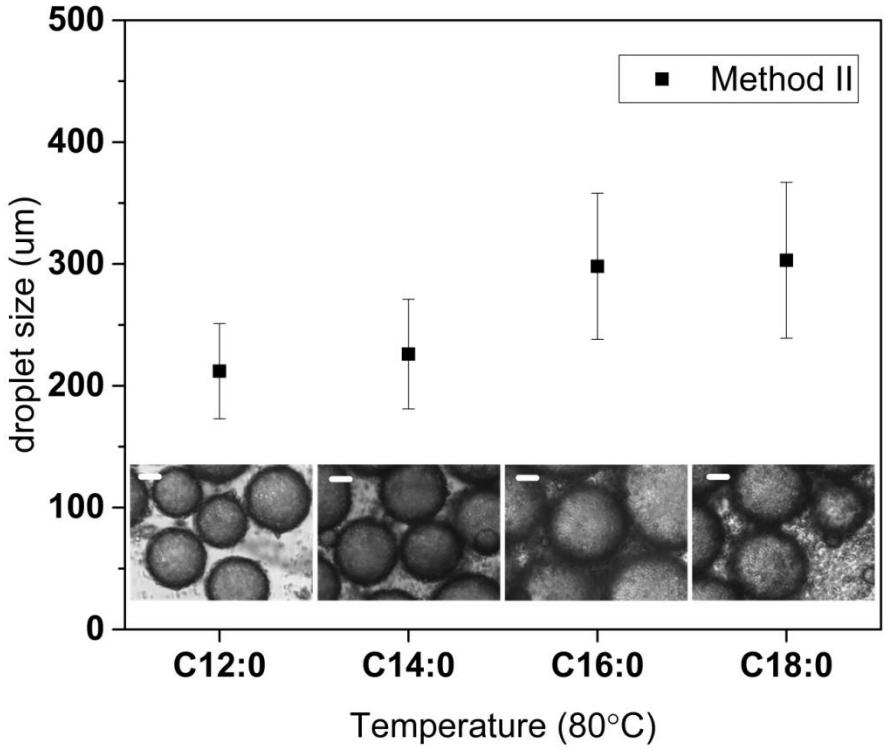
Method II
droplet size (um)
500
400
300
200
100
0
C12:0
C14:0
C16:0
C18:0
Temperature (80°C)

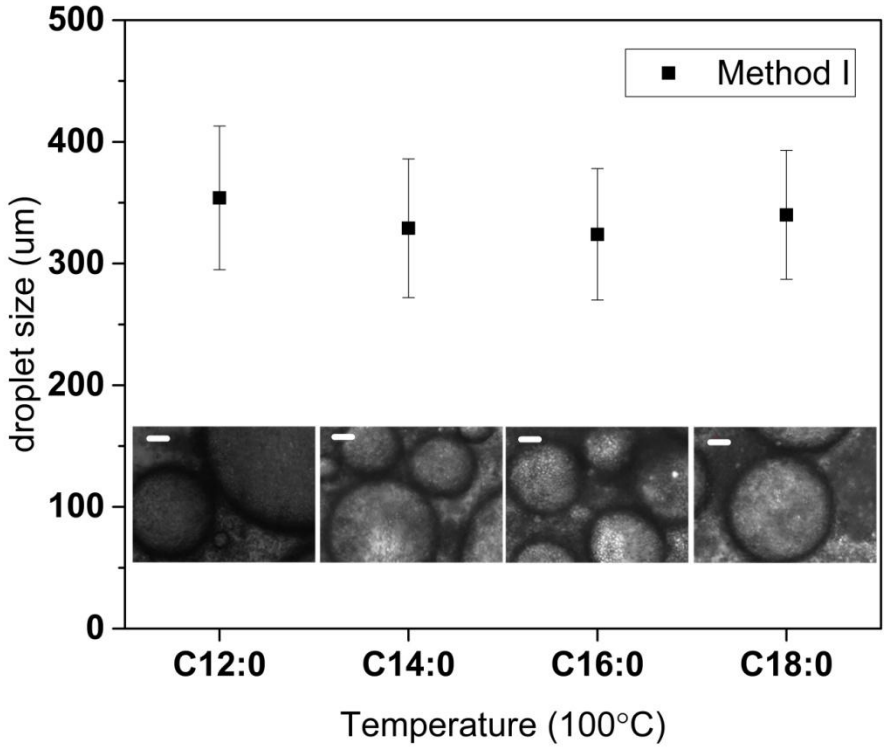
500
400
300
200
100
0
droplet size (um)
Method I
C12:0
C14:0
C16:0
C18:0
Temperature (100°C)

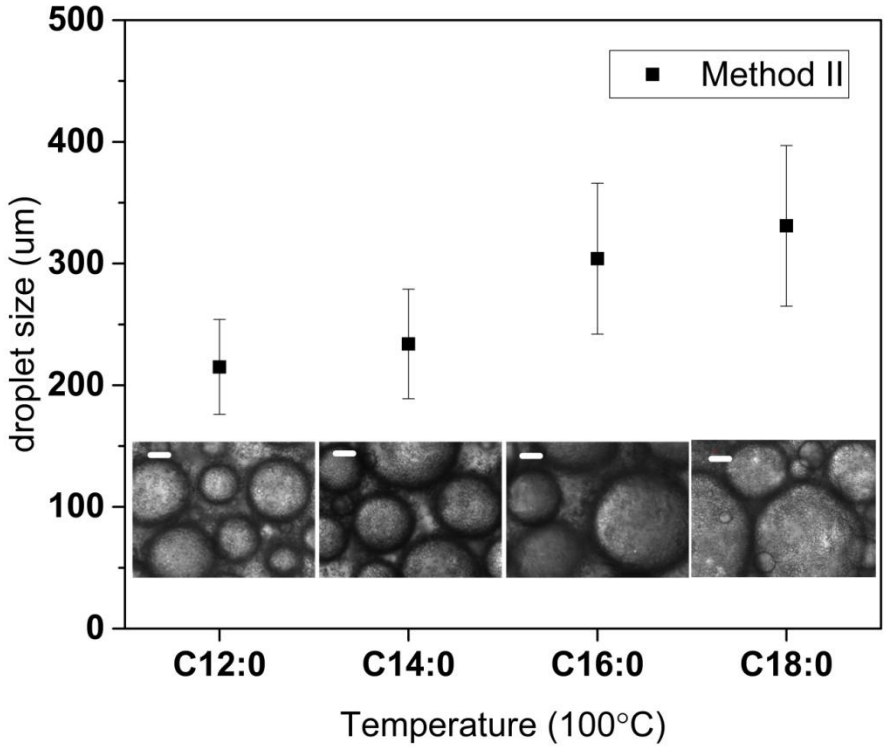

Figure 48. Microscopic images and droplet sizes of emulsions stabilized by different starch-fatty acid complexes after different heat treatments (12 wt% starch complex, o/w 1:1). The solid bars in microscopic images correspond to the length of 100 μm.

7.3.5. Encapsulation of PMFs in starch-fatty acid complexes stabilized Pickering emulsions and their digestion profile under simulated intestinal digestion

Since starch-fatty acid complexes prepared using Method II seemed to exhibit better emulsifying ability, Pickering emulsion systems stabilized these complexes were used to encapsulate two major PMFs (5-demethyltangeretin and 5-demethylnobiletin). The oil/water ratio was set at 1:0.8 to increase the oil faction in the emulsions and decrease the creaming effect. The bulk images of PMFs loaded emulsions stabilized by starch-fatty acid complexes with different fatty acids were presented in **Figure 49(i)**. And the microstructure of these emulsions before and after *in vitro* digestion process were depicted in **Figure 49(ii)**. After encapsulating PMFs, stable emulsions with no creaming

effects were formed. The emulsions exhibited light yellow color coming from PMFs. Discrete emulsion droplets covered with complex granules were observed under optical microscope. The *in vitro* small intestinal digestions of these emulsions were characterized using a pH-stat lipolysis model. The release of fatty acids vs digested time, lipase activity during hydrolysis and bioaccessibility of PMFs after lipolysis were monitored and presented in **Figure 50**. Also, the structure of digestion buffer at the end of lipolysis was observed under optical microscope, seen in **Figure 49(ii)**. After the lipolysis process, the starch-fatty acid complexes remained their intact granular structure despite the fatty acids used, which indicated that starch-fatty acid complexes were resistant to the hydrolysis of amylase (coming from the pancreatin suspension). Compared to emulsions stabilized by complexes with fatty acids (C14:0, C16:0, C18:0), the extent of lipolysis of starch-lauric fatty complexes stabilized emulsions was slower and lower. And its lipase activity recorded was the lowest. The lipolysis progress is the hydrolysis of oil droplets under actions of lipase and gradual detachment of hydrolyzed products (mainly monoglycerides and fatty acids) from the oil droplet surface for further hydrolysis (*209*). The better barrier properties of starch-lauric acid complex against lipase hydrolysis might be resulted from the higher content of fatty acids in the complexes. These complexes covering the surface of oil droplets would restrict the interactions between lipase and oil droplets since the fatty acids in the complexes were hard to be removed from the surface. The bioaccessibility of PMFs during lipolysis was the lowest and the highest in emulsions stabilized by starch-lauric acid complex and starch-palmtic acid complex, respectively. It is worth noting that the transformation of 5-demethyltangeretin to tangeretin or 5-demethylnobiletin to nobiletin was limited (HPLC analysis, data was not

presented), which could explain the much higher bioaccessibility of PMFs in these formulations than that in previous lecithin-based emulsions (bioaccessibility of 5-demethyltangeretin, < 1%) (*266*).

(i)

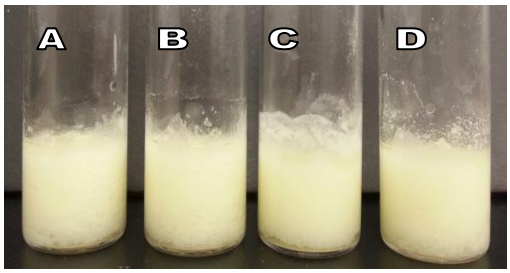

(ii)

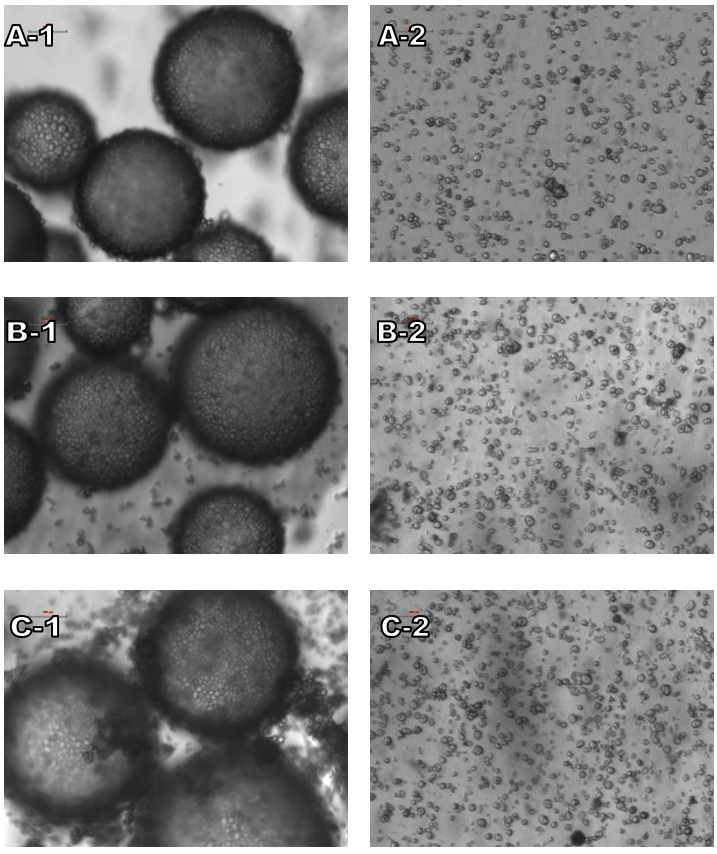

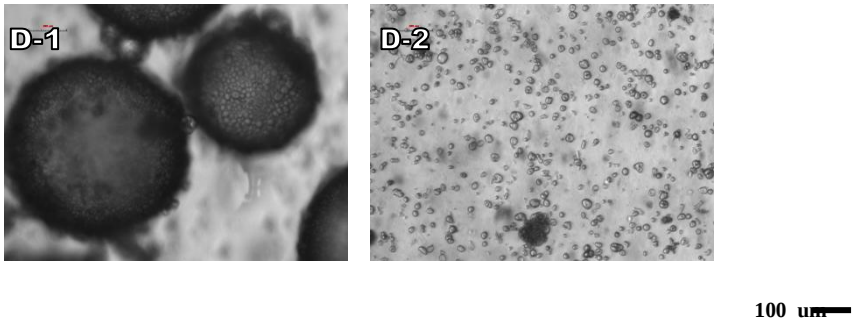

Figure 49. (i) Bulk images and (ii) Microscopic images of PMF-loaded different starch-fatty acid complexes stabilized emulsions before (1) and after lipolysis (2) (12 wt% starch-fatty acid complexes, o/w 1:0.8). From A to D: C12:0, C14:0, C16:0, C18:0.

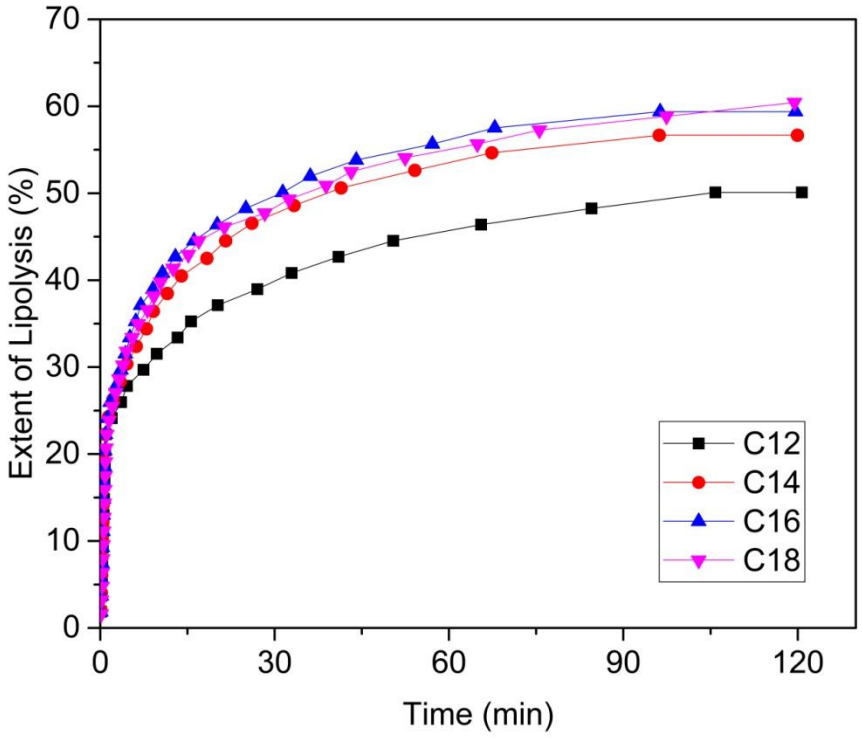

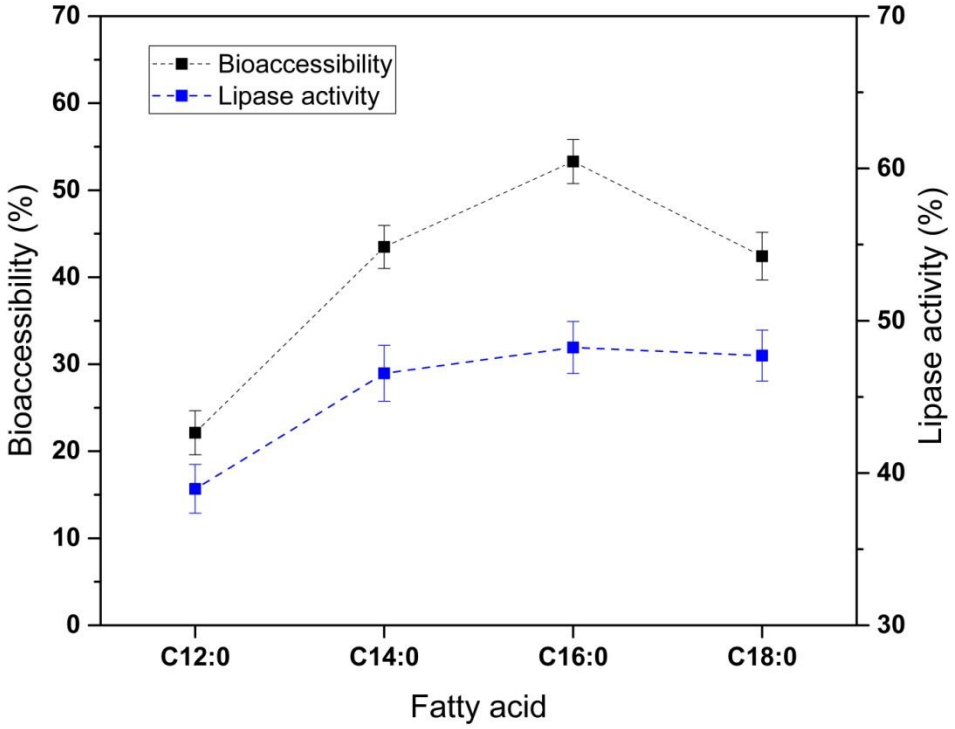

Figure 50. Extent of lipolysis, lipase activity and bioaccessbility of PMFs in different starch-fatty acid complexes stabilized emulsions. Data was presented as mean ± standard deviation.

7.3.6. Effect of starch swelling from heating on lipolysis of PMFs loaded-Pickering emulsions during simulated intestinal digestion

The *in vitro* digestion of Pickering emulsions stabilized by different starch-fatty acid complexes suggested that the barrier properties of emulsions using starch-lauric acid complexes were better than using other complexes. Hence, starch-lauric acid complexes stabilized emulsions were treated with heating process to further investigate the effect of starch swelling on the barrier properties. The bulk images of PMFs loaded emulsions stabilized by starch-lauric acid complexes after heating at different temperature (60, 80, 100℃), the microstructure of these emulsions before and after lipolysis process were presented in **Figure 51**. After heating treatment, a slight creaming effect was observed in

the emulsions. However, these emulsions still remained stable. Discrete emulsion droplets were observed under optical microscope. With the increasing of heating temperature from 60 to 100℃, a noticeable swelling of starch granules was observed, especially at the temperature of 100℃. The swelling of starch granules would make these granules more susceptible to hydrolysis of amylase. As depicted in **Figure 51**, the complexes remained granular structure after lipolysis process, indicating that these complexes possessed resistance to amylase digestion even after certain heat treatment. For emulsions without heat treatment, there would be space between individual granules at the oil-water interface even at close packing. As the result, the oil droplets would be easily accessible for lipase. The partial gelatinized complex granules would form a thickness layer around the emulsion droplets, which made them more impermeable for lipase activity as compared to non-heated emulsions. The digestion profile of these emulsions, lipase activity and bioaccessibility of PMFs after lipolysis process were presented in **Figure 52**. Compared to non-heat emulsions, the extent of lipolysis was slower and lower when the emulsions were heated at 60 and 80℃. And the lipolysis rate of emulsions became similar to that of non-heat emulsions when the heating temperature increased to 100℃. Accordingly, the lipase activity dropped to the lowest at 60℃. It then slightly increased after heating at 80℃, which was still much lower than non-heated samples. These phenomena could be interpreted as higher barrier properties of swelling starch to cover oil droplet surface resulting from heating process. The release of PMFs during lipolysis was reduced at heating temperature of 60 and 80℃ due to the improved barrier properties (**Figure 52**). However, the enhanced barrier effect from swelling starch was not observed in emulsions with heat treatment of 100℃, which might be attributed to

the high level of starch gelatinization resulting in the broken down of some starch granular structure.

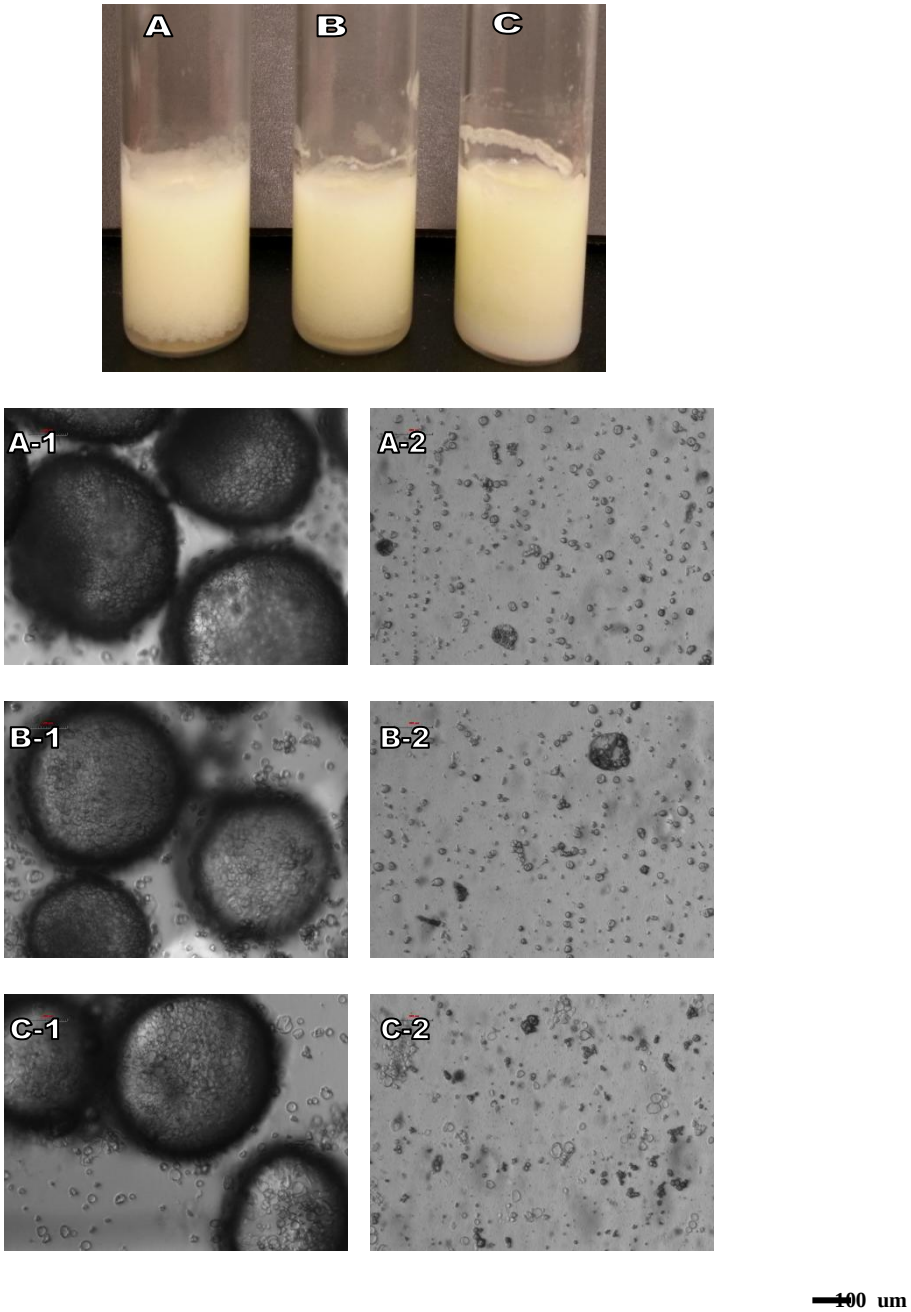

Figure 51. Microscopic images of PMFs-loaded starch-fatty acid complexes stabilized emulsions with different heat-treatments before (1) and after lipolysis (2) (12 wt% starch-lauric acid complexes, o/w 1:0.8). From A to C: 60, 80,100℃.

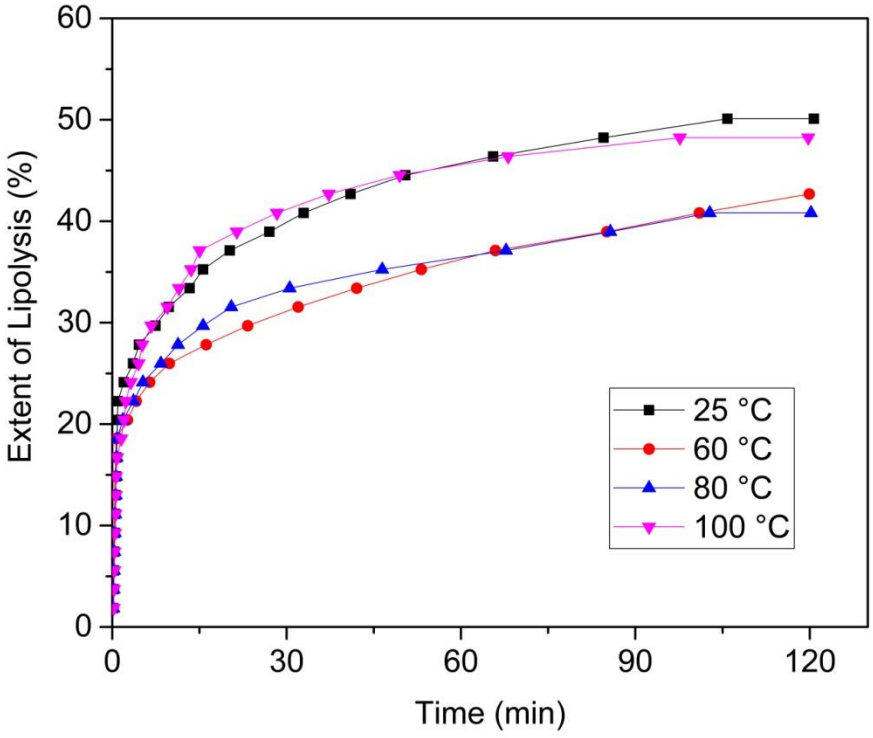
Extent of Lipolysis (%)
Time (min)
25 °C
60 °C
80 °C
100 °C

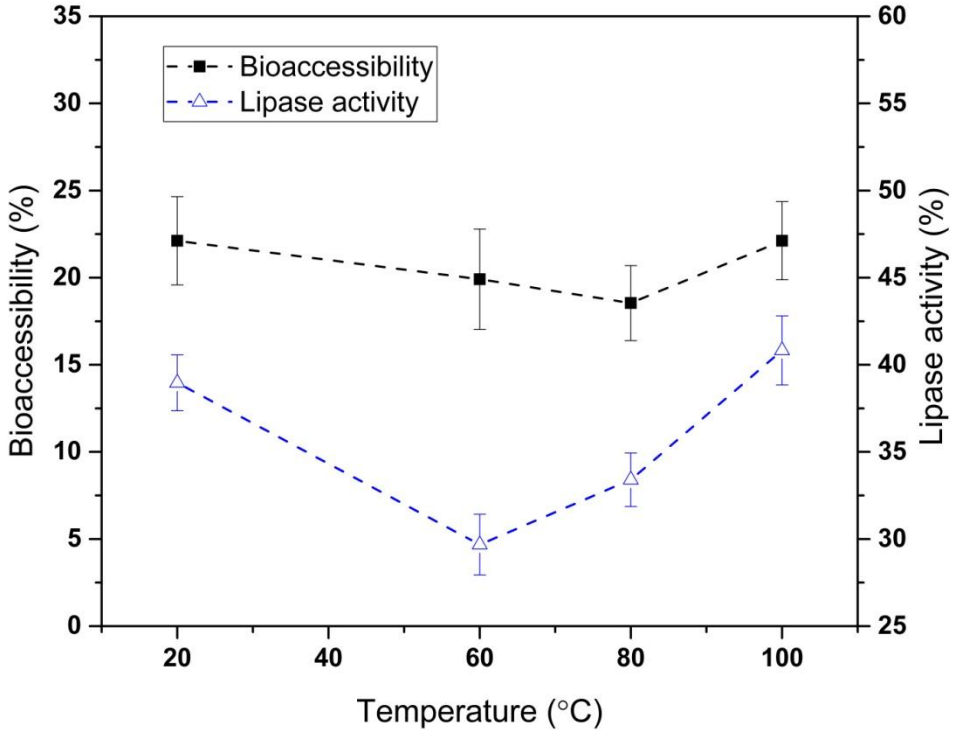
Bioaccessibility
Lipase activity
Bioaccessibility (%)
Lipase activity (%)
Temperature (°C)

Figure 52. Extent of lipolysis, lipase activity and bioaccessbility of PMFs in starch-fatty acid complexes stabilized emulsions after different heat treatments. Data was presented as mean ± standard deviation.

7.4. Conclusion

V-amylose complexes were formed by complexing starch and fatty acid with different chain lengths using two heat-moisture treatment methods. *In vitro* digestibility study suggested that these complexes exhibited enzymatic resistance compared to native starch. The hydrophilic properties of starch were improved when complexing with fatty acids. With improved affinity towards oil and water phases, starch complexes with saturated fatty acids of chain length ranging from 12 to 18 were able to form stable Pickering emulsion and exhibited different emulsifying efficiencies. However, the emulsifying ability of complexes with unsaturated fatty acid was poor. The addition of fatty acids into the starch retarded the gelatinization of starch. Emulsions stabilized by these complexes were stable under heat treatment of 60, 80 and 100℃. Starch-fatty acid complexes stabilized Pickering emulsions were used to encapsulate PMFs (5-demethyltangeretin and 5-demethylnobiletin). The *in vitro* lipolysis of PMFs loaded emulsions suggested that starch-lauric acid complexes provided better barrier properties during lipolysis process compared to other complexes. Heating treatment of emulsions under 60 and 80℃ improved the barrier properties of the emulsions due to the swelling of starch. The lipase activity during lipolysis reached a minimum at heat treatment of 60℃. But this enhanced barrier effect was disappeared when the heating temperature was 100℃ since the partial gelatinization of starch was more severe. These results revealed the potential to create resistant starch based emulsion encapsulation systems with controlled barrier properties using heating process. This emulsion system could be used

for encapsulation and release of lipophilic compounds in various food and pharmaceutical products.

CHAPTER 8 SUMMARY AND FUTURE WORK

8.1. Summary of the dissertation

This study provided three approaches to develop Pickering emulsifiers derived from two major biomass materials, cellulose and starch. Media milling was found to effectively modify native starch and cellulose. The particle size of starch and cellulose was largely reduced through the milling process. And some of the physicochemical properties were also modified. The resulting milled starch and cellulose particles were able to stabilize Pickering emulsions with good stability. Milled starch and cellulose stabilized Pickering emulsions were proved to be effective encapsulation and delivery systems for model lipophilic bioactive compound, curcumin. Encapsulated curcumin maintained benign stability during storage. And enhanced release of curcumin from these Pickering emulsions during *in vitro* digestion condition was also observed compared to control samples.

Starch-fatty acid complexes were formed through complexing long/medium chain fatty acids with starch under heat-moisture treatment. Due to collapsed helical conformation and crystalline structure resulting from the hydrophobic interaction between amylose and fatty acids, these starch-fatty acid complexes were resistant to enzyme hydrolysis, which largely maintained the original granular shape of native starch. Their hydropobicity was increased steadily. As the result, the dual wettability of the resistant starch in the oil-water interface was largely enhanced. Pickering emulsions stabilized by these resistant starches exhibited good stability under different heating conditions. Certain heat treatment was found to enhance the barrier properties of these Pickering emulsions when encapsulating liphophilic compounds, PMFs.

This study provides approaches of producing natural particle emulsifiers, which could fulfill the strong market trend of formulating product, that is edible in theory and maintain the consumer perception of being natural and “green” and still on a scale or at a suitable price for general industrial use, including food, cosmetic and pharmaceutical industry.

8.2. Future work and directions

Due to the limitation of experimental design, time and resources, some meaningful experiments related to this study were not able to be performed. However, they are worth mentioning and thus can be proposed as future work and directions.

Although native starch and cellulose have extremely different structure, media milling process was able to modify them with effectiveness. And a variety of nano/submicrometer particles from other food materials, such as yam (*54*), soybean (*52*), wheat bran dietary fiber (*69*), chitosan (*70*) and *Ganoderma tsugae* (*53*) have been produced using media milling process. Therefore, it is highly possible that media milling would be able to modify other materials as particular emulsifiers for Pickering emulsions. These nano/submicrometer particles might form Pickering emulsions with different properties. And some functional properties could also be brought into these Pickering emulsion systems when materials with bioactive compounds were used.

Since resistant starch was resistant to the digestion of human and will reach the large intestine to interact with the gut microbiota. Studies have suggested that resistant starch would be fermented by the gut microorganism and produced some fermentation products, such as methane, carbon dioxide, hydrogen, organic acids (e.g. lactic acid) and short chain fatty acids (SCFA), which could lower luminal pH, enhance colonic blood flow,

and restrict the development of abnormal colonic cells (*88*). Consumption of Pickering emulsions formed by starch-fatty acid complexes might not only reduce the possible blood glucose increase, but also bring health beneficial effects coming from the resistant starch. To investigate the interactions of starch-fatty acid complex stabilized Pickering emulsion systems with the gut microbiota would be extremely meaningful to reveal the functional benefits of these Pickering emulsion systems.

The single helix structure of amylose has been proven to form inclusion complexes with a variety of lipophilic guest molecules, such as fatty acids, alcohols, aldehydes, and ketones (*221*). And it has also been proved to form inclusion complexes with bulkier molecules, such as genistein and aroma compounds, increasing stability, modulating release, and improving sensory properties of guest compounds (*221, 274, 275*). Therefore, it is possible for the single helix molecules to form complex structure with lipophilic bioactive compounds and the resulting complexes to stabilize Pickering emulsion. In the future, the formation of lipophilic bioactive compound-amylose complexes and their ability to stabilize novel Pickering emulsion system could be developed.

Reference

1. Rayner, M.; Marku, D.; Eriksson, M.; Sjoo, M.; Dejmek, P.; Wahlgren, M., Biomass-based particles for the formulation of Pickering type emulsions in food and topical applications. *Colloid Surface A* **2014,** *458*, 48-62.
2. Ramsden, W., Separation of Solids in the Surface-Layers of Solutions and'Suspensions'(Observations on Surface-Membranes, Bubbles, Emulsions, and Mechanical Coagulation).--Preliminary Account. *Proceedings of the royal Society of London* **1903,** *72*, 156-164.
3. Pickering, S. U., CXCVI.—emulsions. *Journal of the Chemical Society, Transactions* **1907,** *91*, 2001-2021.
4. Binks, B. P., Particles as surfactants - similarities and differences. *Curr Opin Colloid In* **2002,** *7*, 21-41.
5. Hunter, T. N.; Pugh, R. J.; Franks, G. V.; Jameson, G. J., The role of particles in stabilising foams and emulsions. *Adv Colloid Interfac* **2008,** *137*, 57-81.
6. Miller, R.; Fainerman, V. B.; Kovalchuk, V. I.; Grigoriev, D. O.; Leser, M. E.; Michel, M., Composite interfacial layers containing micro-size and nano-size particles. *Adv Colloid Interfac* **2006,** *128*, 17-26.
7. Wilhelm, K. P.; Cua, A. B.; Wolff, H. H.; Maibach, H. I., Surfactant-Induced Stratum-Corneum Hydration in-Vivo - Prediction of the Irritation Potential of Anionic Surfactants. *J Invest Dermatol* **1993,** *101*, 310-315.
8. Friberg, S. E., Foams from non-aqueous systems. *Curr Opin Colloid In* **2010,** *15*, 359-364.
9. Chassaing, B.; Koren, O.; Goodrich, J. K.; Poole, A. C.; Srinivasan, S.; Ley, R. E.; Gewirtz, A. T., Dietary emulsifiers impact the mouse gut microbiota promoting colitis and metabolic syndrome. *Nature* **2015,** *519*, 92-U192.
10. Tan, K. Y.; Gautrot, J. E.; Huck, W. T. S., Formation of Pickering Emulsions Using Ion-Specific Responsive Colloids. *Langmuir* **2011,** *27*, 1251-1259.
11. Eskandar, N. G.; Simovic, S.; Prestidge, C. A., Chemical stability and phase distribution of all-trans-retinol in nanoparticle-coated emulsions. *Int J Pharmaceut* **2009,** *376*, 186-194.
12. Binks, B. P.; Lumsdon, S. O., Pickering emulsions stabilized by monodisperse latex particles: Effects of particle size. *Langmuir* **2001,** *17*, 4540-4547.
13. Ashby, N. P.; Binks, B. P., Pickering emulsions stabilised by Laponite clay particles. *Phys Chem Chem Phys* **2000,** *2*, 5640-5646.
14. Augustin, M. A.; Hemar, Y., Nano- and micro-structured assemblies for encapsulation of food ingredients. *Chem Soc Rev* **2009,** *38*, 902-912.
15. Dickinson, E., Use of nanoparticles and microparticles in the formation and stabilization of food emulsions. *Trends in Food Science & Technology* **2012,** *24*, 4-12.
16. Tan, Y.; Xu, K.; Niu, C.; Liu, C.; Li, Y.; Wang, P.; Binks, B. P., Triglyceride–water emulsions stabilised by starch-based nanoparticles. *Food Hydrocolloids* **2014,** *36*, 70-75.
17. Andresen, M.; Stenius, P., Water-in-oil emulsions stabilized by hydrophobized microfibrillated cellulose. *J Disper Sci Technol* **2007,** *28*, 837-844.
18. Tzoumaki, M. V.; Moschakis, T.; Kiosseoglou, V.; Biliaderis, C. G., Oil-in-water emulsions stabilized by chitin nanocrystal particles. *Food Hydrocolloids* **2011,** *25*, 1521-1529.
19. Gupta, R.; Rousseau, D., Surface-active solid lipid nanoparticles as Pickering

stabilizers for oil-in-water emulsions. *Food & function* **2012,** *3*, 302-311.
20. de Folter, J. W. J.; van Ruijven, M. W. M.; Velikov, K. P., Oil-in-water Pickering emulsions stabilized by colloidal particles from the water-insoluble protein zein. *Soft Matter* **2012,** *8*, 6807-6815.
21. Xiao, J.; Li, C.; Huang, Q., Kafirin Nanoparticle-Stabilized Pickering Emulsions as Oral Delivery Vehicles: Physicochemical Stability and in Vitro Digestion Profile. *J Agric Food Chem* **2015,** *63*, 10263-70.
22. Luo, Z. J.; Murray, B. S.; Ross, A. L.; Povey, M. J. W.; Morgan, M. R. A.; Day, A. J., Effects of pH on the ability of flavonoids to act as Pickering emulsion stabilizers. *Colloid Surface B* **2012,** *92*, 84-90.
23. Gould, J.; Vieira, J.; Wolf, B., Cocoa particles for food emulsion stabilisation. *Food & function* **2013,** *4*, 1369-1375.
24. Tan, Y.; Xu, K.; Liu, C.; Li, Y.; Lu, C.; Wang, P., Fabrication of starch-based nanospheres to stabilize pickering emulsion. *Carbohydrate Polymers* **2012,** *88*, 1358-1363.
25. Kalashnikova, I.; Bizot, H.; Bertoncini, P.; Cathala, B.; Capron, I., Cellulosic nanorods of various aspect ratios for oil in water Pickering emulsions. *Soft Matter* **2013,** *9*, 952-959.
26. Yusoff, A.; Murray, B. S., Modified starch granules as particle-stabilizers of oil-in-water emulsions. *Food Hydrocolloids* **2011,** *25*, 42-55.
27. Shimoni, G.; Levi, C. S.; Tal, S. L.; Lesmes, U., Emulsions stabilization by lactoferrin nano-particles under in vitro digestion conditions. *Food Hydrocolloids* **2013,** *33*, 264-272.
28. Wongkongkatep, P.; Manopwisedjaroen, K.; Tiposoth, P.; Archakunakorn, S.; Pongtharangkul, T.; Suphantharika, M.; Honda, K.; Hamachi, I.; Wongkongkatep, J., Bacteria Interface Pickering Emulsions Stabilized by Self-assembled Bacteria-Chitosan Network. *Langmuir* **2012,** *28*, 5729-5736.
29. Sylvia. Lansky, M. K., Thomas John. Schoch, Properties of the fractions and linear subfractions from various starches. *J. Am. Chem. Soc* **1949,** *71*, 4066-4075.
30. Le Corre, D.; Bras, J.; Dufresne, A., Starch Nanoparticles: A Review. *Biomacromolecules* **2010,** *11*, 1139-1153.
31. Waigh, T. A.; Donald, A. M.; Heidelbach, F.; Riekel, C.; Gidley, M. J., Analysis of the native structure of starch granules with small angle x-ray microfocus scattering. *Biopolymers* **1999,** *49*, 91-105.
32. Jenkins, P. J.; Donald, A. M., The influence of amylose on starch granule structure. *Int J Biol Macromol* **1995,** *17*, 315-321.
33. Matveev, Y. I.; Elankin, N. Y.; Kalistrova, E. N.; Danilenko, A. N.; Niemann, C.; Yuryev, V. P., Estimation of contributions of hydration and glass transition to heat capacity changes curing melting of native starches in excess water. *Starch-Starke* **1998,** *50*, 141-147.
34. Cheetham, N. W. H.; Tao, L. P., The effects of amylose content on the molecular size of amylose, and on the distribution of amylopectin chain length in maize starches. *Carbohyd Polym* **1997,** *33*, 251-261.
35. Cheetham, N. W. H.; Tao, L. P., Variation in crystalline type with amylose content in maize starch granules: an X-ray powder diffraction study. *Carbohydrate Polymers* **1998,** *36*, 277-284.

36. Gerard, C.; Planchot, V.; Buleon, A.; Colonna, P., Crystalline structure and gelatinisation behaviour of genetically modified maize starches. *Colloq Inra* **1999**, 59-63.
37. Sievert, D.; Wursch, P., Amylose Chain Association Based on Differential Scanning Calorimetry. *J Food Sci* **1993,** *58*, 1332-1334.
38. Li, C.; Li, Y.; Sun, P.; Yang, C., Pickering emulsions stabilized by native starch granules. *Colloids and Surfaces A: Physicochemical and Engineering Aspects* **2013,** *431*, 142-149.
39. Li, C.; Li, Y.; Sun, P.; Yang, C., Starch nanocrystals as particle stabilisers of oil-in-water emulsions. *Journal of the science of food and agriculture* **2014,** *94*, 1802-7.
40. Li, C.; Sun, P.; Yang, C., Emulsion stabilized by starch nanocrystals. *Starch - Stärke* **2012**, n/a-n/a.
41. Zhou, J.; Chang, C.; Zhang, R.; Zhang, L., Hydrogels prepared from unsubstituted cellulose in NaOH/Urea aqueous solution. *Macromol Biosci* **2007,** *7*, 804-809.
42. Mazeau, K.; Heux, L., Molecular dynamics simulations of bulk native crystalline and amorphous structures of cellulose. *J Phys Chem B* **2003,** *107*, 2394-2403.
43. Kalashnikova, I.; Bizot, H.; Cathala, B.; Capron, I., New Pickering Emulsions Stabilized by Bacterial Cellulose Nanocrystals. *Langmuir* **2011,** *27*, 7471-7479.
44. Capron, I.; Cathala, B., Surfactant-Free High Internal Phase Emulsions Stabilized by Cellulose Nanocrystals. *Biomacromolecules* **2013,** *14*, 291-296.
45. Pereda, M.; Dufresne, A.; Aranguren, M. I.; Marcovich, N. E., Polyelectrolyte films based on chitosan/olive oil and reinforced with cellulose nanocrystals. *Carbohydrate Polymers* **2014,** *101*, 1018-1026.
46. Xhanari, K.; Syverud, K.; Chinga-Carrasco, G.; Paso, K.; Stenius, P., Structure of nanofibrillated cellulose layers at the o/w interface. *Journal of colloid and interface science* **2011,** *356*, 58-62.
47. Kargar, M.; Fayazmanesh, K.; Alavi, M.; Spyropoulos, F.; Norton, I. T., Investigation into the potential ability of Pickering emulsions (food-grade particles) to enhance the oxidative stability of oil-in-water emulsions. *Journal of colloid and interface science* **2012,** *366*, 209-215.
48. Blaker, J. J.; Lee, K. Y.; Li, X. X.; Menner, A.; Bismarck, A., Renewable nanocomposite polymer foams synthesized from Pickering emulsion templates. *Green Chem* **2009,** *11*, 1321-1326.
49. Ougiya, H.; Watanabe, K.; Morinaga, Y.; Yoshinaga, F., Emulsion-stabilizing effect of bacterial cellulose. *Biosci Biotech Bioch* **1997,** *61*, 1541-1545.
50. Wege, H. A.; Kim, S.; Paunov, V. N.; Zhong, Q. X.; Velev, O. D., Long-term stabilization of foams and emulsions with in-situ formed microparticles from hydrophobic cellulose. *Langmuir* **2008,** *24*, 9245-9253.
51. DOE, U., Genomics:GTL Roadmap, DOE/SC-0090. In *U.S. Department of Energy Office of Science*, 2005; p 204.
52. Kuo, H. Y.; Chen, S. H.; Yeh, A. I., Preparation and Physicochemical Properties of Whole-Bean Soymilk. *J Agr Food Chem* **2014,** *62*, 742-749.
53. Chiang, Y. H.; Chen, S. H.; Yeh, A. I., Preparation of Nano/Submicrometer Ganoderma tsugae and Its Mutagenic Potencies and Cytotoxicity. *J Agr Food Chem* **2014,** *62*, 12244-12255.
54. Chiang, L. H.; Chen, S. H.; Yeh, A. I., Preparation of Nano/Submicrometer Yam and Its Benefits on Collagen Secretion from Skin Fibroblast Cells. *J Agr Food Chem* **2012,** *60*,

12332-12340.
55. Stehr, N., Recent Developments in Stirred Ball Milling. *Int J Miner Process* **1988,** *22*, 431-444.
56. Gao, M. W.; Forssberg, E., Prediction of Product Size Distributions for a Stirred Ball Mill. *Powder Technol* **1995,** *84*, 101-106.
57. Merisko-Liversidge, E.; Liversidge, G. G.; Cooper, E. R., Nanosizing: a formulation approach for poorly-water-soluble compounds. *Eur J Pharm Sci* **2003,** *18*, 113-120.
58. Date, A. A.; Patravale, V. B., Current strategies for engineering drug nanoparticles. *Curr Opin Colloid In* **2004,** *9*, 222-235.
59. Shinohara, K.; Golman, B.; Uchiyama, T.; Otani, M., Fine-grinding characteristics of hard materials by attrition mill. *Powder Technol* **1999,** *103*, 292-296.
60. Yeh, A. I.; Huang, Y. C.; Chen, S. H., Effect of particle size on the rate of enzymatic hydrolysis of cellulose. *Carbohydrate Polymers* **2010,** *79*, 192-199.
61. Huang, Z. Q.; Xie, X. L.; Chen, Y.; Lu, J. P.; Tong, Z. F., Ball-milling treatment effect on physicochemical properties and features for cassava and maize starches. *Cr Chim* **2008,** *11*, 73-79.
62. Ren, G. Y.; Li, D.; Wang, L. J.; Ozkan, N.; Mao, Z. H., Morphological properties and thermoanalysis of micronized cassava starch. *Carbohydrate Polymers* **2010,** *79*, 101-105.
63. Chen, J. J.; Lii, C. Y.; Lu, S., Physicochemical and morphological analyses on damaged rice starches. *J Food Drug Anal* **2003,** *11*, 283-289.
64. Devi, A. F.; Fibrianto, K.; Torley, P. J.; Bhandari, B., Physical properties of cryomilled rice starch. *J Cereal Sci* **2009,** *49*, 278-284.
65. Tamaki, S.; Hisamatsu, M.; Teranishi, K.; Adachi, T.; Yamada, T., Structural change of maize starch granules by ball-mill treatment. *Starch-Starke* **1998,** *50*, 342-348.
66. Huang, Z. Q.; Lu, J. P.; Li, X. H.; Tong, Z. F., Effect of mechanical activation on physico-chemical properties and structure of cassava starch. *Carbohydrate Polymers* **2007,** *68*, 128-135.
67. Chen, C. J.; Shen, Y. C.; Yeh, A. I., Physico-Chemical Characteristics of Media-Milled Corn Starch. *J Agr Food Chem* **2010,** *58*, 9083-9091.
68. Liimatainen, H.; Sirvio, J.; Haapala, A.; Hormi, O.; Niinimaki, J., Characterization of highly accessible cellulose microfibers generated by wet stirred media milling. *Carbohydrate Polymers* **2011,** *83*, 2005-2010.
69. Zhu, K. X.; Huang, S.; Peng, W.; Qian, H. F.; Zhou, H. M., Effect of ultrafine grinding on hydration and antioxidant properties of wheat bran dietary fiber. *Food Res Int* **2010,** *43*, 943-948.
70. Zhang, W.; Zhang, J. L.; Xia, W. S., The preparation of chitosan nanoparticles by wet media milling. *Int J Food Sci Tech* **2012,** *47*, 2266-2272.
71. Englyst, H. N.; Kingman, S. M.; Cummings, J. H., Classification and Measurement of Nutritionally Important Starch Fractions. *Eur J Clin Nutr* **1992,** *46*, S33-S50.
72. Englyst, H.; Wiggins, H. S.; Cummings, J. H., Determination of the Non-Starch Polysaccharides in Plant Foods by Gas-Liquid-Chromatography of Constituent Sugars as Alditol Acetates. *Analyst* **1982,** *107*, 307-318.
73. Sajilata, M. G.; Singhal, R. S.; Kulkarni, P. R., Resistant starch - A review. *Compr Rev Food Sci F* **2006,** *5*, 1-17.
74. Hernandez, O.; Emaldi, U.; Tovar, J., In vitro digestibility of edible films from various starch sources. *Carbohydrate Polymers* **2008,** *71*, 648-655.

75. Hsien-Chih, H. W.; Sarko, A., The double-helical molecular structure of crystalline A-amylose. *Carbohyd Res* **1978,** *61*, 27-40.
76. Asp, N.-G.; Björck, I., Resistant starch. *Trends in Food Science & Technology* **1992,** *3*, 111-114.
77. Putseys, J. A.; Lamberts, L.; Delcour, J. A., Amylose-inclusion complexes: Formation, identity and physico-chemical properties. *J Cereal Sci* **2010,** *51*, 238-247.
78. Ai, Y. F.; Hasjim, J.; Jane, J. L., Effects of lipids on enzymatic hydrolysis and physical properties of starch. *Carbohydrate Polymers* **2013,** *92*, 120-127.
79. Hasjim, J.; Lee, S. O.; Hendrich, S.; Setiawan, S.; Ai, Y. F.; Jane, J. L., Characterization of a Novel Resistant-Starch and Its Effects on Postprandial Plasma-Glucose and Insulin Responses. *Cereal Chem* **2010,** *87*, 257-262.
80. Ludwig, D. D. S., The glycemic index - Physiological mechanisms relating to obesity, diabetes, and cardiovascular disease. *Jama-J Am Med Assoc* **2002,** *287*, 2414-2423.
81. Jenkins, D. J. A.; Vuksan, V.; Kendall, C. W. C.; Wursch, P.; Jeffcoat, R.; Waring, S.; Mehling, C. C.; Vidgen, E.; Augustin, L. S. A.; Wong, E., Physiological effects of resistant starches on fecal bulk, short chain fatty acids, blood lipids and glycemic index. *J Am Coll Nutr* **1998,** *17*, 609-616.
82. Englyst, K. N.; Englyst, H. N.; Hudson, G. J.; Cole, T. J.; Cummings, J. H., Rapidly available glucose in foods: an in vitro measurement that reflects the glycemic response. *Am J Clin Nutr* **1999,** *69*, 448-454.
83. Dedeckere, E. A. M.; Kloots, W. J.; Vanamelsvoort, J. M. M., Resistant Starch Decreases Serum Total Cholesterol and Triacylglycerol Concentrations in Rats. *J Nutr* **1993,** *123*, 2142-2151.
84. Mathe, D.; Riottot, M.; Rostaqui, N.; Sacquet, E.; Navarro, N.; Lecuyer, B.; Lutton, C., Effect of Amylomaize Starch on Plasma-Lipoproteins of Lean and Obese Zucker Rats. *J Clin Biochem Nutr* **1993,** *14*, 17-24.
85. Nugent, A. P., Health properties of resistant starch. *Nutrition Bulletin* **2005,** *30*, 27-54.
86. Christl, S. U.; Murgatroyd, P. R.; Gibson, G. R.; Cummings, J. H., Production, Metabolism, and Excretion of Hydrogen in the Large-Intestine. *Gastroenterology* **1992,** *102*, 1269-1277.
87. Topping, D. L.; Fukushima, M.; Bird, A. R., Resistant starch as a prebiotic and synbiotic: state of the art. *P Nutr Soc* **2003,** *62*, 171-176.
88. Topping, D. L.; Clifton, P. M., Short-chain fatty acids and human colonic function: Roles of resistant starch and nonstarch polysaccharides. *Physiol Rev* **2001,** *81*, 1031-1064.
89. Raben, A.; Tagliabue, A.; Christensen, N. J.; Madsen, J.; Holst, J. J.; Astrup, A., Resistant Starch - the Effect on Postprandial Glycemia, Hormonal Response, and Satiety. *Am J Clin Nutr* **1994,** *60*, 544-551.
90. Brown, I. L., McNaught, K. J., Ganly, R. N.; Conway, P. L., Evans, A. J., Topping, D. L., Wang, X. Probiotic compositions. March 21., 1996.
91. Higgins, J. A., Resistant starch: Metabolic effects and potential health benefits. *J Aoac Int* **2004,** *87*, 761-768.
92. Morais, M. B.; Feste, A.; Miller, R. G.; Lifschitz, C. H., Effect of resistant and digestible starch on intestinal absorption of calcium, iron, and zinc in infant pigs. *Pediatr Res* **1996,** *39*, 872-876.

93. Gelders, G. G.; Duyck, J. P.; Goesaert, H.; Delcour, J. A., Enzyme and acid resistance of amylose-lipid complexes differing in amylose chain length, lipid and complexation temperature. *Carbohydrate Polymers* **2005,** *60*, 379-389.
94. Biliaderis, C. G.; Galloway, G., Crystallization Behavior of Amylose-V Complexes - Structure Property Relationships. *Carbohyd Res* **1989,** *189*, 31-48.
95. Tufvesson, F.; Wahlgren, M.; Eliasson, A. C., Formation of amylose-lipid complexes and effects of temperature treatment. part 2. Fatty acids. *Starch-Starke* **2003,** *55*, 138-149.
96. Cui, R.; Oates, C., + The effect of amylose–lipid complex formation on enzyme susceptibility of sago starch. *Food Chem* **1999,** *65*, 417-425.
97. Yamada, Y.; Hosoya, S.; Nishimura, S.; Tanaka, T.; Kajimoto, Y.; Nishimura, A.; Kajimoto, O., Effect of bread containing resistant starch on postprandial blood glucose levels in humans. *Biosci Biotech Bioch* **2005,** *69*, 559-566.
98. Zhao, Y. S.; Hasjim, J.; Li, L.; Jane, J. L.; Hendrich, S.; Birt, D. F., Inhibition of Azoxymethane-Induced Preneoplastic Lesions in the Rat Colon by a Cooked Stearic Acid Complexed High-Amylose Cornstarch. *J Agr Food Chem* **2011,** *59*, 9700-9708.
99. Zhang, B.; Huang, Q.; Luo, F. X.; Fu, X., Structural characterizations and digestibility of debranched high-amylose maize starch complexed with lauric acid. *Food Hydrocolloids* **2012,** *28*, 174-181.
100. Nakazawa, Y.; Wang, Y. J., Effect of annealing on starch-palmitic acid interaction. *Carbohydrate Polymers* **2004,** *57*, 327-335.
101. Zabar, S.; Lesmes, U.; Katz, I.; Shimoni, E.; Bianco-Peled, H., Studying different dimensions of amylose-long chain fatty acid complexes: Molecular, nano and micro level characteristics. *Food Hydrocolloids* **2009,** *23*, 1918-1925.
102. Zabar, S.; Lesmes, U.; Katz, I.; Shimoni, E.; Bianco-Peled, H., Structural characterization of amylose-long chain fatty acid complexes produced via the acidification method. *Food Hydrocolloids* **2010,** *24*, 347-357.
103. Chang, F. D.; He, X. W.; Huang, Q., Effect of lauric acid on the V-amylose complex distribution and properties of swelled normal cornstarch granules. *J Cereal Sci* **2013,** *58*, 89-95.
104. Obiro, W. C.; Ray, S. S.; Emmambux, M. N., V-amylose Structural Characteristics, Methods of Preparation, Significance, and Potential Applications. *Food Rev Int* **2012,** *28*, 412-438.
105. Aveyard, R.; Binks, B. P.; Clint, J. H., Emulsions stabilised solely by colloidal particles. *Adv Colloid Interfac* **2003,** *100*, 503-546.
106. Zoppe, J. O.; Venditti, R. A.; Rojas, O. J., Pickering emulsions stabilized by cellulose nanocrystals grafted with thermo-responsive polymer brushes. *Journal of colloid and interface science* **2012,** *369*, 202-9.
107. Fujii, S.; Aichi, A.; Muraoka, M.; Kishimoto, N.; Iwahori, K.; Nakamura, Y.; Yamashita, I., Ferritin as a bionano-particulate emulsifier. *Journal of colloid and interface science* **2009,** *338*, 222-228.
108. Russell, J. T.; Lin, Y.; Boker, A.; Su, L.; Carl, P.; Zettl, H.; He, J. B.; Sill, K.; Tangirala, R.; Emrick, T.; Littrell, K.; Thiyagarajan, P.; Cookson, D.; Fery, A.; Wang, Q.; Russell, T. P., Self-assembly and cross-linking of bionanoparticles at liquid-liquid interfaces. *Angew Chem Int Edit* **2005,** *44*, 2420-2426.
109. Sanguanpong, V.; Chotineeranat, S.; Piyachomkwan, K.; Oates, C. G.; Chinachoti, P.; Sriroth, K., Preparation and structural properties of small-particle cassava

starch. *Journal of the science of food and agriculture* **2003,** *83*, 760-768.
110. Sharma, S.; Stutzman, J. D.; Kelloff, G. J.; Steele, V. E., Screening of Potential Chemopreventive Agents Using Biochemical Markers of Carcinogenesis. *Cancer Res* **1994,** *54*, 5848-5855.
111. Hachisuka, H.; Tsujita, Y.; Takizawa, A.; Kinoshita, T., Co2 Sorption Properties and Enthalpy Relaxation in Alternating Copoly(Vinylidene Cyanide Vinyl Acetate)S. *Polymer* **1988,** *29*, 2050-2055.
112. Hermans, P.; Weidinger, A., Quantitative X-Ray Investigations on the Crystallinity of Cellulose Fibers. A Background Analysis. *Journal of Applied Physics* **1948,** *19*, 491-506.
113. Timgren, A.; Rayner, M.; Dejmek, P.; Marku, D.; Sjöö, M., Emulsion stabilizing capacity of intact starch granules modified by heat treatment or octenyl succinic anhydride. *Food science & nutrition* **2013,** *1*, 157-171.
114. Han, X. Z.; Campanella, O. H.; Mix, N. C.; Hamaker, B. R., Consequence of starch damage on rheological properties of maize starch pastes. *Cereal Chem* **2002,** *79*, 897-901.
115. Dhital, S.; Shrestha, A. K.; Flanagan, B. M.; Hasjim, J.; Gidley, M. J., Cryo-milling of starch granules leads to differential effects on molecular size and conformation. *Carbohydrate Polymers* **2011,** *84*, 1133-1140.
116. Vandeputte, G. E.; Vermeylen, R.; Geeroms, J.; Delcour, J. A., Rice starches. I. Structural aspects provide insight into crystallinity characteristics and gelatinisation behaviour of granular starch. *J Cereal Sci* **2003,** *38*, 43-52.
117. Fiedorowicz, M.; Para, A., Structural and molecular properties of dialdehyde starch. *Carbohydrate Polymers* **2006,** *63*, 360-366.
118. Gallant, D. J.; Bouchet, B.; Baldwin, P. M., Microscopy of starch: Evidence of a new level of granule organization. *Carbohydrate Polymers* **1997,** *32*, 177-191.
119. Zhang, Z. M.; Zhao, S. M.; Xiong, S. B., Morphology and physicochemical properties of mechanically activated rice starch. *Carbohydrate Polymers* **2010,** *79*, 341-348.
120. Morrison, W.; Tester, R., Properties of damaged starch granules. IV. Composition of ball-milled wheat starches and of fractions obtained on hydration. *J Cereal Sci* **1994,** *20*, 69-77.
121. Matveev, Y. I.; van Soest, J. J. G.; Nieman, C.; Wasserman, L. A.; Protserov, V.; Ezernitskaja, M.; Yuryev, V. P., The relationship between thermodynamic and structural properties of low and high amylose maize starches. *Carbohydrate Polymers* **2001,** *44*, 151-160.
122. Matveev, Y. I.; Elankin, N. Y.; Kalistrova, E.; Danilenko, A.; Niemann, C.; Yuryev, V., Estimation of Contributions of Hydration and Glass Transition to Heat Capacity Changes During Melting of Native Starches in Excess Wate. *Starch-Stärke* **1998,** *50*, 141-147.
123. Yuryev, V. P.; Kalistratova, E. N.; van Soest, J. G. J.; Niemann, C., Thermodynamic properties of barley starches with different amylose content. *Starch-Starke* **1998,** *50*, 463-466.
124. Rayner, M.; Timgren, A.; Sjoo, M.; Dejmek, P., Quinoa starch granules: a candidate for stabilising food-grade Pickering emulsions. *Journal of the science of food and agriculture* **2012,** *92*, 1841-7.
125. Vignati, E.; Piazza, R.; Lockhart, T. P., Pickering emulsions: Interfacial tension,

colloidal layer morphology, and trapped-particle motion. *Langmuir* **2003,** *19*, 6650-6656.
126. Marku, D.; Wahlgren, M.; Rayner, M.; Sjoo, M.; Timgren, A., Characterization of starch Pickering emulsions for potential applications in topical formulations. *Int J Pharmaceut* **2012,** *428*, 1-7.
127. Laredj-Bourezg, F.; Chevalier, Y.; Boyron, O.; Bolzinger, M. A., Emulsions stabilized with organic solid particles. *Colloid Surface A* **2012,** *413*, 252-259.
128. Clark, A. H., Structural and Mechanical-Properties of Biopolymer Gels. *Roy Soc Ch* **1991,** *82*, 322-338.
129. Jager-Lezer, N.; Tranchant, J. F.; Alard, V.; Vu, C.; Tchoreloff, P. C.; Grossiord, J. L., Rheological analysis of highly concentrated w/o emulsions. *Rheol Acta* **1998,** *37*, 129-138.
130. Barreiro-Iglesias, R.; Alvarez-Lorenzo, C.; Concheiro, A., Poly(acrylic acid) microgels (carbopol (R) 934)/surfactant interactions in aqueous media Part I: Nonionic surfactants. *Int J Pharmaceut* **2003,** *258*, 165-177.
131. Lii, C. Y.; Tsai, M. L.; Tseng, K. H., Effect of amylose content on the rheological property of rice starch. *Cereal Chem* **1996,** *73*, 415-420.
132. Loveday, S. M.; Singh, H., Recent advances in technologies for vitamin A protection in foods. *Trends in Food Science & Technology* **2008,** *19*, 657-668.
133. Folmer, B. M.; Barron, D.; Hughes, E.; Miguet, L.; Sanchez, B.; Heudi, O.; Rouvet, M.; Sagalowicz, L.; Callier, P.; Michel, M., Monocomponent hexa-and dodecaethylene glycol succinyl-tocopherol esters: Self-assembly structures, cellular uptake and sensitivity to enzyme hydrolysis. *Biochemical pharmacology* **2009,** *78*, 1464-1474.
134. McClements, D. J.; Li, Y., Structured emulsion-based delivery systems: Controlling the digestion and release of lipophilic food components. *Adv Colloid Interfac* **2010,** *159*, 213-228.
135. McClements, D. J., Emulsion Design to Improve the Delivery of Functional Lipophilic Components. *Annu Rev Food Sci T* **2010,** *1*, 241-269.
136. Tamayo-Esquivel, D.; Ganem-Quintanar, A.; Martinez, A.; Navarrete-Rodriguez, M.; Rodriguez-Romo, S.; Quintanar-Guerrero, D., Evaluation of the enhanced oral effect of omapatrilat-monolein nanoparticles prepared by the emulsification-diffusion method. *Journal of nanoscience and nanotechnology* **2006,** *6*, 3134-3138.
137. Ahmed, K.; Li, Y.; McClements, D. J.; Xiao, H., Nanoemulsion- and emulsion-based delivery systems for curcumin: Encapsulation and release properties. *Food Chem* **2012,** *132*, 799-807.
138. Porter, C. J. H.; Trevaskis, N. L.; Charman, W. N., Lipids and lipid-based formulations: optimizing the oral delivery of lipophilic drugs. *Nat Rev Drug Discov* **2007,** *6*, 231-248.
139. Paunov, V. N.; Cayre, O. J.; Noble, P. F.; Stoyanov, S. D.; Velikov, K. P.; Golding, M., Emulsions stabilised by food colloid particles: Role of particle adsorption and wettability at the liquid interface. *Journal of colloid and interface science* **2007,** *312*, 381-389.
140. Barany, E.; Lindberg, M.; Loden, M., Unexpected skin barrier influence from nonionic emulsifiers. *Int J Pharmaceut* **2000,** *195*, 189-195.
141. McClements, D. J.; Li, Y., Review of in vitro digestion models for rapid screening of emulsion-based systems. *Food & function* **2010,** *1*, 32-59.

142. Das, R. K.; Kasoju, N.; Bora, U., Encapsulation of curcumin in alginate-chitosan-pluronic composite nanoparticles for delivery to cancer cells. *Nanomed-Nanotechnol* **2010,** *6*, 153-160.
143. Nayak, A. P.; Tiyaboonchai, W.; Patankar, S.; Madhusudhan, B.; Souto, E. B., Curcuminoids-loaded lipid nanoparticles: Novel approach towards malaria treatment. *Colloid Surface B* **2010,** *81*, 263-273.
144. Tikekar, R. V.; Pan, Y. J.; Nitin, N., Fate of curcumin encapsulated in silica nanoparticle stabilized Pickering emulsion during storage and simulated digestion. *Food Res Int* **2013,** *51*, 370-377.
145. Ruiz-Rodriguez, P. E.; Meshulam, D.; Lesmes, U., Characterization of Pickering O/W Emulsions Stabilized by Silica Nanoparticles and Their Responsiveness to In vitro Digestion Conditions. *Food Biophys* **2014,** *9*, 406-415.
146. Dahan, A.; Hoffman, A., Rationalizing the selection of oral lipid based drug delivery systems by an in vitro dynamic lipolysis model for improved oral bioavailability of poorly water soluble drugs. *J Control Release* **2008,** *129*, 1-10.
147. Blanquet, S.; Zeijdner, E.; Beyssac, E.; Meunier, J. P.; Denis, S.; Havenaar, R.; Alric, M., A dynamic artificial gastrointestinal system for studying the behavior of orally administered drug dosage forms under various physiological conditions. *Pharm Res-Dordr* **2004,** *21*, 585-591.
148. Speranza, A.; Corradini, M. G.; Hartman, T. G.; Ribnicky, D.; Oren, A.; Rogers, M. A., Influence of Emulsifier Structure on Lipid Bioaccessibility in Oil-Water Nanoemulsions. *J Agr Food Chem* **2013,** *61*, 6505-6515.
149. Minekus, M.; Marteau, P.; Havenaar, R.; Huisintveld, J. H. J., A Multicompartmental Dynamic Computer-Controlled Model Simulating the Stomach and Small-Intestine. *Atla-Altern Lab Anim* **1995,** *23*, 197-209.
150. Smeets-Peeters, M. J. E.; Minekus, M.; Havenaar, R.; Schaafsma, G.; Verstegen, M. W. A., Description of a dynamic in vitro model of the dog gastrointestinal tract and an evaluation of various transit times for protein and calcium. *Atla-Altern Lab Anim* **1999,** *27*, 935-949.
151. Chen, L.; Hebrard, G.; Beyssac, E.; Denis, S.; Subirade, M., In Vitro Study of the Release Properties of Soy-Zein Protein Microspheres with a Dynamic Artificial Digestive System. *J Agr Food Chem* **2010,** *58*, 9861-9867.
152. Ting, Y. W.; Jian, Y. K.; Lan, Y. Q.; Xia, C. X.; Lin, Z. Y.; Rogers, M. A.; Huang, Q. R., Viscoelastic Emulsion Improved the Bioaccessibility and Oral Bioavailability of Crystalline Compound: A Mechanistic Study Using in Vitro and in Vivo Models. *Mol Pharmaceut* **2015,** *12*, 2229-2236.
153. Wang, X. Y.; Jiang, Y.; Wang, Y. W.; Huang, M. T.; Ho, C. T.; Huang, Q. R., Enhancing anti-inflammation activity of curcumin through O/W nanoemulsions. *Food Chem* **2008,** *108*, 419-424.
154. Sarkar, A.; Goh, K. K. T.; Singh, R. P.; Singh, H., Behaviour of an oil-in-water emulsion stabilized by beta-lactoglobulin in an in vitro gastric model. *Food Hydrocolloids* **2009,** *23*, 1563-1569.
155. Fu, T. T.; Abbott, U. R.; Hatzos, C., Digestibility of food allergens and nonallergenic proteins in simulated gastric fluid and simulated intestinal fluid - A comparative study. *J Agr Food Chem* **2002,** *50*, 7154-7160.
156. Sarkar, A.; Horne, D. S.; Singh, H., Interactions of milk protein-stabilized

oil-in-water emulsions with bile salts in a simulated upper intestinal model. *Food Hydrocolloids* **2010,** *24*, 142-151.
157. Sek, L.; Porter, C. J. H.; Charman, W. N., Characterisation and quantification of medium chain and long chain triglycerides and their in vitro digestion products, by HPTLC coupled with in situ densitometric analysis. *J Pharmaceut Biomed* **2001,** *25*, 651-661.
158. Anson, N. M.; Selinheimo, E.; Havenaar, R.; Aura, A. M.; Mattila, I.; Lehtinen, P.; Bast, A.; Poutanen, K.; Haenen, G. R. M. M., Bioprocessing of Wheat Bran Improves in vitro Bioaccessibility and Colonic Metabolism of Phenolic Compounds. *J Agr Food Chem* **2009,** *57*, 6148-6155.
159. Pak, Y.; Patek, R.; Mayersohn, M., Sensitive and rapid isocratic liquid chromatography method for the quantitation of curcumin in plasma. *J Chromatogr B* **2003,** *796*, 339-346.
160. Anal, A. K.; Singh, H., Recent advances in microencapsulation of probiotics for industrial applications and targeted delivery. *Trends in Food Science & Technology* **2007,** *18*, 240-251.
161. Vandenberg, G. W.; Drolet, C.; Scott, S. L.; de la Noue, J., Factors affecting protein release from alginate-chitosan coacervate microcapsules during production and gastric/intestinal simulation. *J Control Release* **2001,** *77*, 297-307.
162. Dickinson, E., Food emulsions and foams: Stabilization by particles. *Curr Opin Colloid In* **2010,** *15*, 40-49.
163. Amiri, A.; Oye, G.; Sjoblom, J., Influence of pH, high salinity and particle concentration on stability and rheological properties of aqueous suspensions of fumed silica. *Colloid Surface A* **2009,** *349*, 43-54.
164. Deng, Z. B.; Liu, Y. L.; Liu, C. R.; Xiang, X. Y.; Wang, J. H.; Cheng, Z. Q.; Shah, S. V.; Zhang, S. Y.; Zhang, L. M.; Zhuang, X. Y.; Michalek, S.; Grizzle, W. E.; Zhang, H. G., Immature Myeloid Cells Induced by a High-Fat Diet Contribute to Liver Inflammation. *Hepatology* **2009,** *50*, 1412-1420.
165. Wang, Y. J.; Pan, M. H.; Cheng, A. L.; Lin, L. I.; Ho, Y. S.; Hsieh, C. Y.; Lin, J. K., Stability of curcumin in buffer solutions and characterization of its degradation products. *J Pharmaceut Biomed* **1997,** *15*, 1867-1876.
166. Raveendran, R.; Bhuvaneshwar, G. S.; Sharma, C. P., In vitro cytotoxicity and cellular uptake of curcumin-loaded Pluronic/Polycaprolactone micelles in colorectal adenocarcinoma cells. *J Biomater Appl* **2013,** *27*, 811-827.
167. Liu, C. S.; Glahn, R. P.; Liu, R. H., Assessment of carotenoid bioavailability of whole foods using a Caco-2 cell culture model coupled with an in vitro digestion. *J Agr Food Chem* **2004,** *52*, 4330-4337.
168. Puyol, P.; Perez, M. D.; Sanchez, L.; Ena, J. M.; Calvo, M., Uptake and Passage of Beta-Lactoglobulin, Palmitic Acid and Retinol across the Caco-2 Monolayer. *Bba-Biomembranes* **1995,** *1236*, 149-154.
169. Peters, R.; Kramer, E.; Oomen, A. G.; Rivera, Z. E. H.; Oegema, G.; Tromp, P. C.; Fokkink, R.; Rietveld, A.; Marvin, H. J. P.; Weigel, S.; Peijnenburg, A. A. C. M.; Bouwmeester, H., Presence of Nano-Sized Silica during In Vitro Digestion of Foods Containing Silica as a Food Additive. *Acs Nano* **2012,** *6*, 2441-2451.
170. van Kesteren, P. C. E.; Cubadda, F.; Bouwmeester, H.; van Eijkeren, J. C. H.; Dekkers, S.; de Jong, W. H.; Oomen, A. G., Novel insights into the risk assessment of the

nanomaterial synthetic amorphous silica, additive E551, in food. *Nanotoxicology* **2015,** *9*, 442-452.
171. Xiao, J.; Li, Y. Q.; Huang, Q. R., Recent advances on food-grade particles stabilized Pickering emulsions: Fabrication, characterization and research trends. *Trends in Food Science & Technology* **2016,** *55*, 48-60.
172. Eichhorn, S. J.; Dufresne, A.; Aranguren, M.; Marcovich, N. E.; Capadona, J. R.; Rowan, S. J.; Weder, C.; Thielemans, W.; Roman, M.; Renneckar, S.; Gindl, W.; Veigel, S.; Keckes, J.; Yano, H.; Abe, K.; Nogi, M.; Nakagaito, A. N.; Mangalam, A.; Simonsen, J.; Benight, A. S.; Bismarck, A.; Berglund, L. A.; Peijs, T., Review: current international research into cellulose nanofibres and nanocomposites. *J Mater Sci* **2010,** *45*, 1-33.
173. Elazzouzi-Hafraoui, S.; Nishiyama, Y.; Putaux, J. L.; Heux, L.; Dubreuil, F.; Rochas, C., The shape and size distribution of crystalline nanoparticles prepared by acid hydrolysis of native cellulose. *Biomacromolecules* **2008,** *9*, 57-65.
174. Klemm, D.; Kramer, F.; Moritz, S.; Lindstrom, T.; Ankerfors, M.; Gray, D.; Dorris, A., Nanocelluloses: A New Family of Nature-Based Materials. *Angew Chem Int Edit* **2011,** *50*, 5438-5466.
175. Samir, M. A. S. A.; Alloin, F.; Dufresne, A., Review of recent research into cellulosic whiskers, their properties and their application in nanocomposite field. *Biomacromolecules* **2005,** *6*, 612-626.
176. Tasset, S.; Cathala, B.; Bizot, H.; Capron, I., Versatile cellular foams derived from CNC-stabilized Pickering emulsions. *Rsc Adv* **2014,** *4*, 893-898.
177. French, A. D. B., N. R.; Brown, R. M.; Chanzy, H.; Gray, D. G.; Hattori, K.; Glasser, W. G., *Encyclopedia of Polymer Science and Technology*. 3rd ed.; John Wiley & Sons: New York, 2003.
178. Pinkert, A.; Marsh, K. N.; Pang, S. S., Reflections on the Solubility of Cellulose. *Ind Eng Chem Res* **2010,** *49*, 11121-11130.
179. El-Sakhawy, M.; Hassan, M. L., Physical and mechanical properties of microcrystalline cellulose prepared from agricultural residues. *Carbohydrate Polymers* **2007,** *67*, 1-10.
180. Cheng, G.; Varanasi, P.; Li, C. L.; Liu, H. B.; Menichenko, Y. B.; Simmons, B. A.; Kent, M. S.; Singh, S., Transition of Cellulose Crystalline Structure and Surface Morphology of Biomass as a Function of Ionic Liquid Pretreatment and Its Relation to Enzymatic Hydrolysis. *Biomacromolecules* **2011,** *12*, 933-941.
181. Hu, Z.; Ballinger, S.; Pelton, R.; Cranston, E. D., Surfactant-enhanced cellulose nanocrystal Pickering emulsions. *Journal of colloid and interface science* **2015,** *439*, 139-148.
182. Frelichowska, J.; Bolzinger, M. A.; Chevalier, Y., Pickering emulsions with bare silica. *Colloid Surface A* **2009,** *343*, 70-74.
183. Frelichowska, J.; Bolzinger, M. A.; Chevalier, Y., Effects of solid particle content on properties of o/w Pickering emulsions. *Journal of colloid and interface science* **2010,** *351*, 348-356.
184. Chevalier, Y.; Bolzinger, M. A., Emulsions stabilized with solid nanoparticles: Pickering emulsions. *Colloid Surface A* **2013,** *439*, 23-34.
185. Tcholakova, S.; Denkov, N. D.; Lips, A., Comparison of solid particles, globular proteins and surfactants as emulsifiers. *Phys Chem Chem Phys* **2008,** *10*, 1608-1627.
186. Whitby, C. P.; Fornasiero, D.; Ralston, J., Effect of adding anionic surfactant on

the stability of Pickering emulsions. *Journal of colloid and interface science* **2009,** *329*, 173-181.
187. Zhao, H. B.; Kwak, J. H.; Wang, Y.; Franz, J. A.; White, J. M.; Holladay, J. E., Effects of crystallinity on dilute acid hydrolysis of cellulose by cellulose ball-milling study. *Energ Fuel* **2006,** *20*, 807-811.
188. Jeoh, T.; Ishizawa, C. I.; Davis, M. F.; Himmel, M. E.; Adney, W. S.; Johnson, D. K., Cellulase digestibility of pretreated biomass is limited by cellulose accessibility. *Biotechnol Bioeng* **2007,** *98*, 112-122.
189. Uetani, K.; Yano, H., Nanofibrillation of Wood Pulp Using a High-Speed Blender. *Biomacromolecules* **2011,** *12*, 348-353.
190. Liu, P.; Sehaqui, H.; Tingaut, P.; Wichser, A.; Oksman, K.; Mathew, A. P., Cellulose and chitin nanomaterials for capturing silver ions (Ag+) from water via surface adsorption. *Cellulose* **2014,** *21*, 449-461.
191. Yu, Y.; Wu, H. W., Significant Differences in the Hydrolysis Behavior of Amorphous and Crystalline Portions within Microcrystalline Cellulose in Hot-Compressed Water. *Ind Eng Chem Res* **2010,** *49*, 3902-3909.
192. Xiao, J.; Wang, X. A.; Gonzalez, A. J. P.; Huang, Q. R., Kafirin nanoparticles-stabilized Pickering emulsions: Microstructure and rheological behavior. *Food Hydrocolloids* **2016,** *54*, 30-39.
193. Singh, H.; Sarkar, A., Behaviour of protein-stabilised emulsions under various physiological conditions. *Adv Colloid Interfac* **2011,** *165*, 47-57.
194. Charman, W. N.; Porter, C. J. H.; Mithani, S.; Dressman, J. B., Physicochemical and physiological mechanisms for the effects of food on drug absorption: The role of lipids and pH. *J Pharm Sci* **1997,** *86*, 269-282.
195. Humberstone, A. J.; Charman, W. N., Lipid-based vehicles for the oral delivery of poorly water soluble drugs. *Adv Drug Deliver Rev* **1997,** *25*, 103-128.
196. Simovic, S.; Hui, H.; Song, Y. M.; Davey, A. K.; Rades, T.; Prestidge, C. A., An oral delivery system for indomethicin engineered from cationic lipid emulsions and silica nanoparticles. *J Control Release* **2010,** *143*, 367-373.
197. Wagberg, L.; Decher, G.; Norgren, M.; Lindstrom, T.; Ankerfors, M.; Axnas, K., The build-up of polyelectrolyte multilayers of microfibrillated cellulose and cationic polyelectrolytes. *Langmuir* **2008,** *24*, 784-795.
198. Kunnumakkara, A. B.; Anand, P.; Aggarwal, B. B., Curcumin inhibits proliferation, invasion, angiogenesis and metastasis of different cancers through interaction with multiple cell signaling proteins. *Cancer letters* **2008,** *269*, 199-225.
199. Ireson, C.; Orr, S.; Jones, D. J. L.; Verschoyle, R.; Lim, C. K.; Luo, J. L.; Howells, L.; Plummer, S.; Jukes, R.; Williams, M.; Steward, W. P.; Gescher, A., Characterization of metabolites of the chemopreventive agent curcumin in human and rat hepatocytes and in the rat in vivo, and evaluation of their ability to inhibit phorbol ester-induced prostaglandin E-2 production. *Cancer Res* **2001,** *61*, 1058-1064.
200. Ireson, C. R.; Jones, D. J.; Orr, S.; Coughtrie, M. W.; Boocock, D. J.; Williams, M. L.; Farmer, P. B.; Steward, W. P.; Gescher, A. J., Metabolism of the cancer chemopreventive agent curcumin in human and rat intestine. *Cancer Epidemiology Biomarkers & Prevention* **2002,** *11*, 105-111.
201. Kaminaga, Y.; Nagatsu, A.; Akiyama, T.; Sugimoto, N.; Yamazaki, T.; Maitani, T.; Mizukami, H., Production of unnatural glucosides of curcumin with drastically

enhanced water solubility by cell suspension cultures of Catharanthus roseus. *Febs Lett* **2003,** *555*, 311-316.
202. Sharma, R. A.; Gescher, A. J.; Steward, W. P., Curcumin: The story so far. *Eur J Cancer* **2005,** *41*, 1955-1968.
203. Mukerjee, A.; Vishwanatha, J. K., Formulation, Characterization and Evaluation of Curcumin-loaded PLGA Nanospheres for Cancer Therapy. *Anticancer Res* **2009,** *29*, 3867-3875.
204. Yu, H. L.; Huang, Q. R., Enhanced in vitro anti-cancer activity of curcumin encapsulated in hydrophobically modified starch. *Food Chem* **2010,** *119*, 669-674.
205. Leung, M. H.; Colangelo, H.; Kee, T. W., Encapsulation of curcumin in cationic micelles suppresses alkaline hydrolysis. *Langmuir* **2008,** *24*, 5672-5675.
206. Chen, C.; Johnston, T. D.; Jeon, H.; Gedaly, R.; McHugh, P. P.; Burke, T. G.; Ranjan, D., An in vitro study of liposomal curcumin: stability, toxicity and biological activity in human lymphocytes and Epstein-Barr virus-transformed human B-cells. *Int J Pharmaceut* **2009,** *366*, 133-139.
207. Cistola, D. P.; Hamilton, J. A.; Jackson, D.; Small, D. M., Ionization and Phase-Behavior of Fatty-Acids in Water - Application of the Gibbs Phase Rule. *Biochemistry-Us* **1988,** *27*, 1881-1888.
208. Sek, L.; Porter, C. J. H.; Kaukonen, A. M.; Charman, W. N., Evaluation of the in-vitro digestion profiles of long and medium chain glycerides and the phase behaviour of their lipolytic products. *J Pharm Pharmacol* **2002,** *54*, 29-41.
209. MacGregor, K. J.; Embleton, J. K.; Lacy, J. E.; Perry, E. A.; Solomon, L. J.; Seager, H.; Pouton, C. W., Influence of lipolysis on drug absorption from the gastro-intestinal tract. *Adv Drug Deliver Rev* **1997,** *25*, 33-46.
210. Lykidis, A.; Avranas, A.; Arzoglou, P., Combined effect of a lecithin and a bile salt on pancreatic lipase activity. *Comp Biochem Phys B* **1997,** *116*, 51-55.
211.Hernell, O.; Staggers, J. E.; Carey, M. C., Physical-Chemical Behavior of Dietary and Biliary Lipids during Intestinal Digestion and Absorption .2. Phase-Analysis and Aggregation States of Luminal Lipids during Duodenal Fat Digestion in Healthy Adult Human-Beings. *Biochemistry-Us* **1990,** *29*, 2041-2056.
212. Kossena, G. A.; Boyd, B. J.; Porter, C. J. H.; Charman, W. N., Separation and characterization of the colloidal phases produced on digestion of common formulation lipids and assessment of their impact on the apparent solubility of selected poorly water-soluble drugs. *J Pharm Sci* **2003,** *92*, 634-648.
213. Li, Y.; McClements, D. J., New Mathematical Model for Interpreting pH-Stat Digestion Profiles: Impact of Lipid Droplet Characteristics on in Vitro Digestibility. *J Agr Food Chem* **2010,** *58*, 8085-8092.
214. Gargouri, Y.; Julien, R.; Bois, A. G.; Verger, R.; Sarda, L., Studies on the Detergent Inhibition of Pancreatic Lipase Activity. *J Lipid Res* **1983,** *24*, 1336-1342.
215. Mun, S.; Decker, E. A.; McClements, D. J., Influence of emulsifier type on in vitro digestibility of lipid droplets by pancreatic lipase. *Food Res Int* **2007,** *40*, 770-781.
216. Pafumi, Y.; Lairon, D.; de la Porte, P. L.; Juhel, C.; Storch, J.; Hamosh, M.; Armand, M., Mechanisms of inhibition of triacylglycerol hydrolysis by human gastric lipase. *J Biol Chem* **2002,** *277*, 28070-28079.
217. Porter, C. J. H.; Kaukonen, A. M.; Taillardat-Bertschinger, A.; Boyd, B. J.; O'Connor, J. M.; Edwards, G. A.; Charman, W. N., Use of in vitro lipid digestion data to

explain the in vivo performance of triglyceride-based oral lipid formulations of poorly water-soluble drugs: Studies with halofantrine. *J Pharm Sci* **2004,** *93*, 1110-1121.
218. Yu, H. L.; Shi, K.; Liu, D.; Huang, Q. R., Development of a food-grade organogel with high bioaccessibility and loading of curcuminoids. *Food Chem* **2012,** *131*, 48-54.
219. Helbert, W.; Chanzy, H., Single-Crystals of V-Amylose Complexed with N-Butanol or N-Pentanol - Structural Features and Properties. *Int J Biol Macromol* **1994,** *16*, 207-213.
220. Godet, M. C.; Bouchet, B.; Colonna, P.; Gallant, D. J.; Buleon, A., Crystalline amylose fatty acid complexes: Morphology and crystal thickness. *J Food Sci* **1996,** *61*, 1196-1201.
221. Conde-Petit, B.; Escher, F.; Nuessli, J., Structural features of starch-flavor complexation in food model systems. *Trends in Food Science & Technology* **2006,** *17*, 227-235.
222. Kaneko, Y.; Kadokawa, J. I., Vine-twining polymerization: A new preparation method for well-defined supramolecules composed of amylose and synthetic polymers. *Chem Rec* **2005,** *5*, 36-46.
223. Lalush, I.; Bar, H.; Zakaria, I.; Eichler, S.; Shimoni, E., Utilization of amylose-lipid complexes as molecular nanocapsules for conjugated linoleic acid. *Biomacromolecules* **2005,** *6*, 121-130.
224. Nuessli, J.; CondePetit, B.; Trommsdorff, U. R.; Escher, F., Influence of starch flavour interactions on rheological properties of low concentration starch systems. *Carbohydrate Polymers* **1995,** *28*, 167-170.
225. D'Silva, T. V.; Taylor, J. R. N.; Emmambux, M. N., Enhancement of the pasting properties of teff and maize starches through wet-heat processing with added stearic acid. *J Cereal Sci* **2011,** *53*, 192-197.
226. Kim, O. K.; Je, J. T.; Baldwin, J. W.; Kooi, S.; Pehrsson, P. E.; Buckley, L. J., Solubilization of single-wall carbon nanotubes by supramolecular encapsulation of helical amylose. *J Am Chem Soc* **2003,** *125*, 4426-4427.
227. Crowe, T. C.; Seligman, S. A.; Copeland, L., Inhibition of enzymic digestion of amylose by free fatty acids in vitro contributes to resistant starch formation. *J Nutr* **2000,** *130*, 2006-2008.
228. Lauro, M.; Poutanen, K.; Forssell, P., Effect of partial gelatinization and lipid addition on alpha-amylolysis of barley starch granules. *Cereal Chem* **2000,** *77*, 595-601.
229. Chang, F. D.; He, X. W.; Fu, X.; Huang, Q.; Jane, J. L., Effects of Heat Treatment and Moisture Contents on Interactions Between Lauric Acid and Starch Granules. *J Agr Food Chem* **2014,** *62*, 7862-7868.
230. Ai, Y. F.; Zhao, Y. S.; Nelson, B.; Birt, D. F.; Wang, T.; Jane, J. L., Characterization and In Vivo Hydrolysis of Amylose Stearic Acid Complex. *Cereal Chem* **2014,** *91*, 466-472.
231. Gelders, G. G.; Goesaert, H.; Delcour, J. A., Amylose-lipid complexes as controlled lipid release agents during starch gelatinization and pasting. *J Agr Food Chem* **2006,** *54*, 1493-1499.
232. Biais, B.; Le Bail, P.; Robert, P.; Pontoire, B.; Buleon, A., Structural and stoichiometric studies of complexes between aroma compounds and amylose. Polymorphic transitions and quantification in amorphous and crystalline areas.

Carbohydrate Polymers **2006,** *66*, 306-315.
233. Godet, M. C.; Tran, V.; Colonna, P.; Buleon, A.; Pezolet, M., Inclusion exclusion of fatty acids in amylose complexes as a function of the fatty acid chain length. *Int J Biol Macromol* **1995,** *17*, 405-408.
234. Godet, M. C.; Buleon, A.; Tran, V.; Colonna, P., Structural Features of Fatty Acid-Amylose Complexes. *Carbohydrate Polymers* **1993,** *21*, 91-95.
235. Lebail, P.; Buleon, A.; Shiftan, D.; Marchessault, R. H., Mobility of lipid in complexes of amylose-fatty acids by deuterium and C-13 solid state NMR. *Carbohydrate Polymers* **2000,** *43*, 317-326.
236. Lesmes, U.; Cohen, S. H.; Shener, Y.; Shimoni, E., Effects of long chain fatty acid unsaturation on the structure and controlled release properties of amylose complexes. *Food Hydrocolloids* **2009,** *23*, 667-675.
237. Jane, J.; Chen, Y. Y.; Lee, L. F.; McPherson, A. E.; Wong, K. S.; Radosavljevic, M.; Kasemsuwan, T., Effects of amylopectin branch chain length and amylose content on the gelatinization and pasting properties of starch. *Cereal Chem* **1999,** *76*, 629-637.
238. Rondeau-Mouro, C.; Le Bail, P.; Buleon, A., Structural investigation of amylose complexes with small ligands: inter- or intra-helical associations? *Int J Biol Macromol* **2004,** *34*, 309-315.
239. Bhatnagar, S.; Hanna, M. A., Amylose Lipid Complex-Formation during Single-Screw Extrusion of Various Corn Starches. *Cereal Chem* **1994,** *71*, 582-587.
240. Hoover, R.; Hadziyev, D., Characterization of Potato Starch and Its Monoglyceride Complexes. *Starke* **1981,** *33*, 290-300.
241. Krog, N., Amylose complexing effect of food grade emulsifiers. *Starch-Stärke* **1971,** *23*, 206-210.
242. Blazek, J.; Gilbert, E. P., Application of small-angle X-ray and neutron scattering techniques to the characterisation of starch structure: A review. *Carbohydrate Polymers* **2011,** *85*, 281-293.
243. McArdle, C. B., *Side chain liquid crystal polymers*. Springer Science & Business Media: 1990.
244. Glatter, O., Determination of Particle-Size Distribution-Functions from Small-Angle Scattering Data by Means of the Indirect Transformation Method. *J Appl Crystallogr* **1980,** *13*, 7-11.
245. Sarko, A.; Wu, H. C., The Crystal Structures of A-, B-and C-Polymorphs of Amylose and Starch. *Starch-Stärke* **1978,** *30*, 73-78.
246. Lopez-Rubio, A.; Htoon, A.; Gilbert, E. P., Influence of extrusion and digestion on the nanostructure of high-amylose maize starch. *Biomacromolecules* **2007,** *8*, 1564-1572.
247. Foster, M. D., X-Ray-Scattering Methods for the Study of Polymer Interfaces. *Crit Rev Anal Chem* **1993,** *24*, 179-241.
248. Debye, P.; Bueche, A., Scattering by an inhomogeneous solid. *Journal of Applied Physics* **1949,** *20*, 518-525.
249. Godet, M. C.; Bizot, H.; Buleon, A., Crystallization of Amylose-Fatty Acid Complexes Prepared with Different Amylose Chain Lengths. *Carbohydrate Polymers* **1995,** *27*, 47-52.
250. Raphaelides, S.; Karkalas, J., Thermal-Dissociation of Amylose Fatty-Acid Complexes. *Carbohyd Res* **1988,** *172*, 65-82.

251. Gelders, G. G.; Vanderstukken, T. C.; Goesaert, H.; Delcour, J. A., Amylose-lipid complexation: a new fractionation method. *Carbohydrate Polymers* **2004,** *56*, 447-458.
252. Siswoyo, T. A.; Morita, N., Physicochemical studies of defatted wheat starch complexes with mono and diacyl-sn-glycerophosphatidylcholine of varying fatty acid chain lengths. *Food Res Int* **2003,** *36*, 729-737.
253. Jane, J. L.; Shen, J. J., Internal Structure of the Potato Starch Granule Revealed by Chemical Gelatinization. *Carbohyd Res* **1993,** *247*, 279-290.
254. Kasemsuwan, T.; Jane, J.-L., Location of amylose in normal starch granules. II: Locations of phosphodiester cross-linking revealed by phosphorus-31 nuclear magnetic resonance. *Cereal Chem* **1994,** *71*, 282-287.
255. Phillips, J.; Muir, J. G.; Birkett, A.; Lu, Z. X.; Jones, G. P.; Odea, K.; Young, G. P., Effect of Resistant Starch on Fecal Bulk and Fermentation-Dependent Events in Humans. *Am J Clin Nutr* **1995,** *62*, 121-130.
256. Henningsson, A. M.; Margareta, E.; Nyman, G. L.; Bjorck, I. M. E., Influences of dietary adaptation and source of resistant starch on short-chain fatty acids in the hindgut of rats. *Brit J Nutr* **2003,** *89*, 319-327.
257. Sjoo, M.; Emek, S. C.; Hall, T.; Rayner, M.; Wahlgren, M., Barrier properties of heat treated starch Pickering emulsions. *Journal of colloid and interface science* **2015,** *450*, 182-188.
258. Lai, C. S.; Li, S. M.; Miyauchi, Y.; Suzawa, M.; Ho, C. T.; Pan, M. H., Potent anti-cancer effects of citrus peel flavonoids in human prostate xenograft tumors. *Food & function* **2013,** *4*, 944-949.
259. Middleton, E.; Kandaswami, C.; Theoharides, T. C., The effects of plant flavonoids on mammalian cells: Implications for inflammation, heart disease, and cancer. *Pharmacol Rev* **2000,** *52*, 673-751.
260. Benavente-Garcia, O.; Castillo, J., Update on uses and properties of citrus flavonoids: new findings in anticancer, cardiovascular, and anti-inflammatory activity. *J Agr Food Chem* **2008,** *56*, 6185-6205.
261. Arivazhagan, L.; Pillai, S. S., Tangeretin, a citrus pentamethoxyflavone, exerts cytostatic effect via p53/p21 up-regulation and suppresses metastasis in 7, 12-dimethylbenz (α) anthracene-induced rat mammary carcinoma. *The Journal of nutritional biochemistry* **2014,** *25*, 1140-1153.
262. Lai, H. C.; Wu, M. J.; Chen, P. Y.; Sheu, T. T.; Chiu, S. P.; Lin, M. H.; Ho, C. T.; Yen, J. H., Neurotrophic Effect of Citrus 5-Hydroxy-3,6,7,8,3 ',4 '-Hexamethoxyflavone: Promotion of Neurite Outgrowth via cAMP/PKA/CREB Pathway in PC12 Cells. *Plos One* **2011,** *6*.
263. Li, S. M.; Pan, M. H.; Lai, C. S.; Lo, C. Y.; Dushenkov, S.; Ho, C. T., Isolation and syntheses of polymethoxyflavones and hydroxylated polymethoxyflavones as inhibitors of HL-60 cell lines. *Bioorgan Med Chem* **2007,** *15*, 3381-3389.
264. Qiu, P. J.; Dong, P.; Guan, H. S.; Li, S. M.; Ho, C. T.; Pan, M. H.; McClements, D. J.; Xiao, H., Inhibitory effects of 5-hydroxy polymethoxyflavones on colon cancer cells. *Mol Nutr Food Res* **2010,** *54*, S244-S252.
265. Xiao, H.; Yang, C. S.; Li, S. M.; Jin, H. Y.; Ho, C. T.; Patel, T., Monodemethylated polymethoxyflavones from sweet orange (Citrus sinensis) peel inhibit growth of human lung cancer cells by apoptosis. *Mol Nutr Food Res* **2009,** *53*, 398-406.
266. Ting, Y. W.; Li, C. C.; Pan, M. H.; Ho, C. T.; Huang, Q. R., Effect of a Labile

Methyl Donor on the Transformation of 5-Demethyltangeretin and the Related Implication on Bioactivity. *J Agr Food Chem* **2013,** *61*, 8090-8097.
267. Li, S. M.; Pan, M. H.; Lo, C. Y.; Tan, D.; Wang, Y.; Shahidi, F.; Ho, C. T., Chemistry and health effects of polymethoxyflavones and hydroxylated polymethoxyflavones. *J Funct Food* **2009,** *1*, 2-12.
268. Eerlingen, R. C.; Cillen, G.; Delcour, J. A., Enzyme-Resistant Starch .4. Effect of Endogenous Lipids and Added Sodium Dodecyl-Sulfate on Formation of Resistant Starch. *Cereal Chem* **1994,** *71*, 170-177.
269. Luykx, D. M. A. M.; Peters, R. J. B.; van Ruth, S. M.; Bouwmeester, H., A review of analytical methods for the identification and characterization of nano delivery systems in food. *J Agr Food Chem* **2008,** *56*, 8231-8247.
270. Karkalas, J.; Ma, S.; Morrison, W. R.; Pethrick, R. A., Some Factors Determining the Thermal-Properties of Amylose Inclusion Complexes with Fatty-Acids. *Carbohyd Res* **1995,** *268*, 233-247.
271. Nakazawa, Y.; Wang, Y. J., Acid hydrolysis of native and annealed starches and branch-Structure of their Naegeli dextrins. *Carbohyd Res* **2003,** *338*, 2871-2882.
272. Raphaelides, S. N.; Georgiadis, N., Effect of fatty acids on the rheological behaviour of maize starch dispersions during heating. *Carbohydrate Polymers* **2006,** *65*, 81-92.
273. Marefati, A.; Rayner, M.; Timgren, A.; Dejmek, P.; Sjoo, M., Freezing and freeze-drying of Pickering emulsions stabilized by starch granules. *Colloid Surface A* **2013,** *436*, 512-520.
274. Arvisenet, G.; Le Bail, P.; Voilley, A.; Cayot, N., Influence of physicochemical interactions between amylose and aroma compounds on the retention of aroma in food-like matrices. *J Agr Food Chem* **2002,** *50*, 7088-7093.
275. Cohen, R.; Schwartz, B.; Peri, I.; Shimoni, E., Improving Bioavailability and Stability of Genistein by Complexation with High-Amylose Corn Starch. *J Agr Food Chem* **2011,** *59*, 7932-7938.